ANNUAL REPORT 99

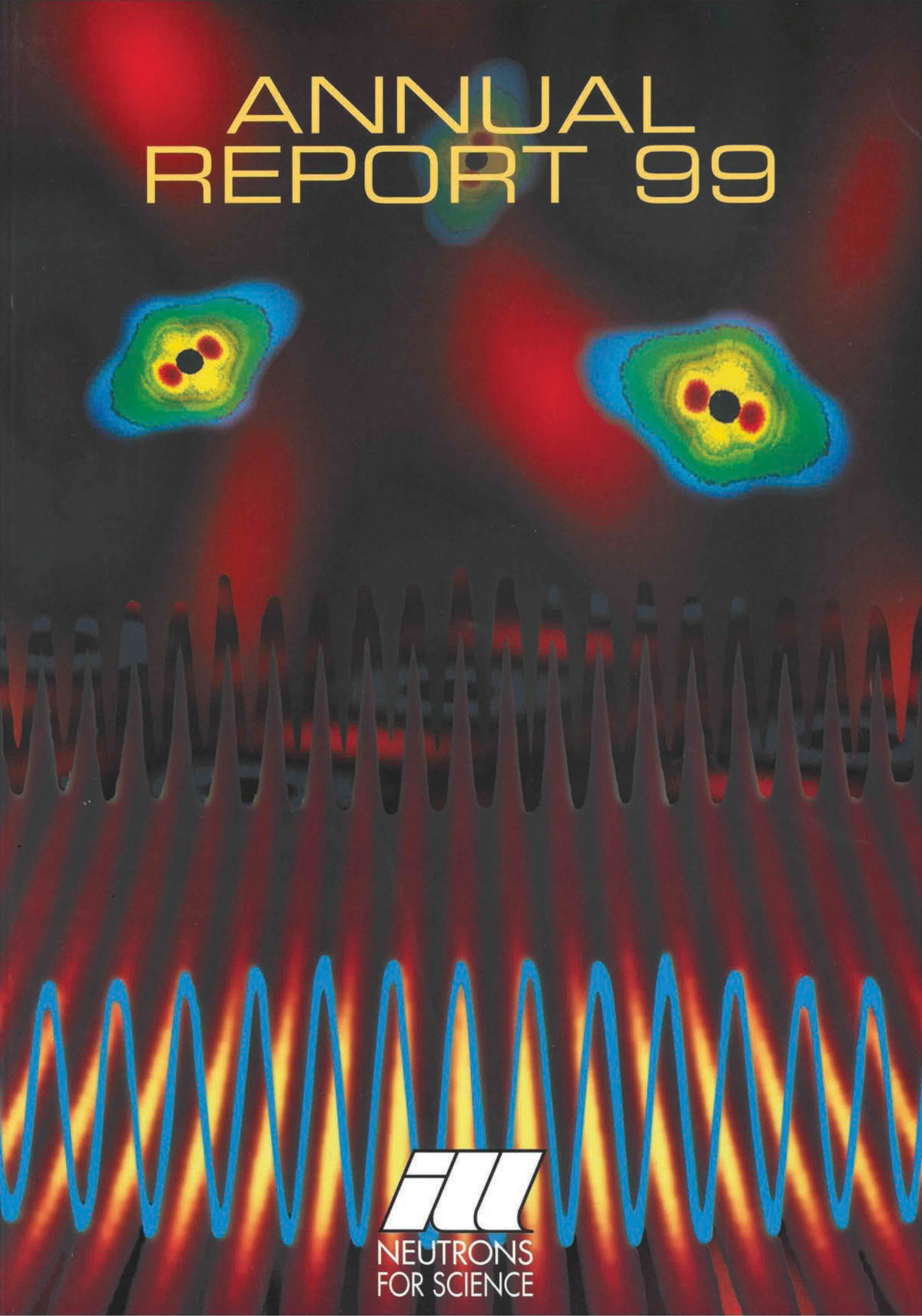

NEUTRONS FOR SCIENCE

ANNUAL REPORT 99

The Institut Max von Laue - Paul Langevin

The Institut Laue-Langevin (ILL) is an international research centre using neutrons to probe the microscopic structure and dynamics of a broad range of materials. The combination of the world's most powerful neutron source with dedicated instrumentation enables the study of a wide variety of scientific questions. Problems in materials science, chemistry, biology, solid-state physics and nuclear physics are investigated. For these diverse studies, the Institute offers its experimental facilities (some 30 instruments) to scientists world-wide via a peer-review system, and confidential industrial experiments are also welcomed.

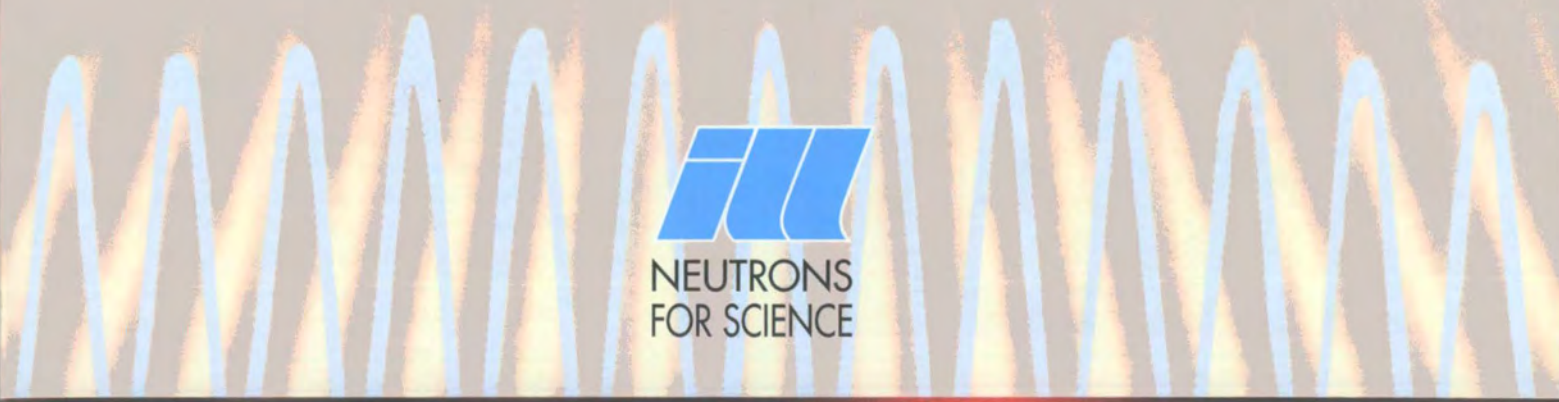

The MENI consortium (Austria and Czech Republic) signs the membership contract during a ceremony for all scientific members, held at the ILL on the 3rd of May 1999. The Czech Republic became a member at the beginning of 1999.

The Prefect Alain Rondepierre (centre) visits the ILL on the 24th of November 1999; on the left Ekkehard Bauer, head of the reactor division.

David Schildt (left), head of the British associates delegation and chairman of the steering committee, and Dirk Dubbers (centre), the ILL director, welcome the mayor of Grenoble, Michel Destot, during the steering committee meeting on 29 November 1999.

Vittorio De Giorgio (left), vice-president of INFM, University of Pavia, and Manuela Arata (centre), general director of INFM, INFM Genova, inaugurate the OGG (Operative Group in Grenoble) of the Italian scientific community INFM on the ESRF/ILL site, here together with Yves Petroff, the ESRF director. This group co-ordinates the activities of INFM scientists and technicians working at the ESRF and ILL and gives scientific, technical and logistic support to Italian users.

CONTENTS

DIRECTOR'S REPORT 4

1 SCIENTIFIC HIGHLIGHTS 7

BIOLOGY 8

SOFT MATTER 18

LIQUIDS & GLASSES 22

CHEMISTRY & STRUCTURE 30

MATERIALS SCIENCE 36

THIN FILMS 44

MAGNETISM 48

FUNDAMENTAL PHYSICS 59

QUANTUM SYSTEMS 64

2 WORKSHOPS 69

3 NEW DEVELOPMENTS 73

4 EXPERIMENTAL PROGRAMME 89

5 FACTS AND FIGURES 97

6 PUBLICATIONS 101

DIRECTOR'S REPORT

1999 started on a high point for ILL. The long-awaited delivery of reactor fuel coincided with the new year, ensuring supplies for the ILL neutron source well into the new Millennium. At the same time, 1999 saw a positive improvement in inputs to funding, due largely to the coming into force on 1 January 1999 of new contracts with our six "Scientific Members". Scientific Member countries include our latest partner the Czech Republic, together with Austria, Italy, Russia, Spain and Switzerland. ILL's associate members are France, Germany and the United Kingdom. The formal signing of the new contracts was celebrated at ILL in early May 1999, with representatives of political and scientific bodies.

New funds gave the ILL sufficient means to meet some of the fluctuating costs being encountered in 1999, such as the fuel cycle, but also to come to grips with projects launched in the past but recently becalmed due to lack of funding. Most significantly, however, it was in 1999 that ILL was able, for the first time in fifteen years, to give serious attention to the systematic renovation of its instrument suite - a point which allows me to move from the necessary question of "inputs" to the main topic of this report, namely ILL's essential "output".

The ILL's output is the operation of the highest quality instrumentation for the benefit of its numerous researchers, to produce groundbreaking scientific results. In the pages that follow you will find a cross-section of recent results - I hope you enjoy reading it.

Preparatory work on the Millennium development programme was a part of ILL's scientific output in 1999. Early in the year, a 200-page programme document was produced, which gave details of more than thirty proposals for the renewal of the instrument suite. The first five of these projects will be launched early in 2000. This modernisation is particularly urgent, if we are to carry into the future the Institute's capacity to optimise returns from the sums with which it is entrusted. Whilst it is true that the Millennium Programme has a relatively slim financial base and is prey to a number of uncertainties, given the imagination, determination and confidence which exists at ILL, a great deal of progress will certainly be achieved.

1999 also saw the departure of Alan Leadbetter and Philippe Leconte, our former British and French directors. We take this opportunity to thank them again most sincerely for the depth and quality of the services rendered during their five years at ILL. Their work has been taken up with great enthusiasm by their successors, Colin Carlile and Christian Vettier.

There were other noteworthy events in 1999. The beginning of the year 2000 brings the new French 35-hour week into force at ILL. Negotiations between management and staff ended in a timely agreement on the framework to be adopted. ILL's industrial R&D unit was developed and the nucleus of a scientific communication unit was established. The ILL's organisation of the 1999 Winter Atomiades at Les Gets in Haute-Savoie was a great success, with 250 participants from 5 different countries competing in various skiing disciplines.

Finally, I must report the breakdown of ILL's hot neutron source at the end of the year which affects four instruments. However, this only serves to underline the real need to renew ILL's infrastructure. A new hot source will be available in 2001.

All in all, 1999 was a good year for ILL. May the new Millennium bring many more!

L'année 1999 a très bien débutée avec un événement capital pour l'ILL : la livraison de combustible tant attendue, qui permettra également d'assurer l'approvisionnement de la source neutronique de l'ILL au cours du prochain millénaire, est arrivée juste à temps pour la Nouvelle Année. La situation financière de l'ILL s'est également améliorée en 1999, en particulier grâce à l'entrée en vigueur des nouveaux contrats avec nos six partenaires scientifiques : l'Autriche, l'Espagne, l'Italie, la Russie, la Suisse, et, depuis peu, la République tchèque. Les pays membres sont l'Allemagne, la France et le Royaume-Uni. Début mai 1999, la signature des nouveaux contrats a été dûment célébrée à l'ILL en présence des représentants politiques et scientifiques des différents pays.

Les ressources supplémentaires ont permis à l'ILL de faire face à l'augmentation de certains coûts, dans le cycle du combustible par exemple, mais aussi de mener à bien certains projets entrepris il y a plusieurs années mais restés inachevés par manque de moyens. Avant tout, elles ont permis à l'ILL d'envisager, pour la première fois depuis quinze ans, un renouvellement systématique de son parc instrumental.

Ainsi, après avoir parlé des ressources nécessaires au fonctionnement de l'Institut, j'en viens maintenant à la partie essentielle de ce rapport, c'est-à-dire la production de l'ILL. Celle-ci émane de l'exploitation des dispositifs expérimentaux par de nombreux scientifiques des laboratoires et des universités des pays membres et par les chercheurs de l'Institut. Les pages suivantes de ce rapport vous donnent, comme d'habitude, une vue d'ensemble des travaux effectués au cours de l'année écoulée, en mettant l'accent sur une série de résultats marquants et parfois innovateurs. J'espère que, cette année encore, leur lecture vous procurera un certain plaisir.

L'élaboration du programme de renouvellement des instruments,

le Programme Millenium, fait également partie des réalisations scientifiques de l'année 1999. Plus de 30 propositions détaillées pour le renouvellement du parc instrumental de l'ILL ont été présentées au printemps dans un document de 200 pages. Les cinq premières propositions doivent être mises en œuvre dès le début de l'an 2000. Cette modernisation de l'ILL est d'une importance primordiale si l'on veut rentabiliser dans les années à venir le capital investi dans l'Institut. La base financière du Programme Millenium est certes étroite et de nombreuses incertitudes persistent, cependant, grâce à l'imagination, la confiance et la ténacité déjà à l'œuvre à l'ILL, des progrès importants seront réalisés.

Au cours de l'année 1999, les Directeurs britannique et français, Alan Leadbetter et Philippe Leconte, ont quitté l'Institut à l'issue de leur mandat de cinq ans. Nous voudrions une fois de plus les remercier pour les immenses services qu'ils ont rendus à l'ILL au cours de cette période. Leur travail est poursuivi avec enthousiasme par leurs successeurs, Colin Carlile et Christian Vettier.

D'autres événements ont également marqué cette année 1999. Au début 2000, la semaine de 35 heures sera introduite en France. Le personnel et la Direction de l'ILL sont parvenus, dans les délais fixés, à trouver un accord sur les modalités d'application à l'Institut de la réduction du temps de travail. D'autre part, l'ILL a renforcé ses équipes à la fois au sein du groupe chargé des relations avec l'industrie, et dans le domaine de la communication. Enfin, l'Atomiade d'hiver 1999 organisée aux Gets par l'ILL a regroupé 250 participants de 5 pays différents et a remporté un franc succès.

Je dois malheureusement terminer ce bilan sur une note d'amertume et annoncer la défaillance de la source chaude de l'ILL. Quatre instruments seront affectés par cet événement survenu à la fin de l'année. Cette défaillance souligne la nécessité de renouveler les infrastructures de l'ILL. Une nouvelle source chaude sera disponible en 2001.

Dans l'ensemble, 1999 aura été une bonne année pour l'ILL. Que de nombreuses années tout aussi fructueuses lui succèdent au cours du prochain millénaire !

Das Jahr 1999 hatte für das ILL einen guten Start: Pünktlich zum Neuen Jahr erreichte uns die langerwartete Lieferung Brennstoff, die die Versorgung der Neutronenquelle des ILL auch im neuen Millennium sicherstellen wird. Auch die Versorgung des ILL mit den notwendigen Geldmitteln hat sich 1999 etwas erholt. Dies lag zu einem guten Teil daran, dass am 1. Januar 1999 die neuen Verträge mit unseren sechs sog. "wissenschaftlichen Mitgliedsländern" in Kraft traten. Die Mitgliedsländer sind Italien, Österreich, Russland, Schweiz, Spanien, sowie die neu hinzugekommene Tschechische Republik; die Stammländer des ILL sind Deutschland, Frankreich und Grossbritannien. Anfang Mai 1999 wurde die Unterzeichnung der neuen Verträge mit Delegierten aus Politik und Wissenschaft am ILL gebührend gefeiert.

Die neuen Geldmittel erlaubten es dem ILL in 1999, nicht nur einige Teuerungen zum Beispiel im Brennstoffkreislauf aufzufangen, sondern auch vor Jahren begonnene, aber durch Geldknappheit ins Stocken geratene Vorhaben abzuschliessen. Vor allem aber wurde es dem ILL erstmals seit 1 1/2 Jahrzehnten überhaupt wieder möglich, über eine systematische Erneuerung seines Instrumentenparks nachzudenken. Und hiermit komme ich, nach der Diskussion des notwendigen "Inputs", zum wesentlichen Teil dieses Berichtes - dem "Output" des ILL.

Unser Produkt ist die Nutzung der wissenschaftlichen Instrumente durch unsere vielen auswärtigen Gäste und durch die Mitarbeiter des ILL. Auf den folgenden Seiten der vorliegenden Broschüre wird, wie gewohnt, das Produkt dieser Nutzung, nämlich die oft hervorragenden, manchmal bahnbrechenden wissenschaftlichen Arbeiten am ILL aus jüngster Zeit dargestellt, und ich wünsche wieder viel Vergnügen bei der Lektüre.

Zur wissenschaftlichen Produktion des Jahres 1999 gehört auch die Ausarbeitung des Millennium-Erneuerungsprogramms. In dem im Frühjahr vorgelegten Dokument werden auf 200 Seiten mehr als 30 detaillierte Vorschläge zur instrumentellen Erneuerung des ILL vorgestellt. Die ersten fünf Erneuerungsvorschläge sollen ab Beginn des Jahres 2000 in die Tat umgesetzt werden. Diese Erneuerung des ILL ist von grosser Dringlichkeit, um die hohe Rentabilität der im Institut investierten Mittel auch in Zukunft zu gewährleisten. Zwar ist die finanzielle Basis des Millennium-Programms schmal und durch manche Unwägbarkeiten gefährdet, aber mit Phantasie, Zuversicht und Hartnäckigkeit wird sich viel erreichen lassen.

Im Laufe des Jahres 1999 verliessen uns die bisherigen britischen und französischen Direktoren, Alan Leadbetter und Philippe Leconte, die in ihrer jeweils fünfjährigen Amtszeit dem ILL immense Dienste geleistet haben, für die wir Ihnen hier nochmals herzlich danken. Ihre Arbeit wird mit grossem Enthusiasmus von ihren Nachfolgern Colin Carlile und Christian Vettier weitergeführt.

An weiteren Ereignissen des Jahres 1999 sind zu vermerken: Mit dem Jahr 2000 wird in Frankreich die 35-Stundenwoche eingeführt, auf deren Modalitäten sich Belegschaft und Institutsleitung auf dem Verhandlungswege rechtzeitig zum Jahresende geeinigt haben. Die Gruppe zur industriellen Nutzung des ILL wurde ausgebaut, und es wurde der Kern einer Gruppe zur professionellen Öffentlichkeitsarbeit ins Leben gerufen. Die Wintersport-Atomiade 1999 wurde in Les Gets für 250 Teilnehmer aus 5 Ländern mit grossem Erfolg vom ILL ausgerichtet.

Schliesslich muss, als Wermutstropfen in diesem Bericht, der Ausfall der heissen Neutronenquelle des ILL gemeldet werden. Von diesem gegen Ende des Jahres aufgetretenen Ereignis sind vier Instrumente betroffen. Eine neue Heisse Quelle wird 2001 zur Verfügung stehen.

Alles in allem war 1999 ein gutes Jahr für das ILL, mögen viele weitere im neuen Millennium folgen.

Dirk Dubbers

Dirk Dubbers (centre) sees off his colleagues, Alan Leadbetter (left, white shirt), the British director and head of science, and Philippe Leconte (right, white shirt), the French director and head of projects & techniques.

Alan Leadbetter welcomes his successor Christian Vettier, the new French director coming from ESRF.

Colin Carlile, the new British director and head of the projects & techniques division, enjoying his first ILL Steering Committee meeting; on the left Michel Destot, the Mayor of Grenoble.

The ILL finishes champion of the medal table at the Atomiade in Les Gets; from left Bob Pratt, Barbara Standke, Ariel Brun and Heinz Rhein, FZ Jülich. The 7th Atomiade, organised by the ILL works committee on 13-20 March 1999, gathered about 250 people from European research centres to compete in a variety of skiing disciplines.

SCIENTIFIC HIGHLIGHTS

1

Our goal at the Institut Laue Langevin (ILL) is to achieve scientific excellence. This volume of the Annual Report for the year 1999 provides the best illustration of this attempt: 30 highlights are presented covering a remarkable range of science and technique. As with last year's report, a wide spectrum of neutron science is embraced from biology, through to studies in chemistry, materials science and magnetism, to particle physics. To maintain this excellence, important efforts have been made in instrumentation; they are described in the technical section together with the Millennium Programme. This report is an appropriate illustration of the unique value of neutron methods for the study of a wide range of materials proving the usefulness of large-scale facilities such as the ILL.

In 1999, the reactor operated for 208 days and more than 700 experiments were carried out in over 4400 days of scheduled beam time. Unfortunately, there was a failure of the hot source in December 1999 leading to a loss of about 20 days of beam time. Therefore, in 2000 the reactor will operate without the hot source. However, this will only affect 10% of ILL's instruments. As in previous years, a large number of high-quality experiments was proposed and performed to tackle a broad range of scientific questions. For example in biology, the results presented here demonstrate that the contrast-variation method combined with small-angle scattering and neutron reflectivity techniques is a remarkable and unique tool for the investigation of biological materials. In the field of soft matter and liquids, it is known that confined geometry substantially modifies the properties of systems as diverse as simple water, polymers and quantum fluids. Neutron scattering experiments, presented here, have revealed the static and dynamic characteristics of these materials under conditions of confinement. In materials sciences, the penetration and contrast properties of neutrons are exploited, particularly in the case of small-angle scattering applied to alloys. Finally, the exploration of magnetism with neutrons continues to be very productive: simply to mention the discovery of a new class of phase transitions involving magnetic chirality and the observation of super high-spin magnetic clusters.

We thank all our collaborators who have submitted highlight reports for this Annual Report, but we regret that we had to make a selection. For the year 2000 report, we invite our users again to submit highlights. Note that this version of the 1999 Annual Report will be followed by a version dedicated to the general public. Herma Büttner who has been the editor of the ILL Annual Report for the last 4 years, has announced her departure from ILL to start a new career. The staff and the management of ILL would like to reiterate their grateful thanks to Herma for her dedication to Scientific Coordination and Communication at ILL.

Critical role of micelles in pancreatic lipase activation

D. Pignol, J. Hermoso and J. C. Fontecilla-Camps (LCCP, CEA-CRNS Grenoble),
L. Ayvazian, B. Kerfelec, I. Crenon and C. Chapus (CNRS Marseille),
P. Timmins (ILL).

The digestive process is carried out by secretions from several organs: the salivary glands, the stomach, the gall bladder and the pancreas. In the small intestine, pancreatic lipase (PL) hydrolyses insoluble triglyceride by binding to the oil-droplets in the presence of its protein cofactor colipase (PC) and bile-salt micelles. Combined x-ray and neutron diffraction experiments have previously revealed the crystal structure of an activated lipase-colipase non- physiological micelle complex. This structure suggested that the adsorption of the enzyme to the emulsified oil-droplets is mediated by this ternary complex. We decided to carry out small-angle neutron scattering experiments with D_2O/H_2O contrast variation in order to characterise the physiological ternary PC/PL/bile salt micelle complex in solution. The experimental radii of gyration and match point of the protein/micelle solutions correspond to those expected for a ternary complex, similar to the one observed in the crystal structure. This preformed ternary complex would be the entity that adsorbs to the water-insoluble substrate.

Triglycerides (TG) comprise more than 95% of the dietary fats in the western diet. TG are mainly cleaved in the small intestine by pancreatic lipase (PL) into triglycerol and fatty-acids. TG, which are insoluble in water, form oil-droplets. As a consequence, TG hydrolysis implies the adsorption of PL to the oil-water interface [1]. In the intestine, PL alone would not be able to react against the emulsified oil-droplets: its active site is covered by a loop that prevents the access of the substrate. Two other physiological components are required for PL activation (the unmasking of the active site and the adsorption of the enzyme to the substrate interface): 1, colipase (PC), a small protein also produced by the pancreas that forms a complex with PL and 2, bile-salts, that solubilise fatty-acids (the product of the hydrolysis) into mixed micelles that are later discharged into lymph or blood. The aim of our studies is to understand, at a molecular level, the interactions between the different components of the system (PL, PC, bile-salts micelles, substrate oil-droplets). We initially solved the crystal structure of a PL-PC-micelle complex using x-rays [2]. In this complex, the detergent micelles were non-physiological.

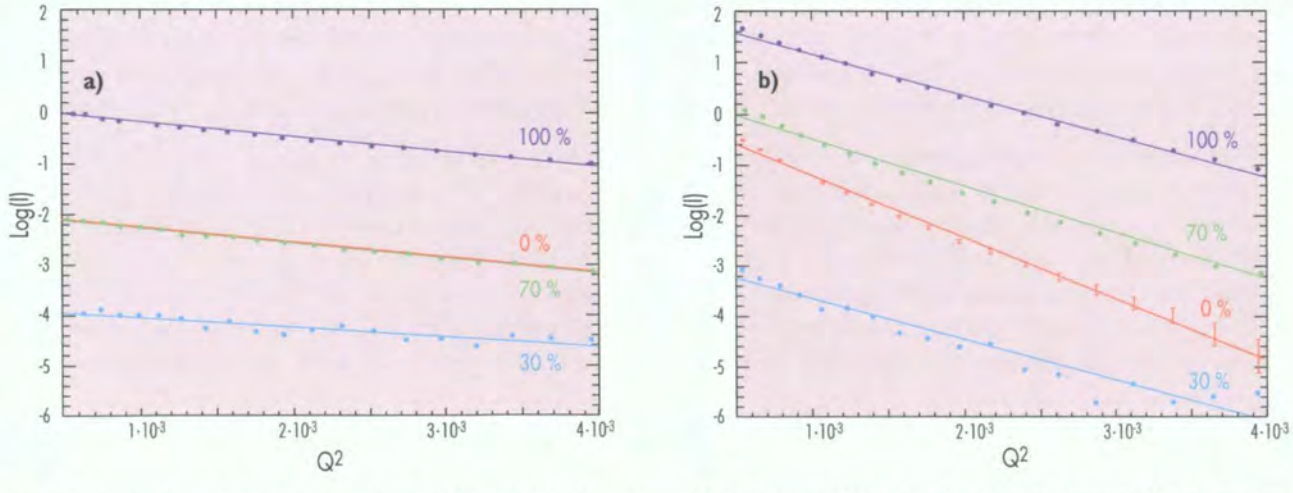

*Figure 1: Guinier plots of PL/PC complex solutions at different D_2O concentrations: **a)** in the absence of bile-salt micelles, **b)** in the presence of bile-salt micelles.*

The structure solved at 2.8 Å resolution, only revealed the structural organisation of the protein components of the system (PC/PL). Subsequently, we decided to carry out a neutron-diffraction analysis. Neutron diffraction data collected to 15 Å resolution allowed us to obtain the structure of the micellar partner of the system in the crystal [3].

In the resulting ternary complex, both PC and the micelle help stabilising the PL activated conformation. The aim of the work reported here was to characterise the ternary PC/PL/bile salt micelles in solution. We carried out neutron small-angle scattering experiments on D22, combined with the D_2O/H_2O contrast variation method because this procedure is very well adapted to obtain structural information on systems composed of two components of different scattering density (such as lipid-protein associations).

Initial experiments were carried out on PC/PL complex solutions, in the absence of bile-salt micelles. The Guinier plots at different D_2O concentrations are presented in Fig. 1a. The resulting radius of gyration at infinite contrast is 26 Å and the match point of the solution is 41.6% D_2O. These values are in good agreement with those calculated for the PC-PL complex using the x-ray structure coordinates (Rg = 25 Å, match point = 42% D_2O).

We applied the same procedure to spectra obtained from the PL/PC complex solutions in the presence of bile-salt micelles (sodium taurodeoxycholate micelles). The Guinier plots at different D_2O concentrations are presented in Fig. 1b. The resulting radius of gyration is 56 Å, and the match point of the solution is 38.5% D_2O. Since both values differ significantly from the ones obtained in the absence of micelles, different protein-micelle associations were modelled.

The experimental values are very close to those calculated for a model built with a stoichiometry of 2 lipase/colipase molecules per micelle (Rg = 55 Å Match point = 39.2% D_2O), which corresponds to that observed in the neutron low-resolution crystal structure (Fig. 2). All the other models we built did not fit the experimental results.

These results clearly demonstrate for the first time, in solution, the formation of a ternary PC/PL/bile-salt micelle complex. This complex is similar to the one observed previously in crystals with a non-physiological detergent. Our results strongly suggest that the association of PC and bile-salt micelle stabilises the enzyme in its active conformation. The preformed complex behaves as an entity that adsorbs to the substrate oil-droplets [4].

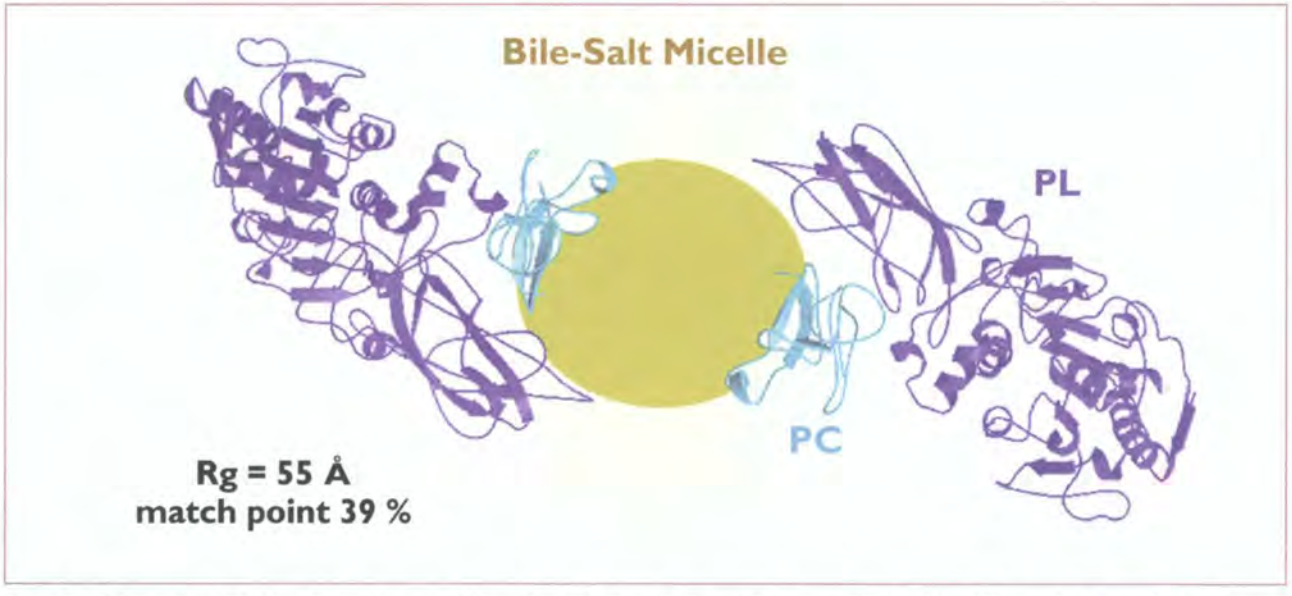

Figure 2: *Calculated model built with a stoichiometry of 2 lipase/colipase molecules per micelle corresponding to observed low-resolution crystal structure.*

References

■ [1] B. Borgström et al., Eur. J. Biochem. 37 (1973) 60 ■ [2] J. Hermoso et al., J.Biol. Chem. 271 (1996) 18007 ■ [3] J. Hermoso et al., Embo J. 16 (1197) 5531 ■ [4] D. Pignol et al., J. Biol. Chem. 275 (2000) 4220.

New insights to cellulose structure

- H. Chanzy (CERMAV-CNRS, Grenoble),
- Y. Nishiyama (Univ. Tokyo),
- P. Langan (Los Alamos National Laboratory).

Neutron fibre diffraction experiments carried out at the ILL on instrument D19 have provided detailed new information on the position of hydrogen atoms in cellulose II and on the hydrogen bonding network that holds the cellulose structure together. D19 is currently the only instrument in the world that is capable of this type of fibre diffraction study; this work on cellulose illustrates its potential for the investigation of other biological and non-biological polymer systems.

Cellulose is often said to be the most abundant polymer on earth. It is certainly one of the most important structural elements in plants and other living systems. In nature it is synthesised as slender rod-like crystalline microfibrils. One of the key features of cellulose is that each of its monomers bears three hydroxyl groups. It is these hydroxyl groups and their hydrogen bonding ability that not only play a major role in directing crystalline packing but also in governing important physical properties of cellulose materials.

Cellulose can occur in a number of different forms. Native cellulose is known as cellulose I, but other forms such as cellulose II, cellulose III and cellulose IV have been described. We are involved in a long-term study, using the neutron and synchrotron x-ray facilities in Grenoble, to unravel the fine details of these allomorphs. In this report, the focus is on cellulose II fibres that result from the swelling of fibres in concentrated sodium hydroxide. By using deuterated solvents, crystalline fibres can also be prepared in which all the OH groups in the crystalline unit cell are replaced by ODs. Neutron fibre diffraction data recorded from these samples can then be used to locate these groups using Fourier imaging methods.

Neutron fibre diffraction patterns of cellulose II, obtained at D19 (wavelength 1.529 Å) are shown in Fig. 1 (the left part of the diagram shows data recorded from the hydrogenated sample, and the right part shows the data recorded from the deuterated sample). Both data sets show diffraction extending to 1.2 Å resolution. The data have been indexed with a $P2_1$ unit cell having lattice parameters a = 8.01 Å, b = 9.04 Å, c (chain axis) = 10.36 Å, $\gamma = 117.1°$. Despite strong similarities between the left and right parts of the diagram, there are nevertheless substantial differences in the distribution of intensities, particularly on the equator and on the 4th layer line where for instance the reflection 004 is very strong in the deuterated pattern, but almost absent in the hydrogenated one. These differences can be used to image the OH groups in the cellulose unit cell.

Using the CCP13 program suite [1], 97 independent intensities (I) were measured for each part of the diagram in Fig. 1; 41 with $I > 2\sigma$ and 56 with $I < 2\sigma$. These intensities and

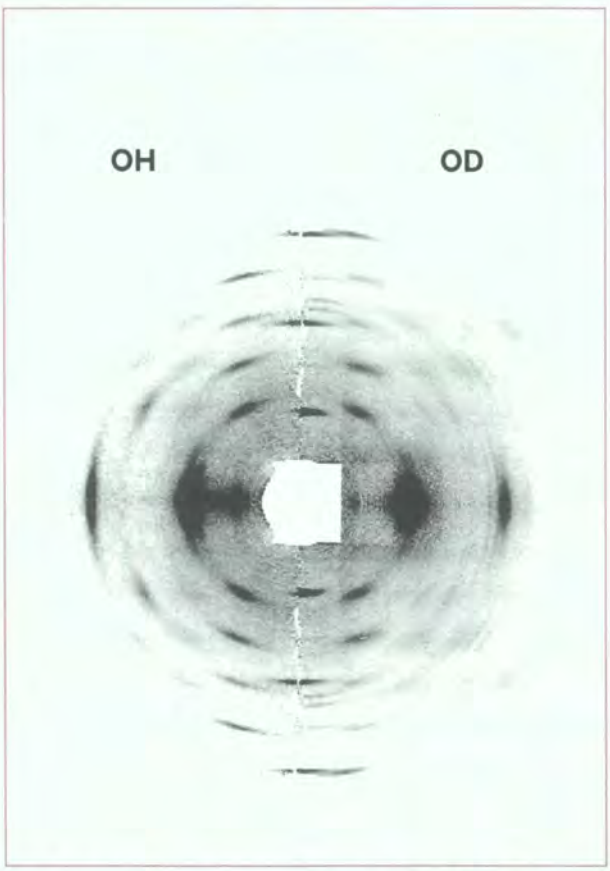

Figure 1: *Neutron fibre diffraction patterns collected from two cellulose samples, one treated with $NaOH/H_2O$ (left hand side) and the other treated in $NaOD/D_2O$ (right hand side). The fibre axis is vertical and the two patterns have been displayed together by joining equivalent halves along the meridian.*

their differences were tested against two different models existing already in literature, which we refer to here as model 1 [2,3] and model 2 [4,5]. Both models agree on several points, namely that the structure of cellulose II is based on a two chain unit cell where the chains are antiparallel and that the chains are located on the 2_1 axes of the monoclinic cell. However, the two models differ significantly in the description of their chain conformations. We could not differentiate between these two models on the basis of their agreement with the x-ray data alone.

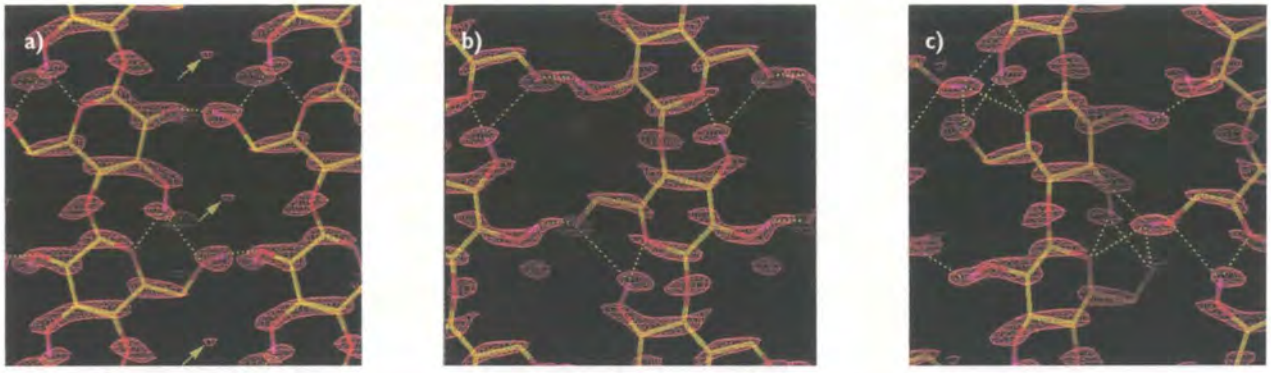

Figure 2: *Final 2Fd-Fc map (red density) of cellulose II, showing views of the planes containing* **a)** *the centre chains* **b)** *the origin chains and* **c)** *origin and centre chains. Cellulose chains are represented by a skeletal model in which carbon atoms are yellow, oxygen atoms are red and exchangeable hydrogen atoms are pink. The arrows in* **a)** *indicate density peaks which could not be accounted for by exchangeable hydrogen atom positions. The potential hydrogen bonds are represented by broken lines.*

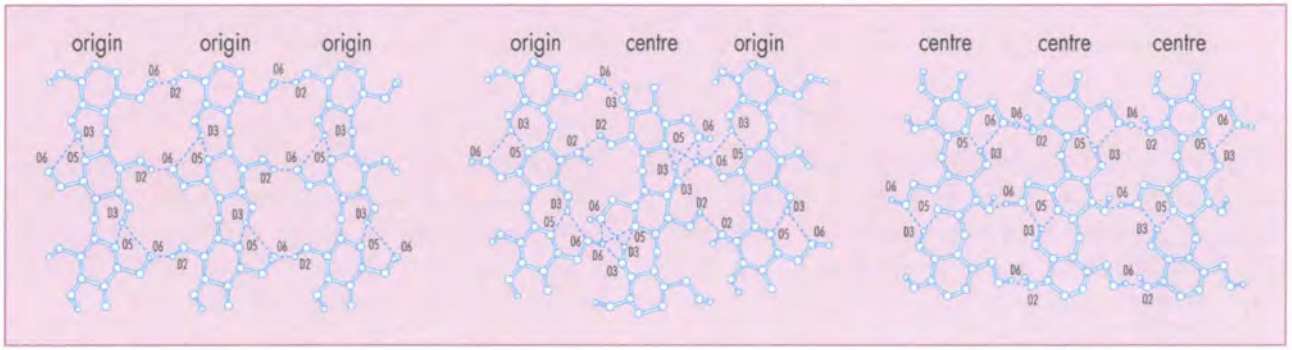

Figure 3: *A schematic representation of the hydrogen bonding in cellulose II.*

The H/D atom positions of both models were then refined against our D19 neutron diffraction data. Model 2 was in significantly better agreement with the data than model 1 and we were able to reject model 1. A final 2Fd-Fc difference Fourier map is shown in Fig. 2. The identified hydrogen bonding system, shown schematically in Fig. 3, reveals some interesting three and four centred hydrogen bonding arrangements [6].

This study, which has now been followed by similar evaluations for cellulose I and III, is the first three-dimensional description of the hydrogen bonding system in a fibrous polysaccharide.

References

■ [1] Fibre Diffraction Review 7 (1998) 12 ■ [2] F. J. Kolpak and J. Blackwell, Macromolecules 9 (1976) 273 ■ [3] A. Stipanovic and A. Sarko, Macromolecules 9 (1976) 851 ■ [4] K. Gessler, N. Krauss, T. Steiner, C. Betzel, C. Sandman and W. Saenger, Science 266 (1994) 1027 ■ [5] S. Raymond, A. Heyraud, D. Tran Qui, Å. Kvick and H. Chanzy, Macromolecules 28 (1995) 2096 ■ [6] P. Langan, Y. Nishiyama and H. Chanzy, J. Am Chem. Soc. 121 (1999) 9940.

Are all disordered regions of native cellulose of the same nature?

- C. Czihak (ILL, Univ. Wien and HMI Berlin),
- G. Vogl (Univ. Wien and HMI Berlin),
- M. Müller (ESRF),
- H. Schober (ILL),
- Y. Nishiyama (Univ. Tokyo).

Cellulose is the most abundant structural biopolymer. Despite considerable research efforts the structural details of native cellulose, in particular on the morphological level, are still controversial. Inelastic neutron scattering provides important clues to understand the problem. Using the hydroxyl groups of cellulose as a microscopic probe, it is possible to investigate the dynamic response (spectrum of vibrational modes) of regions accessible to water. For these disordered regions the dynamic response is distinctly different from that obtained for the crystal cores and therefore constitutes a signature of the disordered parts. This signature turns out identical when comparing cellulose types of different crystallinity and origin indicating its universal character.

Cellulose is a complex composite material which structurally comprises three hierarchical levels: (i) The *molecular* level of the single molecule; (ii) the *supermolecular* level concerning the packing and aggregation of the molecules in crystals called *microfibrils*; and (iii) the morphological level, i.e., the arrangement of microfibrils and interstitial voids in relation to the cell wall (see Fig. 1). On the molecular level, cellulose is composed of linear chains of glucose units. These chains form whisker-like crystals which are assembled in a superstructure. Details about the arrangement of the chains both inside the crystals and in the interface between the crystals have been discussed extensively over the last years [1].

The structural organisation at all levels influences the macroscopic properties of the material and is equally of importance for the chemical reactions taking place during industrial processing. In addition, from structural properties conclusions can be drawn for the cellulose synthesis in plants.

The "classical" two-phase model assuming a composite arrangement of distinct crystalline and extended amorphous regions [2] to describe the superstructure of cellulose apparently has to be revised. Concepts like crystallinity and amorphicity are well adapted to describe homogeneous states of matter. They are, however, rather ill-defined when it comes to treat dense composite materials like cellulose given that

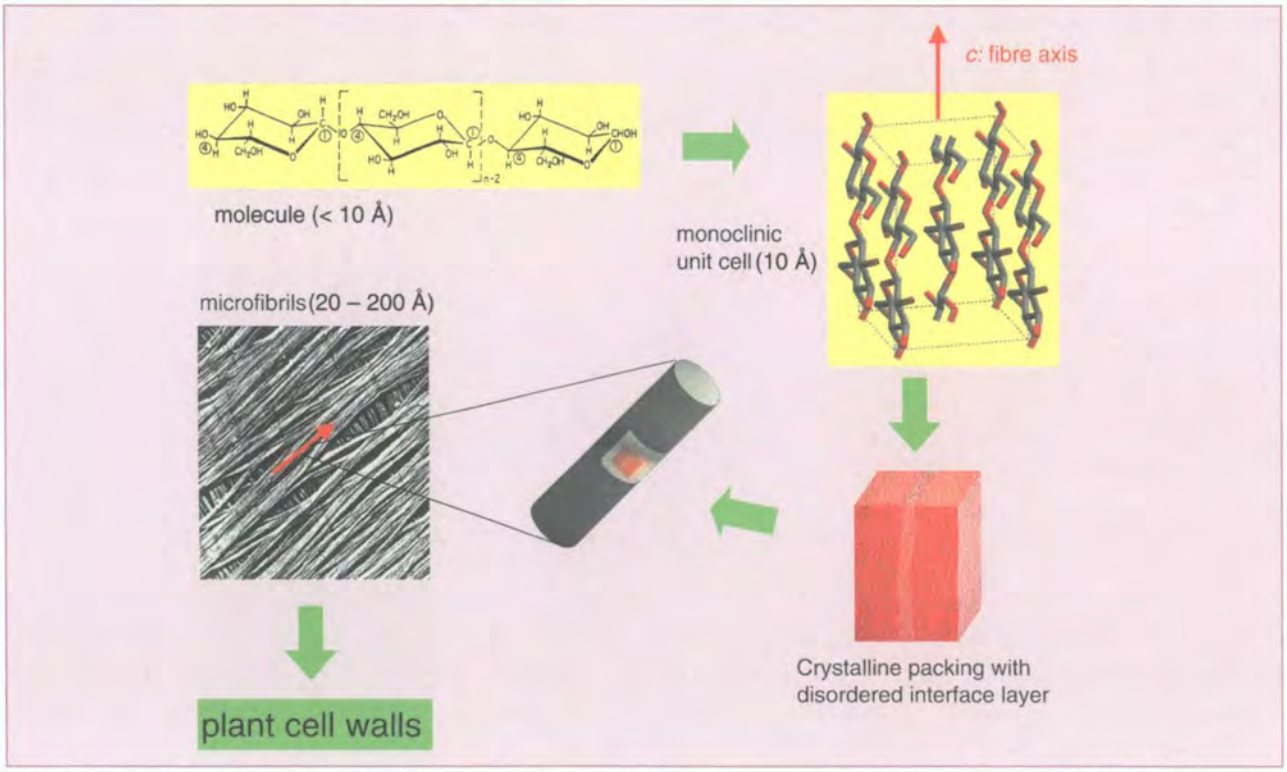

Figure 1: *Hierarchical organisation of cellulose. The polymer (top left) aggregates to cellulose nano-crystallites, which are interconnected by disordered interface layers (bottom right). These crystallites (20 – 200 Å) are organised in bundles of single fibres (bottom left).*

intermolecular correlations do not build up or die off abruptly at some fictitious interfaces. This equally makes the interpretation of diffraction experiments problematic.

A by far better defined quantity than crystallinity or amorphicity is the *accessibility* of cellulose to various guest molecules, in particular water [3]. Inelastic neutron scattering in conjunction with deuteration becomes a very powerful tool of investigation. Using the hydroxyl groups of the cellulose as a microscopic probe inelastic neutron scattering allows to investigate the dynamic response of regions accessible to water. The low-energy dynamics of the accessible OH groups in natural cellulose was carried out on the cold neutron time-of-flight spectrometer IN6 and is shown in Fig. 2 for cellulose material of different origin. Even without quantitative analysis it is evident that the native samples with no preferential orientation, namely cotton and sugar beet pulp, show spectra identical to a completely disordered reference sample – *amorphous* cellulose, all within the experimental uncertainties.

The restoring forces which are locally encountered by OH groups are averaged over the accessible parts of cellulose and therefore do not depend on the cellulose origin.

In addition, the dynamic OH response is indistinguishable from that obtained on artificial amorphous cellulose and, therefore, it is of universal nature. As amorphous cellulose is fully accessible to water it constitutes the ideal reference to which the accessible regions of the native samples should be compared. In conclusion the accessible regions seem to correspond to disordered regions, which are all similar to each other.

Albeit universal, the spectral response is not isotropic as can be seen in the spectrum from oriented flax fibres. This demonstrates that the disordered regions retain a high degree of directionality. The latter can be linked to the morphology by identifying disordered regions with surface and single interface layers. There is no evidence for the presence of largely extended amorphous regions [4].

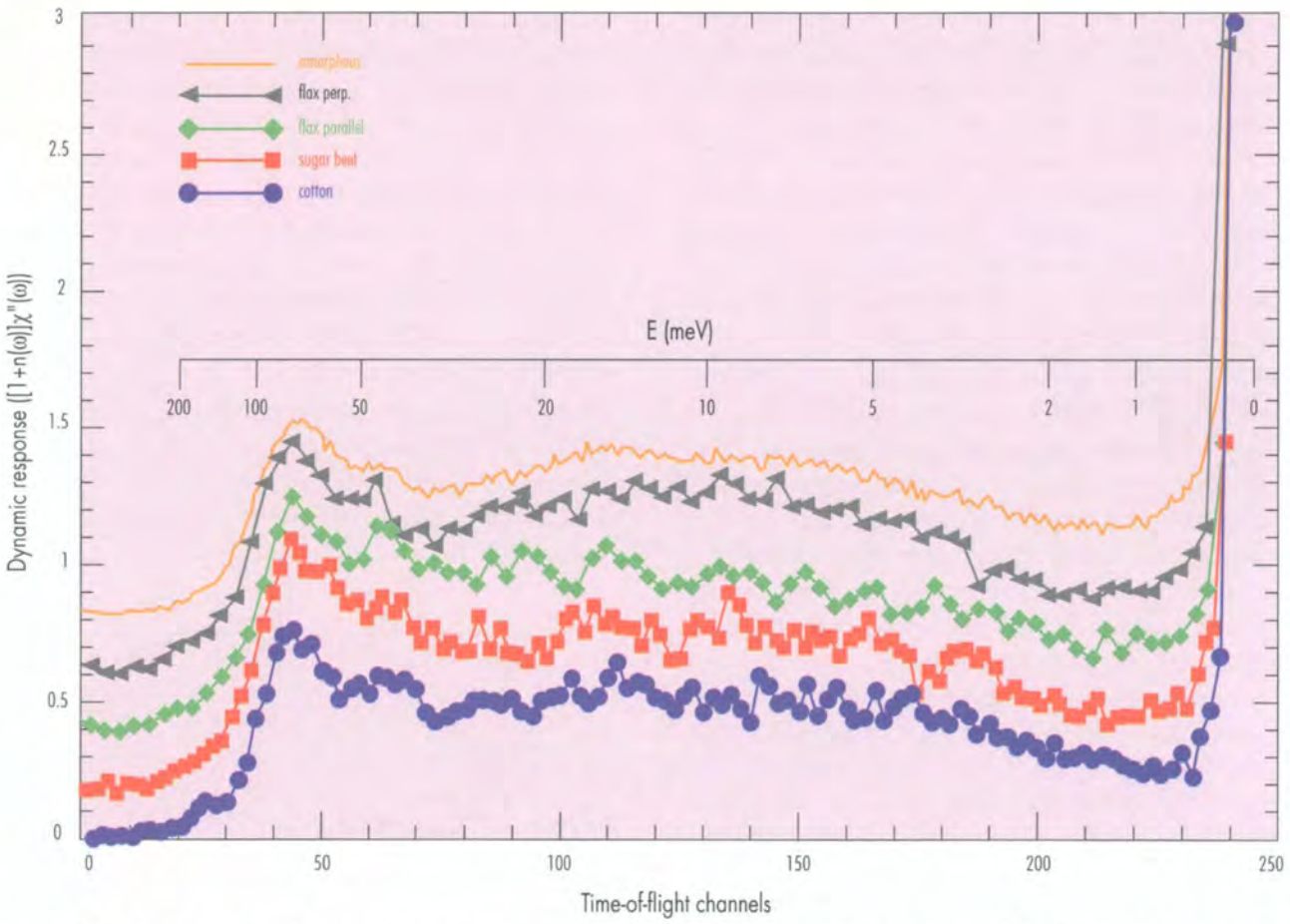

Figure 2: *The dynamic response of disordered regions of cellulose samples which are of different origin. " Flax parallel " stands for flax fibres that are aligned in the scattering plane, so does "flax perp", but perpendicularly aligned.*

References

■ [1] A. C. O'Sullivan, Cellulose 4 (1997) 173 ■ [2] H. Krässig, Cellulose: Structure, Accessibility and Reactivity; Polymer Monographs 11, Gordon and Breach Science Publ.: Yverdon 1993 ■ [3] M. Ioelovitch and M. Gordeev, Acta Polymer 45 (1994) 123 ■ [4] M. Müller, C. Czihak, H. Schober, Y. Nishiyama, and G. Vogl, Macromolecules 33 (2000) 1834-1840.

Free bilayer: a new model for biological membranes

- G. Fragneto, E. Bellet-Amalric (ILL),
- F. Graner, L. Perino-Gallice (UJF, Grenoble),
- T. Charitat (ICS, Strasbourg).

Neutron reflection has been applied to the study of a new physical model of cell membranes consisting of a well controlled phospholipid bilayer (free bilayer) floating in water. This system offers several advantages with respect to classical models of biological membranes and it has great potential for studies of membrane/protein interactions and bilayer fluctuations. Measurements were carried out at several temperatures ranging from 25.4°C, where lipids are in the gel phase, to 64.1°C, where lipids are in the liquid-crystalline phase, the transition occuring at 52°C. Around the phase transition large fluctuations inducing giant swelling were observed. In the liquid-crystalline phase the system has a similar structure as in the gel phase and it is stable over several hours.

The structure and composition of cell membranes is well known and described in classical books. Less known are the nature and mechanisms of interaction of membranes with other biological entities like peptides, proteins, DNA, etc. The complicated structure of cell membranes and the variety of events happening around them makes it difficult to study such mechanisms at the molecular level with real cells. For that reason biophysicists have searched for decades for simple and easily-controlled physical models of membranes and several systems are now available including lipid-stacked multibilayers, vesicles, lamellae, monolayers on the water surface, bilayers on solid surfaces.

We have recently succeeded in preparing double phospholipid bilayers assembled at the silicon/water interface [1]. This is a new system, promising for membrane/protein interaction studies and ideal for the study of bilayer fluctuations. The first bilayer is adsorbed on the flat solid substrate while the second one, named the free bilayer, floats at 15 to 30 Å above the first and, by interacting less strongly with the solid substrate, it is a better model than the single bilayer. The free bilayer has many remarkable properties: it exists in bulk water, unlike stacked bilayers or monolayers; it fluctuates like real membranes; it is stable in the biologically relevant fluid phase (as it will be shown below); it can be investigated alone (that is without averaging the effect of several layers as in lamellae, stacked bilayers and vesicles), with techniques able to reveal details at the Ångstrom scale like neutron or x-ray reflectivity; finally it is a useful model for determining how fluctuations influence the interactions of peptides or transmembrane proteins with the cell membrane.

Phospholipid bilayers exhibit a main phase transition from a gel phase, where lipid chains are rigid and well ordered, to a liquid crystalline phase (L_α), where chains are disordered and fluid-like. Here, we present the results of a neutron specular reflectivity study of the structural modifications induced on double phosphocholine bilayers by changing the temperature and going from the gel to the liquid-crystalline lipid-phases. Preliminary data were collected on the reflectometer ADAM while a more complete study was done recently on the rebuilt diffractometer D16 specially adapted for reflectivity measurements. Samples were double bilayers of hydrogenated DSPC (di-stearylphosphatidil-choline) in D_2O and deuterated DSPC in H_2O and SMW (silicon-matched water, that is water with the same scattering-length density of silicon). Phosphocholines were used since they are the main components of cell membranes. The double bilayers were assembled on very smooth and highly hydrophilic silicon single crystals with the Langmuir-Blodgett and Langmuir-Schaeffer techniques. For full details on the deposition and measurement procedures see [1,2].

For hydrogenated DSPC in D_2O the phase transition occurs at 52°C [3]. As expected deuterated lipids show a transition temperature different from that of the hydrogenated ones. Data analysis is still in progress and only the analysis for the hydrogenated lipids will be discussed here. Figure 1 shows

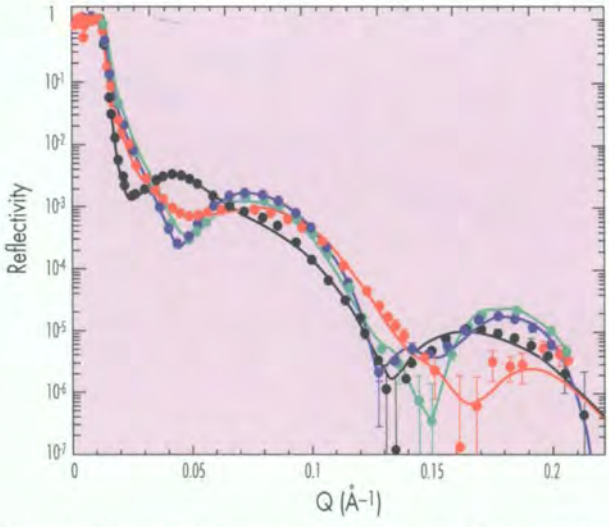

Figure 1: *Measured reflectivity profiles and fitted curves for DSPC double bilayers in D_2O at (●) 25.4°C; (●) 51.5°C; (●) 55.4°C; (●) 64.1°C. For details on model used see text and Fig. 2.*

the reflectivity curves recorded at room temperature (25.4°C), in the pre-transitional phase (51.5°C), just above (53.4°C) and well above (64.1°C) the transition for fully hydrogenated DSPC in D_2O. Data were analysed by model fitting using the optical matrix method [4]: the interface is divided in several boxes, each characterised by a scattering-length density, a thickness and the interfacial roughness between two consecutive boxes. These parameters are varied until the optimum fit to the data is found. Between 25.4°C and 42°C, curves were very similar and data were interpreted with the same model. Figure 2a shows a cartoon of such a model. Lipid headgroups and chains could be distinguished and their thickness determined with 1 Å precision. No measurement is available for the hydrogenated lipids between 42°C and 51.5°C but at 51.5°C and 52.5°C the curves differ dramatically from those at lower temperature indicating major changes in the bilayer structure (cf. Fig. 1). Data analysis indicates that the water layer between the bilayers becomes much thicker (60 to 90 Å) and the second bilayer much rougher (~ 30 Å). With such high value of the roughness the box-model used to fit the data is not very efficient anymore. Figure 2b is a cartoon of a speculative interpretation of the model. Additional work is needed for a more precise interpretation. Plans for future work include off-specular reflectivity and atomic force microscopy measurements for extracting information in the membrane plane. Moreover, a study of the theoretical explanation of the experimental observation is in progress [2].

A further increase of temperature brings the system nearly back to the initial state in terms of total thickness (immediately noticeable from the positions of the first minimum in Fig. 1). The water layer thickness is 21 ± 1 Å. The second bilayer chain thickness decreases from 37 ± 1 Å to 31 ± 1 Å (cf. Fig. 2c). The highest temperature measured was 64.1°C. Surprisingly, the double bilayer is still at the surface although the chain thickness of both bilayers decreases to 27 ± 1 Å and the roughness of the free bilayer is of 10 ± 2 Å (cf. Fig. 2d).

Finally, this work has confirmed the good stability of double bilayer systems over several days and at all temperatures investigated and therefore of their suitability as model biological membranes. Results are reproducible and pre-transitional effects on the structure are remarkable. The giant increase of both the thickness and the roughness at the transition (i.e. where the bilayer is extremely flexible) might be the first direct observation of the fluctuation-induced repulsion predicted by Helfrich [5] using entropy arguments and considered a key ingredient of bilayer-bilayer interactions.

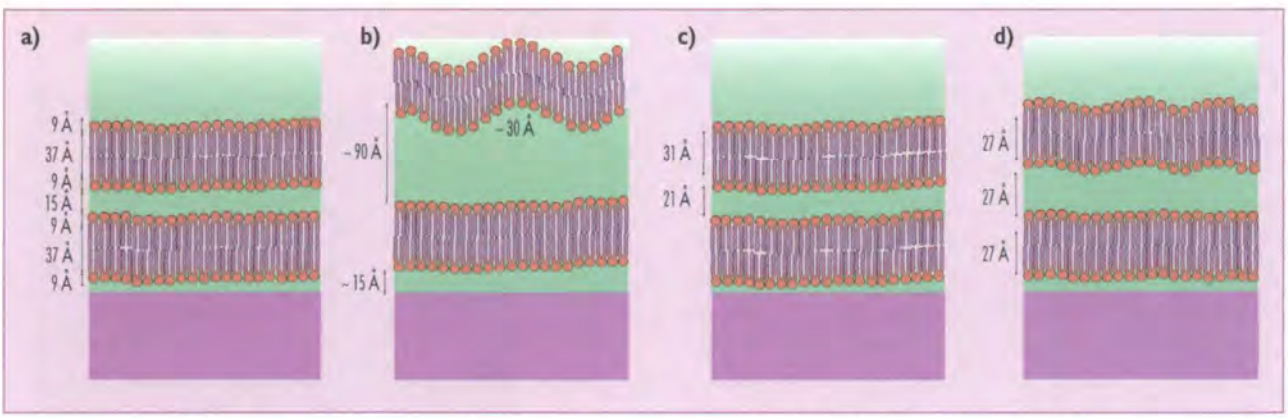

Figure 2: *Cartoons of a possible interpretation of models found to fit the data measured at* ***a)*** *25.4°C,* ***b)*** *51.5°C,* ***c)*** *55.4°C and* ***d)*** *64.1°C. For clarity, in* ***b), c)*** *and* ***d)*** *only the thickness parameters that change with respect to* ***a)*** *are indicated. Vertical dimensions are drawn to scale.*

References

■ [1] T. Charitat, E. Bellet-Almalric, G. Fragneto and F. Graner, Eur. Phys. J. B. 8 (1999) 583 ■ [2] G. Fragneto, T. Charitat, F. Graner, K. Mecke, L. Perino-Gallice and E.Bellet-Amalric, submitted to Europhysics Letters ■ [3] NIST Online Reference Databases (LIPIDAT) ■ [4] M. Born and E. Wolf. Principles of Optics (1989) Pergamon Press, Oxford ■ [5] W. Helfrich, Z. Naturforschung 33a (1978) 305.

Nonspecular neutron scattering from highly aligned lipid membranes

C. Münster, T. Salditt (Univ. München),
B. Bechinger (MPI Biochemie, Martinsried),
R. Siebrecht, V. Leiner (ILL and Univ. Bochum).

We report a neutron-scattering study of multilamellar membranes supported on solid silicon substrates. In contrast to previous work, the high degree of orientational alignment allows for a clear distinction between specular and nonspecular reflectivity contributions. In particular, we demonstrate that by using the specific advantages of neutron optics the nonspecular diffuse scattering can be mapped over a wide range of reciprocal space, which is usually not accessible by x-rays. In the neutron case, as is often argued, a lack of intensity severely limits the practicability of neutron diffuse studies, which are therefore rather scarce. Contrarily, we demonstrate in this study that several orders of magnitude in scattering signal and parallel momentum transfer can easily be recorded in multilamellar stacks of lipid membranes. This opens up the possibility to study fluctuations and lateral structure parameters of membranes on length scales between a few Å up to several µm.

Lipid bilayers are the basic building blocks of biological membranes [1]. A quantitative understanding of the elastic properties, the thermal fluctuations, and the interactions governing membrane self-assembly has significant impact on various research areas, including the biophysics of biological membranes, synthetic biomaterial engineering, and pharmaceutical applications. In this context, the interaction between lipid bilayers and antimicrobial peptides, such as magainin 2, is of particular interest, since the peptides exhibit a broad antibacterial, fungicidal and antitumor activities [2]. However, the structural motifs of the interaction are presently poorly understood. Therefore, we study fundamental aspects of structure, elasticity and fluctuations in model systems composed of neutral and charged phospholipids with and without membrane-active peptides such as magainin.

Neutron reflectivity offers unique possibilities to study the vertical density profile of lipid membranes on solid substrates with molecular resolution and is widely used for this purpose complementing x-ray techniques by means of contrast variation. Apart from contrast variation, a unique advantage of neutron diffuse scattering over x-rays results from the simple fact that most standard substrates are essentially transparent, such that the diffuse scattering can be measured continuously for positive and negative angles of incidence and scattering, see Fig. 1. Consequently, a much wider range of the parallel momentum transfer Q_{II} is accessible. Important information on the lateral membrane structure can

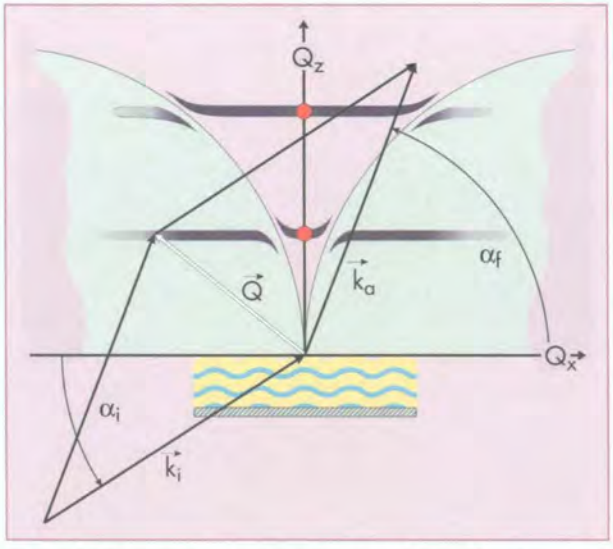

Figure 1: *The scattering experiment in reciprocal space. The schematics of the incident, the scattered beam and the scattering vector are sketched relative to the sample surface. The Laue region, which is not accessible in x-ray experiments, is shaded in gray.*

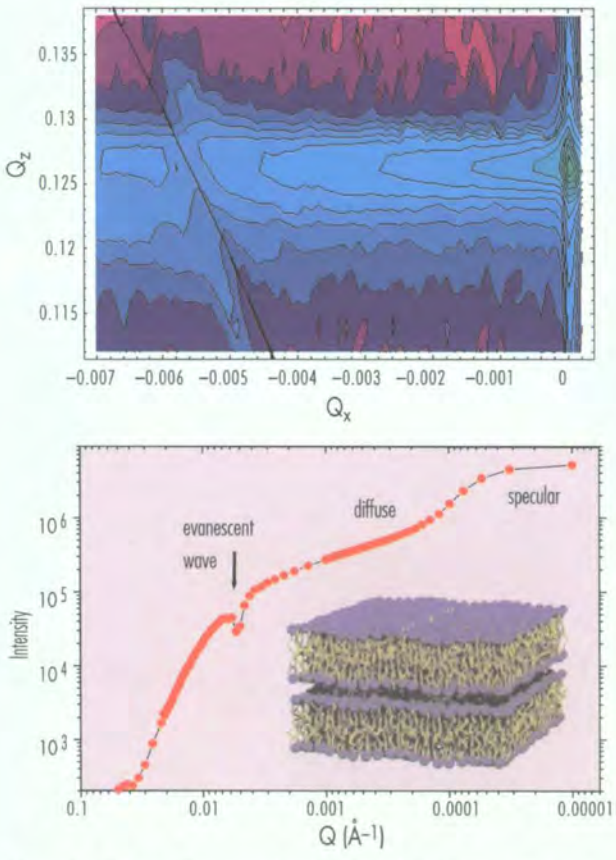

Figure 2: *Top: a one-dimensional cross-section of the diffuse scattering as a function of parallel momentum-transfer. Bottom: Reciprocal space mapping around the first Bragg peak of a stack of multilamellar phospholipid membranes (DMPC).*

be revealed, yielding new and previously inaccessible information on the membrane fluctuation spectrum, i.e. the height-height self- and cross-correlations.

For the experiments it is a prerequisite to prepare samples of several hundred bilayers oriented perfectly on a silicon substrate. The degree of membrane mosaicity achieved is typically better than 0.02°, compared to 1-5° in conventional measurements. These samples show a tremendous amount of diffuse intensity reflecting the softness of the system. For the investigation the samples were either partially hydrated (water layer of 10–15 Å in between membranes) and kept at constant temperature in a humidity cell or completely immersed under water in a chamber of full hydration, with the neutron beam impinging from the side of the silicon substrate [3].

The contour plot of a reciprocal space mapping around the first multilamellar Bragg peak is shown in Fig. 2 (lower part). The so-called diffuse Bragg sheet arises from layer fluctuations which are correlated over several adjacent layers (conformal fluctuations) such that the diffuse scattering is concentrated along ridges of constant Q_z corresponding to the specular Bragg peak positions. From the Q_z value, a mean distance *d* of the DMPC membranes of d = 49.8 Å can be inferred, corresponding to a water layer of about 14 Å in between adjacent membranes. Note that the mapping combines data taken in reflection and transmission geometry. The collapse of the intensity along the Laue sphere (black line) marks the loci in reciprocal space where the incident beam impinges at an angle of 0°, in the vicinity of which evanescent waves are excited. A one-dimensional transverse scan is also shown for comparison (Fig. 2, upper part). A lateral correlation length of ξ_{II} = 1000 Å is inferred from the crossover point around 0.006 $Å^{-1}$ between the two characteristic slopes. Note that the nonspecular scattering can be measured over an unprecedented range of up to four orders of magnitude in intensity and four orders of magnitude in parallel momentum-transfer. From this data, the membrane fluctuation spectrum can be determined and directly compared to theoretical models [4].

Upon the insertion of antibacterial peptides such as magainin 2, drastic changes in the specular and nonspecular reflectivity are observed at increasing peptide/lipid ratio (P/L). The first and second order peaks are shown in Fig. 3 (right) as a function of Q_z for increasing molar peptide concentration (P/L). Note that the data is clean enough to perform a line shape analysis of the Bragg peaks. Futhermore, the scattering-length density-profile can be modelled from the data and provides information on the configuration of the peptides with respect to the lipid bilayer [5].

In summary, the static structure-factor of solid supported membranes was measured as a function of the perpendicular and lateral momentum transfer, making use of the special advantages of neutron optics. From the data the fluctuation spectrum of the membrane system was determined [4]. The results may be put in perspective to the relevant microscopic interactions and also be compared to current theoretic predictions of membrane distortions by inclusions (peptides, proteins). In future, the method presented here to map out the reciprocal space over a wide range and with high resolution may be applied to many interesting lipid-membrane based materials, including lipid/peptide, lipid/protein or lipid/DNA systems. The technique can reveal lateral structures on length scales between a few Å up to several µm at *in situ* conditions.

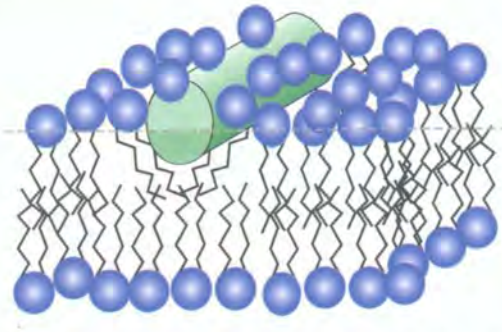

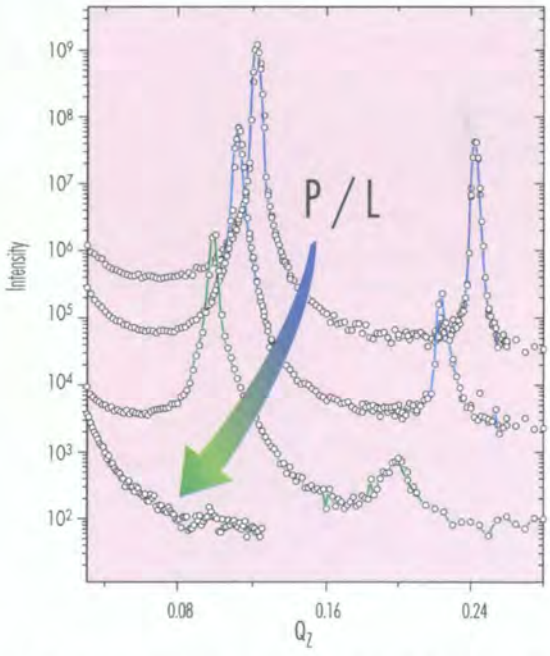

Figure 3: *Left: Sketch of a peptide (green) adsorbed on the lipid bilayer (blue). Right: Details of the reflectivity curves (1st and 2nd Bragg peaks of multilamellar DMPC) at increasing peptide concentration (from top to bottom: pure DMPC (P/L=0), P/L=0.025, 0.05, 0.1). The peptides affect the multilamellar order.*

References

■ [1] R. Lipowsky, E. Sackmann, Structure and Dynamics of Membranes, Handbook of Biological Physics, Vol 1, Amsterdam, North-Holland (1995) ■ [2] B. Bechinger, J.Membrane Biol. 156 (1997) 197 and references therein ■ [3] M. Vogel, C. Münster, W. Fenzl, T. Salditt, Phys. Rev. Lett. 84 (2000) 390 ■ [4] C. Münster, T. Salditt, M. Vogel, J. Peisl, Europhys. Lett. 46 (1999) 486 ■ [5] C. Münster, J. Lu, S. Schinzel, B. Bechinger, T. Salditt, Euro. Biophys. J. 28 (2000) 0683.

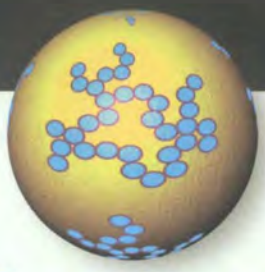

Investigation of confined polymer films

- P. Müller-Buschbaum (TU München),
- J.S. Gutmann, O. Wunnicke, M. Wolkenhauer (MPI Polymerforschung Mainz),
- R. Cubitt (ILL),
- M. Stamm (IPF Dresden),
- W. Petry (TU München).

Surface morphology of thin films is another probe of the method of grazing-incidence small-angle neutron scattering (GISANS). In case of homopolymer samples, GISANS yields the surface topology. In addition for blend samples the chemical composition is determined with GISANS. Compared to common transmission experiments GISANS enables the determination of very small sample volumes.

Polymer films are extensively used in many applications. With the ongoing miniaturisation of any type of application a reduction of the polymer-film thickness is required. In the limit of ultra-thin films the thickness is in the order of the polymer dimension. This induces a different conformation, morphology and kinetics. To determine these confinement effects, the film thickness of the polymer sample has to be small compared to the unperturbed radius of gyration of the polymer molecule (e.g. only 30 Å). In this film-thickness regime, a free-standing film is unstable. Thus, a preparation on top of a solid support is required. In a common transmission set-up the scattering volume of the confined polymer film is very small as compared to the one of the substrate. The scattering signal contains only a small contribution of the polymer film.

Therefore, a transmission geometry is extremely disadvantageous. One way to overcome this problem is the use of a reflection set-up as demonstrated previously with x-ray scattering techniques. With grazing-incidence small-angle scattering, a small scattering volume located near the sample surface is probed. In contrast to x-ray experiments this geometry is only rarely applied in neutron experiments. This may result from the limited fluxes available with neutrons compared to x-ray experiments.

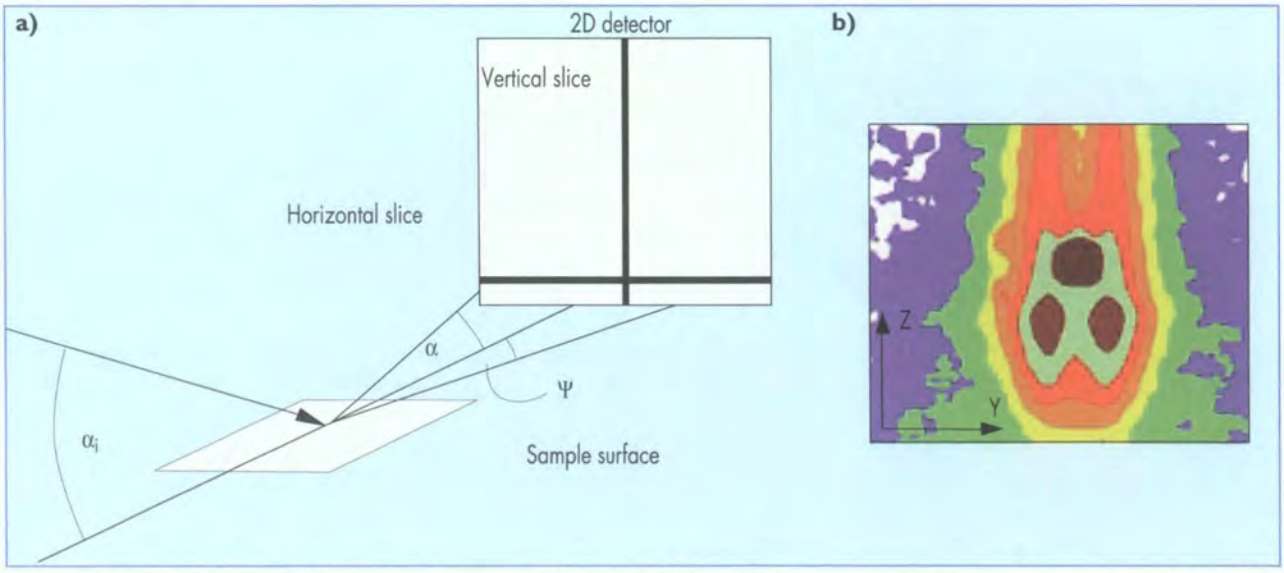

Figure 1: a) *Schematic drawing of the reflection set up performing GISANS at D22.* ***b)*** *Example of the two-dimensional intensity distribution measured with GISANS. In the contour plot a logarithmic contour line spacing with an alternating colour scheme is used.*

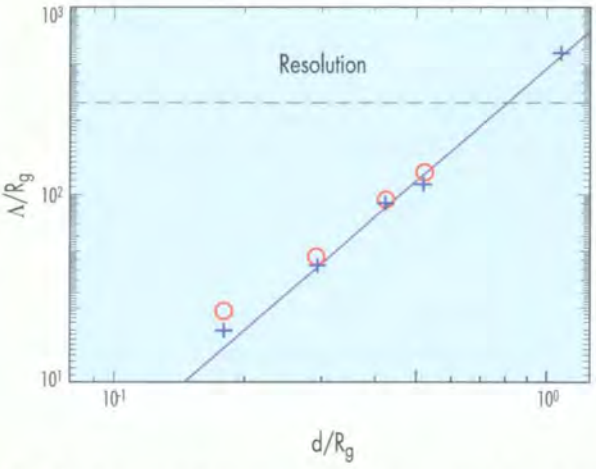

Figure 2: *Comparison of surface topographics determined with atomic force microscopy (+) and with GISANS (○). The mean droplet distance Λ and the originally prepared film thickness d are normalised by the radius of gyration R_g. The resolution of the scattering experiment is shown with the dashed line. The solid line shows a fit to the data based on a spinodal dewetting model.*

However, in the case of x-rays, the contrast, even for significantly different polymers is not large, whereas with neutrons strong contrast between two components can be generated by deuteration. This is extremely useful for investigations on blends of weakly incompatible polymers and is commonly applied in neutron reflectometry. The first successful experiments applying GISANS have been performed at the D22 instrument.

In general, the D22 instrument is used in transmission geometry. The scattering signal of interest is located near the beam stop which limits the largest resolvable length-scale. We applied a reflection geometry for GISANS. Thus, the signal of interest is reflected out-of-plane of incidence and geometrical constraints due to a beam stop are not present. This enables the detection of in-plane length-scales Λ up to 3.3 µm. It is a significant increase compared to the highest resolvable length-scale in transmission geometry under comparable conditions.

A schematic drawing of the experimental set-up is shown in Fig. 1a. At one fixed angle of incidence α_i the scattered intensity is detected at exit angles α_f and out-of-plane angles ψ. The two-dimensional intensity distribution consists of several vertical and horizontal slices. Figure 1b shows a typical two-dimensional scattering distribution. In the centre of the picture the specular peak is located. Horizontal slices contain information parallel to the sample surface. Vertical slices basically carry information perpendicular to the sample surface.

In the case of a dewetted confined homopolymer film the length Λ can be attributed to the mean distance between the droplets. During the dewetting of a originally homogeneous film isolated monodisperse droplets are created. Thus, the resulting sample is no longer continuous. With increasing film thickness, d, the mean droplet diameter and distance increases as well. In the past, the investigation of these small surface structures were only possible with atomic force microscopy. Thus, only locally very limited information has been available. Due to the progress in the GISANS technique it is now possible to determine heterogenieties on surfaces by scattering. In a scattering experiment, the mean droplet distance is determined on basis of a much larger surface area and therefore with a greater statistical significance. As demonstrated previously with atomic force microscopy and grazing incidence small-angle scattering, using x-rays as well as neutrons yields identical information in the case of dewetted confined homopolymer films [1].

In more complex systems such as confined blend samples, in addition to the dewetting, a phase separation is possible. In Fig. 2 the mean droplet distances as determined with GISANS (circles) and with atomic force microscopy (crosses) are similar for the complete range of confined films ($R_g/3 < d < R_g$). Thus the local technique atomic force microscopy and the averaging technique GISANS deliver the same topological information. The observed droplets are explained by a spinodal dewetting model (solid line in Fig. 2).

An internal contrast within single droplets is available with neutrons whereas with atomic force microscopy and x-ray scattering only the surface topology is detected. Using GISANS in addition to the topological signal, the internal chemical composition has been determined [2]. A periodic variation of different polymer phases can be induced by careful sample preparation and this internal structure has been observed with the GISANS technique [3].

Of course, the GISANS technique is not limited to polymer samples. The topology and chemical composition of any type of sample surface can be probed.

In addition, GISANS enables the investigation of non-homogeneous samples consisting of isolated structures. In-plane distances up to several micrometres are accessible. Due the need for a very high neutron flux, GISANS experiments are limited to a few neutron instruments such as D22.

References

■ [1] P. Müller-Buschbaum, J.S. Gutmann, M. Stamm, Phys. Chem. Chem. Phys. 1 (1999) 3857 ■ [2] P. Müller-Buschbaum, J.S. Gutmann, M. Stamm, R. Cubitt, Macromol.Symp., in press. ■ [3] P. Müller-Buschbaum, J.S. Gutmann, R. Cubitt, M. Stamm, Colloid Polym. Sci. 277 (1999) 1193.

Surfactant lamellar phase alignment under shear

S. Bare, A. R. Rennie (Kings College London),
E. Bellet-Amalric, G. Fragneto (ILL).

Shear has a profound influence on the behaviour of complex fluids due to their non-newtonian behaviour and neutron scattering is an important method for the characterisation of shear induced transformations. A new rotating disc shear-cell has been built and measurements on the wide-angle diffractometer D16 on concentrated surfactant solutions under shear have allowed to determine orientations not visible with the geometries used in the past on similar systems. A complete study will be useful for many applications where it is important to know how shear may effect phase behaviour such as micelle to lamellar phase transitions or induce formation of vesicles.

Amphiphilic molecules such as surfactants are used in many applications that range from emulsion stabilisers, detergents, cosmetics, food and mineral processing. Surfactants at high concentrations in water often form lamellar phases with bilayers packed together to give a regular interlayer spacing (Fig. 1). In some circumstances other concentrated phases (cubic, hexagonal, etc.) may form. The properties of concentrated phases of surfactants can be of importance in many areas: such as the formulation of concentrated detergents, properties of foods and behaviour of cosmetic preparations. Flow of soft materials has attracted considerable interest and the rheological properties of surfactants are no exception.

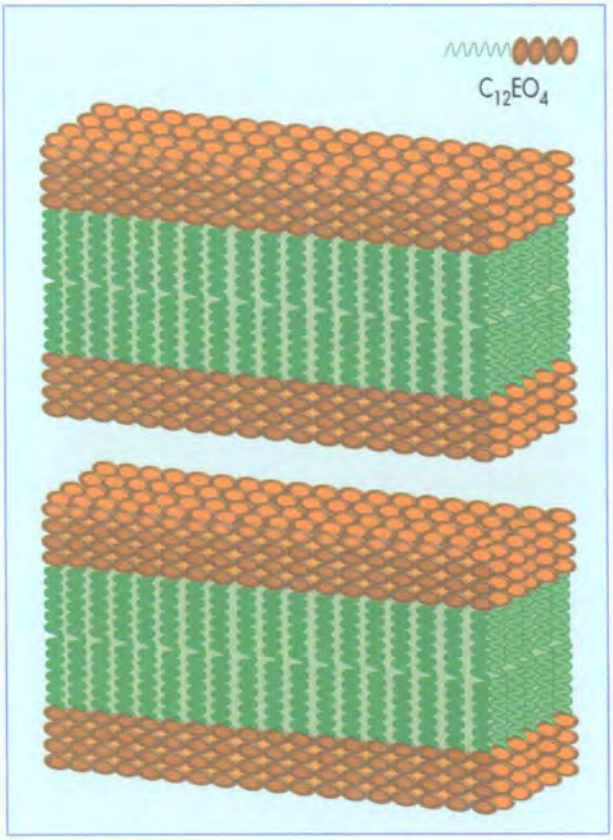

Figure 1: *Schematic diagram of lamellar phase structure of surfactants showing the inter-lamellar spacing used to determine the orientation.*

For some years small-angle neutron scattering (SANS) has been used to produce detailed pictures of structures under flow [1,2]. In the presence of shear field two different orientations of the lamellar layers have been observed, respectively with the normal to the layers parallel to the velocity gradient direction (orientation *c*) and perpendicular to it (orientation *a*). Orientational transitions have been observed depending on the shear rate and the system studied. In particular, Penfold et al. [1] observed a transition from orientation *a* at low shear rate to orientation *c* at high shear rate for the $C_{16}EO_6$ (hexaethylene glycol monohexadecyl ether)/water system. In a recent work Richtering at al. [2] observed the same transition for a system of SDS/decanol/water.
Additionally, they observed two more orientational transitions at very low and intermediate shear rates and the formation of vesicles. Both the transitions and the formation of vesicles were influenced by the content of decanol. Also in block copolymer melts, a transition from the *a* to the *c* alignment was observed, but there is no evidence of vesicle formation. Recently, neutron diffraction has been used to determine orientational order in dispersions of crystalline, anisotropic colloidal particles [3]. Measurement of the distribution of intensity of a particular Bragg reflection directly determines the orientation distribution of the plate-like particles. In many respects lamellar surfactant phases resemble the structure of dispersions of plate-like particles. The distribution of scattered intensity arising from the lamellar spacing can be used to determine the orientation distribution. The flexibility and dynamic equilibrium of lamellae can give rise to new and interesting phenomena.

The principal directions in a shear flow field are shown in Fig. 2 and a full description of the alignment will require determination of the full three-dimensional structure, or distribution of orientation, in relation to these axes. In order to achieve a better understanding of the flow behaviour of lamellae under shear, a rotating disc shear-cell has been built. This has been used on the diffractometer D16 to investigate the orientational alignment, using a sample geometry that is not readily accessible with a Couette shear cell and conven-

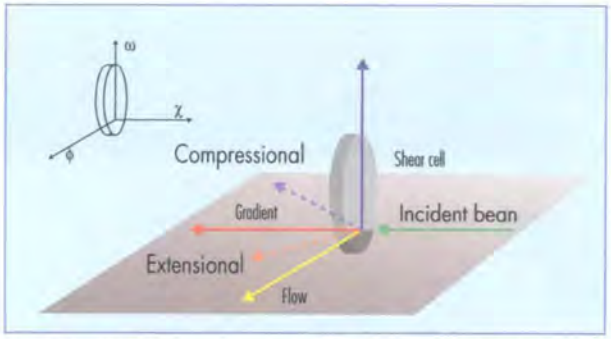

Figure 2: *Shear-cell orientation on the diffractometer. The principal axes of the shear field can be aligned with respect to the scattering vector to allow full determination of the orientation distribution. It is useful to identify not just the axes of flow, shear gradient and vorticity but also to distinguish in measurements between the extensional and compressional quadrants associated with the shear flow.*

tional SANS measurements. Data were collected for the non-ionic surfactant tetraoxyethylene glycol monododecyl ether ($C_{12}EO_4$) in D_2O, which has a wide range of lamellar phases at room temperature. The cell geometry allowed scans to determine the orientation distribution of the lamellar phases in the plane of shear velocity and shear gradient. With the cell normal to the incident beam the measured intensity corresponds to scattering from the lamellae with normals almost in the flow direction. As ω increases to 90° this angle approaches the condition of lamellae normal to gradient direction. Two concentrations corresponding to 40 and 60%wt surfactant were studied.

First results from these studies are shown in Fig. 3. Data were collected over a range of angles and corrected for detector efficiency, sample thickness and transmission. Spectra were acquired varying the angle ω from –75° to +75° (see Fig. 2) at different values of ϕ and χ (ranging between 0° and 24° for ϕ and 0° and 20° for χ). All experiments were repeated at different shear rates. A strong Bragg reflection at $Q \approx 0.1$ Å^{-1} for the 60% sample and at $Q \approx 0.07$ Å^{-1} for the 40% sample was observed. This corresponds to a d-spacing of 63 Å and 90 Å respectively corresponding to the distance between adjacent lamellar planes. Two less intense peaks were observed in the diffraction pattern of the 60% sample, at $Q \approx 0.075$ Å^{-1} (d = 82 Å) and at $Q \approx 0.2$ Å^{-1}. Peaks have been fitted with a Gaussian and their intensities have been normalised making allowance for the variation of the scattering volume, which depends on the cell orientation. The plot of the intensity of the Bragg reflection at $Q \approx 0.1$ Å^{-1} versus the rotation angle ω is shown in Fig. 3b. A maximum is observed for $\omega \approx 50°$. A similar pattern is observed at higher shear rates. The experimental arrangement allowed to investigate only small a range of ϕ and χ; small variations are observed in the peak intensities for experiment recorded after rotating the cell through ϕ and χ. For the less concentrated sample the plot of the intensity of the Bragg reflection at $Q \approx 0.07$ Å^{-1} versus the rotation angle ω showed a different pattern with a maximum corresponding to $0 < \omega < 20$ depending on the shear rate (Fig. 3a). These preliminary data clearly show alignment that changes with concentration and in directions that have not been reported previously. Suprisingly for the sample at 60%wt fraction, the maximum is seen well away from either the flow or gradient directions. The positive ω direction corresponds to the extensional quadrant that lies between the flow and gradient directions (see Fig. 2). The normals to the lamellae are seen to lie in this quadrant.

Under the flow conditions studied, orientation is observed in a rather different manner to that reported in previous work on concentrated surfactants. The lamellae are oriented with the normal to the plane in the flow gradient-plane and forming an angle with the vorticity-flow plane. The tilt depends both on the concentration of the surfactant and the applied shear rate. The orientation of the particles is only observable when scanning a large part of reciprocal space. The observed orientation of the layers with the peak in the compressional direction of the flow field shows certain similarities to the behaviour of plate-like colloidal particles [4]. Further work is required to determine the exact orientation of the layers as a function of surfactant concentration and shear rate.

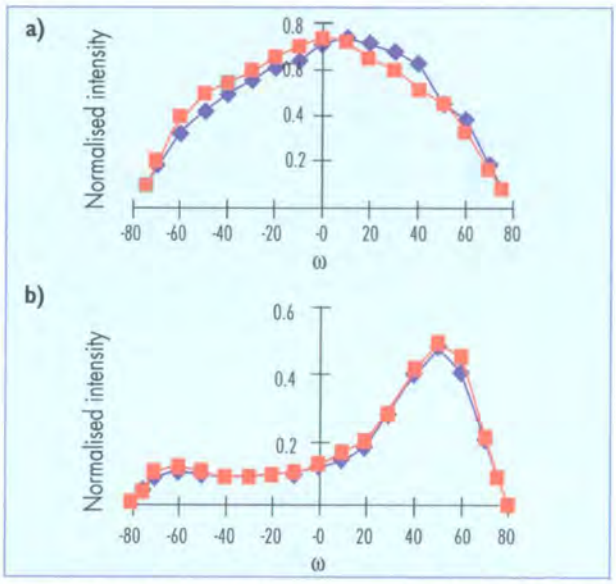

Figure 3: *Plots of the normalised intensity versus the angle ω for* ***a)*** *$C_{12}E_4$ at 40 wt% and* ***b)*** *60 wt% at two different shear rates (■ 0.5 s^{-1} and ◆30 s^{-1}). For the 60% sample the maximum is at ω = 50 for both shear rates, while for the 40% sample the maximum is at ω = 0 for 30 s^{-1} and at 10 < ω < 20 for 0.5 s^{-1}.*

References

■ [1] J. Penfold, E. Staples, A. Klan Lodhi and G. J. T. Tiddy, J. Phys. Chem B 101 (1997) 66 ■ [2] J. Zipfel, J. Berghausen, P. Lindner and W. Richtering, J. Phys. Chem B 103 (1999) 2841 ■ [3] S.M. Clarke, A.R. Rennie and P. Convert Europhysics Letters 35 (1996) 233 ■ [4] A.B.D. Brown 'Order in Concentrated Colloidal Dispersions of Anisotropic Particles Under Shear' Ph.D. Thesis, University of Cambridge (1998). A.B.D. Brown and A.R. Rennie, submitted to Phys. Rev. E.

Fast strain fluctuations in a polymer melt

W. Schmidt, U. Buchenau (FZ Jülich).

Can a quantitative connection be established between the low temperature anomalies of glasses and the fast picosecond motion in the melt? Very recent inelastic neutron scattering experiments on IN12 seem to show such a connection.

A reasonably successful description of the low-temperature glass anomalies is the soft potential model [1], an extension of the tunnelling model, which postulates a co-existence of localised tunnelling, relaxational and vibrational localised modes with the sound waves at low frequencies, below the boson peak at 2 meV. This peak may arise from scattering of the phonon modes of the whole Brillouin-zone due to disorder effects in these systems. The localised modes are supposed to interact bilinearly with elastic strains, in order to explain the strong sound absorption. In terms of that model, an extended strain field is expected around each of these localised modes, fluctuating with the mode amplitude.

A calculation of the coherent inelastic scattering from such a fluctuating strain field yields a weakly Q-dependent inelastic signal at small momentum transfer Q, as long as Q remains larger than the Brillouin scattering wave-vector at the given frequency [2]. If these localised modes exist not only at low temperatures, but also in the melt, one should be able to see this small-Q inelastic signal.

The measurements were carried out on the CRG-instrument IN12, a three-axis spectrometer for cold neutrons, with a sample of amorphous deuterated 1,4-polybutadiene at 288 K (the glass transition temperature is 186 K). For comparison, a protonated polybutadiene sample was also examined under the same conditions. Measurements on the empty sample container were used for background corrections.

The instrument was optimised for lowest background at low momentum transfer. In addition to 30'-collimation, we used a large vacuum tank (1 m in diameter) around the cryostat to suppress the air scattering of the direct beam which produces a strong inelastic signal at small angles. Its efficiency for the present problem is demonstrated in Fig.1 which compares the scans before and after evacuation of the tank. In general, this set-up can be considered as a competitive alternative to time-of-flight instruments for this kind of measurements.

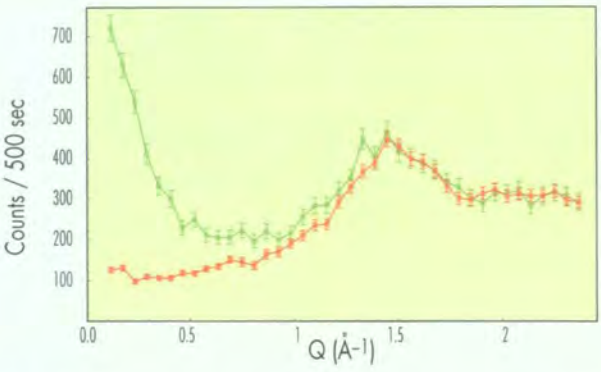

Figure 1: *Inelastic scattering on deuterated polybutadiene at 288 K and an energy transfer of 0.5 meV. The green curve shows the signal with surrounding air while the red curve demonstrates the drastic background reduction at low Q after evacuating the tank.*

The soft-potential model postulates modes with a stabilising fourth-order term in the potential, but with varying first and second order terms, eventually even negative ones, to account for the asymmetric double-well potentials of the tunnelling states. These modes are assumed to couple to the uniaxial and shear strains of the long-wavelength longitudinal and transverse sound-waves, respectively. So far, this is the only model capable to explain consistently the low-temperature glassy anomalies in the heat capacity, the thermal conductivity and the acoustic absorption [3].

If the soft-potential model is correct, there should be fluctuating strain fields around each of these localised modes. The simplest theoretical description of the strain field around a localised mode is to assume an elastic dipole in the centre of the mode, proportional to the mode displacement. The coherent inelastic small-angle scattering from such an elastic dipole, fluctuating or oscillating in an elastically isotropic medium, has been calculated recently [2]. This calculation assumes a homogeneous deformation within an inner sphere of radius r_s, continuity at the sphere boundary, and a decay

according to the elastic dipole field outside. Besides the radius r_s the model requires two further parameters: The squared ratio of the transversal and longitudinal sound velocity called f, and the dipole strength which is expressed in terms of a value Q_0 which also can be calculated from the soft potential model in the glass phase.

The main difficulty of the measurements is the multiple-scattering intensity from the strong inelastic scattering at higher Q. These processes produce a sizeable linear background at low Q of the same order of magnitude as the contribution we are looking for. Therefore the multiple-scattering calculations must be reliable. With this aim a protonated sample with the same scattering power was measured, too. For an incoherent scatterer the low Q inelastic signal should be absent, it should start with a Q^2 dependence. Indeed, the offset at low Q confirms the calculations (Fig. 2).

The data of the deuterated sample are shown in Fig. 3. For the fit we took into account that the data consist of a mixture of localised modes and sound waves. Both contributions must be considered. For the latter the structure factor is taken as $Q^2\, S_{el}(Q)$ where $S_{el}(Q)$ is obtained from the elastic data. The fit gives about 50% for that contribution. Further, the fit provides the three relevant parameters for the model of the localised modes which have been described above. The resulting values are $Q_0 = 0.48 \pm 0.04$ Å^{-1}, $r_s = 8.3 \pm 0.8$ Å and $f = 0.25 \pm 0.03$. From soft potential data [3], $Q_0 = 0.46$ Å^{-1} has been calculated. Also the radius r_s of the distorted sphere is a reasonable value in the order of the distance of neighbouring polymer chains. Further, the ratio of the sound velocities f is consistent with the value calculated from the sound velocities in the glass phase ($f = 0.21$). Figure 3 shows the data with the corresponding fit. The low Q contribution is indicated separately.

Inelastic neutron scattering data from deuterated amorphous polybutadiene show a clearly discernible inelastic coherent contribution at small momentum transfer well above the glass transition. The result is consistent with the existence of elastic dipoles in the polymer melt, fluctuating on a picosecond scale. Within experimental error the dipole strength (in terms of Q_0) from the high-temperature data equals the one expected from the soft-potential model parameters for the low-temperature anomalies. For the first time this provides a quantitative connection between the low temperature glass anomalies and the properties of the melt.

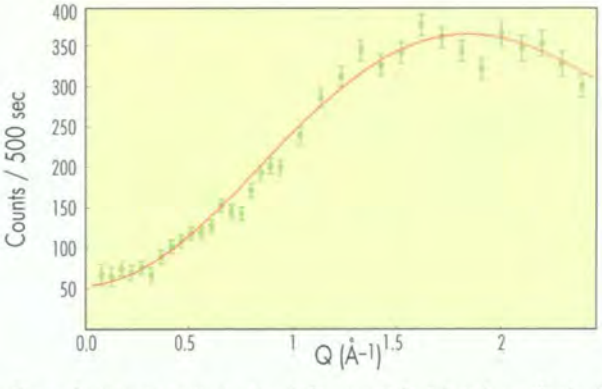

Figure 2: *Inelastic scattering signal of protonated polybutadiene after background correction at 0.5 meV. In contrast to the deuterated sample the data at low Q show the expected $Q^2 \cdot \exp(-\alpha Q^2)$ dependence plus a constant multiple scattering contribution. The solid line shows the corresponding fit.*

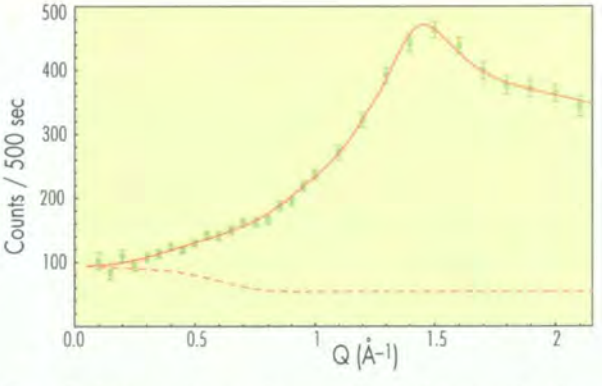

Figure 3: *Background corrected scattering signal of deuterated polybutadiene at 288 K with an energy transfer of 0.5 meV. The solid line shows the fit for the inelastic structure factor while the dashed line indicates the contribution of the localised modes as calculated in the model, plus again the constant multiple-scattering contribution.*

References

■ [1] D. A. Parshin, Phys. Solid State 36 (1994) 991 ■ [2] U. Buchenau, A. Wischnewski, M. Monkenbusch and W. Schmidt, Phil. Mag. B 79 (1999) 2021 ■ [3] M. A. Ramos and U. Buchenau, Phys. Rev. B 55 (1997) 5749.

A purely dynamical signature of the orientational glass transition

- M. Jiménez-Ruiz, A. Criado, F. J. Bermejo, C. Cabrillo (CSIC, Madrid),
- G. J. Cuello (ILL),
- F. R. Trouw, R. Fernández-Perea (Argonne National Laboratory),
- H. Lowen (Univ. Düsseldorf),
- H. E. Fischer (LURE, Orsay).

The dynamics of the freezing transition of the rotator phase crystal of ethanol into its orientational glass phase is monitored by measurements of molecular rotational components using quasielastic neutron scattering. The phenomena observed at microscopic scales are mapped onto those shown by a model of infinitely thin hard needles rotating around body-centred-cubic lattice positions. The basic signatures across the orientational glass transition are similar in the needle model and in the neutron scattering data for ethanol. As the model's glass transition is of purely dynamical origin, our findings support the idea that the glass transition is purely dynamical and not associated with any thermodynamic phase-transition [1].

Despite recent progress in understanding the nature of the liquid-glass transition, a clearer view is still needed. It can be viewed either as a purely dynamical phenomenon without any associated changes in static quantities or as a remnant of an underlying thermodynamic phase-change that is partially obscured due to kinetics reasons. Arguments in favour of both views are partially supported by experiment. The difficulties in evaluating the merits of both approaches concern the wide range of complex phenomena involved within the glass-transition of a real material, which tend to hide some of the characteristic signatures of glassy behaviour.

Here we concentrate our efforts in studying the rotational freezing transition of ethanol, Rotator Phase (RP) → Orientational Glass (OG), which takes place in the same range of temperatures that the Supercooled Liquid (SCL) → Glass (G) transition (see Fig. 1). The measured macroscopic phenomena associated with the RP → OG transition (jumps in specific heat and in the thermal expansion coefficient) are tantalisingly similar to those exhibited by the SCL → G transformation. Both RP and OG crystals have the same lattice structure (the molecular centres of mass sit in both phases at the nodes of a bcc lattice), which implies that the transition is purely rotational. The quantitative similiarity of the two transitions was revealed by dielectric spectroscopy [2], where α and sub-T_g relaxations appear to be very close in frequency. This suggests that if there is evidence that the RP → OG transition is purely dynamical, the same conclusion should then be pertinent for the canonical glass-transition (SCL → G).

We compare neutron-scattering data for ethanol across the transition RP → OG with result of a simple, albeit non-trivial, model [3] consisting of a set of hard-needles reorienting on a bcc lattice. This simple model exhibits a purely dynamical crossover from free needle rotation down to a "glassy" phase depending upon a sole control parameter: the ratio $\ell = L/a$ of needle length to lattice parameter (see Fig. 2). The transition is monitored by following the relaxational behaviour of $\Phi_1(t)$, a correlation function associated with single-needle reorientations. For $\ell \sim 3.4$ the autocorrelation is almost blocked on the timescale explored by the simulation. For $\ell = 4.5$ the orientational autocorrelation is almost equal to unity, i.e., the orientations become frozen within a very narrow solid angle.

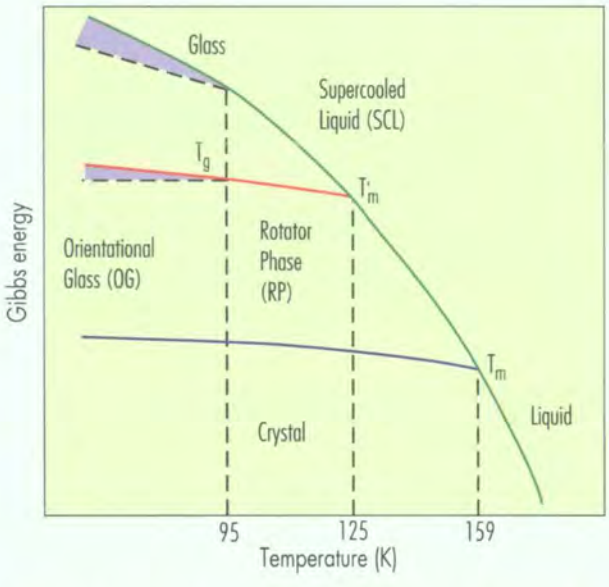

Figure 1: *Schematic phase diagram of ethanol where the transition temperatures of the condensed phases are shown. Depending upon temperatures and cooling rates, ethanol presents four different solid-state phases at ambient pressure: the stable monoclinic crystal, the structural glass obtained by quenching the liquid, the rotator phase RP (bcc crystal with rotational disorder, obtained after an annealing of the Supercooled Liquid), and finally the orientational glass (OG) obtained by cooling the RP.*

Two sets of neutron-scattering experiments were carried out. Exploration of the microscopic dynamics within a scale of about 1 meV was pursued using the inverted-geometry time-of-flight spectrometer QENS at the intense pulsed neutron source at Argonne, whereas that taking place at μeV scales was monitored using the IN16 backscattering spectrometer at ILL. The spectra show a strong elastic (resolution-limited) component plus a quasielastic intensity and the concomitant decrease of the elastic peak, as shown in Fig. 3. There it is shown that the transition is nicely monitored by following

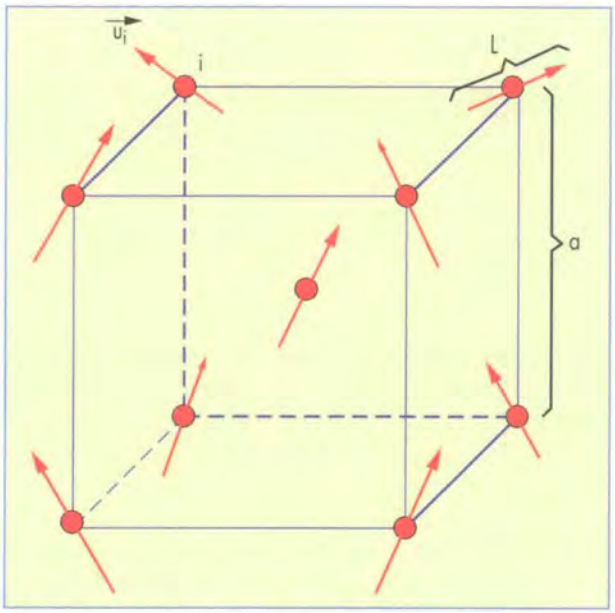

Figure 2: *Unit cell of the bcc lattice together with the needles of length L whose centre-of-mass positions are fixed to lattice sites.*

the transfer of spectral intensity from elastic to quasi- (or inelastic) scattering and this shows very similar characteristics for both frequency windows. The time scale of the needle model can be mapped directly into the physical space using the time $\tau = (mL^2/24k_BT)^{1/2}$. If we identify the moment of inertia of the needles, $J = mL^2/12$, with that of one ethanol molecule ($J = 0.741 \times 10^{-45}$ kg·m^2), we obtain that τ is of the order of 1 ps at T = 100 K.

Consequently, we can translate experimental frequencies into simulation data and vice versa. Finally, in the athermal needle model only ℓ enters, whereas temperature is the crucial parameter for our measurements. Hence, the translation of temperatures in the experiment into effective ratios ℓ of our model is given by $\ell = \ell_0 \exp(T_g/T^*)$.

The comparison between experiment and model results is carried out by transforming $\Phi_1(t)$ into the frequency domain and then convolving with the instrumental resolution functions in order to mimic the measurements. The resulting function $\Phi(\omega)$ was split into elastic and quasielastic parts. The width and the amplitude of the quasielastic part were determined afterwards. The results for the widths and the intensity fractions are given in Fig. 3. One clearly sees a kink in the quasielastic intensity both in the experimental data and in the transformed needle model data at temperatures of about 97 K and 75 K, respectively, which is a clear-cut fingerprint of the orientational glass-transition.

The elastic intensity exhibits a similar kink. The effective widths of the quasielastic spectra of both model and experiment (Fig. 3) also exhibit kinks at the same temperatures as do the intensities. This gives compelling evidence that the essential signatures of the orientational glass-transition can be understood from a purely dynamical model. The implications of such an analogy in dynamical behaviour can, in the light of previous data, to a large extent be applied to the glass/liquid transition inasmuch as the latter must carry a large rotational component.

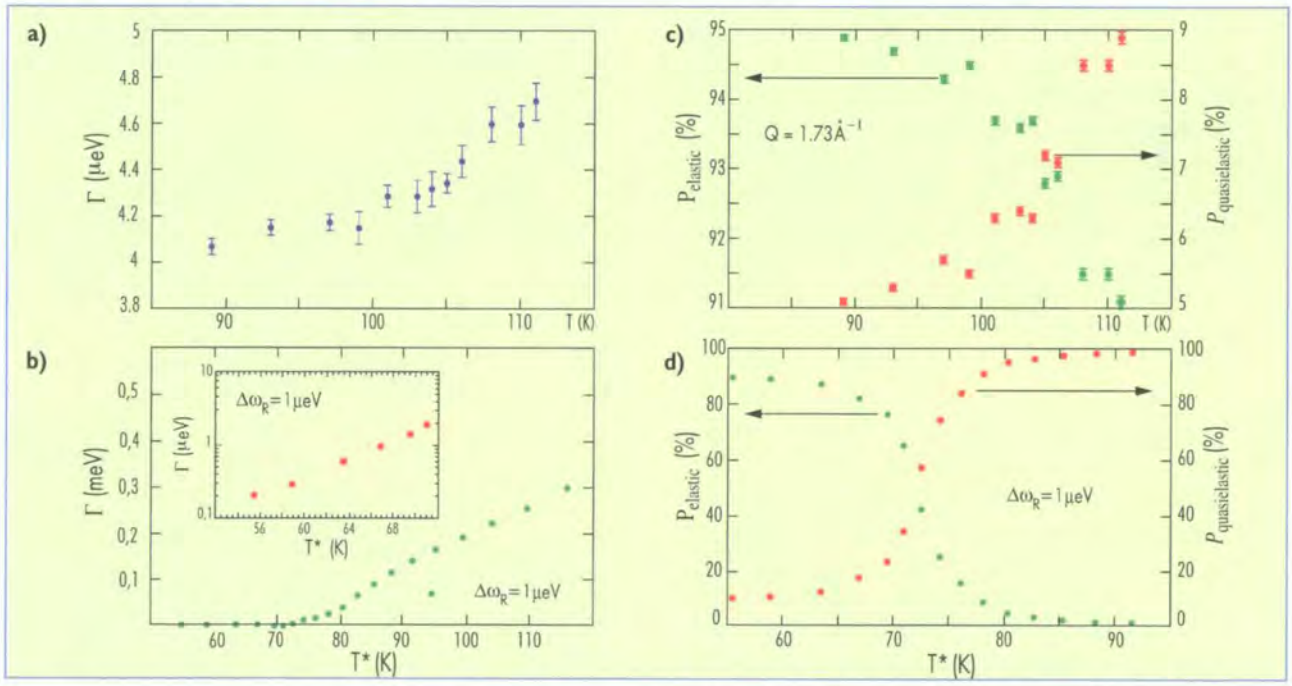

Figure 3: ***a)*** *Temperature dependence of the quasielastic linewidth as measured on IN16.* ***b)*** *Variation of the width of $\Phi(\omega)$ as calculated from results for the system of hard needles. The inset shows data in the μeV scale on a semi-logarithmic plot.* ***c)*** *Temperature dependence of the elastic (green) and quasielastic (red symbols) intensities across the RP-OG transition measured on IN16.* ***d)*** *Contributions from $\Phi(\omega)$ to the elastic (green) and quasielastic (red symbols) frequency windows versus the equivalent temperature T* for the resolution width $\Delta\omega_R$ = 1 μeV.*

References

[1] M. Jiménez-Ruiz et al., Phys. Rev. Lett. 83 (1999) 2757 ■ [2] M. Jiménez-Ruiz et al., Phys. Rev. B 59 (1999) 9155 ■ [3] C. Renner et al., Phys. Rev. E 52 (1995) 5091.

High-resolution Brillouin neutron scattering from heavy water

C. Petrillo, F. Sacchetti (INFM, Perugia),
B. Dorner (ILL),
J. B. Suck (TU Chemnitz).

The dynamics of water has been investigated previously by Brillouin scattering with neutrons and x-rays. Our new neutron data can explain the complexity of the inelastic signals by a simple model of two interacting modes, one acoustic-like and one optic-like. The different structure-factors allow for a detailed distinction of mode intensities.

Water is probably the most studied liquid and, nonetheless, there remain open questions due to its intrinsic complexity. The investigation of the dynamics of water is of basic interest because of its role for the existence and the behaviour of living systems. The dynamics of water has also attracted much attention because it is the prototype of a hydrogen-bonded network, where many of the complex features are connected to the presence of the medium-strength hydrogen-bonds. As the local structure of water is very close to that of its solid phase under normal conditions, i.e. hexagonal ice, it is quite reasonable to expect the dynamics of the liquid to develop in a way similar to that of the solid. In contrast to this anticipation, the sound velocity in water is found to be twice smaller than in ice.

A first investigation of the collective dynamics of (heavy) water by means of inelastic neutron scattering [1] has revealed an acoustic-like collective mode with an associated velocity of about 3000 m/s, to be compared with 1360 m/s, the measured sound velocity in heavy water. This rather striking effect is known as positive dispersion. The recently developed ultra-high resolution x-ray inelastic scattering technique [2-4] made it possible to perform Brillouin scattering in water over rather extended energy and momentum regions. The good energy-resolution achieved in x-ray inelastic scattering experiments (up to 1.5 meV), although limited by the quasi-Lorentzian shape of the resolution function, has confirmed the existence of the fast sound and, in addition, revealed dispersion-less signals around 5 meV [4].

The inelastic scattering function probed by x-rays originates from the electron density which, in water, is concentrated on the oxygen site. Therefore, the information obtained is limited to the motion of the oxygen atom. In contrast, in inelastic neutron scattering from heavy water the deuterium contributes equally well as oxygen and this favourable property of neutrons was the reason why we carried out experiments on the three-axis spectrometer IN1.

The experiment was performed with a rather high (constant analyser) energy of 120 meV. To push the resolution as much as possible, we used vertically focusing Cu(331) and Cu(400) as monochromator and analyser respectively. The collimation was squeezed to 25', 20', 20', 20' from reactor to detector. This set-up resulted in a resolution of 2.6 meV full-width half-maximum (FWHM), a value which is the top performance presently achievable on a three-axis spectrometer at such a high incoming neutron energy. Moreover, such a resolution is comparable with the best ultra-high resolution x-ray measurements which attain a FWHM of ~ 1.5 meV. However, it is not only the FWHM, which counts in resolution but also the line shape. Particularly, if one wants to distinguish signals at small energy-transfers, a Gaussian shape, as in the present case, has enormous advantages over a Lorentzian shape as in the x-ray case.

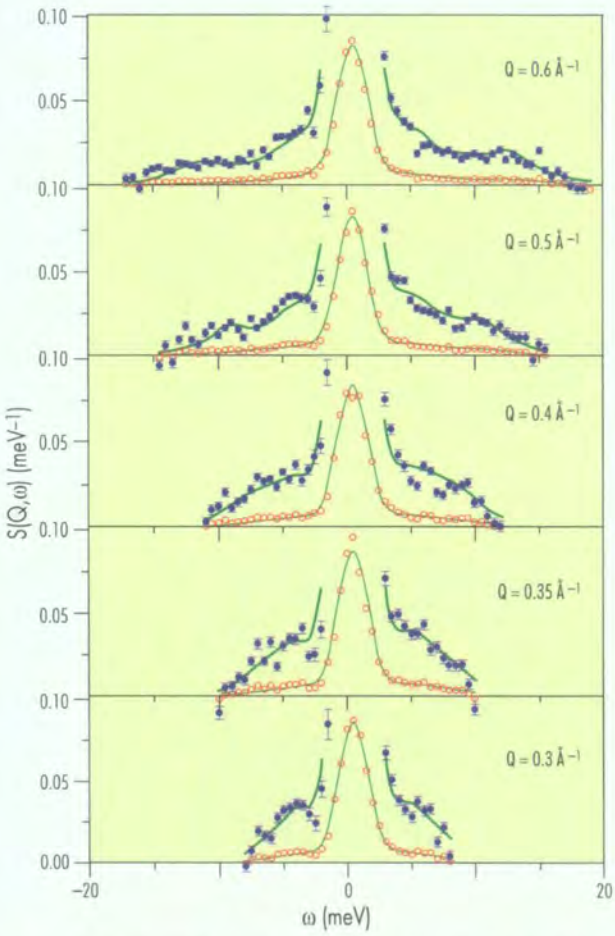

Figure 1: *Experimental dynamic structure-factor of heavy water versus energy transfer and at the wavevector transfer values of the measurements. The experimental data (○) are also shown on a scale expanded five times (●) to emphasise the inelastic structures. The full lines are the curves calculated according to the fitted model described in the text.*

At 293 K, constant Q-scans were carried out at five wavevector transfers Q. Figure 1 shows the coherent scattering-function S(Q,ω) as a function of energy and wavevector transfer. Details on the data reduction are given in Ref. [5]. Q-values smaller than 0.3 Å^{-1} were not investigated because of kinematical limitations in Q and ω transfers.

To interpret the present experimental data, we tried to develop a model requiring a limited number of parameters and also accounting for the observations in Refs. [1-4], i.e. the low macroscopic sound velocity at very small Qs, the high sound velocity at large Qs and the low energy signals around 5.5 meV at Q greater than 0.3 Å^{-1}. We assumed two interacting modes, one acoustic-like and one optic-like. Due to the interaction, the resulting dispersion curves do not cross, see Fig. 2. In the fitting procedure, the low Q sound velocity, which was out of the range of our data, was kept fixed to C_0 = 1360 m/s as taken from the literature. Then, the essential parameters of the model were ω_0 (5.5 ± 0.3 meV), the frequency of the optic-like mode, c_∞ (3200 ± 320 m/s), the sound velocity at high Qs, and a factor to account for the frequency-proportional broadening of the excitation. The values obtained by the fit are given in parenthesis. Note that, by keeping C_0 fixed, there was no additional free parameter to describe the mode coupling. It is important to remind that a low frequency optic mode has been observed in a single crystal of hexagonal ice [6]. The dispersion curves in Fig. 2 have been obtained by using all present neutron data of the different constant Q-scans for the fit. The open symbols in Fig. 2 indicate the frequencies determined by the fit. They coincide necessarily with the curves. We were very satisfied when we compared our result to the x-ray data [2-4] which are also shown in Fig. 2. The model fitted to the neutron data reproduces the x-ray data very well.

For the investigation of interacting (mixing) modes, the analysis of intensities is of high interest because the eigenvectors of the modes mix to produce two composite (still orthogonal) eigenvectors. We derived experimental values for structure factors, which are quantities independent of Q and ω but which reflect the eigenvectors. With increasing Q, the structure factor of the upper dispersion curve should vary from optic-like (vanishing value for Q towards zero) to acoustic-like, while the opposite should be the case for the lower dispersion curve varying from acoustic-like to optic-like. The optic structure-factor is expected to be smaller than the acoustic one. The results are shown in Fig. 3. At Q ≈ 0.35 Å^{-1} both structure factors have the same value indicating a maximum (50%–50%) of mixing of eigenvectors. Finally, the sum of both structure factors is constant within the error bars, as it should be. The sum must be independent of the interaction.

We analysed also one scan from the x-ray data using our model with our parameters. We observed that the structure factor of the optic mode relative to the acoustic mode was weaker in the x-ray case than in the neutron case. We take this as a hint that deuterium (hydrogen) amplitudes dominate the optic eigenvector.

Such a model for mode mixing is taken from solid-state physics, where modes and their interaction are well defined. The application to a liquid is an approximation which works well in the present case. The interpretation of the two sound velocities leads us to call c_∞ = 3200 ± 320 m/s the unperturbed sound velocity which, in fact, is close to the sound velocity in the solid with about 4000 m/s. The macroscopic sound velocity c_0 = 1360 m/s is, following the model, perturbed due to the coupling to a low frequency optic mode, which is supposed to be similar to the one observed in ice.

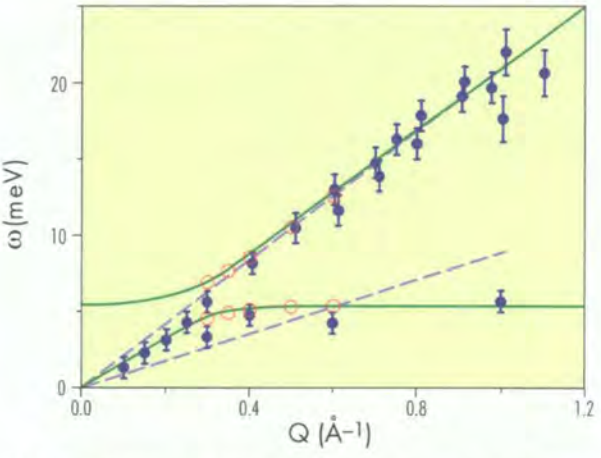

Figure 2: *Dispersion relation as deduced from the present experiment (full line) in comparison with the results of the x-ray scattering experiments reported in Refs. [2-4] (●). The open symbols (○) indicate the results from neutron scattering which lie on the calculated curves (see text). The dashed lines are reference linear dispersion curves corresponding to the velocities c_∞ and c_0.*

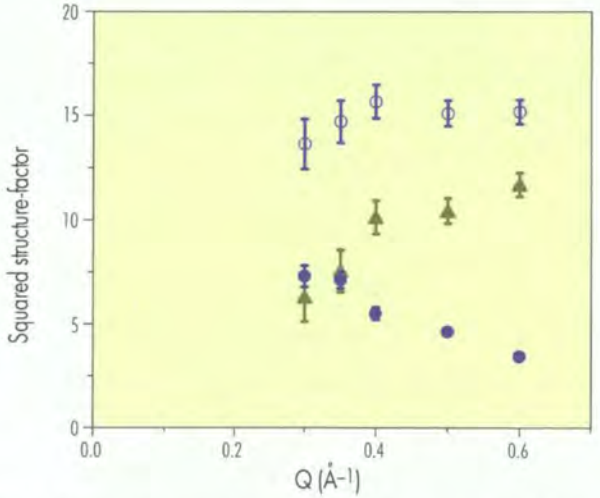

Figure 3: *Squared structure-factors provided by the present model versus wavevector transfer. Lower branch: ●. Upper branch: ▲. The sum of the two squared structure-factors is also shown by open circles (○).*

References

■ [1] J. Teixeira et al., Phys. Rev. Lett. 54 (1985) 2681 ■ [2] F. Sette et al., Phys. Rev. Lett. 75 (1995) 850 ■ [3] G. Ruocco et al., Nature 379 (1996) 521 ■ [4] F. Sette et al., Phys. Rev. Lett. 77 (1996) 83 ■ [5] C. Petrillo, F. Sacchetti, B. Dorner and J. B. Suck, unpublished ■ [6] B. Renker, Lattice Dynamics of Hexagonal Ice. (In Physics and Chemistry of Ice: edited by E. Whalley et al., Ottawa, Canada (1972) 82.

Liquid water at – 45°C, the effects of confinement

J. Dore (Univ. of Kent, Canterbury),
C. Haggenmüller (Univ. München),
P. Behrens (Univ. Hannover),
H. Fischer (LURE, Orsay).

Structural studies of water in ordered mesoporous MCM silicas have shown that the liquid phase remains stable to temperatures of – 45°C, below the normal phase transition to hexagonal ice. This deeply super-cooled liquid is characterised by a well developed hydrogen-bond connectivity and eventually undergoes a reversible phase transition to cubic, not hexagonal, ice.

Characteristics of bulk water

Water has a number of distinctive properties which distinguish it from other molecular liquids. Earlier neutron diffraction measurements have shown that the hydrogen-bonding interaction has a direct influence on the structural characteristics. At low temperatures, particularly in the super-cooled region, the orientational correlations are enhanced [1] and the system seems to be evolving towards the continuous random network which characterises the structure of low-density amorphous ice [2], made by vapour deposition onto a cold substrate plate at < 100 K. At ambient pressures there appears to be a limit, the homogenous nucleation temperature, to the stability of the super-cooled phase which is –45°C for H_2O and –40°C for D_2O. Special techniques using water droplets in emulsions have been developed to study deeply super-cooled D_2O water over a temperature regime extending down to –30°C. The main diffraction peak, $Q_0(T)$, changes systematically to lower values [3] as shown in Fig. 1; the corresponding density change is given in the inset. The nature of the eventual transition to the ice phase remains controversial and several different theories have been advanced. The situation is puzzling because the glass-transition temperature and the upper limit to the stability of bulk amorphous ice are at much lower temperatures, in the region of 140 K.

Water/ice in mesoporous sol-gel silicas

The properties of water are substantially modified when the liquid is contained in the voids of a mesoporous solid. Neutron diffraction studies [4] of water in sol-gel silicas have shown that the water readily super-cools between –15 and –25°C (depending on the pore size) and subsequently nucleates to produce cubic ice rather than the hexagonal ice formed in the bulk phase. The super-cooled liquid phase shows enhanced hydrogen-bonding over bulk water at the same temperature indicating that the confinement has a direct effect on the hydrogen-bond structure and the nucleation process. Unfortunately, sol-gel derived silicas have rather broad pore-sized distributions and a poorly defined pore topology.

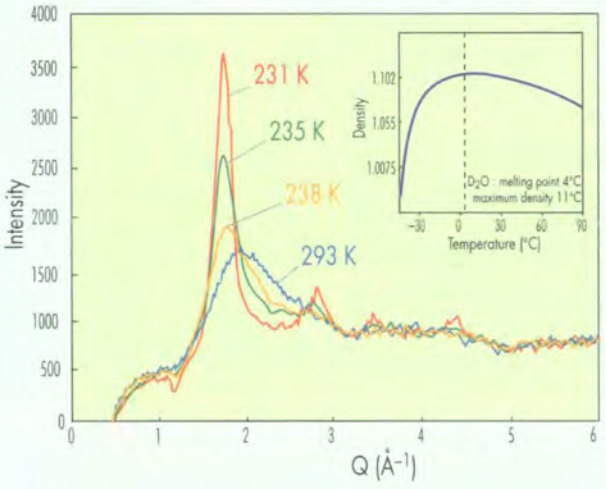

Figure 1: *The diffraction patterns for D_2O water in MCM silica showing the deep super-cooling and transition to cubic ice.*

Water and ice nucleation in M41S silicas

Only recently, a new form of ordered mesoporous silica has become available. It has a well defined geometrical structure based on a regular array of cylindrical pores with narrow pore-size distributions and diameters typically in the range 25-35 Å. The MCM silicas [5] have different geometries categorised as M41S (hexagonal) and M48S (cubic) and are shown schematically in Fig. 2. These new silicas provide a superb means of extending the investigation of water in confined geometries and have produced some remarkable and unexpected results.

Neutron diffraction measurements [6] indicated that the water confined in MCM silicas super-cooled to even lower temperatures, down to – 45°C, before nucleation, as shown in the variable temperature plot of Fig. 1. Furthermore, the liquid phase could be re-gained by re-heating the sample to just above the nucleation point and showed no hysteresis. This behaviour is totally different to that observed in the previous studies and represents a reversible phase transition between two states that are both metastable with respect to the bulk phase! The MCM silicas therefore provide a suitable system for the production of liquid water at temperatures

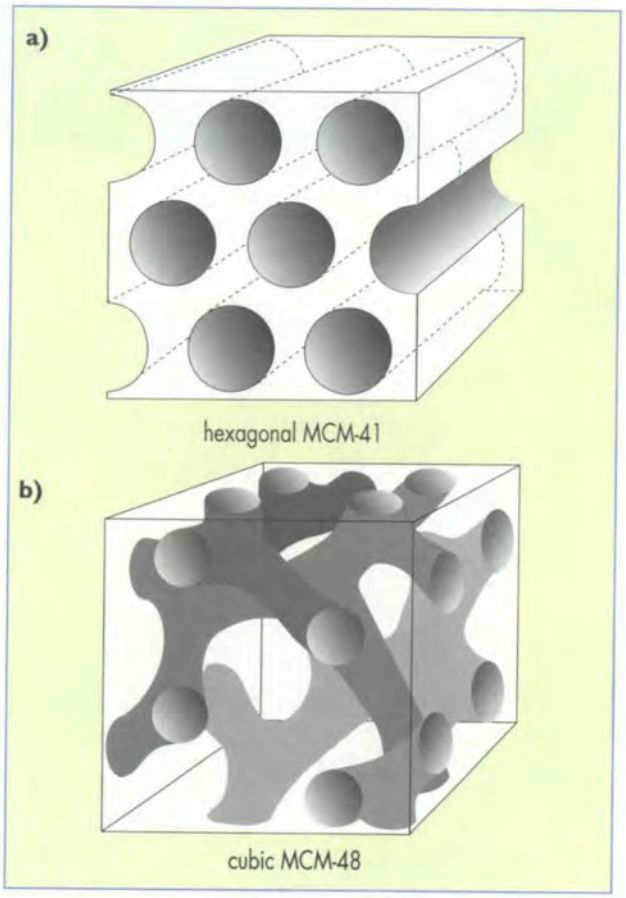

Figure 2: *The geometry of mesoporous MCM silicas:* ***a)*** *hexagonal,* ***b)*** *cubic.*

well below those normally available and open up new possibilities for studying liquid water under extreme low temperature conditions.

Characteristics of confined water

The reasons for this unusual behaviour are thought to depend on the interaction of the water molecules with the surrounding pore walls which have a low density of surface silanol groups. The largely hydrophobic surface causes an effective isolation of the water volume from the surrounding solid matrix. The hydrogen-bond connectivity is expected to be well developed with a disordered tetrahedral geometry such that the structure could be more accurately described as a gel network than a molecular liquid, as shown schematically in Fig. 3.

Clearly, it will be interesting to study other characteristics, such as the dynamics, of this 'strange' form of liquid water. This investigation also has implications for the properties of water at other more complex interfaces, particularly in a biosciences context.

Water has a relatively simple molecular conformation involving just three atoms but the complexities of its collective behaviour remain a major challenge for current scientific understanding.

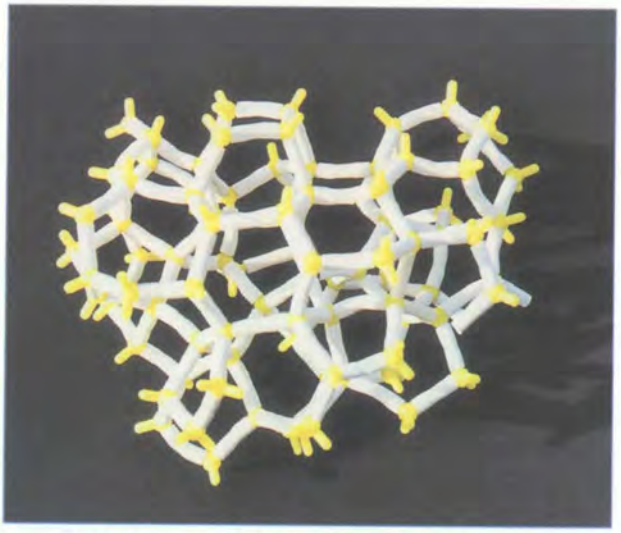

Figure 3: *A schematic model of low-temperature water based on the structure of low-density amorphous ice.*

References

■ [1] D.C. Steytler, J.C. Dore and C.J. Wright, Mol. Phys. 48 (1983) 1031 ■ [2] M.R. Chowdhury, J.C. Dore and J.T. Wenzel, J. Non. Cryst. Solids 53 (1984) 247, J.C. Dore and D.M. Blakey, J. Mol. Liq. 65 (1995) 85 ■ [3] M.C. Bellissent-Funel, J. Teixeira, L. Bosio, J.C. Dore,and P. Chieux, Europhys Letts. 2 (1986) 241 ■ [4] J.M. Baker, J.C. Dore and P. Behrens, J. Phys. Chem. B101 (1997) 6226 ■ [5] P. Behrens and G.D. Stucky, Angew. Chem. Int. Ed. Engl. 32 (1993) 696 ■ [6] J.C. Dore, P. Behrens, C. Haggenmüller and H.E. Fischer, submitted to Phys. Chem. Chem. Phys.

Proliferation of ice XII in water's phase diagram

M. M. Koza, A. Tölle, F. Fujara (Univ. Dortmund),
H. Schober, T. Hansen (ILL).

Water possesses a large number of crystalline phases. The latest phase which has been discovered is ice XII. Originally produced within a narrow band of pressure and temperature ice XII turns out to be a rather prolific form of water. It competes successfully with other crystalline and amorphous phases along production routes at low temperature and high pressure.

Although, water has been the object of extensive experimental and theoretical investigation it still rewards us with new and unexpected properties. This has been demonstrated recently by the discovery of polyamorphism [1], i.e. the existence of two different amorphous phases of water, and by the identification of a twelfth crystalline ice-phase (ice XII) [2]. Having been observed in different regions of water's phase diagram the two phenomena were originally thought to be disconnected.

Ice XII is produced at about 0.55 GPa and 260 K. It provides the first example of a four-connected network which is built up by seven- and eight-membered rings [3]. These rings are arranged such that they lead to the densest crystalline water-phase known so far which does not show hydrogen bond interpenetration.

Polyamorphism is experimentally confined to much lower temperatures. At T below 150 K common crystalline hexagonal ice I_h can be compressed into a high-density amorphous state (HDA) by the application of pressure exceeding 1 GPa. HDA can be recovered at ambient pressure below 80 K. Upon heating HDA transforms into a low-density amorphous phase (LDA). While the microscopic structure of HDA is still a matter of speculation there are strong experimental indications that LDA consists of a random network of fully connected water tetrahedra. LDA can be maintained at ambient pressure up to T = 140 K before it crystallises into a cubic phase I_c of nearly equal density.

In the past, HDA has often been found to be contaminated by crystalline phases. As these phases could not be properly indexed in a diffraction experiment, they were given only little attention. Our recent study, performed on the instruments

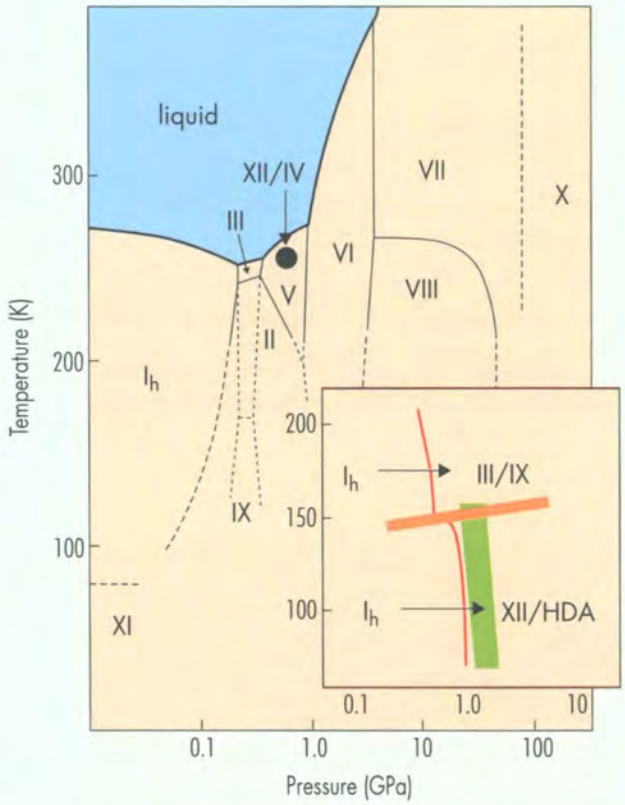

Figure 1: *The phase diagram of water. ● represents the region in which ice XII has been observed by Lobban et al. (T = 260 K, p = 0.55 GPa) [2]. Please note that this region is fully surrounded by the stability range of ice V. The inset sketches the pressure induced transition line of I_h (red line) as studied by O. Mishima [1]. The green area indicates the region in which ice XII is successfully formed. Horizontal arrows indicate that I_h transforms by compression below 150 K to ice XII or high-density amorphous state (HDA) and above 150 K to ice III/IX. The orange area displays the 150 K boundary studied by O. Mishima for HDA which is equally observed for ice XII.*

D20 and D2B at ILL, reveals that all contaminations correspond to the recently detected ice XII modification [4,5]. This implies that ice XII forms under identical thermodynamic conditions as HDA, i.e. at temperatures T below 150 K and at pressures p above 1 GPa. By properly choosing the compression rate it is possible to favour the production of either ice XII or HDA. Under rapid compression the formation of ice XII dominates, whereby compression rates exceeding 1 GPa/min lead to pure bulk ice XII samples.

When increasing the temperature beyond 77 K, the formation of ice XII does not only compete with HDA but also with other crystalline phases. Above 150 K no ice XII formation has been observed in our experiments [5]. Ice XII, therefore, is rather prolific in water's phase diagram existing in at least two topologically unconnected regions. The study of the formation of ice I_h to ice XII contributes valuable clues to the understanding of water amorphisation under pressure. Crystallisation implies a reorganisation of water's hydrogen bond network and not merely its deformation. The latter is sufficient for amorphisation. A molecular reorganisation requires a high molecular mobility as provided by a thermodynamic mechanical instability or a melting process. The instability or melting may be followed either by recrystallisation or amorphisation. Moreover, since the structure of ice XII has been established as the first example of a non-self-clathrating network built up by seven- and eight-membered rings of water molecules it may help us to deduce some structural characteristics for HDA. It may even be possible to model the structure of HDA by putting disorder into the molecular network of ice XII. This process has been successfully performed on the I_h network leading to a model structure for LDA.

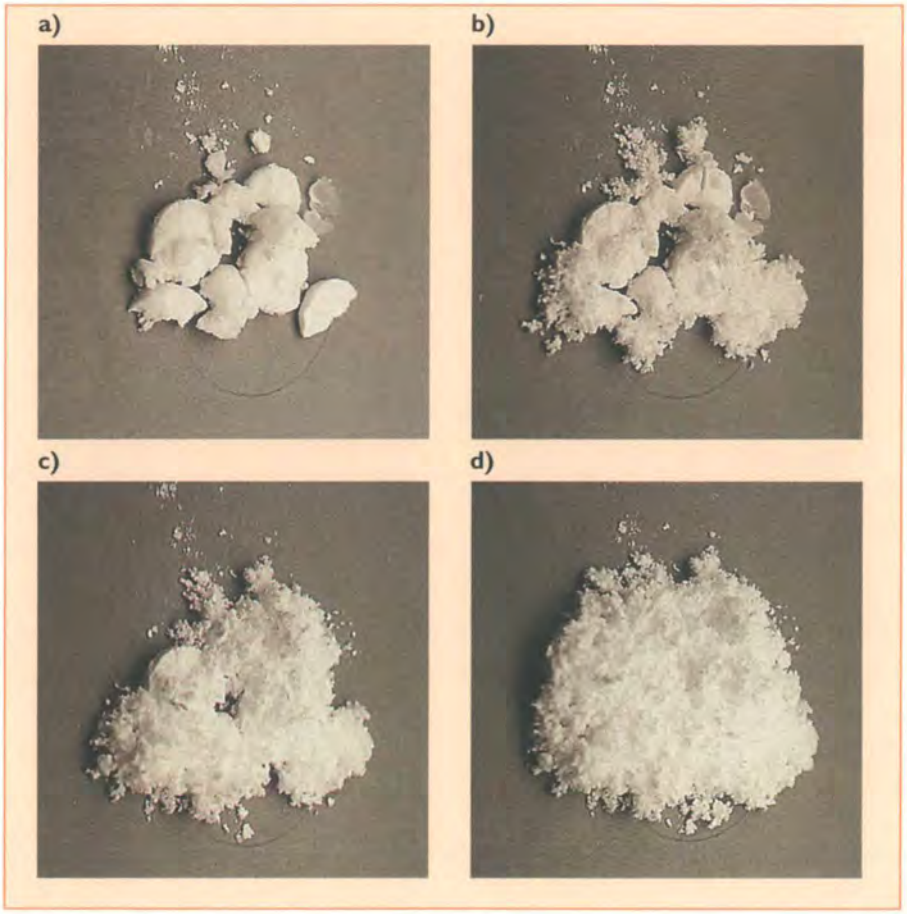

Figure 2: *Transition of ice XII towards hexagonal ice upon heating. The upper left photograph a) shows ice XII as recovered from the pressure cell at low temperature. In contrast to high-density amorphous ice it has a milky appearance. The following photographs show the floking of ice XII as it transforms to the lower density forms cubic ice and hexagonal ice (b-d).*

References

■ [1] O. Mishima, Nature 384 (1996) 546 ■ [2] C. Lobban, J. L. Finney and W. F. Kuhs, Nature 391 (1998) 268 ■ [3] M. O'Keeffe, Nature 392 (1998) 879 ■ [4] M. Koza, H. Schober, A. Tölle, F. Fujara, and T. Hansen, Nature 397 (1999) 660 ■ [5] M. Koza, H. Schober, T. Hansen, A. Tolle and F. Fujara, PRL, in print.

Observation of nitrogen insertion in $NdFe_{11}Ti$

PH. OLEINEK, K.-H. MÜLLER, L. SCHULTZ (INSTITUT FÜR METALLISCHE WERKSTOFFE, IFW DRESDEN),
O. ISNARD (LAB. CRISTALLOGRAPHIE CNRS, GRENOBLE),
P. CONVERT (ILL),
M. LOEWENHAUPT (INST. F. ANGEWANDTE PHYSIK, TU DRESDEN).

Recently discovered new hard magnetic materials are made of rare-earth element and transition-metal intermetallics whose properties are optimised by insertion of light element within the crystal structure (H, C, N). These elements are inserted in the interstices of the crystal structure. The understanding of the gas-solid reaction process is crucial for achieving new hard magnetic material with optimum magnetic properties. High intensity kinetic neutron diffraction, such as that available by the D20 diffractometer, has been used to investigate *in situ* the reaction of the $NdFe_{11}Ti$ with nitrogen gas. The location of N atoms is determined unambiguously, the gas-solid reaction characterised and the stability domain of the new $NdFe_{11}TiN$ type phase has been revealed.

The study of the physical properties of the rare-earth (R) transition-metal intermetallic (T) compounds is a major field of research in solid-state physics. Some of these compounds are industrially used such as $SmCo_5$ or the $Nd_2Fe_{14}B$ phases which are produced for permanent magnet purposes. The requirements for such applications are good intrinsic magnetic properties, i.e. high Curie temperature, magnetisation and anisotropy field combined with a suitable microstructure generating a high coercivity. To fulfil these requirements, research has turned towards alloys composed mainly of the ferromagnetic 3d elements, iron or cobalt, thus leading to high magnetisation and Curie temperature: their association with rare-earth elements may induce strong uniaxial anisotropy. Since the discovery of $Nd_2Fe_{14}B$ in 1983, many studies have been devoted to iron-containing materials leading to new series of intermetallic compounds such as $R(FeT)_{12}$ which crystallise in the $ThMn_{12}$ structure type (space group I4/mmm).

More recently, it was reported that R_2Fe_{17} compounds can be interstitially modified with N atoms by means of a heat treatment in ammonia [1,2]. Gas-solid reaction has become a new method for producing interstitially modified R-T compounds with C or N atoms. New high-performance hard-magnetic materials have been obtained such as $Sm_2Fe_{17}N_3$ and $Sm_2Fe_{17}C_3$ which are the most promising in terms of possible permanent magnet applications [3]. This technique was transferred to $R(Fe,T)_{12}$ compounds soon after [4]. Among the $R(Fe,T)_{12}$ compounds, R = Nd and T = Ti, V or Mo showed the best magnetic properties after absorption of N atoms [5,6]. Significant improvement of the magnetic features of the $NdFe_{11}Ti$ phases can be achieved by insertion of nitrogen atoms. An increase of the saturation magnetisation is observed as well as a spectacular increase of the Curie temperature which goes from 547 K in $NdFe_{11}Ti$ to 740 K in $NdFe_{11}TiN$. The saturation magnetisation increases from 16.8 μ_B per formula unit in $NdFe_{11}Ti$ to 19.2 μ_B in $NdFe_{11}TiN$.

The Nd sublattice contribution to the magnetocrystalline anisotropy changes of sign upon N insertion in the $RFe_{12-x}M_x$ structure. Finally, whereas the magnetisation of $NdFe_{11}Ti$ is not aligned along the c-axis of the structure, the $NdFe_{11}TiN$ phase exhibits a strong uniaxial anisotropy field of about 8 T. The control of the gas-solid reaction process is crucial in order to obtain materials with optimum magnetic properties.

The *in situ* neutron diffraction was carried out on the high-flux two-axis diffractometer D20, using a position-sensitive ^3He microstrip gas-detector covering an angular range

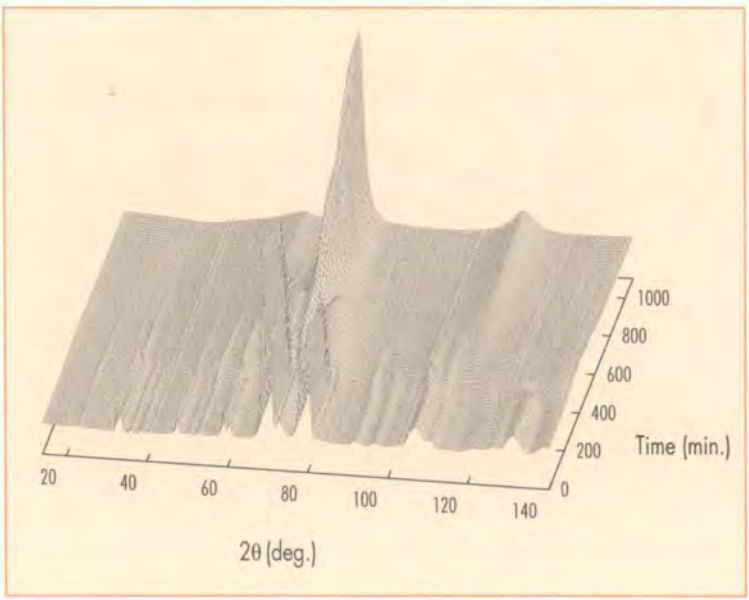

Figure 1: *Neutron thermodiffractogram of the reaction of $NdFe_{11}Ti$ with nitrogen gas at ambient pressure. The final phase is α-Fe plus an amorphous phase containing Nd, N and probably some Fe.*

of 160°. The N_2-gas pressure was kept constant at ambient pressure during the measurements so that the pressure at the sample was constant throughout the whole measurement. The nitrogenation and nitrogen disproportionation behaviour of $NdFe_{11}Ti$ was investigated by in situ neutron powder diffraction at temperatures between 100°C and 800°C. The neutron diffraction diagram recorded at each step is given in Fig. 1.

The nitrogen content and lattice parameters were measured as a function of temperature and time. The amount of interstitial nitrogen atoms is estimated to be 0.7 atoms per formula unit. Anisotropic cell expansion occurs upon N insertion. The lattice parameters a and c increase by 0.8% and 2% respectively, leading to a relative cell-volume increase $\Delta V/V$ of about 3.7%.

The interstitial modification starts at a temperature of 360°C and is complete at 440°C. A decrease of the Bragg intensities and an increase of the background occurs simultaneously to the peak shift, which means that interstitial modification and decomposition reactions overlap. The experiment demonstrates that in $NdFe_{11}Ti$ the shift of the Bragg peaks due to the insertion of N atoms continues until a temperature of 440°C is reached. The nitrogen atoms are located in the rare earth neighbourhood in a pseudo-octahedral site 2b drawn in Fig. 2.

These sites are surrounded by two rare-earth and two iron atoms. After 5 hours at 450°C the decomposition reaction is finished. Figures 1 and 3 clearly evidence that the product of the nitrogen disproportionation is a mixture of α–Fe an amorphous phase, which is stable up to temperatures of 800°C.

Incomplete interstitial modification may result in an inhomogeneous distribution of the N atoms within the crystal lattice, causing inhomogeneous magnetic properties. Excessive nitrogenation for too long times or at too high temperatures may lead to the destruction of the crystal structure and, in consequence, of the hard magnetic properties [7]. We found that the N atoms fills only the 2b sites in the $R(Fe,T)_{12}$ structure and no other interstitial sites are significantly occupied. This means that the decomposition reaction is not dependent on the occupation of other interstitial sites.

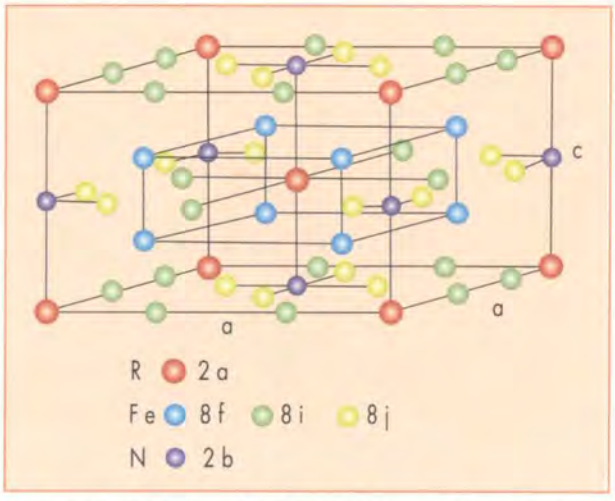

Figure 2: *Crystal structure of the $NdFe_{11}TiN$ phase. The Ti atoms are partly filling the Fe 8i site.*

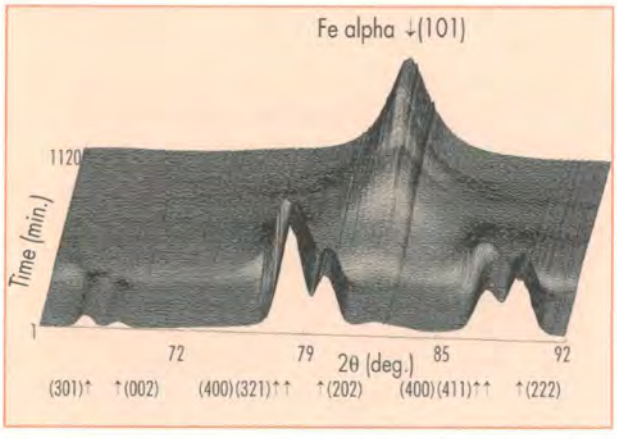

Figure 3: *Details of the neutron diffraction pattern evidencing the peak shift induced by the insertion of N atoms within the crystal structure and the appearance of α-iron Bragg reflection due to the decomposition of the $NdFe_{11}TiN$ phase.*

References

■ [1] J.M.D. Coey and Hong Sun, J. Magn. Mater 87 (1990) L 251 ■ [2] K.H.J. Buschow et al., J. Magn. Magn. Mater. 92 (1990) L35 ■ [4] O. Isnard, S. Miraglia, M. Guillot and D. Fruchart, J. Appl. Phys. 75 (1994) 5988 ■ [3] Y.Z. Wang and G.C. Hadjipanayis, J. Appl. Phys. 70 (1991) 6009 ■ [5] Y.Z. Wang et al., J. Magn. Magn. Mater. 104-107 (1992) 1132 ■ [6] J.M.D. Coey, Hong Sun and D.P.F. Hurley, J. Magn. Magn. Mater. 101 (1991) 301 ■ [7] Ph. Oleinek et al., Mat. Lett. 35 (1998) 126.

Structure and dynamics of single-wall carbon nanotubes

- S. Rols (GDPC Université Montpellier II and ILL),
- E. Anglaret, J-L. Sauvajol (GDPC Université Montpellier),
- A. J. Dianoux, H. Schober, A. Ivanov, P. Convert (ILL),
- G. Coddens (LLB, CEA Saclay).

We report the first study of the structure and dynamics of single-wall carbon nanotubes using elastic and inelastic neutron scattering. Good agreement between structural information derived from local techniques (electron microscopy, Raman spectroscopy) and macroscopic techniques (x-ray and neutron diffraction) is found by taking into account a Gaussian distribution of tubes' diameter in the sample. The phonon density-of-states of single-wall nanotubes is also shown and constitutes the first study of the dynamical properties of this system in the whole energy range.

Because of their tremendous potential for future technological applications, carbon nanotubes are presently one of the most exciting molecular systems. Their exceptional electronic and mechanical properties make them the best candidates for future nano-scale electronic devices and composite materials having the strongest strength resistivity for minimum weight. But beside these two principal applications, an incredible theoretical and experimental work is actually done in nanotubes sciences covering almost all scientific fields. Chemistry, theoretical and applied physics, as well as biology and biomechanics expect this new material to be the solution for future developments and advances.

The structure of perfect single-wall carbon nanotubes (SWNT) is that of a graphene sheet rolled up into a cylindrical shape so that they are only composed of sp^2 carbon atoms. They usually self-organise into bundle-like 2D crystals with hexagonal symmetry containing tens to hundreds parallel tubes (called "bundles" in the following) [1]. The physical in-plane properties of graphene are transposed to SWNT along their cylindrical axis and are modified depending on the way the graphene sheet has been rolled. Therefore, a large number of their physical properties can be tuned depending on their structure, e.g., diameter, helical pitch and two-dimensional packing. Moreover, it has been recently suggested [2] that the peculiar dependence of the transport properties (electronic conductivity and heat capacity) of this material with temperature could be related to low energy intra and inter-tube excitations, and to an orientational disorder of the tubes in the bundles leading to a lack of intertube atomic correlation. Up to now, only a few Raman and infrared active modes have been studied, and no information on modes for which the frequencies are smaller than 20 meV have ever been collected. Fortunately, recent advances in the production techniques allow to synthesise SWNT in sufficient quantity and quality for inelastic neutron scattering experiments. We present in the following a complete neutron scattering study of single-wall carbon nanotube that correlates structural information (especially tube diameter and 2D packing) derived from neutron diffraction to dynamics measured in the whole energy range by the use of two different experimental apparatus.

Figure 1 displays the diffraction diagram of a 300 mg powder sample recorded at room temperature on the neutron high-flux diffractometer D20. The organisation of the tubes into bundles is evidenced by the presence of peaks in the low-scattering wave-vector range ($Q < 2$ Å^{-1}). The most intense one is located at 0.44 Å^{-1} and corresponds to Bragg reflections on the (1 0) planes of the 2D hexagonal lattice. For a correct interpretation of the diffraction diagram, we developed a detailed numerical study of the diffraction response of a SWNT bundle [3,4]. By taking into account the finite size of the lattice as well as a distribution of tube diameters in the sample, one can study the influence of the structural parameters on the diffracted signal. The best agreement between calculations and experiments was obtained for a mean tube diameter of 13.4 Å and a distribution of 2 Å. The number of tubes per bundle was estimated to be of the order of 40. These results are in good quantitative agreement with those

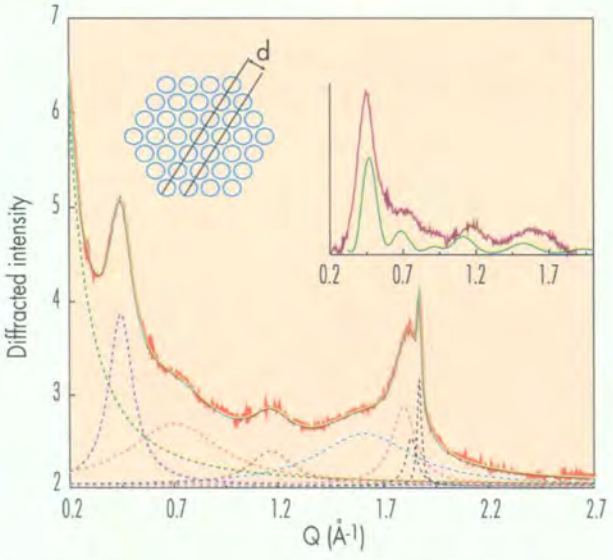

Figure 1: *Raw diffraction diagram (red line) of a single-wall carbon nanotube sample fitted by a set of 8 lorentzians (dotted curves). The low-Q peak at 0.44 Å^{-1} is characteristic of the 2D packing of the tubes and is related to Bragg reflections on the (10) plane of the lattice (top left). After removing the low-Q background and the graphite and nanoparticles contributions (located around 1.8 Å^{-1}) the coherent part of the signal due to the bundles is compared to calculation of numerical bundles with 40 tubes of 13.4 Å diameter (full line inset).*

deduced from local characterisation techniques. We derived the generalised phonon density-of-states (GDOS) from the one phonon coherent cross-section measured at 300 K on the time-of-flight spectrometer IN6 (full symbols) and at 5 K on the IN1 Be-Filter analyser spectrometer (open symbols). The singularities in the GDOS spectrum are characteristic of modes for which the dispersion curves present flat behaviour.

We compare in Fig. 2 the GDOS of the same SWNT sample used for diffraction experiments (Fig. 2b) with that of a standard graphite sample (Fig. 2a). Both graphite and SWNT GDOS spectra display five bands located around 58, 80, 100, 180 and 200 meV, while two additional bands in the nanotube spectrum are observed at 36 and 22 meV (Fig. 3a). These differences and analogies can be explained as follows: in graphite, normal modes involving in-plane and out-of-plane motions are decoupled. This is no more the case in SWNT for which out-of-plane modes with motions in the radial direction involve a mixing of out-of-plane bond bending and in-plane bond bending and bond stretching. It is thus expected that the main differences in the GDOS between graphite and SWNT occur at low energy where modes with a dominant out-of-plane *radial* component dominate the dynamics. According to this, the 22 and 36 meV bands are attributed to radial modes for which the frequencies are calculated to be inversely proportional to the tubes diameter. As an example, the A1g *radial breathing mode* is Raman active and provides a powerful tool to probe the diameter of the tube in the sample under study. In Fig. 3a, we compare the profile of the 22 meV band with the Raman signature of this mode (dotted line) where each well defined peak corresponds to a fixed tube diameter. From the envelope of these contributions and from the width of the corresponding band in the GDOS spectrum we derived a mean diameter and a diameter distribution that were found to be in good agreement with those deduced from diffraction experiments and calculations. Finally, the detailed analysis of the 0-12 meV range (Fig. 3b) reveals, in addition to the obvious contribution of other low energy excitations, a linear behaviour of the GDOS with energy from 0 to 3 meV. This range corresponds to acoustic modes for which the contribution to the density of states is sensitive to the dimensionality of the system. This linear behaviour can be tentatively assigned to the dominant contributions of intertube modes in the 2D packing of the bundle. A possible reason for this enhancement could be related to an orientational disorder of the tubes in the 2D lattice of the bundle. Preliminary studies of the temperature dependence of the GDOS shows changes in the low frequency profile at low temperature that can be assigned to freezing of orientational fluctuation.

Finally, neutron diffraction was used to derive a statistical picture of the purity and structure of our sample. Consequently, inelastic neutron scattering experiments could be performed and were shown to be efficient to derive the GDOS of SWNT where additional information about vibrational modes are clearly observed with regards to Raman data. A real effort in the synthesis (monodisperse samples) and in modelisation is now required in order to interpret unambiguously these data. A first step consist also to separate the low energy intra and inter-tube excitations. For that, a special sample containing mostly isolated tubes is actually prepared, and further time-of-flight experiments are planned.

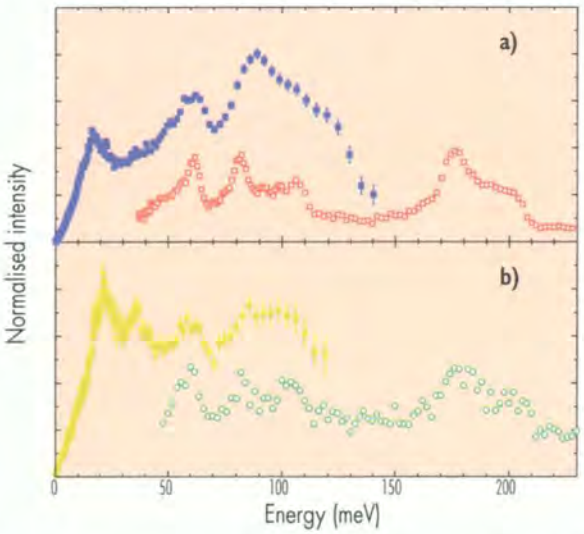

Figure 2: *Generalised phonon density-of-states of* ***a)*** *graphite and* ***b)*** *single-wall nanotubes derived from time-of-flight measurements (filled symbols) at 300 K and from three axis Be-Filter analyser experiments (open symbols) at 5 K.*

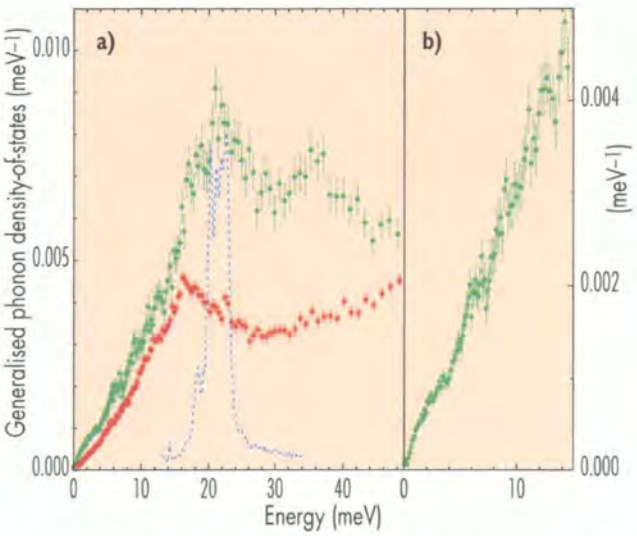

Figure 3: *Low energy parts of the generalised phonon density-of-states of graphite (red) and single-wall nanotubes (green). The energy of the radial breathing modes as measured in Raman spectroscopy (dashed blue line) is in good agreement with that of the main low-frequency peak observed at 22 meV peak in the generalised phonon density-of-states of single-wall nanotubes.*

References

■ [1] R. Saito, G. Dresselhauss and M.S. Dresselhauss, Physical properties of carbon nanotubes (Imperial College Press, London (1998) ■ [2] A. Mizel et al., Phys. Rev. B 60 (1999) 3264; C.L. Kane et al., Europhys. Lett. 41 (1998) 683; P. Petit et al., Phys. Rev. B 56 (1997) 9275 ■ [3] S. Rols et al., Eur. Phys. J. B 10 (1999) 263 ■ [4] E. Anglaret et al., Phys. Rev. Lett. 81 (1998) 4780.

The fractal geometry of rocks

A. P. Radlinski (Australian Geological Survey Organisation, Canberra),
E. Z. Radlinska (The Australian National University, Canberra),
M. Agamalian, G. D. Wignall (Oak Ridge National Laboratory),
P. Lindner, O. G. Randl (ILL).

Neutron scattering has been used to study the fractal microstructure of sedimentary rocks. The results have proven to be useful in prospecting for oil. "Immature" shales, which have the right geochemical characteristics to produce oil but have not yet generated, typically have a high fractal dimension, like the rocks in this study. By contrast, in "mature" oil-bearing rock, the fractal dimension for large pores drops to nearly 2, reflecting a smooth interface between the grain-surface-covering mobile bitumen and the pore space.

Sedimentary rocks are formed from a mixture of organic and inorganic debris deposited in an aqueous environment, buried and compacted at elevated temperatures over geological periods of time. The fractal structure of these systems is of great interest to oil industry because it could indicate a rock's oil-producing potential.

The small-angle scattering technique (SANS), using cold neutrons, has been applied to a hydrocarbon source rock U116, originating from the Urapunga 4 well in the MacArthur Basin, Northern Territory, Australia [1]. A series of SANS experiments have been performed using the instrument D11 at ILL at the wavelength of 14 Å, as well as with the ORNL facility at 4.75 Å. Recent progress in neutron scattering instrumentation at ORNL allowed the microstructure of rocks to be studied well beyond the conventional limit and into the range of ultra small angle scattering (USANS). In particular, the ORNL ultra-small angle neutron scattering (USANS) facility [2] can probe Q-ranges down to $Q \sim 2 \cdot 10^{-5}$ Å^{-1} (momentum transfer $Q = 4\pi\lambda^{-1} \sin\theta$, scattering angle = 2θ).

Figure 1 shows a combination of SANS data taken on the ILL and ORNL SANS instruments, along with USANS data [3]. It may be seen that all three data sets overlap smoothly with no adjustable parameters and the differential scattering cross section in the log-log representation can be approximated by a straight line above $Q = 2 \cdot 10^{-4}$ Å^{-1}. Detailed analysis of the data in Fig. 1 shows that the pore-rock fabric interface is a surface fractal with dimension $D_S = 2.82$ over three orders of magnitude of the length scale and ten orders of magnitude in cross section. To our knowledge, these data represent the largest range to date over which fractal behaviour has been observed in a natural system. Such an extent of fractal microstructure in a rock is remarkable, when compared with the limited size range over which the fractal properties are usually observed (typically one order of magnitude) [4].

This study extends the widest fractal length range previously observed in sedimentary rocks, which covered 2 decades in length scale and 7.5 decades in intensity [5], and shows that sedimentary rocks are in fact one of the most extensive fractal systems found in nature.

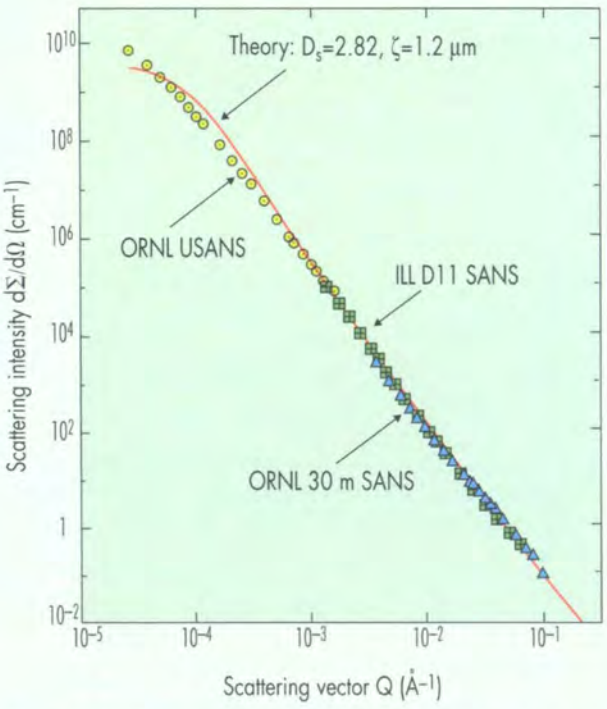

Figure 1: *SANS and USANS data from sedimentary rock showing that the pore-rock interface is a surface fractal (D_s = 2.82) over three orders of magnitude in length scale and ten orders of magnitude in cross section (intensity).*

The fractal character of the scattering cross-section eventually breaks down at scales larger than several micrometres. This is reflected in a flattening out of the scattering curve in Fig. 1 for smallest Q-values. In real space, the fractal dimension can be quantified by counting the frequency of structural features of given size on scanning electron microscope (SEM) images of the rock. Figure 2 illustrates statistical data for SEM images of rock U116, with the breakdown of fractal properties at the scale of 4 micrometres clearly observed as a sharp change of slope.

In conclusion, a "mature" (oil bearing) sample would have its fractal dimension decreased compared to the immature sample. Also, due to the decrease of contrast (bitumen-filled pores as opposed to water filled pores), the scattering intensity at a given Q-value is smaller for mature samples that have generated hydrocarbons than for immature samples. Therefore, the technique has the potential to distinguish the source rocks that have produced hydrocarbons from those that have not.

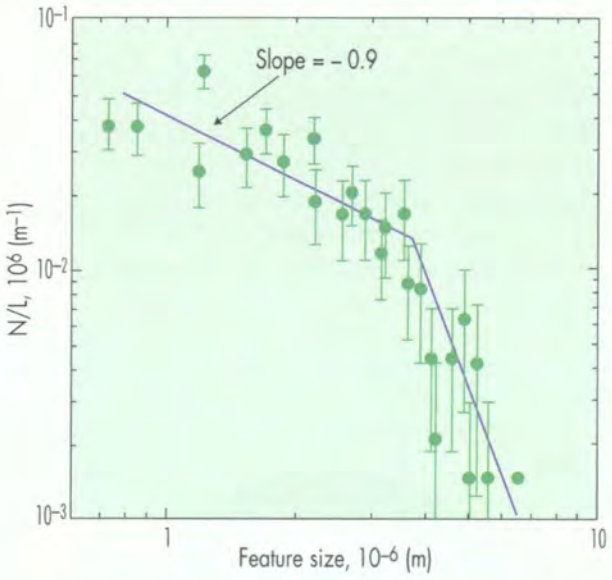

Figure 2: *Variation of the average number of SEM features per unit length (N/L) with feature size obtained from SEM images of the cleaved surface of sedimentary rock U116. Note the breakdown of fractality (D_s = 2.8 to 2.9) for length scales larger than 4 micrometres.*

As observed in *Physical Review Focus* [6], "The constancy of the fractal dimension over so many scales is astounding, considering what a messy, heterogeneous material sedimentary rock appears to be... This study will enhance the idea that you can describe rock with simple concepts ... There will be certain *bona fide* uses of fractal concepts, and one of them will be in the geological sciences".

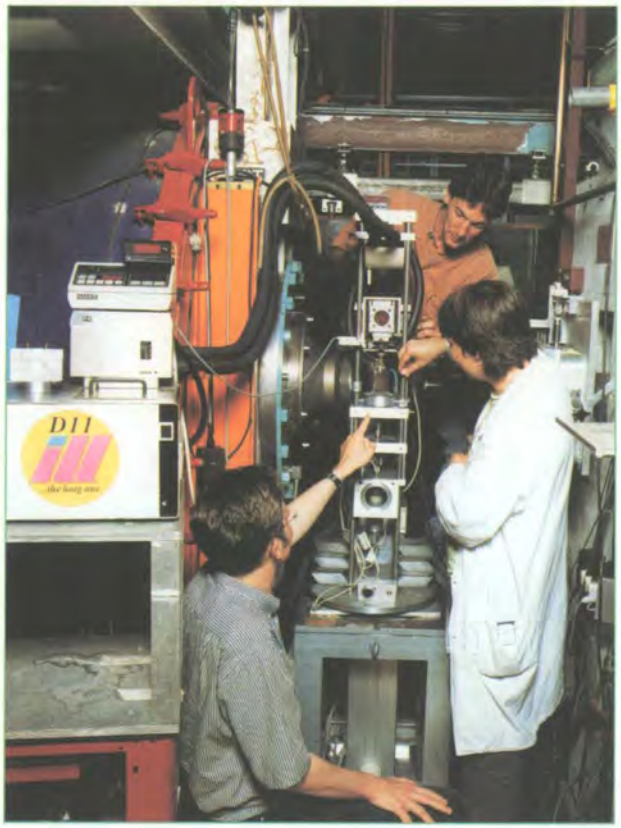

Peter Lindner (centre) and his collaborators aligning a sample on D11.

References

■ [1] A. P. Radlinski, C. J. Boreham, G. D. Wignall and J. S. Lin, Phys. Rev. B53 (1996) 14152 ■ [2] M. M. Agamalian, G. D. Wignall and R. Triolo, J. Appl. Cryst. 30 (1997) 345 ■ [3] A. P. Radlinski, E. Z. Radlinska, M. Agamalian, G. D. Wignall, P. Lindner, O. G. Randl, Phys. Rev. Lett. 82 (1999) 3078 ■ [4] D. Avnir, O. Biham, D. Lidar, O. Malcai, Science 279 (1997) 39 ■ [5] H. D. Bale, P. W. Schmidt, Phys. Rev. Letters 53 (1984) 596 ■ [6] Physical Review Focus, 20/04/99.

Decomposition and microstructure in Ni-Al-Mo and Ni-Ti alloys

G. Kostorz, J. Hecht, M. Kompatscher, J.-M. Schneider and B. Schönfeld (ETH Zürich),
B. Deme (ILL),
J. Kohlbrecher and W. Wagner (PSI Villigen).

Nickel-rich alloys are technologically useful, especially as high-temperature structural materials. They often contain submicroscopic, finely dispersed precipitates. The properties of this two-phase microstructure, especially the (meta-)stability and evolution of the precipitate population, are of considerable interest. Small-angle neutron scattering experiments were performed on Ni-alloy single crystals containing aluminium and molybdenum or titanium to follow closely their phase separation paths. The analysis of the anisotropic scattering patterns of Ni-Al-Mo single crystals yields a detailed description of the average precipitate morphology. Thus, a separation of the influence of interfacial energy and elastic strain energy of the precipitates during decomposition becomes feasible. The complex decomposition process of binary Ni-Ti alloys involves a sequence of metastable states which can be distinguished by small-angle neutron scattering. The transformation from the metastable state to the stable hexagonal phase was also followed *in-situ*.

Ni-base alloys are widely used in structural applications owing to their good mechanical properties and their resistance to corrosion. Especially, Ni superalloys exhibit high mechanical strength at temperatures exceeding 1300 K owing to the presence of an internally ordered phase of hard, structurally coherent precipitates embedded in the Ni-rich matrix. Although the technological development of superalloys is quite advanced, there is still a general need to better understand the basic physical processes controlling microstructural changes and long-term stabilisation of decomposed states with favourable properties. In the present experiments, small-angle neutron scattering (SANS) has been employed to characterise the microstructure of Ni-Al-Mo and to investigate the decomposition sequence in Ni-Ti.

The formation of coherent ordered precipitates from supersaturated Ni-rich solid solutions in Ni-Al-Mo is strongly influenced by temperature and overall composition as the solid solubility of both alloying elements varies sharply with temperature. Additions of Mo modify the lattice parameter mismatch between matrix and coherent precipitates [1-3]. Strain fields are built up during precipitate growth and may slow down the decomposition kinetics. The strain fields, coupled with the anisotropic elastic properties of the two phases, lead to non-spherical precipitate shapes and a preferred arrangement of precipitates along <100> crystallographic directions.

Experiments on Mo single crystals with Ni–12at.%, Al–2at.% and Ni–10at.% Al–5at.% (during ageing, for up to 10 h at 973 K and 1073 K) were performed on the SANS instrument D11 with neutrons of a wavelength of 6 Å. With advancing decomposition, the two-dimensional scattering patterns recorded on the D11 detector show an increasing anisotropy. For large scattering vectors ($Q \geq 0.05\,Å^{-1}$ where $Q = 4\pi \sin\theta/\lambda$, θ is half the scattering angle, and λ the wavelength of incident neutrons), the scattering intensity mainly represents the tail of the scattering function of the average precipitate. From transmission electron microscopy it is known that the precipitates are cuboidal in shape. The small-angle scattering of such objects can be described by a one-parameter analytical expression able to pass continuously from a sphere to a cube. Comparison with experimental data shows that, as decomposition proceeds, cuboidal precipitates progressively approach the shape of a perfect cube. Figure 1 illustrates the results obtained for one of the crystals. The average particle shape is found to correspond to the particle outlined in Fig. 1b [4]. The evolution of the particle shape

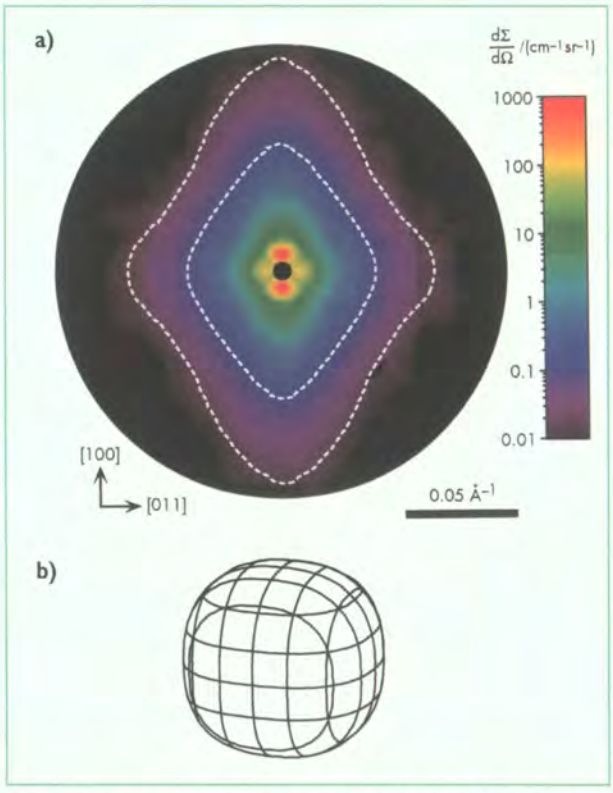

Figure 1: a) *Measured SANS pattern of a Ni–10at.% Al–5at.% Mo single crystal (face-centred cubic) after ageing at 1073 K for 3 h. The incident beam was parallel to the <110> surface normal of the sample. The dotted lines represent lines of equal intensity as calculated for a cuboidal precipitate (Fig. 1b).* ***b)*** *Best-fitting cuboidal shape.*

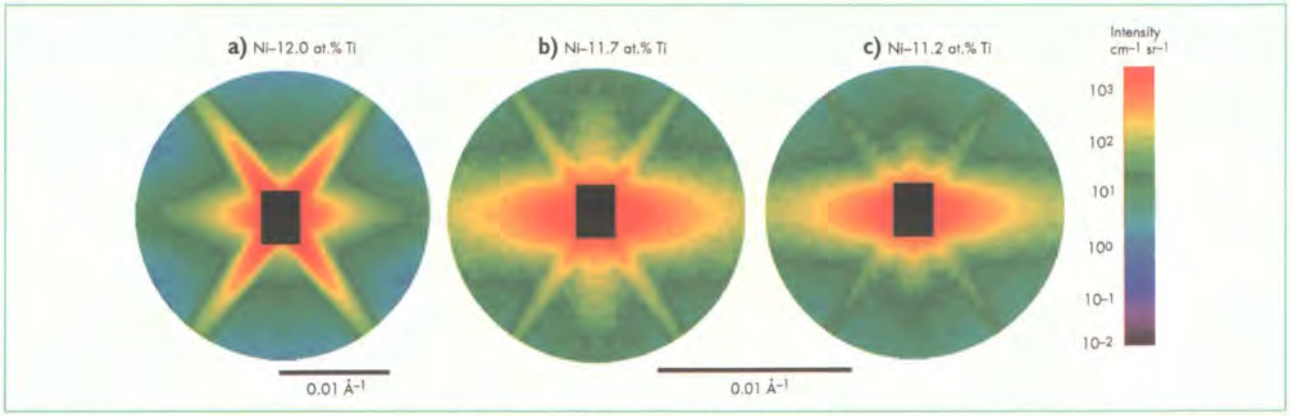

Figure 2: *SANS patterns of Ni-rich Ni-Ti single crystals (face-centred cubic) homogenised at 1440 K and annealed in-situ for* ***a)*** *46 min at 1240 K,* ***b)*** *10 min at 1220 K,* ***c)*** *43 min at 1200 K. The patterns were symmetrised to highlight the dominating features. The incident beam was parallel to the <110> surface normal of the sample, the horizontal axis is along <100>.*

and size gives information on the competition between interfacial energy and elastic strain energy. This allows macroscopic properties to be interpreted on the basis of microstructural parameters.

The decomposition sequence in Ni-rich Ni-Ti is more complex than in Ni-Al-Mo, as intermediate (metastable) states appear during phase separation, whereas the stable ordered hexagonal phase Ni_3Ti is observed only after extended ageing above about 1200 K. Previous SANS studies had indicated that the metastable precipitates may pass through two successive regimes with Ti concentrations of about 18 and 22 at.% [5,6]. The coexistence of these metastable states and the subsequent formation of the stable hexagonal phase are still to be explored in more detail.

In situ SANS investigations were performed to follow the decomposition progressively within individual samples. Polycrystals were investigated at SINQ/PSI (Villigen, Switzerland) with a heatable (up to 1020 K) sample holder, while single crystals were measured at D11 with a special furnace (up to 1470 K) for SANS, built in collaboration with the ILL. With this furnace, rapid temperature changes and *in situ* solid-solution treatments at high temperatures become feasible.

Polycrystalline Ni-Ti quenched in water after homogenisation treatment at 1440 K develops a SANS interference peak upon ageing at 900 K; this peak reflects the alignment of the coherent metastable precipitates along <100>. After an initial rapid increase of the integrated SANS intensity (the integrated intensity yields the total amount of Ti in precipitates), a temporary slowing down is observed between 1 and 5 h for Ni-11.3at.% Ti. Plateaus in the temporal evolution of the integrated intensity of such alloys confirm the succession of two states [7,8].

For single crystals at temperatures near and slightly above the suggested coherent miscibility gap, an unexpected result was obtained, as shown in Fig. 2; the metastable states still prevail, as indicated by the strong SANS intensity along <100>, and are still present after 1 h. After some time a new feature progressively dominates the scattering pattern. Sharp intensity streaks start growing along the <111> directions. They are due to the formation of platelets of the stable hexagonal phase. The direct formation of the hexagonal phase without the preceding appearance of metastable states was observed just below the incoherent solvus line.

These SANS investigations are accompanied by high-temperature, high-resolution x-ray diffraction close to fundamental and superstructure Bragg peaks as well as by transmission electron microscopy. The interplay between local atomic ordering and decomposition in the presence of coherency stresses will thus be clarified, and the results may be used in the numerical modelling of high-temperature stability and strength of superalloys.

References

■ [1] H.A. Calderon and G. Kostorz, in 'Morris E. Fine Symposium', edited by P.K. Liaw, J.R. Weertman, H.L. Marcus, and J.S. Santner, The Minerals, Metals & Materials Society (1991) 11 ■ [2] M. Fährmann, P. Fratzl, O. Paris, E. Fährmann, and W.C. Johnson, Acta Metall. Mater. 43 (1995) 1007 ■ [3] A.D. Sequeira, H.A. Calderon, G. Kostorz, and J.S. Pedersen, Acta Metall. Mater. 43 (1995) 3427 ■ [4] J.-M. Schneider, B. Schönfeld, B. Demé, and G. Kostorz, J. Appl. Cryst. 33 (2000) ■ [5] A. Cerri, B. Schönfeld, and G. Kostorz, Phys. Rev. B 42 (1990) 958 ■ [6] P. Vyskocil, J.S. Pedersen, G. Kostorz, and B. Schönfeld, Acta Mater. 45 (1997) 3311 ■ [7] G. Kostorz, M. Kompatscher, and B. Schönfeld, 'Coherent Precipitation in Ni-Rich Single Crystals', Solid-Solid Phase Transformation '99, edited by M. Koiwa, K. Otsuka, and T. Miyazaki, Kyoto, Japan (1999) 305 ■ [8] M. Kompatscher, B. Schönfeld, H. Heinrich, and G. Kostorz, J. Appl. Cryst.33 (2000).

He-bubble growth in a martensitic steel for fusion reactors

R. Coppola (ENEA, Casaccia),
G. Cicognani, R. P. May (ILL),
M. Magnani (ENEA, Bologna),
A. Moeslang (FZ Karlsruhey).

Small-angle neutron scattering has been employed to study the growth of He bubbles in a martensitic steel developed for fusion reactor technology. The He-bubble volume distribution functions obtained from our small-angle neutron scattering data show that a uniform distribution of small bubbles (about 15 Å) evolves during high temperature annealing within a few hours into a bimodal one with an additional population of larger bubbles (approximately 100 Å). Transmission electron microscopy can give insight into the morphology and size of He bubbles in the range from 20 to 50 Å. However, quantitative information cannot be derived, because only a small fraction of bubbles are visible by transmission electron microscopy.

One of the problems to be solved in the design of a future fusion reactor is the choice of the most adequate structural materials. Dramatic changes in both mechanical properties and microstructure are expected especially in the first wall (the element that is closest to the plasma), due to the very high neutron irradiation and the thermal stresses expected [1]. Fast neutrons and α particles produced by the fusion reaction induce radiation damage in the materials and lead to helium accumulation in the first wall. Helium is not soluble in solids and it precipitates by forming bubbles, whose growth causes the swelling and consequent embrittlement of the components. The growth of He bubbles under high-energy neutron irradiation is therefore one of the key factors determining the lifetime and the reliability of structural materials for fusion reactors steels. For a better understanding of the growth mechanism of He bubbles, and the influence of temperature on their formation, evolution, and size distribution should be determined.

To simulate the effect of the radiation from the fusion reaction on the first-wall components, and in particular helium-bubble formation, one can irradiate steels with accelerated α-particles. As shown in Fig. 1, the experimental observation of the bubbles using transmission electron microscopy (TEM) is difficult because of their tiny sizes (typically 10 Å), and because the electron beam is defocused by the martensitic matrix. Small-angle neutron scattering (SANS), on the other hand, is a particularly appropriate technique for this study, for several reasons. Neutrons have a wavelength that is of the order of the size of these particles, they penetrate easily relatively thick samples (up to several millimetres). Finally, because they have a spin, they sense the magnetisation of the steel; this property can be used to enhance the contrast of the (non-magnetic) He bubbles with respect to the steel matrix.

We investigated [2-4] the martensitic steel F82H[1]. The samples were homogeneously implanted at 250°C with 400 atomic parts per million He, using 104 MeV α-particles at the cyclotron facility at the FZ Karlsruhe. They were then heat treated (at 525°C, 825°C and 975°C) for two hours in high vacuum. These implantation conditions are representative of the effect of helium in fusion reactors. Of course, there are other microstructural effects, such as cavities, loops, segregation, etc., produced by neutron irradiation (that we may study in future).

Figure 1: *Helium bubbles in F82H after implantation of 400 appm He at T_{in} = 250°C (from Ref. [7]).*

One non-implanted sample for each temperature served as a reference to isolate the SANS signal due to the He bubbles from that of the structural changes induced by the thermal treatment. A further non implanted sample was heated at 250°C for 5 days to simulate the heat effects of the implantation process.

The SANS measurements were carried out on the instrument D11 at the ILL with a sample-to-detector distance of 1.46 m and a wavelength λ of 6 Å. A horizontal magnetic field was

[1] composition: 8.0 Cr, 0.10 C, 0.16 Mn, 0.16 V, 2.0 W, 0.02 Ta wt%

applied perpendicular to the incoming neutron beam in order to fully align the magnetic moments in the sample. Since the He bubbles are non-magnetic inhomogeneities imbedded in a magnetised matrix, we observe the scattering from two phases of different scattering density. In this study, we mainly use the stronger signal in the direction perpendicular to the magnetic field, where the magnetic scattering adds to the nuclear contribution.

The contribution of He bubbles of different sizes leads to relatively featureless scattering curves; therefore it is difficult to visually extract quantitative information from them. Using the method described in reference [5], the data were transformed into volume distribution functions D(r) defined as $D(r) = N(r)\, r^3$, where N(r) is the number per unit volume of bubbles (assumed to be spherical) of radius r.

The distribution functions for the three different annealing temperatures are shown in Fig. 2. The large error bands (dashed area in Fig. 2) in the volume distribution function arise both from the uncertainty in background subtraction [3] and from the limited Q range investigated. However, such uncertainties do not affect the relative values we found. The He bubble volume fractions *V*, determined by integration of the D(r)s, are reported in Tab. 1 together with the average bubble radii R_b.

At lower temperatures (Fig. 2a and b) we observe basically one well defined peak centred around 15 Å corresponding to a dense population of bubbles of small size. This value validates the estimation of 16 Å obtained by TEM [6,7].

Annealing temperature	V	R_b
250°C	0.0015	15
825°C	0.0079	5
975°C	0.0123	5*

Table 1: *He bubble volume fraction, V, and average radius, R_b (Å), from SANS analysis (* with a secondary bubble population around 100 Å).*

At 975°C (Fig. 2c), a second distribution of bubbles, one order of magnitude larger, appears. The density of both bubble populations is almost one order of magnitude larger than at 825°C.

The bubbles of large size present at 975°C contribute a high scattering intensity at smaller Q-values than those explored. This accounts for the larger error band found for the distribution associated to this temperature. There is an increase of a factor 5 in the relative value of the bubble volume fraction from 250°C to 825°C and of about 50% from 825°C to 975°C (see Tab.1).

We conclude that the thermal treatment is responsible for the growth of larger bubbles at the expense of the smallest ones and by coalescence of the He atoms initially implanted in the matrix. The latter are "invisible", because individual atoms cannot be resolved by SANS; for this reason the integrated intensity in Fig. 2 increases with temperature.

Nevertheless, SANS turned out to be an essential tool for the quantitative characterisation of the bubble-growth mechanism in these steels.

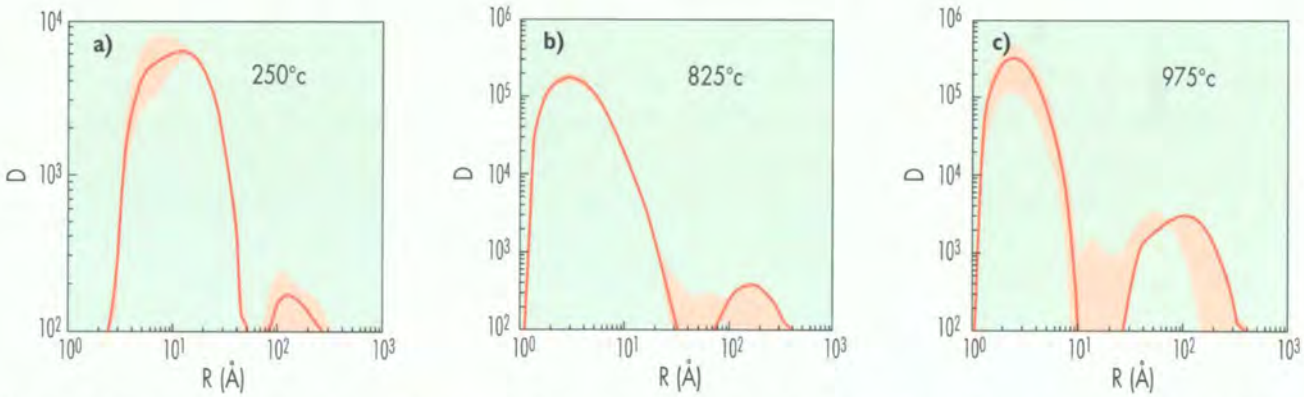

Figure 2: *He-bubble volume distribution functions (arbitrary units proportional to bubble volume per unit volume vs. bubble size in Å) obtained from the SANS data: **a)** 250°C, **b)** 825°C and **c)** 975°C. The dashed areas represent the 80% confidence band.*

References

■ [1] A. Hishinuma, A. Kohyama, R. L. Klueh, D. S. Gelles, W. Dietz, K. Ehrlich, J. Nuc. Mat. 258-263 (1998) 193 ■ [2] ILL Exp. Rep. 7-01-31 (1998) ■ [3] R. Coppola, M. Magnani, R. P. May, A. Moeslang, J. Appl. Cryst, in press ■ [4] R. Coppola, M. Magnani, R. P. May, A. Moeslang, M. Valli, J. Nuc. Mat., submitted ■ [5] M. Magnani, P. Puliti, M. Stefanon, N. Inst. & Meth. A 271 (1988) 611 ■ [6] A. Moeslang, S. Cierjacks and R. Lindau, Proceedings of 12th Intern. Conf. on Cyclotrons and their Applications Berlin 1989, eds. B. Martin and K. Ziegler, World Scientific, London (1991) 545 ■ [7] J. Bertsch, FZK Report 5984 (1997), FZ Karlsruhe.

Reflectivity analysis of Ni nanoclusters in ion-implanted fused silica-glass

- R. Siebrecht (ILL and Ruhr-Univ. Bochum),
- C. Mondelli (ILL),
- G. Battaglin, E. Cattaruzza and F. Gonella (INFM Venice),
- F. D'Acapito (INFM Grenoble and ESRF),
- P. Mazzoldi (INFM Padua).

Ion implantation is a useful technique to obtain composite materials such as metal nanocluster composite glasses (MNCGs), formed by nanometer-size metallic clusters embedded in silicate glasses. Due to quantum and dielectric confinement effects, these composites exhibit several effects such as an enhanced optical Kerr susceptibility, which can be important for application in all-optical switching devices. Moreover, MNCGs obtained by ion implantation of transition elements are important for their magnetic properties itself. Neutron reflectometry was used as a non-destructive method to determine the in-depth metal cluster density distribution and to roughly estimate the cluster size. The data analysis under a multilayer sample approximation gives realistic results: this suggests the possibility to use neutron beams to study very diluted systems such as MNCGs.

Ion implantation of metal elements in glass substrates can lead to the formation of nanometer-radius colloidal particles in a thin surface layer. The formation of nanoclusters depends on the chemical reactivity of the pair "implanted atom-dielectric host". Metal nanocluster composite glasses (MNCGs) exhibit an enhanced intensity-dependent refractive index due to the optical Kerr effect: this feature could be exploited in all-optical switching device technology, with the aim to process light signals without conversion to electronic form. Thus allowing to operate such a device in fast time regimes (tenths of pico seconds). Moreover, MNCGs obtained by ion implantation of transition elements are important for their magnetic properties: when the size of magnetic particles is in the nanometer range inside a non-magnetic matrix, surface effects are dominant. These affect the magnetic properties significantly, in terms of both oxidation and anisotropy effects. For this range of magnetic particle size, the composite material offers new technological possibilities, for example in the field of magnetic recording substrates for high-density information storage. The knowledge of the cluster size distribution, as well as the spatial correlation function, is important in order to relate the morphological characteristics to the physical properties.

The investigated samples are amorphous fused silica-glass slides implanted sequentially with Ni^+ ions at two different energies and (nominal) fluxes, namely, 180 keV ($1.7 \cdot 10^{17}$ ions/cm^2) and 70 keV ($6 \cdot 10^{16}$ ions/cm^2). Only glass slides without voids were chosen to serve as substrates for implantation. The double implantation leads to a flatter depth distribution of the nickel atoms, as suggested by simulations [1]. The average in-plane cluster distribution is constant over the whole sample area, which is known from transmission

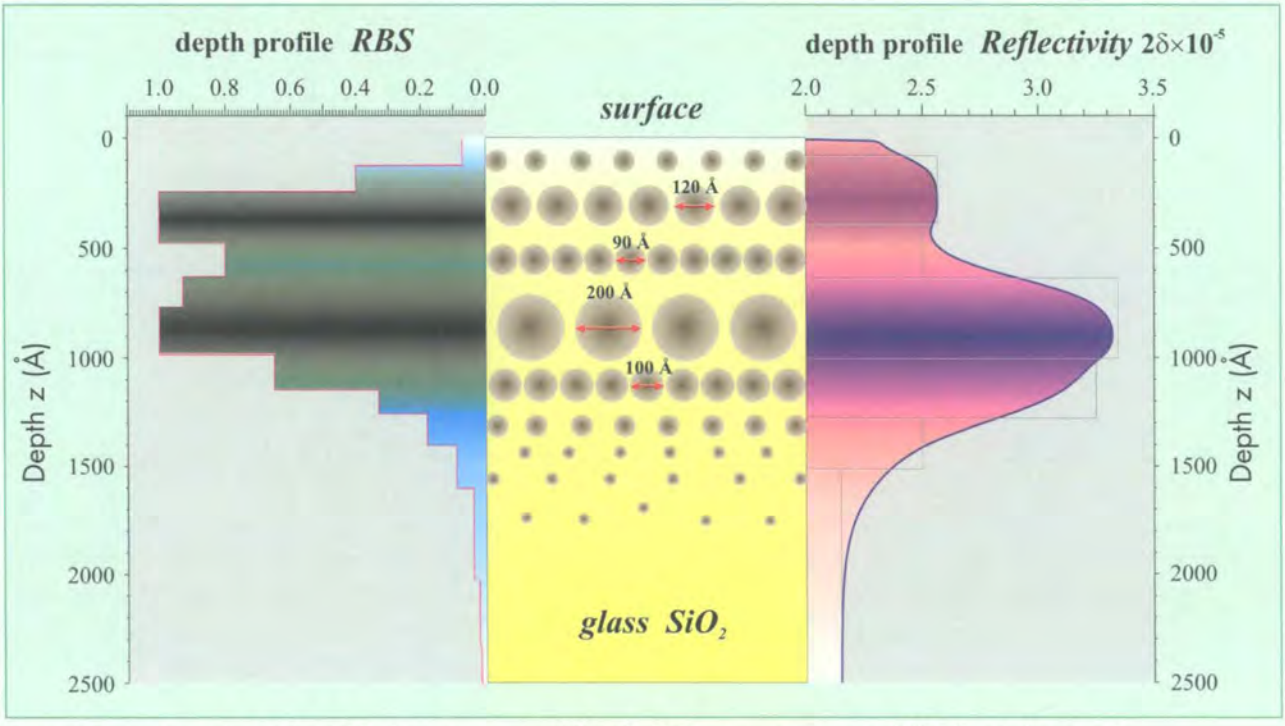

Figure 1: The experimental in-depth nickel distribution measured with Rutherford backscattering spectroscopy (RBS), left, and reflectivity, right.

electron microscopy measurements during former experiments. The experimental in-depth nickel distribution, as measured by Rutherford backscattering spectrometry is reported in Fig. 1 on the left side. The retained implanted dose was about $2.5 \cdot 10^{17}$ ions/cm^2. Grazing incidence x-ray diffraction on these samples gives evidence for fcc nickel nanoclusters. To learn about the sample's magnetic properties a non-destructive method, sensitive to the depth-dependent magnetism is needed. In our case polarised neutron reflectivity with spin analysis comprises all the demanded qualities, making it to the method of choice. The analysis of spin dependent reflectivity data enables one to reveal quantitatively the nuclear and magnetic depth profile at the same time. Nevertheless, due to the relatively low total amount of magnetic material in the sample the scattered magnetic signal may be difficult to sort out from the data. Thus, in a first step one has to confirm that it is possible to reconstruct the nuclear non-magnetic depth profile for such a sample with unpolarised neutron reflectivity.

We performed neutron reflectivity measurements on the diffractometer ADAM [2]. The data were taken at the instrumental wavelength of $\lambda = 4.41$ Å and over a Q-range of 0.1 Å.

Figure 2 shows the reflectivity curve (open circles). The fit to the data is given by the solid line. The basic hypothesis for the fit was to take into account the lateral homogeneity of the potential. The depth variation of the potential in the z-direction, roughly proportional to the local metallic element density, was approximated by potential slabs of different scattering-length density and thickness. On the right side of Fig. 1 the potential obtained from the fit is depicted: two maxima are clearly visible, in agreement with the simulation results. The peaks are both shifted of about 350 Å towards the surface with respect to the positions in the simulation, because of the surface erosion effect of the incident ion beam during the sample preparation. This result is in agreement with the Rutherford backscattering spectrometry measurements shown on the left side of Fig. 1.

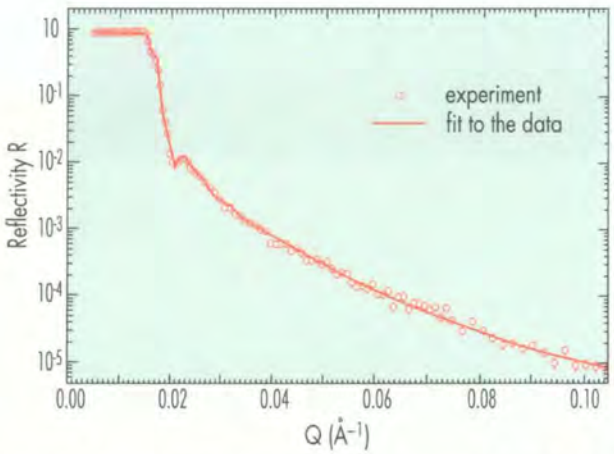

Figure 2: *Reflectivity measurement (open circles) taken on ADAM ($\lambda = 4.41$ Å), solid line fit to the data.*

Furthermore, the roughness of the slabs in the fit can be related to the mean size of the clusters which is sketched in Fig. 1. In fact, due to the high local nickel concentration, Ni clusters are expected to be very close one to each other. Under this assumption, we obtain reasonable values of the cluster size for all the implanted regions, except for the deepest part, where a very large value was found for the roughness. Considering the low nickel concentration in the tail of the in-depth distribution, we interpret this result as due to a large average distance among the metallic clusters.

This unpolarised reflectivity experiment is the first step to set a more general approach to MNCGs using neutron-based techniques, to study their magnetic properties. We clearly demonstrated that with this technique it is possible to reveal the non-magnetic nuclear depth profile. This result is in agreement with precedent Rutherford backscattering spectrometry measurements. The first neutron reflectivity experiments with polarised neutrons and spin analysis on similar samples with magnetic implantations were performed recently. The data obtained looks promising and data treatment is currently in progress.

References

■ [1] J.P. Biersack and L.G. Haggmark, Nucl. Intr. and Meth. 174 (1980) 257 ■ [2] R. Siebrecht, A. Schreyer, U. Pietsch, H. Zabel, Physica B 241 (1998) 169.

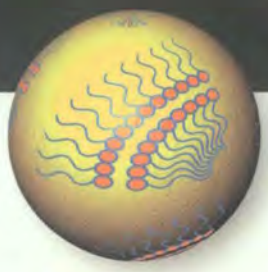

Magnetic ordering in a single 46 Å thick Ho(00.1) film

V. Leiner and R. Siebrecht (ILL),
D. Labergerie, Ch. Sutter, and H. Zabel (Univ. Bochum).

We report on magnetic ordering in an epitaxial Ho single film with a thickness of 46 Å. Using the ADAM diffractometer at ILL, we were able to investigate the evolution of the first magnetic satellite of the Ho magnetic helix in the temperature region between 10 K and T_N. As compared to bulk Ho, the Néel temperature T_N is reduced from 132 K to 105 K. Simultaneously, an increase of the turn angle α for the magnetic moments from one layer to the next is observed, implying a shorter period for the spin helix.

Due to new advances in thin-film deposition techniques it is possible today to grow ultra-thin epitaxial magnetic films with very high structural quality. This allows to raise the question of how the bulk magnetic properties are modified in thin films either due to dimensionality effects or due to proximity with other material layers. Information on nanofabricated magnetic films is of high importance for the design and functionality of magnetic nanostructures integrated in new electronic devices. The most complete information on such ultra-thin structures comes from neutron scattering. For revealing antiferromagnetic or incommensurate spin structures, neutron scattering is unique. However, known as a bulk probe, its applicability to thin films has to be proven. In this context, we have studied the magnetic phase-transition in single ultra-thin Holmium films. The strong magnetic moment of Ho and its long-range magnetic order yield intense magnetic peaks at small Q-values, thus, making Ho a perfect model system for scattering experiments in the ultra-thin regime.

In the bulk, Holmium exhibits an incommensurate spin helix below the Néel temperature, T_N, of ~ 132 K. Between 20 K and 132 K the magnetic moments order ferromagnetically in the hexagonal basal plane. From one plane to the next, the average orientation of the magnetic moments encloses a turn angle α, setting up a magnetic spiral along the direction normal to the planes. The turn angle is about 30° at 20 K and increases continuously to 50° with rising temperature up to the Néel temperature. Below 20 K the magnetic moments lock into a commensurate magnetic cone structure with a turn angle of 30° in the basal plane and a ferromagnetic component normal to the planes. In Fig. 1, the phase diagram is schematically reproduced, which is the result of magnetic neutron scattering [1-3] and resonant magnetic x-ray scattering experiments at the Ho – L_{II} and L_{III} absorption edge [4-6].

In magnetic scattering experiments the helical magnetic structure gives rise to magnetic satellite reflections at distance $\pm \tau^*$ around the allowed Bragg peak along the c* direction. τ^* in units of c* is related to the turn angle α via $\alpha = 180° \cdot \tau^*$.

Using resonant magnetic x-ray scattering at the Ho – L_{III} absorption edge, the minimum thickness which can be studied is around 200 Å. Below this value the charge background from the Laue-oscillations of the nearby Bragg-reflection becomes too strong and buries the magnetic ($00.2 \pm \tau^*$) reflections [7]. Using neutron scattering, we have now succeeded to study the magnetic phase-transition in a single Ho(00.1) film which has a thickness of only 46 Å. The epitaxial Ho film was grown on

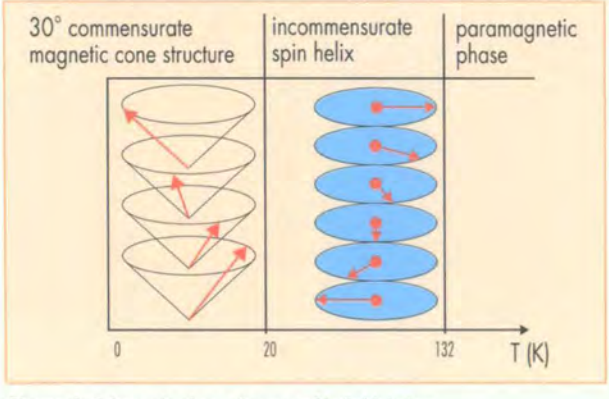

Figure 1: *Schematic phase diagram of bulk Holmium.*

a sapphire substrate with the use of a Nb and Y buffer layer. The Ho film was capped with an Y and Nb layer to prevent it from oxidation. The embedding of Ho between Y layers ensures symmetric structural and magnetic boundary conditions. The film thickness was determined from x-ray reflectivity measurements; the out-of-plane roughness was found to be ~ 10 Å. For the magnetic scattering experiments we use the ADAM reflectometer at the ILL because of its high flux, low background and high Q-resolution. These features are essential for studying weak satellite reflections close to the (00.0) Bragg peak. Throughout the experiments we used a wavelength of 4.41 Å. Figure 2 shows the magnetic $(00.0+\tau^*)$ peak from the Ho film with 46 Å thickness. With increasing temperature the peak shifts to higher Q values due to an increasing turn angle. At the same time the intensity drops due to a decreasing order parameter. For this thin film we measure a Néel temperature of only 105 K which is considerably lower than in the bulk. The inset shows the order parameter as a function of temperature. Below 20 K, we could not observe a transition to a commensurate magnetic structure. The magnetic order in the ultra-thin Ho film remains incommensurate, in agreement with results obtained previously from Ho/Y superlattices [8]. Looking at the length of the magnetic helix at ≈ 20 K, we find $\tau^* \approx 0.251c^*$, i.e. an increase of the turn angle to 46° (as compared to 30° found for bulk Ho).

We have demonstrated for the first time that it is possible to study the magnetism in such ultra-thin films by investigating the magnetic ordering in Ho films as thin as 46 Å using a high-resolution neutron reflectometer. The neutron results indicate that even thinner samples can be investigated with reasonable counting statistics and underline impressively the importance of neutron scattering for the investigation of nanostructured magnetic systems.

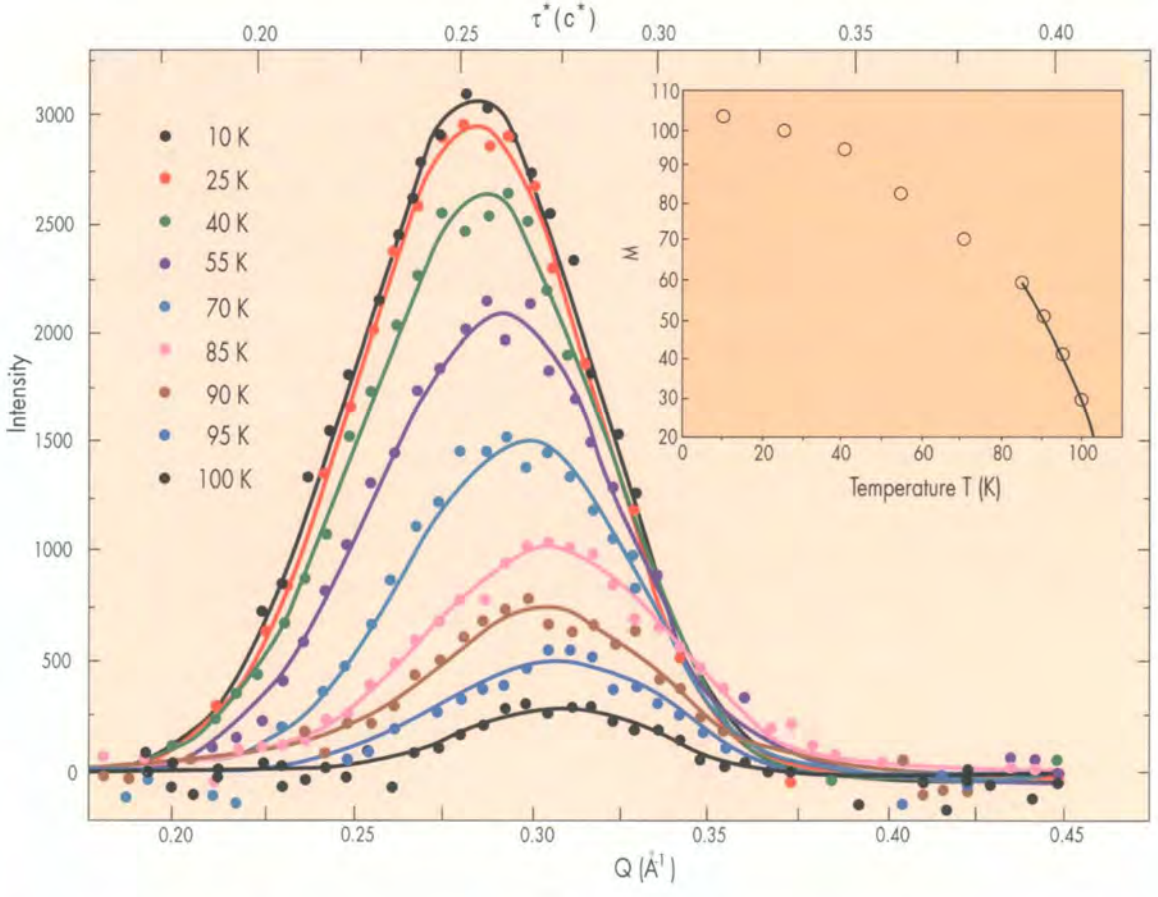

Figure 2: *Radial neutron scans of the $(00.0+\tau^*)$ magnetic satellite peak for the 46 Å thick single epitaxial Ho(00.1) film for different temperatures. The peak shifts to higher scattering vectors due to an increasing turn angle of the Ho spin helix with increasing temperature. Simultaneously the intensity decreases due to a loss of long-range magnetic-order with increasing temperature. In the inset the magnetic-order parameter is plotted as a function of temperature.*

References

■ [1] W.C. Koehler, et al., Rev. 158 (1967) 450 ■ [2] G.P. Felcher, et al., Spedding, Phys. Rev. B 13 (1976) 3034 ■ [3] M.J. Pechan, C. Stassis, J. Appl. Phys. 55 (1984) 1900 ■ [4] D. Gibbs, et al., Phys. Rev. Lett. 55 (1985) 234 ■ [5] J. Bohr, et al., Physica 140A (1986) 349 ■ [6] D. Gibbs, et al., Phys. Rev. B 43 (1991) 5 663 ■ [7] C. Sutter, E. Weschke, R. Meier, C. Schüssler-Langeheine, G. Grübel, D. Abernathy, to be published ■ [8] D.A. Jehan, et al., Phys. Rev. B 48 (1993) 5594.

Magnetic off-specular neutron scattering and GMR effect

- V. Lauter-Pasyuk (Univ. München and JINR Dubna),
- B. Toperverg (ILL and PNPI St. Petersburg),
- H. J. Lauter (ILL),
- O. Nikonov (ILL and JINR Dubna),
- E. Kravtsov, M. A. Milyaev, L. Romashev and V. Ustinov (IMP Ekaterinburg).

Complete polarisation analysis of neutron reflection and simultaneous measurements of polarised neutron off-specular scattering have been employed to verify atomic-spin arrangements in Fe/Cr multilayers, a typical representative of systems showing the giant magnetoresistance (GMR) effect. The quantitative theoretical data analysis shows that in the GMR region small column-like antiferromagnetic domains exist, arranged perpendicularly to the film surface through the whole multilayer depth. The domains may provide an efficient spin-flip mechanism for electron scattering, a crucial ingredient for the GMR effect.

The understanding of a wide range of exciting properties of artificially superstructured magnetic materials including giant magnetoresistance (GMR) [1], oscillating interlayer exchange coupling [2], and non-collinear magnetic ordering [3,4] requires unambiguous microscopic information on the atomic-spin arrangement in those materials. In a set of experiments on magnetic Fe/Cr multilayers we demonstrate that such information can only be obtained if two conditions are fulfilled. Firstly, the interface quality of the sample must be so high, that off-specular scattering originating from magnetic and non-magnetic roughness at the interfaces is negligible. Secondly, the data collection in specular reflection mode (with complete polarisation analysis) must be combined with polarised neutron off-specular scattering measured in a broad range of incident and outgoing angles, so that a model can be compared over a necessary broad off-specular region. This wide map over the specular and off-specular region should be obtained for both, spin-flip (SF) and non spin-flip (NSF) scattering in order to separate unambiguously the true specular signal from the SF off-specular signal, which may appear also along the specular line. These two conditions together with the numerical analysis allowed us to establish a detailed description of the microscopic spin-arrangement. The central issue is that the off-specular SF-scattering arises from small column-like antiferromagnetic domains oriented perpendicular to the film surface. So, our interpretation does not confirm the picture of laterally uniformly magnetised Fe-layers with non-collinear or canted angle structure published before e.g. in [3,4]. Our finding is important due to the fact that the presence of domains cause spin-dependent electron scattering which accounts for the GMR-effect.

The spin-resolved polarised neutron reflectrometry (PNR) experiment from a superlattice [Cr (9 Å) / 57 Fe (68 Å)] × 12 grown by molecular beam epitaxy on an Al_2O_3-substrate was performed on ADAM with its new multidetector. The magnetic field H was applied parallel to the sample surface.

The very good quality of the sample is visible in Fig. 1 which shows the scattered intensity from this multilayer for H = 5.48 kG parallel to the sample surface in the saturation regime. The reflectivity was measured beyond the second structural Bragg-peak. No off-specular scattering is observed within the experimental accuracy around these Bragg-peaks at $\alpha_i = \alpha_f = 0.029$ rad and 0.058 rad. This picture represents the sample with ferromagnetic magnetisation in the Fe-layers, having interfaces free from non-magnetic roughness or magnetic interface disorder within the accuracy of the measurement.

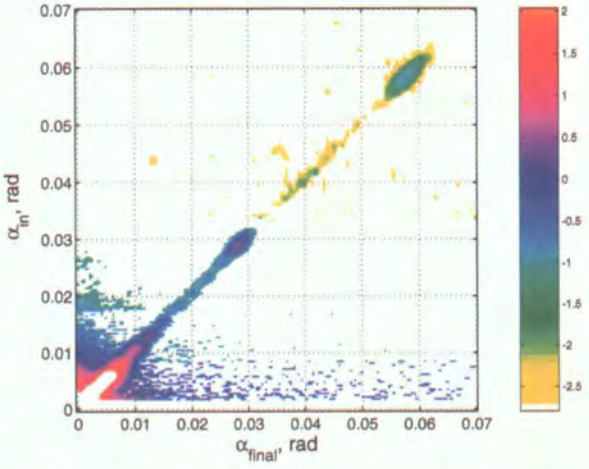

Figure 1: *Intensity map of specular (R^+) and off-specular scattered neutrons from the Fe/Cr multilayer at H = 5.48 kG as a function of α_{in} and α_{final}, the incident and outgoing scattering angle, respectively. The colours reflect the scattered intensity on a log-scale. The horizontal colour lines crossing the pictures are background effects. (Wavelength used: 4.4 Å)*

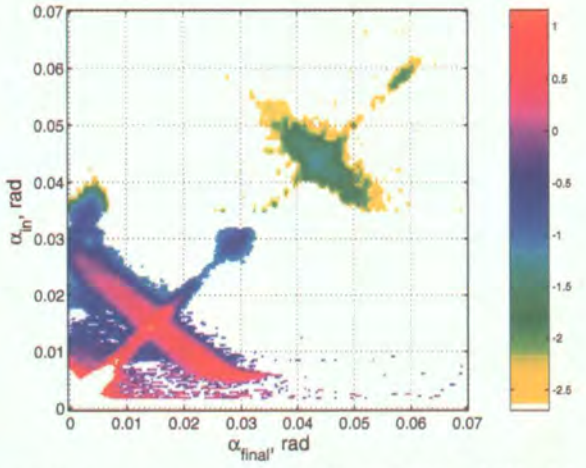

Figure 2: *Intensity map as in Fig. 1 but for the field H = 0.428 kG for $R^+ = R^{++} + R^{+-}$.*

This last statement is very important, because samples with this quality are unique and allow us to separate the effects of interface disorder from other magnetic effects.

In Fig. 2, for the lower field of H = 0.428 kG, additional intensity is observed with respect to Fig. 1 going through the two half-order positions at $\alpha = 0.0145$ rad and $\alpha = 0.0435$ rad. At this field the sample shows the GMR-effect. This additional intensity is off-specular scattering distributed along lines perpendicular to the reflectivity curve forming a superstructure Bragg-sheet. However, in contrast to the usual case when the Bragg sheet crosses the specular line at the Bragg peak position no appreciable enhancement of the intensity at the superstructure position was observed. Thus, the objects giving rise to off-specular scattering must be smaller than the lateral coherence-length. Furthermore, the off-specular scattering is asymmetric, where it approaches the axes near $\alpha_{in} = 0$ and $\alpha_{final} = 0$.

The intensity along the first superstructure Bragg-sheet is cut before reaching $\alpha_{in} = 0$ or $\alpha_{final} = 0$. On one side the intensity is cut at α_{final} nearly zero and on the other side at $\alpha_{in} \sim 0.005$ rad. These angles are related to the critical angle of the Fe-layers which depends on the polarisation direction of the neutrons with respect to the magnetisation direction of Fe; this shows, without spin analysis, that off-specular scattering consists of SF neutrons. With this unusual, but effective method, SF neutrons can be determined. R in the figure caption relates to reflectivity with the polarisation of the neutrons parallel (+) or antiparallel (–) to the external field.

The spin-flip effect is also shown in Fig. 3 which was obtained under the same experimental conditions as Fig. 2 but with an analyser placed between sample and detector and centred at the position of the specular beam. Only NSF neutrons are transmitted by the analyser. The footprint of the analyser covers only a certain angular band of neutrons in transmission scattered from the sample, the width of which is marked in Fig. 3 by the dashed lines.This band is already sufficient for a polarisation analysis. The scattering along the half-order Bragg-sheets crosses the reflectivity curve and consists purely of SF-scattering as can be deduced by comparing figs. 2 and 3.

In our model, the disorder leading to off-specular scattering has a lateral correlation length smaller than the lateral neutron coherence length, which is estimated to be in the order of a few tens of microns. Furthermore, the perturbation must have antiferromagnetic character due to the location at half-order Bragg-sheets. Therefore, antiferromagnetic domains are assumed. The domains extend in the perpendicular direction throughout the film thickness as evidenced by the width of these off-specular Bragg-sheets. The off-specular SF-scattering together with the NSF-specular scattering is calculated with the supermatrix formalism [6] and presented in Fig. 4.

This antiferromagnetic domain model can describe correctly the off-specular scattering appearing as Bragg-sheets through the half order magnetic Bragg-positions reproducing the details like the asymmetry in the lower Q Bragg-sheet and with all the details at the border of the picture. In addition, our model correctly reproduces the relative intensities between first and second Bragg-sheet as well as the off-specular scattering intensities between the half order Bragg-sheets. The average size of the antiferromagnetic regions is around ~3000 Å.

The high quality of the sample and the complete mapping of the off-specular scattering has allowed identifying unambiguously the origin of the spin-flip off-specular scattering. This model of *antiferromagnetic domains* is quite in contrast to the usually used model of homogeneously magnetised layers stacked into a sequence with magnetisation direction varying between alternative Fe-layers, [e.g. 3,4]. The new interpretation may lead to reconsidering electron scattering in these type of samples for a more exact description of the GMR effect.

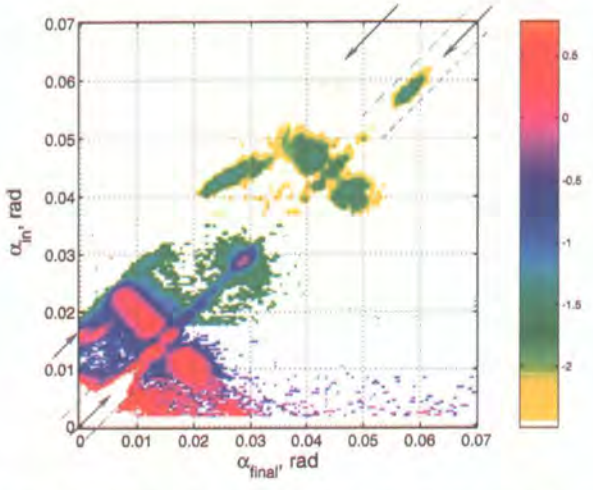

Figure 3: *Intensity map as in Fig. 2 but with analyser. The arrows indicate the specular line in one spin state (transmission; R^{--}) and the specular line in the opposite spin state (reflected; R^{-+}); the region between the dashed lines shows the working area of the analyser in transmission.*

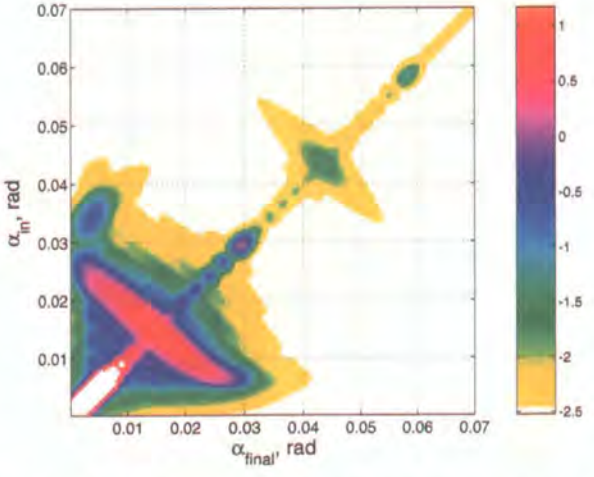

Figure 4: *Intensity map of off-specular spin-flipped and specular non-spin flipped neutrons from the Fe/Cr multilayer calculated with a model of antiferromagnetic domains to be compared to Fig. 2.*

References

■ [1] M.N. Baibich, et al., Phys. Rev. Lett. 61 (1988) 2472 ■ [2] S.S.P. Parkin, N. More, and K.P. Roche, Phys. Rev. Lett. 64 (1990) 2304 ■ [3] A. Schreyer, et al., Europhys. Lett. 32 (1995) 595 ■ [4] A. Schreyer, et al., Phys. Rev. B52 (1995)16066 ■ [5] V. Lauter-Pasyuk, et al., SXNS6 (1999), accepted Physica B ■ [6] B.P. Toperverg, A. Rühm, W. Donner, H. Dosch, Physica B 267-268 (1999) 198.

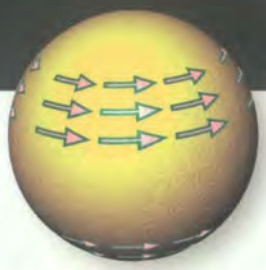

The Mn_{12}-acetate spin cluster

I. Mirebeau, M. Hennion (LLB),
H. Casalta (ILL),
H. Andres, H. U. Güdel (Univ. Bern),
V. Irodova (Inst. Kurchatov Moscow),
A. Caneschi (Univ. Firenze).

Mn_{12}-acetate is a ferrimagnetic spin cluster with total spin S = 10, providing the first and most well known example of macroscopic quantum tunnelling of magnetisation. By inelastic neutron scattering we separated the energy levels corresponding to the splitting of the ground state. We could measure accurately, and for the first time in zero field, a very small energy term, responsible for the quantum tunnelling process.

The study of molecular nanomagnets, besides its great theoretical interest, could help to determine the size limit for information storage. The most attractive clusters consist of a few (typically 10-20) paramagnetic ions coupled by exchange interactions at the borderline between quantum and classical behaviour. Among them, Mn_{12}-acetate (Mn_{12}-ac) is the best-studied spin cluster so far, providing the first experimental evidence of macroscopic quantum tunnelling [1]. The cluster has a plate-like shape, with a total spin S = 10, and a uniaxial anisotropy. Its magnetisation relaxes between two equivalent sublevels of the ground state (M = ± 10) separated by an energy barrier. Above 10 K, it relaxes by thermal activation like a superparamagnet. Below 2 K, the magnetic reversal is governed by a quantum process yielding a spectacular effect, regular steps in the magnetisation curve [2]. The quantum tunnelling which occurs within the S = 10 ground state is governed by extremely small high-order terms of the anisotropy energy. To understand it better, we have studied the energy sublevels of the ground state by inelastic neutron scattering.

The S = 10 ground state arises from a ferrimagnetic coupling between eight Mn^{III} ions (S = 2) and four Mn^{IV} ions (S = 3/2). It is split by crystal fields in 21 sublevels ($-10 \leq M \leq 10$). Using high-energy resolution, we separated all the sublevels of the S ground-state. We could show the presence of high-order spin interactions unambiguously. The main result is the accurate determination in zero field, of a very small non-diagonal term in the spin Hamiltonian (hereafter called transverse term). Its presence has been searched for by many theoreticians and experimentalists to explain the tunnelling effects.

A powder sample:

$$[Mn_{12}(CD_3COO)_{16}(D_2O)_4O12]\cdot 2CD_3COOD\cdot 4D_2O$$

was synthesised using deuterated solvents. The crystal structure was checked between 10 and 290 K by neutron diffraction on the

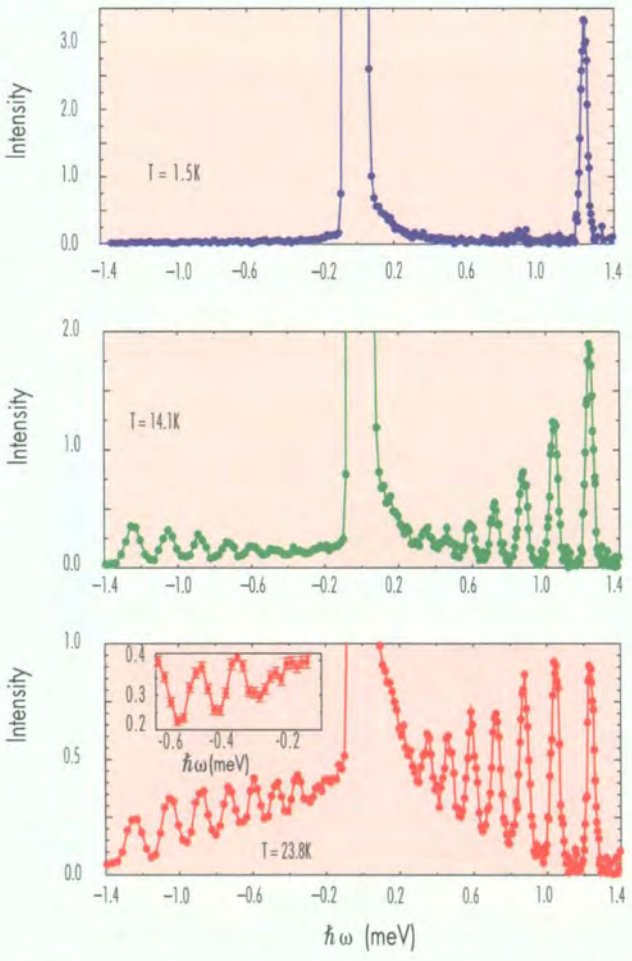

Figure 1: *Energy spectra at three temperatures (raw data, averaged in Q-space). The intensity units are the same but the scales differ for all spectra. In the inset, the low energy range for ω < 0.*

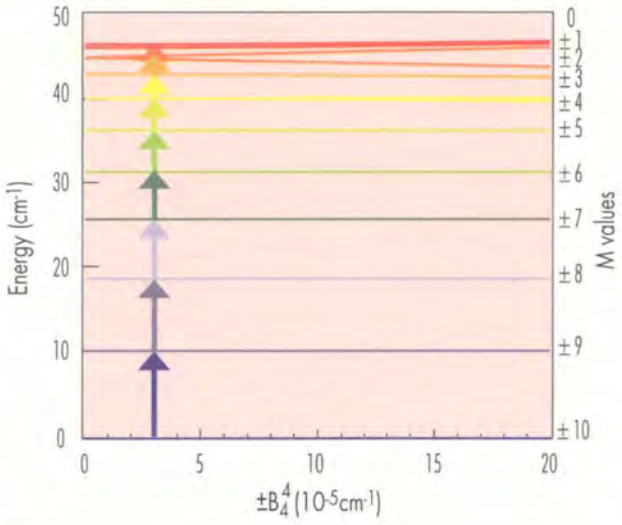

Figure 2: *Energy sublevels of the S = 10 ground state versus the transverse coefficient B_4^4.*

diffractometer G6.1 at LLB. The first inelastic measurements up to 13 meV, were performed on the cold three-axis spectrometer 4F1 at LLB [3]. The present ones with a higher energy resolution were made on the time-of-flight spectrometer IN5 at ILL. The experimental spectra are shown in Fig. 1 for three temperatures. At T = 1.5 K, a well defined excitation is observed at 1.24 meV on the sample energy gain side ($\omega > 0$). It is readily attributed to an excitation from the lowest energy-level (M = ± 10) to the first excited level (M = ± 9). As the temperature increases, higher energy levels are populated so that new excitations appear on both sides of the spectrum. At 23.8 K, we distinctly observe 7 well separated peaks on each side of the spectrum, together with much smaller ones at about ± 0.2 meV (see inset of Fig. 1).

The magnetic neutron cross-section was analysed quantitatively by using the spin Hamiltonian already proposed to interpret electron paramagnetic resonance [4], magnetisation and optical infrared experiments. Due to the neutron selection rules, only the transitions with $\Delta M = 0$ or ± 1 are allowed. When only the diagonal terms are considered, the S = 10 manifold splits into 11 sublevels corresponding to M = ± 10, ± 9, 0. In this case, the ± M degeneracy of these levels is not lifted and when all possible states are populated we expect nine transitions (from M = ±10 to ±9 and so). Seven of these transitions are clearly observed on the spectrum at 23.8 K. The non-equivalent energy-spacing between them arises from the 4th order diagonal term. The transverse term induces a mixing of energy states with different M that becomes more and more effective on approaching the top of the barrier. It is shown in Figure 2 where the energy levels E_i are plotted versus the transverse coefficient B_4^4. The energies of the highest excited states strongly depend on B_4^4 and the degeneracy of some levels is lifted. Figure 3 (top) shows the calculated intensities at 23.8 K for three B_4^4 values. The position, shape and intensity of the low energy peaks are strongly modified, whereas the other peaks remain unaffected. Only B_4^4 values in a very narrow range could explain the low energy features found experimentally. We find that $B_4^4 = \pm 3.0(5) \cdot 10^{-5}$ cm^{-1} gives the best agreement with the data. To compare with experiment (Fig. 3 bottom) we added a small quasielastic background, probably due to hydrogen. The agreement with the calculation is excellent.

The main result of the experiment is the precise determination of the coefficient B_4^4 of the transverse term. This term is very small, but important since only components which do not commute with the longitudinal magnetisation could be responsible for the tunnelling. The fourth order coefficient found here is the lowest order term allowed by the tetragonal symmetry. It allows tunnelling between sublevels with $\Delta M = \pm 4$, as observed in the magnetisation. This could explain the dominant tunnelling process. Other tunnelling transitions between sublevels $\Delta M = \pm 1$ are also observed by magnetisation, and cannot be understood in the expression of the anisotropy with tetragonal symmetry. It suggests that other origins than anisotropy also contribute to the tunnelling, like dipolar coupling, hyperfine interaction or spin-phonon mechanism.

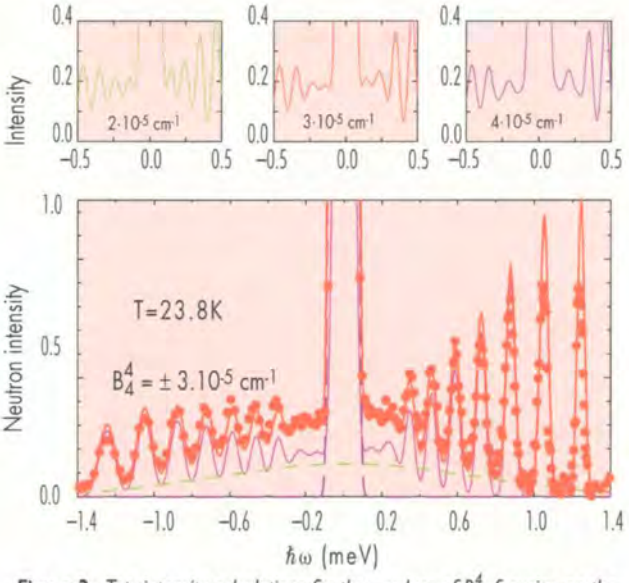

Figure 3: *Top: intensity calculations for three values of B_4^4, focusing on the low energy peaks. Bottom: Energy spectrum. The corrected experimental data are shown by red dots. The intensity calculation (purple line), hydrogen background (green dashed line), elastic intensity (blue dashed line) and the sum of all components (red line) are also shown.*

The above picture mostly relies on the assumption a "single spin" ground-state. This simple picture which neglects the inner features of the cluster, describes the low-energy excitations within the ground state quite well. Very recently a microscopic description of the Mn_{12}-ac was proposed [5], which attempts to describe both low and high-energy excitations observed by neutron scattering. Our new experimental results [6] combined with previous results at higher energies [3], could be a crucial checkpoint for further theoretical work.

References

■ [1] R. Sessoli et al., Nature 365 (1993) 141 ■ [2] L. Thomas et al., Nature 383 (1996) 145 ■ [3] M. Hennion et al., Phys. Rev. B 56 (1997) 8819 ■ [4] A. Barra et al., Phys. Rev. B 56 (1997) 8192 ■ [5] M. I. Katsnelson et al., Phys. Rev. B 59 (1999) 6919 ■ [6] I. Mirebeau et al., Phys. Rev. Lett. 83 (1999) 628.

Chirality in $CsMnBr_3$ – evidence for a new universality class of phase transitions

- V. P. Plakhty, E. Moskvin (PNPI Gatchina St. Petersburg),
- J. Kulda (ILL),
- D. Visser (Univ. Warwick Coventry),
- J. Wosnitza (Physik. Inst. Univ. Karlsruhe),
- R. K. Kremer (MPI Stuttgart).

Using polarised neutrons we have observed spin chirality in the frustrated triangular-lattice antiferromagnet $CsMnBr_3$. We were able to determine both the critical exponent $\beta_C = 0.43(2)$ describing the average chirality in the ordered phase below the Néel temperature $T_N = 8.37$ K and the crossover exponent $\phi_C = 1.27(9)$ corresponding to the dynamical chirality above T_N. These results provide the first experimental proof of the new chiral universality class of phase transitions predicted by theory.

An important feature of phase transitions is their universality, which means that the critical behaviour of physically different systems depends only on the number of the order-parameter components and on the spatial dimensionality of the system. Each universality class has a particular set of exponents which characterises its critical behaviour. The order parameter of frustrated triangular-lattice antiferromagnets, as well as of helimagnets includes, in addition to the ordinary spin variables, S_R, the spin chirality, $C = [S_{R_1} \times S_{R_2}]$, which describes whether the spin structure is a right- or left-handed one. According to Kawamura [1], the chirality results in new universality classes. The conventional critical exponents are modified and, moreover, two new exponents, $\beta_C \approx 0.45$ for the average chirality below the Néel temperature (T_N) and $\gamma_C \approx 0.77$ for the chiral susceptibility above T_N are expected to appear.

Since the observed values of the conventional critical exponents fit different scenarios [2,3] Kawamura's conjecture is under considerable discussion. However, the chiral exponents, were never determined experimentally, in part because of the absence of a suitable technique to produce a single-domain crystal. The original motivation of the present experiment was the proposition by Maleyev [4], suggesting that above the Néel temperature the dynamical chirality, i.e., the projection of the chiral field on the sample magnetisation, results in an inelastic polarisation-dependent cross section that is odd in energy transfer. Its temperature dependence would be described by the crossover chiral exponent, $\phi_C = \beta_C + \gamma_C$.

A convenient representant of planar (XY) frustrated triangular-lattice antiferromagnets is $CsMnBr_3$ whose structure is displayed in Fig. 1. The magnetic moments of the manganese ions lie in the hexagonal plane. The chirality is characterised by the sense of their rotation when passing from a manganese atom to the next one along one of the crystallographic axes in the basal plane. Figure 1 gives an example of domains with spin rotations in the clockwise (A) and counter-clockwise (B) sense.

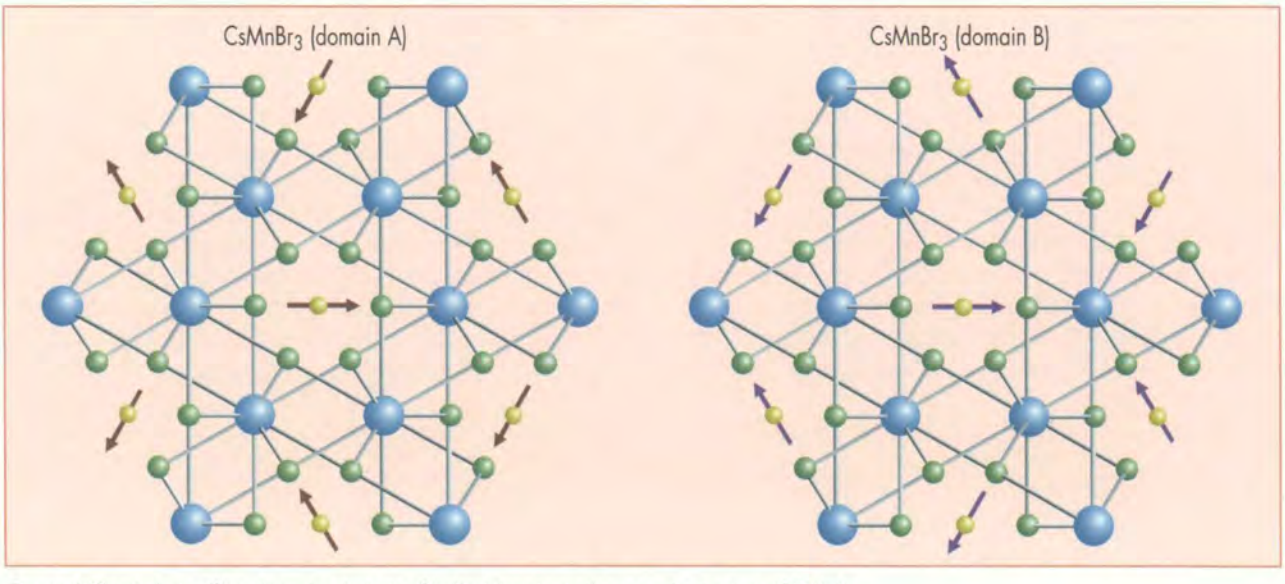

Figure 1: *The clockwise (A) and counter-clockwise (B) chiral domains in the magnetic structure of $CsMnBr_3$.*

The dynamical chirality has been investigated at $Q = (1/3, 1/3, 1)$ using the cold neutron three-axis spectrometer IN14. A crystal of about 3 cm^3 has been mounted in a 4 Tesla horizontal cryomagnet with field parallel to the hexagonal axis. The difference between the scattering intensities of neutrons with incident polarisation parallel and antiparallel to the applied field, $\Delta I(\omega) = I^{\uparrow}(\omega) - I^{\downarrow}(\omega)$, has then been measured. A typical spectrum exhibiting the antisymmetric variation with the energy transfer is shown in the inset of Fig. 2.

An empirical function, a squared Lorentzian multiplied by the energy transfer,

$$\Delta I(\omega) = S\omega\Gamma^3/[\Gamma^2 + (\omega - \omega_0)^2]^2 \quad (1)$$

convoluted with the resolution function has been used to fit these data. According to Ref. [5] the value of the chiral cross-section characterised by S should depend on:

$$\tau = |(T - T_N)/T_N| \text{ as } S = \tau^{-\phi_C} \quad (2)$$

A logarithmic plot of S versus τ is shown in Fig. 2. From the slope at $\tau \geq 0.1$ one obtains the value of the chiral crossover exponent $\phi_C = 1.29(7)$ which is in good agreement with Kawamura's calculated value 1.22(6) for the XY model [1]. At lower τ, the slope decreases, apparently due to the inverse correlation length becoming smaller than the resolution width.

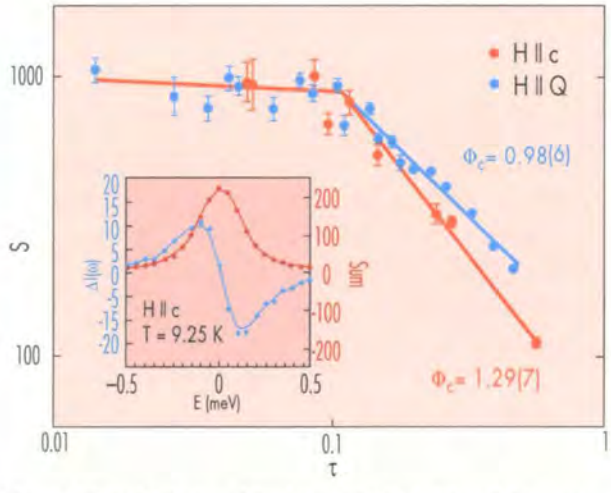

Figure 2: Critical behaviour of the dynamical chirality (above TN) in magnetic field applied along the scattering vector and along the hexagonal axis. Inset: the polarisation-dependent component of the energy spectra.

In the course of the experiment it turned out that in the ordered state, below $T_N = 8.37$ K, different populations of left- and right-handed domains can be frozen in. Their proportion depends, in a random manner, on the cooling history. In the case of unequal populations again a difference in the (1/3,1/3,1) Bragg-peak intensity is observed between the two incident neutron polarisations, parallel and antiparallel to the guide field (about 10 Gauss) along the scattering vector. This part of the study was carried out using polarised thermal neutrons on the IN20 spectrometer ($k = 2.662$ Å^{-1}, Si 111 analyser and PG filter to remove any 2nd order contamination). The sum of the scattered intensities for the two polarisations is proportional to $\tau^{2\beta}$ with the expected exponent $2\beta \approx 0.42$. The difference signal, displayed in Fig. 3, provides the critical exponent $\beta_c \approx 0.43(2)$, being in excellent agreement with Kawamura's theory [1].

Combining the two measured critical exponents, β_c and ϕ_c, the experimental value for the chiral susceptibility exponent, $\gamma_C \approx 0.86(9)$, can be derived. All these results provide support to Kawamura's predictions of a new universality class of chiral phase transitions.

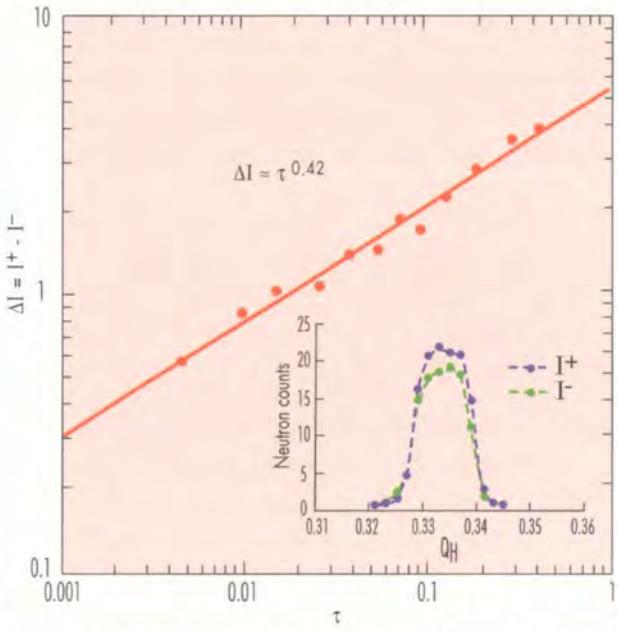

Figure 3: Critical behaviour of the average chirality below TN. Inset: the difference in (1/3, 1/3, 1) Bragg peak intensities I^+, I^-, due to unequal chiral domain population.

References

■ [1] H. Kawamura, J. Phys.: Condens. Matter 10 (1998) 4707 ■ [2] P. Azaria, B. Delamotte, T. Jolicoer, Phys. Rev. Lett. 64 (1990) 3175 ■ [3] S.A. Antonenko And A.I. Sokolov, Phys. Rev. B49 (1994) 15901 ■ [4] S.V. Maleyev, Phys. Rev. Lett. 75 (1995) 4682 ■ [5] V.P. Plakhty, S.V. Maleyev, J. Kulda, J. Wosnitza, D. Visser, E. Moskvin, Europhys. Lett. 48 (1999) 21.

High-precision determination of the antiferromagnetic form-factor of Cr^{3+}

- P. J. Brown (Loughborough University and ILL),
- A. Hillier, H. Humblot, E. Lelièvre-Berna and F. Tasset (ILL),
- J. Dreyer (SPSMS, DRFMC, CEA Grenoble),
- J. B. Forsyth (Clarendon Laboratory, Oxford).

Cryopad II in conjunction with a ^{3}He neutron-spin filter has enabled us to measure the form-factor of the Cr^{3+} ion in Cr_2O_3 out to $\sin\theta/\lambda = 0.75$ Å^{-1}. These new measurements supplement those obtained in a previous experiment in which the limit in $\sin\theta/\lambda$ was restricted by use of IN20 to a maximum of 0.5 Å^{-1}. These measurements provide the first high-precision determination of an antiferromagnetic form-factor with high enough resolution to draw conclusions about the asphericity in the magnetisation due to 3d electrons.

The form-factors of magnetic ions in ferromagnetic and paramagnetic materials have been extensively studied using classical polarised-neutron flipping-ratio measurements and in favourable cases these measurements can be very precise [1]. Such form-factors are much more difficult to measure in antiferromagnetic structures because in antiferromagnets the neutron scattering cross-section is not often polarisation dependent; the classical method is then not applicable. As a consequence, very few measurements of antiferromagnetic form-factors have been made. In the few cases where such measurements have been undertaken they have given very interesting results [2 - 4]. The antiferromagnetic form-factors are more sensitive than ferromagnetic or paramagnetic ones to the effects of covalency. This is because the overlap of positive and negative transferred spin on the ligand ions leads to an actual loss of moment rather than to its redistribution. Up to now no precise measurements of the form factor have been made in antiferromagnetic structures in which the periodicicty of the magnetic and nuclear structures are the same and in which magnetic atoms of opposite spin are related by a centre of symmetry. In such structures, the magnetic and nuclear scattering are superimposed, making their separation difficult. Additionally, the magnetic and nuclear structure factors are in phase quadrature so that there is no interference between them to give a polarisation-dependent cross-section. The newly developed technique of spherical neutron polarimetry [5] allows a precise measurement of the magnetic scattering in such structures, and this can be exploited to determine the antiferromagnetic form-factor.

The technique of neutron polarimetry which we have developed using Cryopad consists in choosing a direction for the incident neutron polarisation and determining the direction of polarisation of the beam scattered by the sample with a chosen momentum and energy transfer. In the present experiment we are looking at elastic Bragg scattering so that the energy transfer is zero. It is convenient to choose three orthogonal directions (**x**,**y**,**z**) for the incident polarisation: **z** perpendicular to the scattering plane, **x** parallel to the momentum transfer vector, and **y** completing the right-handed Cartesian set. The components of the scattered polarisation parallel to the same three directions can be designated P_{ux}, P_{uy}, P_{uz} where the subscript u indicates the direction of incident polarisation (x, y or z).

Cr_2O_3 provides a well known example of an antiferromagnet for which magnetic and nuclear scattering appear in the same Bragg reflections and are in phase quadrature. The components of scattered polarisation in this case can be written [6]:

$$P_{xx} = \beta \qquad P_{xy} = 0 \qquad P_{xz} = \xi$$
$$P_{yx} = 0 \qquad P_{yy} = 1 \qquad P_{yz} = 0$$
$$P_{zx} = -\xi \qquad P_{zy} = 0 \qquad P_{zz} = \beta$$

Where $\beta = (1-\gamma^2)/(1+\gamma^2)$ and $\xi = 2m_y\gamma/(1+\gamma^2)$

γ is the ratio between the magnetic and nuclear structure-factors, and m_y the projection of the magnetic-moment direction on the plane perpendicular to the momentum transfer. There are two possible 180° domains for which m_y is of equal magnitude but opposite in sign. If the volumes of crystal

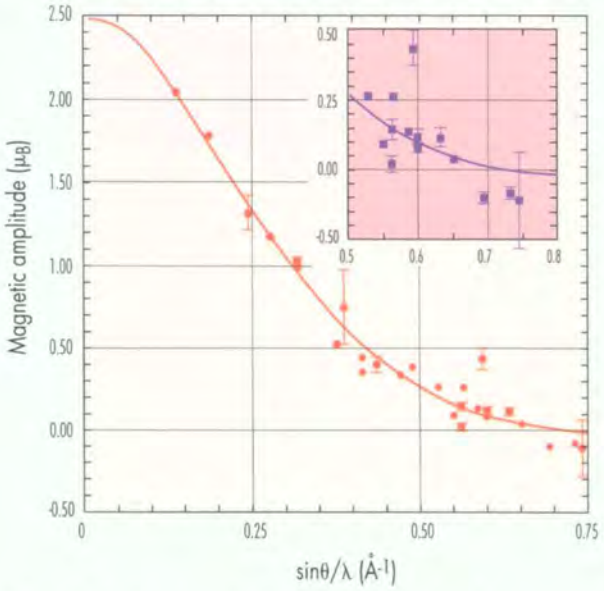

Figure 1: *The experimental values of the magnetic form-factor measured at the h0.ℓ Bragg reflections of Cr_2O_3. The smooth curve is the spin-only free ion form-factor for Cr^{3+} normalised to 2.5 μ_B.*

belonging to the two domains are v+ and v–, the domain ratio is defined as:

$$\eta = (v^+ - v^-)/(v^+ - v^-)$$

and the non-zero off-diagonal terms in the polarisation matrix become :

$$P_{xz} = \eta\xi \quad \text{and} \quad P_{zx} = -\eta\xi.$$

We have already measured the ratios γ of all reflections of the form $h0.\ell$ with $\sin\theta/\lambda < 0.5$ Å^{-1} using Cryopad II on IN20 [6]. These measurements, which were made on two crystals of different sizes in three different degrees of domain imbalance, gave amazingly consistent results which enabled the lower angle part of the Cr^{3+} form factor shown in Fig. 1 to be determined with high precision. It is not, however, possible to extend these measurements to higher $\sin\theta/\lambda$ using IN20 since the highest useable incident wave-vector is 4.1 Å^{-1}.

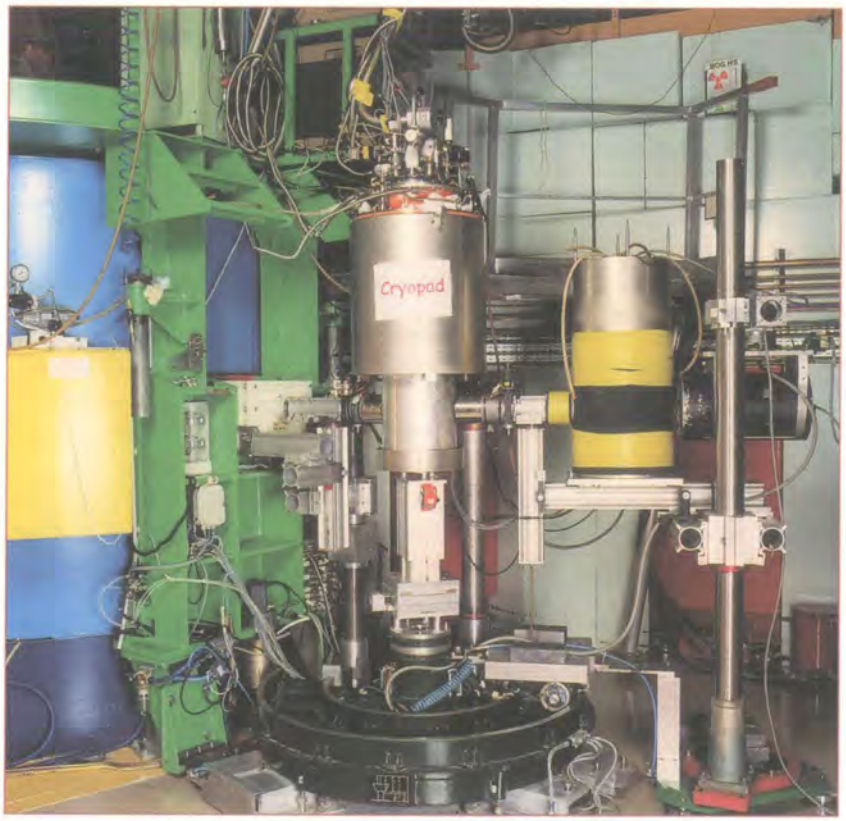

Figure 2: *Cryopad installed on D3 showing the ^{3}He spin filter in the magnetically isolating enclosure "Cryopol".*

We have recently, however, been able to extend our measurements to higher momentum-transfer by installing Cryopad on the hot-source polarised-neutron diffractometer D3 and using the newly available ^{3}He neutron-spin filter to allow polarisation analysis of the diffracted beam. The experimental arrangement is shown in Fig.2.

At the higher $\sin\theta/\lambda$ values the magnetic scattering becomes very weak and it is impractical to carry out the full polarisation analysis. However, if the domain ratio is high and is determined using the lower angle reflections, then it is sufficient to measure just the P_{xz} and P_{zx} components of scattered polarisation. These are linearly rather than quadratically dependent on γ and may be corrected for deficiencies in the transmitted polarisation using the P_{yy} component. Using this method we were able to deduce the magnetic structure-factors of 14 $h0.\ell$ reflections with $\sin\theta/\lambda$ between 0.5 and 0.75 Å^{-1}. Their contributions to the Cr^{3+} form-factor are shown in Fig.1 and are magnified in the inset.

We were able to fit the low angle data to the Cr^{3+} free atom form-factor by assuming a chromium moment of 2.5 μ_B. The rather low value suggests that here is significant covalent transfer to the oxygen ligands.

These lower angle data fit rather well onto a smooth curve. The higher angle data are scattered above and below the curve corresponding to a spherical distribution of moment, this scatter contains information about the deviations from spherical symmetry and can be used to determine the distribution of unpaired electrons amongst the different 3d orbitals.

References

■ [1] H.A. Mook, Phys. Rev. 148 (1966) 495 ■ [2] H.A. Alperin, J. Phys. Soc Japan Supl. B-III (1961) 17 ■ [3] J.W. Lynn, G. Shirane and M. Blume, Phys. Rev. Letters 37 (1976) 154 ■ [4] X.L. Wang, et al., J. Appl. Phys. 69 (1991) 4860 ■ [5] P. J. Brown, J. B. Forsyth and F. Tasset, Proc. R. Soc. London A 442 (1993) 147 ■ [6] P. J. Brown, J. B. Forsyth and F. Tasset, Physica B 267-268 (1999) 215.

Kohlrausch relaxation in random magnets

P. Manuel and R. Cywinski (Univ. St. Andrews),
R. I. Bewley (ISIS, Rutherford Appleton Lab., Chilton),
P. Schleger, B. Farago (ILL).

Whilst the nature of the glass transition is one of the outstanding problems in physics, the spin-glass transition introduces an additional degree of complexity through the orientational disorder of the magnetic spins. It is believed that the clue to the nature of the glass transition in spin glasses lies in the spin dynamics above and close to the glass temperature, yet for the last twenty-five years there has been considerable debate and controversy surrounding the nature of the time dependent spin correlation function in such disordered magnetic systems. Using the amorphous random anisotropy magnets α–Er_7Fe_3 and α–Er_7Ni_3 as model systems, we have used the neutron spin-echo technique to map the evolution of the dynamical spin correlations as a function of temperature. Interestingly, the functional form of the time dependent spin correlations closely follows the stretched exponential form first recognised by Kohlrausch 150 years ago, and points to distribution of relaxation rates which broadens considerably as the glass temperature is approached from above.

In 1847, Kohlrausch [1] discovered that the decay of the residual charge on a glass Leyden jar followed a stretched exponential law defined by $Q(t) = \exp(-(\omega t)^{\beta})$. Since then, this functional form of relaxation has been found to describe a remarkably wide range of physical processes, including phenomena as diverse as the frequency dependence of the complex dielectric constant and the intermediate light scattering function in microgel solutions. The Kohlrausch form, which is often associated with a broad distribution of relaxation times, τ, is also believed by many authors to be characteristic of the time-dependent paramagnetic spin-correlation function, $\langle S(Q,t)S(Q,0)\rangle$, in highly disordered magnets such as spin glasses and random anisotropy systems. Extensive numerical simulations of such random magnets, particularly those by Ogielski [2], have suggested that not only τ but also the exponent β is temperature dependent, taking a value of unity at high temperatures ($4T_g$) and slowly decreasing to 1/3 as the spin freezing or glass temperature, T_g is approached. However, several theoretical models predict that the spin correlation function should instead follow a power-law time dependence. Experimentally it has proved extremely difficult to distinguish between these two models, and the controversy regarding the functional form of the spin dynamics of disordered magnets remains largely unresolved.

Neutron spin-echo is a particularly powerful tool with which to investigate such dynamics. Indeed, it offers the possibility of measuring the spin correlation function directly in the time domain, rather than in the frequency domain as offered by more conventional inelastic neutron scattering techniques. Moreover, the time window covered by the spin-echo technique is of the order of 10^{-8}-10^{-12} s. This window not only effectively bridges the gap between AC susceptibility methods (10^{-1}-10^{-6} s) and conventional neutron scattering techniques (10^{-10}-10^{-13} s), but is also of precisely the same order as predicted for relaxation times in spin glasses and random anisotropy systems close to T_g.

We have performed a series of neutron spin-echo measurements on two amorphous random anisotropy magnets, α-Er_7Fe_3 and α-Er_7Ni_3. Neither the iron nor the nickel carries a magnetic moment in these amorphous alloys, whilst the inherent topological disorder gives rise to crystalline electric fields which are almost random from erbium site to erbium site. Consequently, single ion anisotropy, rather than exchange dominates, and the magnetic ground state is highly disordered [3]. In the present context these random anisotropy alloys have the particular advantage that, although displaying spin-glass-like properties, they have a much higher concentration of magnetic spins than the canonical dilute spin glasses such as CuMn. This feature, together with the relatively large erbium magnetic moment, ensures a sizeable magnetic cross section.

The samples were prepared at the University of St. Andrews, Scotland, using a melt-spinning technique in which molten alloy is ejected onto a rapidly rotating copper wheel, achieving cooling rates of the order of 10^6 K · s^{-1}. The resulting

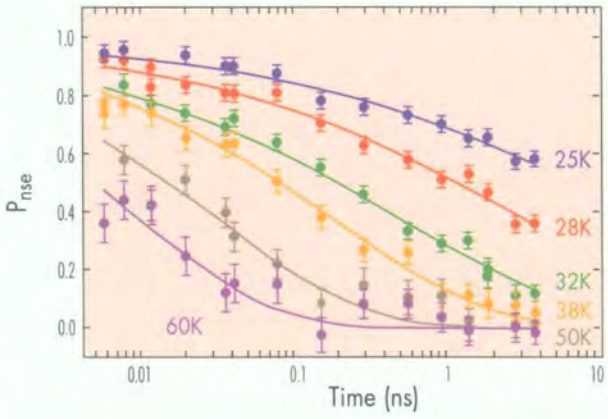

Figure 1: *The normalised spin correlation function Pnse = S(Q,t) / S(Q,0) at Q = 0.12 Å^{-1} for α-Er_7Fe_3 measured by neutron spin-echo for several temperatures. The solid lines represent fits of the Kohlrausch stretched exponential function, $Q(t) = \exp(-(t/\tau)^{\beta})$ to the data. It should be noted that the data are inconsistent with a simple power law dependence upon time.*

amorphous ribbons have a typical width of 2 mm and thickness of 20 μm, and are up to several meters in length. The spin-echo measurements were performed using the IN11 spectrometer with a wavelength of 4.64 Å, allowing relaxation times from $5.75 \cdot 10^{-12}$ s to $3.7 \cdot 10^{-9}$ s to be sampled. The instrumental resolution was determined using spectra collected from the respective samples at 1.5 K, at which temperature all magnetic spins can be assumed to be static.

Figure 1 shows the measured time-dependent spin-correlation function at Q = 0.12 $Å^{-1}$ for the α–Er_7Fe_3 sample at several temperatures up to $2T_g$ (For this sample T_g = 32 K as determined by AC susceptibility). The neutron spin-echo signals were found to be Q-independent within experimental error.

In most paramagnetic metals the spin-spin correlation function is generally of a simple exponential form, and characterised by a single relaxation time, τ. On a plot such as that of Fig. 1, such a relaxation process would appear as a simple rapidly depolarising exponential. As the relaxation rate, τ, changes with temperature the spectra would conserve the same shape but be displaced laterally with respect to one another. However, in the case of the spectra obtained from the α–Er_7Fe_3 sample we observe instead a slow depolarisation associated with a very broad distribution of relaxation times. Moreover, we find that the functional form of the spectra is well described by the Kohlrausch stretched exponential form rather than a simple power law. Fitting the Kohlrausch form to the spin-echo spectra obtained from α–Er_7Fe_3 allows the exponent β and relaxation time τ to be extracted. The temperature dependence of these two parameters is shown in Fig. 2 and 3.

Our neutron-spin echo measurements of the evolution of the spin correlations in the α–Er_7Fe_3 random anisotropy system are in broad agreement with the theoretical predictions of Ogielski [2]. Not only is the time dependence of the correlations well modelled by the Kohlrausch stretched exponential form $Q(t) = \exp(-(t/\tau)^{\beta})$, but the exponent β also decreases with decreasing temperature, approaching 1/3 at T_g as predicted. The temperature dependence of the characteristic relaxation time, τ, shown as a modified Arrhenius plot in Fig. 3, indicates that the spin relaxation arises from a simple activation process. However, two activation regimes, corresponding to two different activation energies, can be distinguished. The crossover point between the regimes coincides with the glass temperature T_g = 32 K. It is likely that whilst the high-temperature regime is dominated by the single ion random anisotropy of the rare earth ions, below T_g exchange interactions begin to play an important, but still not dominant, role. It may be possible in future experiments to investigate this crossover in greater detail by judicious substitution of the rare earth ion to vary the relative balance of exchange to anisotropy.

Neutron spin-echo has therefore provided a unique and invaluable insight into the nature of spin dynamics in disordered spin glass-like magnets as T_g is approached, and it has thereby helped to resolve a long-standing controversy.

We have shown convincingly that it is the 150 year-old Kohlrausch model, rather than a simple power law dependence, that provides an appropriate description of the dynamic spin correlations, at least in the limit of strong random anisotropy considered here. A picture emerges of a broadly distributed relaxation process in which the width of the distribution of relaxation times broadens considerably (i.e. β decreases) as the temperature is lowered. Correspondingly, the mean relaxation time, τ, increases as the glass temperature is approached. However there is also evidence that both β and τ continue to evolve below T_g, although here it might be expected that τ is associated with quite different activation processes to those evident above T_g.

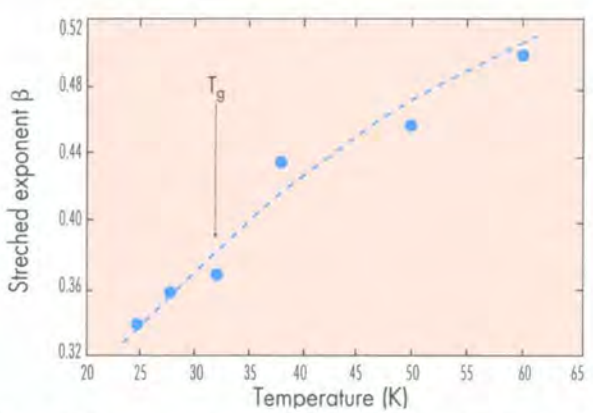

Figure 2: The temperature dependence of the exponent β as a function of temperature. The dashed line is a guide to the eye.

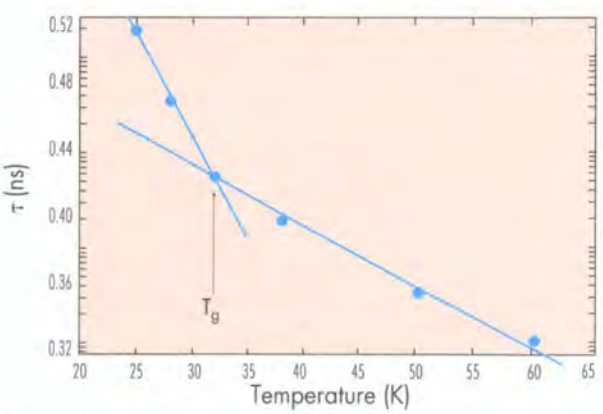

Figure 3: The temperature dependence of the logarithm of the mean relaxation time τ. Note the change in slope of the plot, indicative of a change in the associated activation energy, at T_g = 32 K.

References

■ [1] R. Kohlrausch, Ann. Phys. 12 (1847) 392 ■ [2] A. T. Ogielski, Phys. Rev. B. 32 (1985) 7384 ■ [3] R. I. Bewley and R. Cywinski Phys Rev B. 54 (1996) 15251.

Sublattice interactions in the MFe_4Al_8 compounds

J. A. Paixão (Univ. of Coimbra),
P. J. Brown (ILL),
B. Lebech (Risø Nat. Lab.),
G. H. Lander (Inst. Transuranium Elements, Karlsruhe).

Intermetallics between transition (3d) and rare-earth (4f) elements are vital for many technologies, including those of permanent magnets. However, understanding these interactions at the fundamental level is difficult. We report here a study of stoichiometric MFe_4Al_8 (M = rare-earth and uranium) single crystals. Conflicting explanations of the magnetic interactions of these material have been reported in the past. By using polarised neutrons we have characterised the Fe and M metal magnetism, and their temperature dependence. A further key to their understanding is provided by resonant magnetic scattering of photons (at the ESRF) which characterises the conduction-electron states.

Interactions between elements with d and f magnetism are crucial to many technologies. The richness of their behaviour, as well as the difficulty in establishing detailed models, can be traced partly to the lack of a clear hierarchy of interactions. In addition to the magnetic 3d and 4f states, there are the conduction electrons, which are important in defining the nature of the long-range magnetic order. The MFe_4Al_8 compounds, about which there are many conflicting reports in the literature, including the suggestion that these materials are spin glasses, provide an interesting test case. Using a combination of neutron and synchrotron techniques, including the use in both cases of polarisation analysis, we have established not only magnetic structure as a function of temperatures, but also how the different sublattices interact with one other. This then provides a benchmark for theories addressing these important problems; indeed, one theoretical paper has already appeared.

Since the early work on these systems some 20 years ago [1], it has been recognised that the strongest magnetic interactions are between the Fe atoms and that, at the stoichiometry MFe_4Al_8, it is principally antiferromagnetic in nature. (With further replacement of Fe for Al, up to $MFe_{10}Al_2$ the materials are high-temperature ferromagnets and have potential applications). The tetragonal unit cell is shown in Fig. 1. The M atom is surrounded by 8 Fe atoms. If the latter have an perfect AF configuration, then the molecular field at the M site is zero.

Bulk measurements show the rare-earth materials to be purely antiferromagnetic, and Fe Mössbauer studies [1] establish that the Fe ordering is between 150 and 180 K for all compounds. The use of D10, together with single crystals, allowed us to identify the initial ordering *only* of the Fe sublattice (at 170 K in the Dy material) as incommensurate and probably cycloidal in nature. This was confirmed by using the neutron polarimeter (IN20-cryopad), which showed that the envelope of the Fe modulation is circular. The wavevector is q_{mag} = [0.13, 0.13, 0] and has little temperature dependence. As the temperature is lowered, there is a long-range ordering of the rare-earth component [2]. This starts in $DyFe_4Al_8$ at T_{Dy} ~ 50 K. At the lowest temperature about 60% of the rare-earth moment is ordered; the configuration at ~ 15 K is

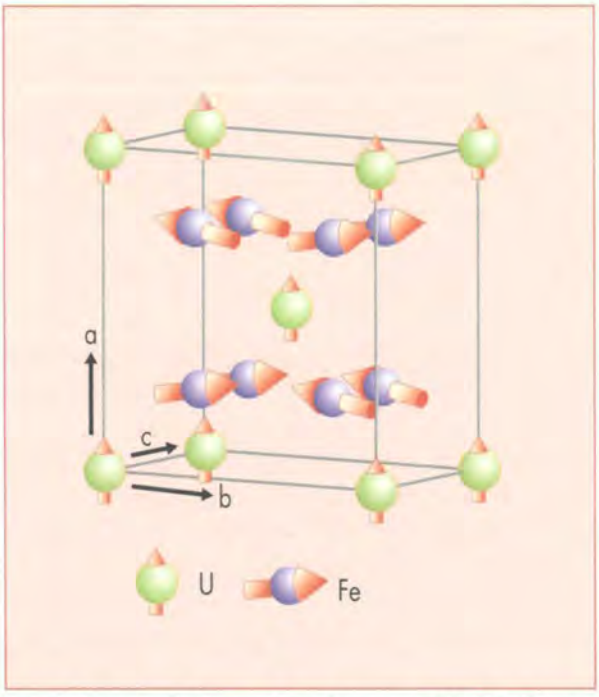

Figure 1: *One unit cell of the crystallographic structure of the MFe_4Al_8 series. Shown also is the unusual magnetic configuration of the UFe_4Al_8 compound. Weak ferromagnetism due to a moment of 0.47(3) μ_B on the U atom is complemented by an almost antiferromagnetic configuration of the Fe sublattice with moments of 1.08(2) μ_B. The Fe moments are canted by 16° in zero field by their interaction with the U sublattice. This canting angle increases with a magnetic field applied in the basal plane. Both sublattices order at ~ 150 K.*

shown in Fig. 2. A careful examination of this cycloid with the neutron polarimeter (IN20-cryopad) shows that the Fe and Dy cycloids are turning in *opposite* directions, but with the same q wavevector. At lower temperatures the ellipticity of the Dy sublattice changes sign and higher-order harmonics (up to 7th order) from the rare-earth moments are seen; however, the envelope of the Fe cycloid remains circular at all temperatures. The higher-order harmonics distort the envelope of the rare-earth cycloid and may be viewed as establishing ferromagnetic interactions between the rare-earth atoms. At the same time, the *disordered* component of the rare-earth moments develop short-range ferromagnetic

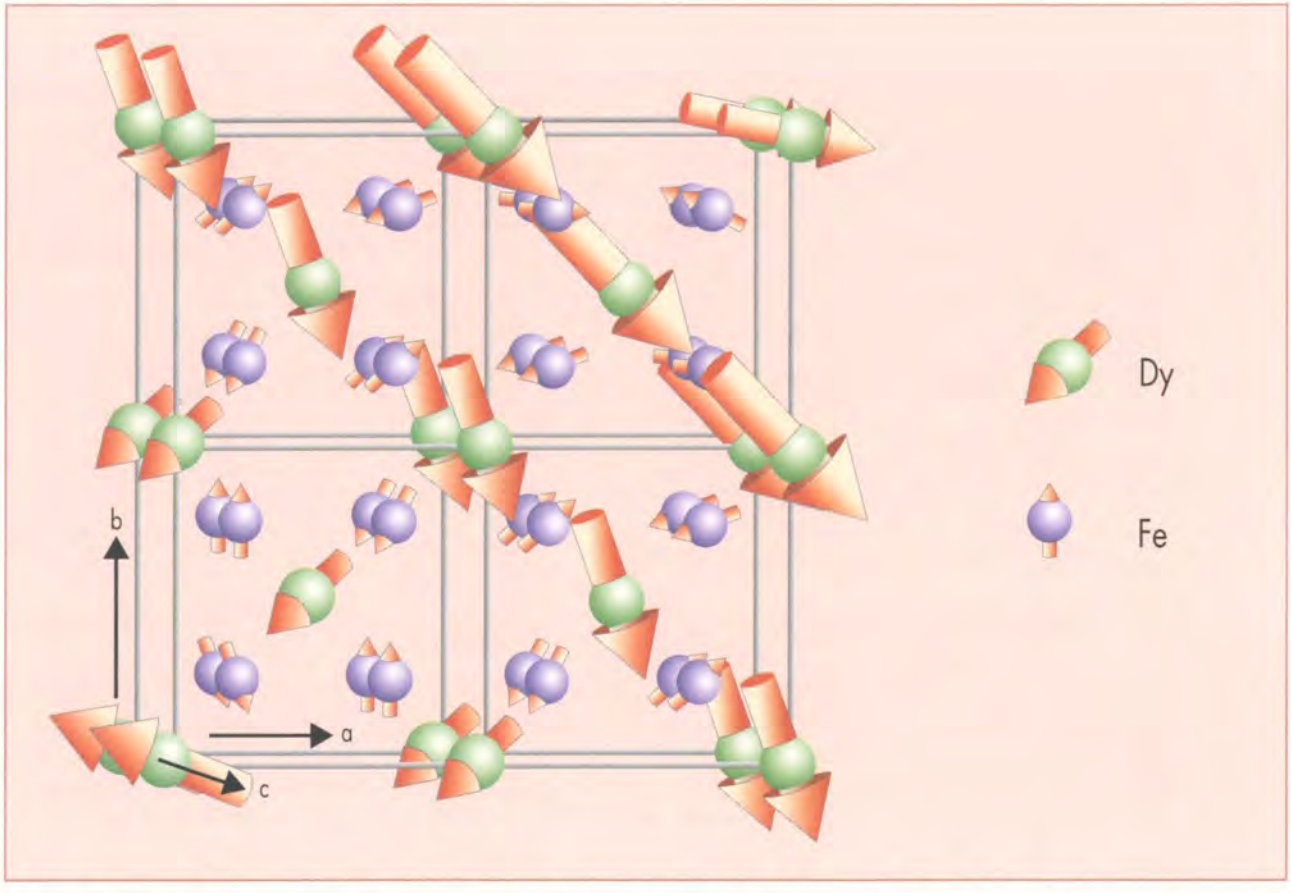

Figure 2: *The complex cycloidal magnetic configuration found in the rare-earth compounds – here shown for $DyFe_4Al_8$ at 15 K. Four unit cells are shown. The magnetic moments are always confined to the ab plane, with their propagation wavevector q_{mag} = [0.13,0.13,0]. Notice that the Fe and Dy cycloids turn in opposite directions. At lower temperature additional higher-order harmonics in the diffraction pattern are observed and signify a further distortion of the envelope of the Dy cycloid. The Fe moment is ≈ 1 μ_B, whereas the Dy moment is ≈ 6 μ_B. The remaining Dy moment (to make up the free-ion moment of 9 μ_B) contributes to ferromagnetic diffuse scattering within the ab plane.*

correlations. This inherent instability of the rare-earth sublattice means that it can be easily modified in a field, an applied field of 0.5 T is sufficient to induce a large moment within the rare-earth sublattice. However, the interaction with the Fe sublattice, which remains antiferromagnetic to very high field, confines the directions of the rare-earth moments to the basal plane. It is this unusual behaviour that led previous authors to claim the materials were spin glasses.

The development with temperature of the ordered rare-earth moment in both the Dy and Ho compounds is shown in Fig. 3. The 110^+ satellite reflection arises from both the Fe and rare-earth sublattices so that it is sensitive to the coherent interference between the two. The different temperature dependencies may be explained by a temperature-independent phase- factor between the modulations of the rare-earth and Fe sublattices.

The final piece to the puzzle is the behaviour of the conduction-electron states. This has been examined by performing resonant x-ray magnetic scattering experiments on the Dy L edges at the ESRF ID20 beamline using the same crystal as for the neutron studies. These x-ray experiments focus on the Dy 5d electrons that belong to the conduction band. We have found that they initially polarise at T_N (170 K); i.e. their interaction with the Fe 3d states is sufficiently strong that they are immediately polarised at T_N rather than T_{Dy} ~ 50 K. Important changes in their polarisation occur at T_{Dy}, which are related to changes in the band splitting of the 5d states [3].

In comparison with the rare earth compounds, the interactions in UFe_4Al_8 are quite different. Previous reports on this material were also confusing, but again single-crystal experiments at Risø and D3 led [4] to a clear-understanding of the magnetic configuration, which is shown in Fig. 1. Here the antiferromagnetic modulation vector is [000] so that no new peaks occur; the unit cell is thus easier to represent, but the interactions are more complex than in the RFe_4Al_8 compounds.

Sandratskii and Kübler [5] have considered this configuration and shown that many of its features can be explained by taking account of the larger (than in the rare earths) spin-orbit coupling and hybridisation between the Fe 3d and U 5f electrons. The local symmetry at the Fe site, which defines the directions for the Fe moments, gives rise to their canting. UFe_4Al_8 is more anisotropic than the RFe_4Al_8 systems, showing interesting hysteresis behaviour when a field is applied within the basal plane [6]. These effects, and the fact that both sublattices order at the same temperature, are a consequence of hybridisation between them [5].

The present measurements illustrate the power of single-crystal neutron and x-ray techniques (in both cases using polarisation analysis) to unravel complex sublattice magnetic interactions in compounds containing d and f electrons. They also demonstrate the profound differences in behaviour between the rare-earths and actinides in an isostructural series.

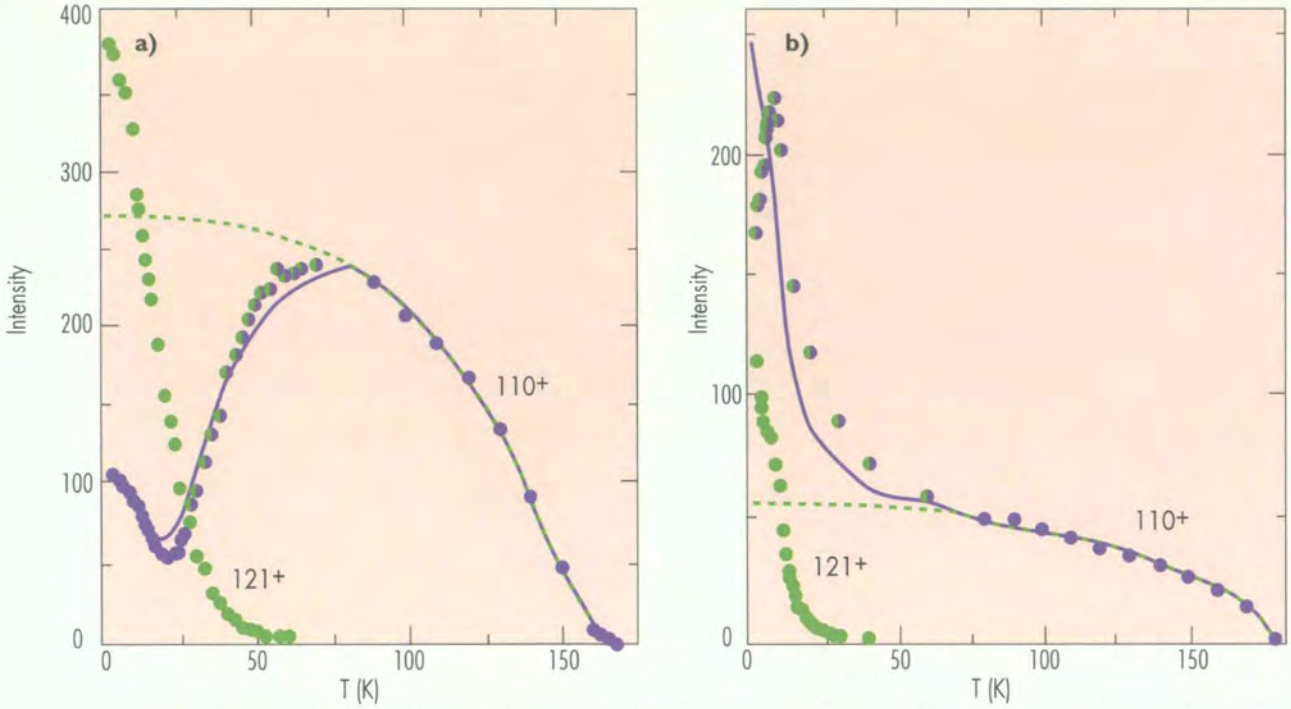

Figure 3: *The temperature dependencies of the 110⁺ and 121⁺ magnetic satellites. The former arise from both sublattices, whereas the latter arise from only the rare-earth sublattice. The changes at $T_{Dy} \sim 50$ K in panel* ***a)*** *and $T_{Ho} \sim 80$ K in panel* ***b)*** *are due to the coherent interference between the two sublattices and indicates the appearance of long-range component at the rare-earth site. This is not observed readily at the 121⁺ position as the amplitude squared is too small. The dashed lines represent the extension of the intensity from the Fe sublattice only, and the solid lines are drawn taking into account a constant (with temperature) phase factor between the Fe and rare-earth magnetic sublattices. These phase factors are 42(6)° for the Dy compound and 150(8)° for the Ho compound. Thus, in panel* ***a)*** *we observe almost constructive interference, whereas in* ***b)*** *the interference is mostly destructive. The drop in intensity in panel* ***a)*** *for $DyFe_4Al_8$ below ≈ 12 K is associated with the appearance of higher-harmonics, which are not included in our simple model.*

References

■ [1] K. H. J. Buschow and A. M. van der Kraan, J. Phys. F 8 (1978) 921 ■ [2] J. A. Paixão et al., Phys. Rev. B, in press
■ [3] S. Langridge et al., Phys. Rev. Letters 82 (1999) 2187 ■ [4] J. A. Paixão et al., Phys. Rev. B 55 (1997) 14370
■ [5] L. M. Sandratskii and J. Kübler, Phys. Rev. B 60 (1999) R6961 ■ [6] G. Bonfait et al., Phys. Rev. B 53 (1996) R480.

Ternary fission as a testing ground for conservation laws

P. Jesinger, A. Kötzle, F. Gönnenwein (Physik. Institut Univ., Tübingen),
G. Petrov, A. Gagarski, V. Petrova (PNPI Gatchina, St. Petersburg),
M. Mutterer, J. von Kalben, S. R. Neumaier (Inst. Kernphysik, Darmstadt),
G. Danilyan, V. Pavlov, V. Chvatchkin (ITEP, Moscow),
W. H. Trzaska (Dep. Physics, Jyväskylä),
V. Nesvishevsky, O. Zimmer (ILL).

The correlations between neutron spin and the momenta of the outgoing fission fragments and ternary charged particles have been investigated in ternary fission of actinide nuclei induced by cold polarised neutrons. These correlations challenge the validity of fundamental conservation laws like time reversal and space parity. While probing time reversal invariance an unexpectedly large effect has been discovered whose mere size appears to rule out violation of time reversal invariance as being responsible for the observation. On the other hand parity non-conservation for ternary fission has been clearly established. This has interesting implications for the process at hand. Furthermore, surprising features of the left-right asymmetries in the emission of fission fragments relative to the incoming polarised beam are catching the eye with the sign of the asymmetry depending on the direction of emission of the ternary particles with respect to the reaction plane. These new findings have attracted interest from theoreticians but a generally accepted theory is still missing.

Time Reversal Invariance

In an ILL report of 1988, it was suggested by K. Schreckenbach [1] that ternary fission might be a nuclear reaction well suited to test Time Reversal Invariance (TRI). In ternary fission three charged particles show up in the final state of a scissioning nucleus. Besides the two main fission fragments (FF) a third charged particle, usually an α-particle or a triton, is emitted. In most cases the ternary particle (TP) is ejected roughly at right angles relative to the fission axis defined by the two FFs receding in opposite directions. The suggestion was that, in analogy to tests of TRI in the decay of free polarised neutrons, also in ternary fission induced by polarised neutrons a triple correlation between neutron spin $\hat{\sigma}$ and the momenta of both, the momenta of FFs $\hat{p}_{LF}$ and the momenta of TPs $\hat{p}_{TP}$ could be investigated. The observable proposed to be studied is:

$$B = \hat{\sigma} \cdot [\hat{p}_{LF} \times \hat{p}_{TP}]. \qquad (1)$$

with all vectors being normalised to unit length and with $\hat{p}_{LF}$ being the momentum of the light fragment by convention.

B runs from – 1 to + 1. The correlation observable B is odd under time reversal and even under the parity operation. Any non-zero expectation value <B> for the correlation could indicate a violation of TRI.

So far two fission reactions have been analysed on the polarised beam facility PF1: ^{233}U (n, f) and ^{235}U (n, f). Two independent reaction chambers were mounted sharing the neutron beam. The measuring principle is different in the two chambers. One of the chambers was developed in Gatchina. It relies on fast ionisation chambers to detect any charged

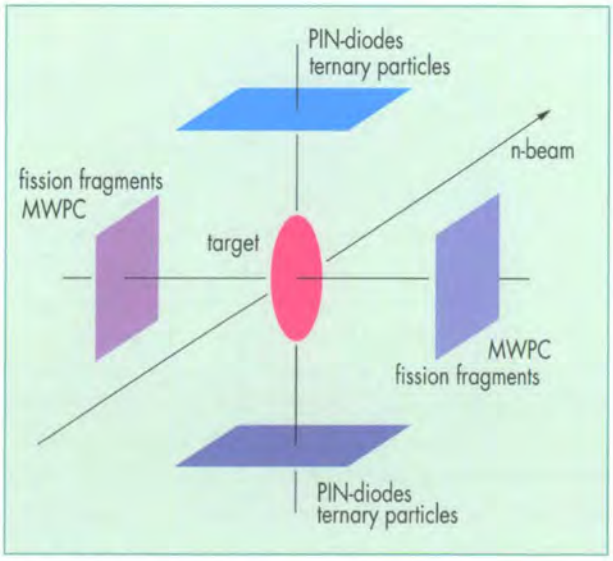

Figure 1: *The experimental setup used on PF1.*

particles. It could be demonstrated that the novel technique works satisfactorily and first results were obtained. The second chamber was built in Tübingen. In the following, mainly results from this latter chamber are reported. A sketch of the experimental setup is given in Fig. 1. The longitudinally polarised neutron beam hits the fissile target and both, the fission fragments and the ternary particles are observed perpendicularly to the neutron beam. The fragment and ternary particle detectors are likewise positioned at right angles relative to each other. This geometry was chosen to give the search for a non-vanishing expectation value <B> maximum sensitivity. The detectors for the two fragments to be registered in coincidence are multiwire proportional counters (MWPC). The ternary particles are identified by PIN diodes of rectangular shape (3×3 cm^2). With these pn-junctions α-particles are distinguished from tritons by inspecting the risetimes of the current signals in the diodes.

A total of up to 40 diodes are grouped into two arrays of 20 diodes each and mounted above and below the reaction plane defined by the neutron beam and the fission axis (Fig. 1). To get rid of instrumental asymmetries the spin flip technique is employed. A current sheet placed in the polarised neutron beam with the current being switched at a rate of 1 Hz serves as a very efficient spin flipper. The technique allows to determine from the count rate differences for the two spin helicities directly a quantity D, called the correlation coefficient, which is linked to the expectation value <B> to good approximation by $D = 3 \cdot \langle B \rangle$.

Since from theory the absolute size for a non-vanishing correlation <B> due to the violation of TRI is expected to be in the 10^{-7} range, the experiment had to aim at large count rates and long measuring times to reach statistically significant results. With a polarised beam flux of $6 \cdot 10^8$ n/cm^2·s and 5 mg of highly enriched ^{233}U or ^{235}U isotopes, count rates of 10^6 coincident fission fragments per sec. and $3 \cdot 10^2$ ternary events per sec. are reached. Beam times allocated so far to these experiments were 2 cycles.

In the following all results are quoted in terms of the correlation coefficient D calculated from the raw data. Any corrections are only to increase the modulus of D. For the two reactions under study the values found for D are

$D = -(1.81 \pm 0.10) \cdot 10^{-3}$ for the ^{233}U target and

$D = +(0.52 \pm 0.06) \cdot 10^{-3}$ for the ^{235}U target.

A first surprise in these results comes from the sizes of the coefficient D and, hence, also the expectation values of the observable B which are huge, at least in comparison to expectations. This raises doubts whether it is really a violation of TRI which is becoming manifest in the present experiments. A further surprise is the change in sign for D (and <B>) for the two reactions studied. Probably, this points to a change in sign of the polarisation of the two compound nuclei which depends on the relative orientations of target and neutron spin in the capture state. Physically it is the spin of the compound nucleus and not the neutron spin which steers the correlation.

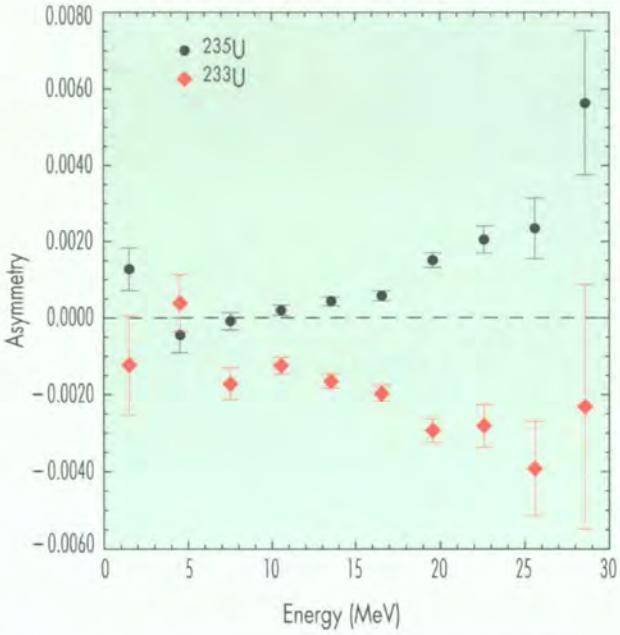

Figure 2: *Dependence of the correlation on energy of the ternary particle for ^{233}U and ^{235}U.*

Offhand it is argued that some initial or final state interactions between the partners of the reaction might be responsible for the observations. However, so far it is not clear which intricate mechanism could be at work and bring about the above correlations.

To gain more detailed information on the characteristics of the triple correlation, the dependence of the coefficient D has been evaluated as a function of both, fragment masses and/or energies and ternary particle energies. As shown in Fig. 2, a very strong variation of the correlation is disclosed as a function of ternary particle energy. For both reactions studied the modulus of the correlation coefficient D increases with the energy of the ternary particle. The pronounced effect appears to be difficult to reconcile with initial state interactions. More details on the experiments are given in [2] and [3].

Parity Non-Conservation and Left-Right Asymmetries

It is a remarkable feature of the target and detector assembly sketched in Fig. 1 that, upon turning around the spin $\hat{\sigma}$ of the incoming neutron into a plane at right angles to the beam direction, experiments with completely different physics can be performed. Two classes of experiments may be distinguished for neutron beams polarised perpendicularly: either probing parity non-conservation (PNC) or measuring left-right asymmetries (LRA). For the neutron spin pointing towards the fragment detectors the pseudoscalar observable

$$A_{PNC} = \hat{\sigma} \cdot \hat{p}_{LF} \qquad (2)$$

and its expectation value $\langle A_{PNC} \rangle$ can be analysed. The ternary particle is only required in this case to be in coincidence with the FFs and, hence, to identify ternary fission. A non-zero expectation value $\langle A_{PNC} \rangle$ is an unambiguous signature for PNC. As with the triple correlation experiments, from the difference in count rates for the two spin orientations from

the flip technique a PNC coefficient α_{PNC} is derived from which the quantity of physical interest $\langle A_{PNC} \rangle$ is calculated through the relation $\alpha_{PNC} = 3 \cdot \langle A_{PNC} \rangle$. The result obtained for the ^{233}U (n, f) reaction is

$$\alpha_{PNC} = (0.32 \pm 0.08) \cdot 10^{-3}.$$

Thus, similar to binary fission, where PNC was discovered more than twenty years ago [4], also in ternary fission parity is non-conserved. But more striking is the fact that the PNC coefficient for ternary fission established here has the same size within experimental uncertainty as the one known since long for binary fission. This property of ternary fission was already disclosed in former work at ILL by a group from ITEP, Moscow [5]. This has interesting implications for the ternary process which are discussed elsewhere [6].

In the second class of experiments the neutron spin is required to face the TP detectors. For this choice of the polarisation the left-right asymmetry of fragment emission may be investigated with the observable:

$$A_{LRA} = \hat{\sigma} \cdot [\hat{p}_n \times \hat{p}_{LF}] \qquad (3)$$

and the corresponding expectation values $\langle A_{LRA} \rangle$. In eq. (3) $\hat{p}_n$ is the unit vector of neutron momentum. The LRA is to be traced to an interference effect between incoming s- and p-waves of the neutron. Again from the count rates of the spinflip technique an LRA coefficient α_{LRA} is deduced which is related to the expectation value $\langle A_{LRA} \rangle$ through $\alpha_{LRA} = 3 \cdot \langle A_{LRA} \rangle$. It should be stressed that similar to the PNC studies also here it has only to be made sure that a TP has been emitted in coincidence with two fragments.

In the LRA experiment another strange observation was made. Referring to Fig. 1 the sign of the LRA coefficient for fragments from ternary fission is found to depend on whether the TP is ejected upwards or downwards, i.e. parallel or antiparallel to neutron spin, while the modulus of the asymmetry is virtually the same for the two directions of TP emission. The modulus is determined for the ^{233}U (n, f) reaction to be:

$$|\alpha_{LRA}| = (0.56 \pm 0.17) \cdot 10^{-3}$$

Yet a different type of PNC and LRA experiments is performed by inspecting the ternary particles instead of the fission fragments. Formally, this is simply achieved by replacing in eqs.(2) and (3) the FF momentum $\hat{p}_{LF}$ by the TP momentum $\hat{p}_{TP}$. In contrast to the fragments, the PNC and LRA coefficients measured for the ternary particles are all compatible with nil. This demonstrates that the main fission fragments and the light ternary particles are not on an equal footing.

Conclusion

Apart from the PNC effects, all of the other results quoted are new. They are intriguing not only because they were not anticipated, but also because even after their discovery no concept for a possible mechanism behind the triple correlation and the curious left-right asymmetries has been proposed so far. It is not clear whether the characteristics of the ternary disintegration process of a fissioning nucleus or violations of conservation laws are responsible for these results.

Finally, it should be mentioned that, beyond the panoply of correlation studies described, in the course of experiments some 10^9 ternary and multiple particle events were collected and registered on tape, and this huge data base enables the detailed investigation of yields and energetic properties of quaternary fission. In quaternary fission two light charged particles in addition to the two main fission fragments are formed in the decay of a heavy nucleus. However, quaternary fission should be the topic of a separate report.

Acknowledgements

This work was supported by grants from BMBF, Bonn and RFBR, Moscow.

References

■ [1] K. Schreckenbach, Internal ILL Report 88SCOCT, 1988 ■ [2] P. Jesinger et al. Nucl. Instr. and Meth. A440 (2000) 618 ■ [3] A. Gagarski et al. "Int. Sem. on Interactions of Neutrons with Nuclei", ed. W. Furman, Dubna 1999, 279 ■ [4] G. Danilyan et al., JETP lett 26 (1977) 186 ■ [5] A.V. Belozerov et al., JEPT lett 54 (1991) 133 ■ [6] F. Gonnenwein et al., Nucl. Phys. A567 (1994) 303.

Testing the proportionality of the neutron's gravitational and inertial mass

G. van der Zouw and A. Zeilinger (Univ. Wien),
P. Høghøj, R. Gähler, P. Geltenbort, J. Butterworth (ILL).

In classical physics the gravitational and the inertial mass of a body are the same up to a proportionality constant. This forms the basis of the General Theory of Relativity. The observation of gravity-induced phase shifts was one of the earliest successes in the field of neutron interferometry and demonstrates, in the quantum limit, the influence of the gravitational potential on systems described by quantum mechanics. However, after corrections, these experiments did not confirm the equivalence of the neutron's gravitational and inertial mass. Because all earlier experiments were carried out with one type of neutron interferometer only, we have repeated them with our interferometer for very-cold-neutrons at ILL. We can now confirm the equivalence of the neutron's gravitational and inertial mass, excluding at the same time earlier experimental results on a 1-σ level.

By dropping masses off the tower of Pisa, Galileo Galilei for the first time demonstrated that all bodies subject only to the gravitational force of the Earth fall the same way, when starting from the same position with the same velocity. In Newton's theory of gravity this is explained phenomenologically by the fact that the gravitational mass and the inertial mass of a body are proportional to each other and therefore cancel in the equation of motion. Einstein's General Theory of Relativity promoted this phenomenon to a ruling principle, called the *weak equivalence principle*, stating that an accelerating system is indistinguishable from a system in a gravitational field.

It is interesting to ask what happens when the equivalence principle is applied to a system, such as the neutron, which is clearly governed by the laws of quantum mechanics. The present consensus is that the principle of proportionality between gravitational and inertial mass also holds for quantum mechanical systems, but not the classically equivalent principle of equal paths [1]. In practice this means that the quantum system can be described by a Schrödinger equation that contains the gravitational potential.

Until 1975 there had been no experiment that demonstrated directly the effect of this gravitational potential *in the quantum limit*, i.e. in the limit where Planck's constant is different from zero. In that year Collela, Overhauser and Werner (COW) [2] demonstrated what has come to be known as *gravity-induced quantum interference*. In their experiment a neutron interferometer made out of a silicon single-crystal was rotated about its optical axis, resulting in a difference in height and thus in gravitational potential energy between the two paths the neutron can take (see Fig. 1).

The potential difference causes a phase shift given by

$$\phi = \frac{2\pi m_i m_g}{h^2} A g \lambda \sin\alpha \,.$$

In this equation m_i and m_g are the inertial mass and gravitational mass of the neutron, respectively, h is Planck's constant, A is the area enclosed by the interferometer, g is the local gravitational acceleration, as measured by a classical device, λ is the neutron de Broglie wavelength and α is the tilt angle. By comparing the measured value of $m_i m_g$ with, for instance, m_i^2 known from other experiments, one can test the proportionality of gravitational and inertial mass. The original COW experiments and subsequent, more sophisticated versions of it, showed beautiful agreement with theoretical prediction within the error of 1%.

However, years later it was pointed out by Bonse and Wroblewski [3] and by Horne [4], independently, that a correction for dynamical diffraction effects inside the silicon slabs, ignored in the original calculations, leads to a *discrepancy* between theory and experiment of the order – 4%.

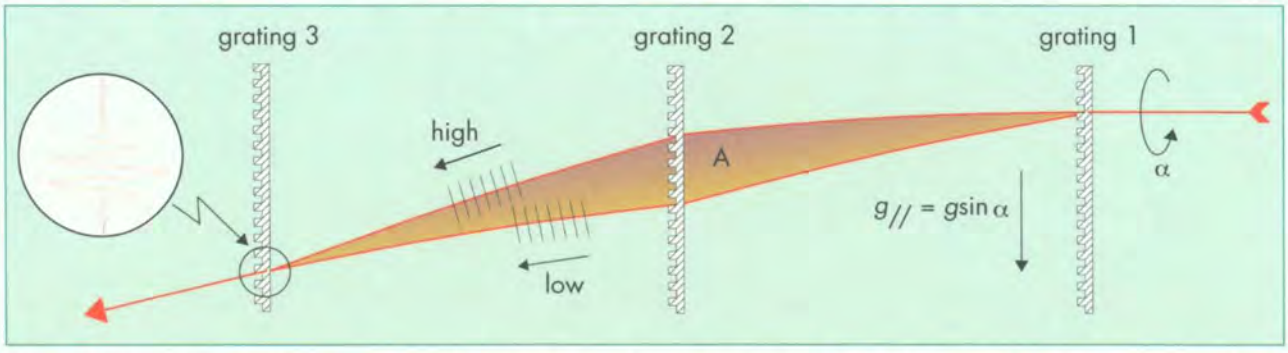

Figure 1: *When a neutron interferometer (here seen from above) is rotated around its optical axis by an angle α the neutron wave in one path travels at a greater height than in the other, causing a phase shift between the two waves due to the difference in gravitational potential energy. This phase difference is measured by interferometry. At the same time the overall envelope of the interference pattern, as shown in the "magnification", shifts by the same amount as the fringes, representing the bending of the classical trajectories.*

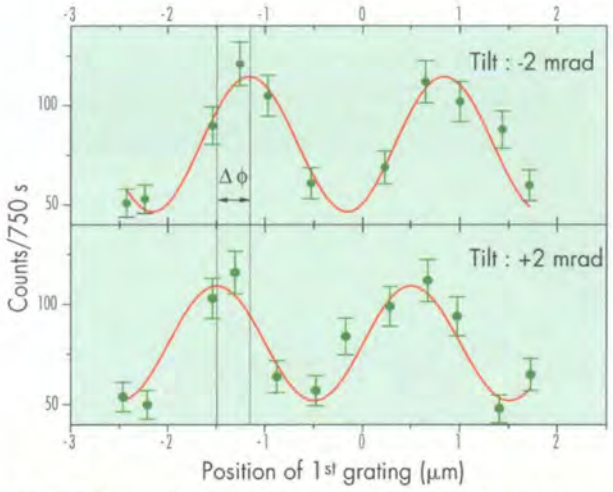

Figure 2: *Two interferograms at tilt angles +2 mrad and –2 mrad showing the count-rate as function of the first grating position. The displacement of the sinusoidal pattern between the top and the bottom graph corresponds to a gravitational phase difference of about 19.6 rad (modulo 2π).*

This discovery was followed by a series of new experiments, of which the recent experiment by Littrell et al. [5] is the most advanced. It nevertheless still shows a $-1.0 \pm 0.1\%$ deviation from theory.

It is important to note that *all these experiment were carried out using essentially the same neutron interferometer*. Recent experiments by Peters et al. [6] using an *atomic* fountain interferometer show no significant discrepancies on a level of 7 parts in 10^9, so the neutron results are most likely due to an unknown systematic effect. To verify this hypothesis, to be sure that no fundamental property of the neutron was overlooked, we carried out a series of COW experiments using a different type of instrument, namely our interferometer for very cold neutrons (VCN) at ILL [7].

This interferometer is based on the principle that for VCN, we can use micro-fabricated quartz glass refractive gratings as beam splitting elements, instead slabs of silicon crystal. Because of the large neutron wavelength of about 100 Å and its large length (1.016 m) our interferometer is also about 50 times more sensitive to gravity than the COW one.

Up to this year, however, we had not been able to measure all parameters in our experiment with high enough accuracy to clearly distinguish between theoretical prediction and earlier experiments. Especially, the uncertainty in the spectrum of our neutron beam contributed to the experimental error of about 1% [8]. This is too large to distinguish between theory and earlier results.

This year we started a new series of measurements, but instead of the full available neutron spectrum, we used only a narrow band that is well-defined by a multi-layer based filter ($\Delta\lambda/\lambda \approx 0.1$) made at ILL. This not only decreases the error from the measurement of the spectrum, but, also makes it possible to measure over a larger range of tilt angles α, which also results in a better accuracy. It, of course, reduces the already low count-rate further to about 0.1 n/s.

The experiment itself consisted of two independent series of measurements. In the first series we measured the gravitational phase shift itself by taking interferograms at different tilt angles. An interferometer (as shown in Fig. 2) measures the intensity as a function of a gravity-independent phase shift: the position of one of the gratings. A change in tilt angle causes this sinusoidal pattern to shift, which directly gives the difference in gravitational phase. The second series of measurements consisted of an accurate time-of-flight measurement of the spectrum detected by the same detector at the same position as during the first series.

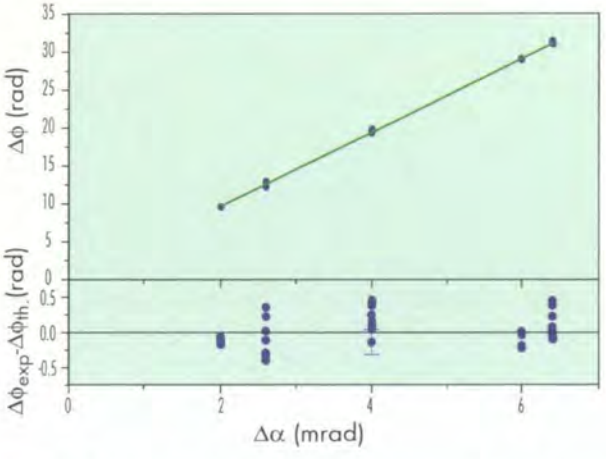

Figure 3: *(Top) Measured gravitationally induced phase shift plotted as function of the difference in tilt angle. Each point represents one set of interferograms as in fig. 2. The line is the theoretical prediction. (Bottom) Measured phase shift minus theoretical prediction. One typical errorbar is indicated.*

In Fig. 3, we show our final results. The graph shows the differences in gravitational phase as a function of the difference in tilt angle. Comparing with the theoretical prediction, calculated from the spectrum measurement, we find no discrepancy on the level of accuracy of about 0.4%. In other words, within the measurement error we have experimentally demonstrated that the gravitational and the inertial mass of the neutron are the same in the quantum limit. At the same time this result *excludes* all earlier results from single-crystal interferometers on the 1-σ level. We thus could clarify a long-standing issue in the field of neutron interferometry.

Acknowledgements

We thank Th. Brenner, C. Gomez and W. Graf for their technical assistance at ILL.

This work was supported by the Austrian Science Foundation FWF, Project No. S65-03. GvdZ gratefully acknowledges support from the TMR European Network No. ERB-FMRX-CT96-0057.

References

■ [1] J. Anandan, Phys. Rev. D 15 (1976) 1448 ■ [2] R. Colella, et al., Phys. Rev. Let. 34 (1975) 1472 ■ [3] U. Bonse and T. Wroblewski, Phys. Rev. D 30 (1984) 1214 ■ [4] M. A. Horne, Physica B 137 (1986) 260. [5] K. C. Littrell, et al., Phys. Rev. A 56 (1997) 1767 ■ [6] A. Peters, et al., Nature 400 (1999) 849 ■ [7] M. Gruber, et al., Phys. Lett. A 140 (1989) 363 ■ [8] G. van der Zouw, et al., Nucl. Instr. and Meth. A 440 (2000) 568.

Excitations of superfluid helium in porous media

B. Fåk, O. Plantevin (CEA Grenoble),
H. R. Glyde, N. Mulders (Univ. of Delaware),
G. Coddens (LLB Saclay),
H. Schober (ILL).

The elementary excitations of superfluid ^{4}He, characterised by the phonon-roton dispersion curve, have been studied in great detail over the last forty years since the first observation of the roton in a pioneering neutron-scattering experiment in Stockholm in 1957 [1]. The interest today is turning towards the effect of disorder and confinement on these excitations, when e.g. helium is immersed in porous media. The key word is here "dirty bosons". We have studied the microscopic dynamics of superfluid ^{4}He in porous media using the IN12 and IN6 spectrometers at the ILL. These measurements suggest that the modifications of the macroscopic properties (specific heat, superfluid fraction) are related to the existence of two-dimensional (2D) excitations rather than to modifications of the three-dimensional (3D) bulk excitations, such as the roton.

The porous media used in this investigation are aerogel and Vycor. Aerogel is a highly tenuous structure of irregularly connected silica (SiO_2) strands with a large distribution of pore sizes and porosities ranging from 85 to 99.5%. Vycor can be considered as a network of worm-like channels in silica with a rather well defined diameter of about 70 Å and a porosity of about 30%. When superfluid helium is immersed in these media, the macroscopic properties are modified due to confinement and/or disorder [2]. In aerogel, the superfluid transition temperature T_s is lowered from that of the bulk ($T_\lambda = 2.17$ K) by only a few mK, while the critical exponent ζ in the expression for the temperature dependence of the superfluid fraction $\rho_s(T)/\rho = (1-T/T_s)^\zeta$ is modified, indicating a possible change in the universality class. In Vycor on the other hand, T_s is lowered to 1.95 K, while ζ is the same as in the bulk.

Our measurements on ^{4}He in aerogel show that the 3D bulk-like excitations are the same as in bulk superfluid helium. In particular, the temperature dependence of the roton energy (Fig. 1) and the roton width is the same in aerogel as in bulk. There are no observable deviations from the bulk behaviour that could explain the differences in the macroscopic properties.

However, additional intensity is observed slightly below the roton energy, as illustrated in Fig. 2 for different filling fractions. The intensity of this low-energy mode saturates quite rapidly with filling fraction, in contrast to the bulk mode whose intensity increases linearly with filling. This suggests that the low-energy mode is propagating in the first liquid layers near the substrate (the two first layers are solid).

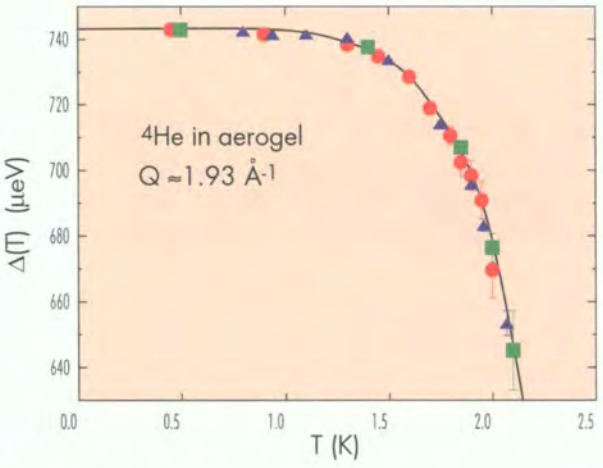

Figure 1: *Temperature dependence of the roton energy measured for different aerogels on IN12 (red and green) and IN6 (blue). No deviations are found from bulk ^{4}He (line).*

Similar excitations have been observed in thin films of helium on graphite surfaces [3,4], but the present result is the first observation of layer modes in aerogel. The dispersion of the layer mode is similar to that of the bulk roton, as shown in the inset of Fig. 2, but with a lower energy.

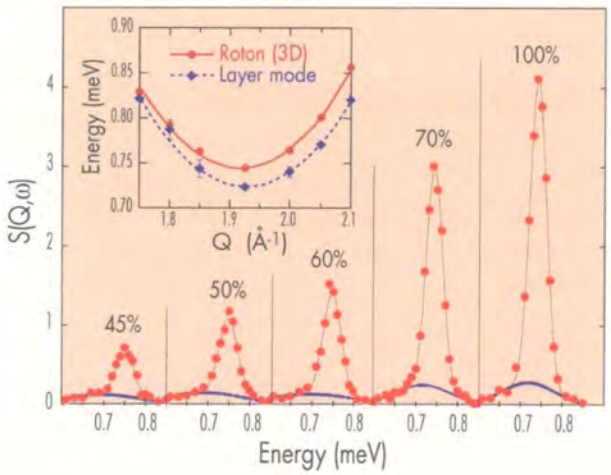

Figure 2: *Dynamical structure-factor for superfluid ^{4}He in 87% porous aerogel at T = 0.5 K for different percentage fillings measured on IN12. The thick blue line shows the 2D layer mode. The inset shows the energy of the bulk 3D roton and the 2D layer mode.*

Layer modes are also observed in our measurements on helium in fully filled Vycor. The energies of these modes are smaller than that of the bulk roton, and consistent with the observed specific heat and $\rho_s(T)/\rho$ at low temperatures. The 3D phonon-roton excitations are very similar to bulk helium, as shown in Fig. 3, with the same energy and width, and the same temperature dependence. With increasing temperature, the intensity of the main (roton) peak decreases. In bulk liquid ^{4}He, the intensity of the roton scales approximately with the superfluid fraction $\rho_s(T)/\rho$ and disappears at $T_\lambda = 2.17$ K [5], where $\rho_s/\rho = 0$. Above T_λ, only a very broad contribution is seen. We find that the roton intensity of helium in Vycor does *not* scale with ρ_s/ρ in Vycor. Specifically, there is a clear peak at T = 1.99 K, which is above the superfluid transition temperature $T_s = 1.95$ K in Vycor. The peak has disappeared by T = 2.3 K. Theoretical work [6] suggests that the roton intensity should scale with the Bose condensate fraction $n_0(T)$ rather than $\rho_s(T)$.

The results in Vycor suggest that if the intensity scales with $n_0(T)$, then the Bose-Einstein condensation temperature (BEC) T_{BEC} must lie above the superfluid transition temperature T_s in Vycor. In other words, T_s and T_{BEC} may be separated in Vycor.

There are sound physical reasons to believe that such a separation due to disorder is possible. Neutron scattering measurements of the condense fraction of helium in Vycor are needed to clarify this intriguing possibility.

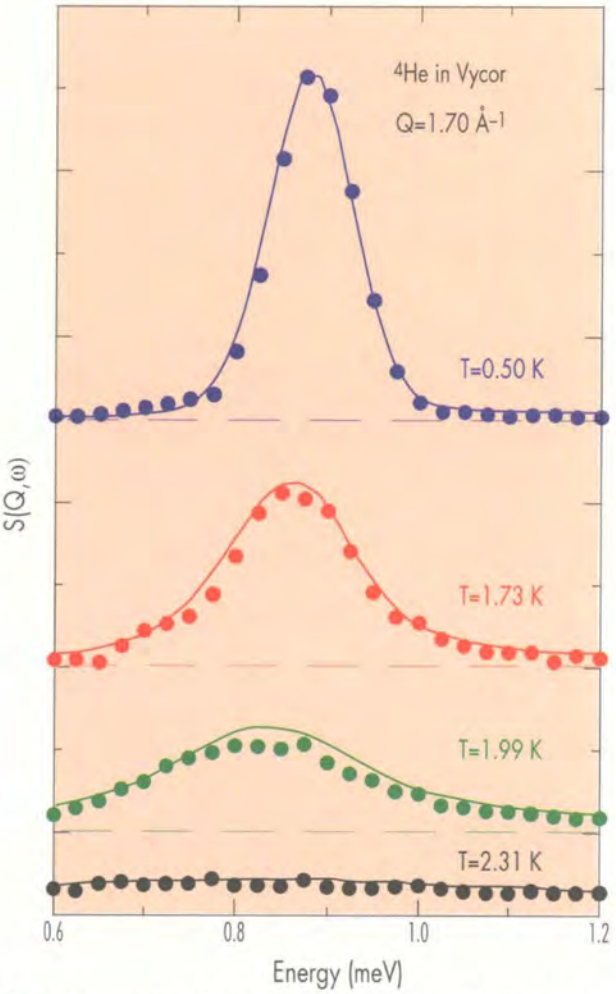

Figure 3: *Comparison of the dynamical structure factor of superfluid ^{4}He in Vycor (filled circles) with bulk helium (lines) at different temperatures measured on IN6 for a wave-vector slightly smaller than the roton wave-vector.*

References

■ [1] H. Palevsky et al., Phys. Rev. 108 (1957) 1346 ■ [2] J. D. Reppy, J. Low Temp. Phys. 87 (1992) 205 ■ [3] W. Thomlinson et al., Phys. Rev. Lett. 44 (1980) 266 ■ [4] H. J. Lauter et al., Phys. Rev. Lett. 68 (1992) 2484; J. Low Temp. Phys. 87 (1992) 425 ■ [5] A. D. B. Woods and E.C. Svensson, Phys. Rev. Lett. 41 (1978) 974 ■ [6] H. R. Glyde and A. Griffin, Phys. Rev. Lett. 65 (1990) 1454.

Giant tunnelling effect of hydrogen and deuterium in α-manganese

A. I. Kolesnikov, V. E. Antonov, V. K. Fedotov (ISSP RAS Chernogolovka),
A. J. Dianoux, B. Dorner, A. Hewat, A. S. Ivanov (ILL),
G. Grosse, F. E. Wagner (TU München).

A neutron diffraction investigation of α-$MnH_{0.07}$ showed that hydrogen atoms randomly occupy interstitial positions which form dumb-bells, 0.68 Å long. Together with the high-energy optical bands, pronounced peaks at 6.3 and 1.6 meV were observed in the inelastic neutron-scattering spectra of α-$MnH_{0.07}$ and α-$MnD_{0.05}$. Our data show that these peaks originate from the splitting of the vibrational ground-state of hydrogen and deuterium atoms due to their tunnelling between the adjacent sites forming a dumb-bell. The intensity and the energy of the tunnelling peak are anomalously high compared to those in metal-hydrogen systems studied earlier. Hydrogen tunnelling in α-MnH_x is one of the very few quantum effects observed at temperatures as high as 100 K.

Apart from their technological importance, metal-hydrogen systems have repeatedly been found to exhibit unique phenomena not observed in other materials. The study of these phenomena helps in understanding fundamental aspects of quantum and solid-state physics. The special geometry of the hydrogen positions in the complex structure α-phase of manganese gives rise to an unusually pronounced tunnelling effect.

A recent high-pressure study showed that the solubility of hydrogen in α-Mn can be increased up to a few atomic percent [1]. The crystal structure of a powder sample of $MnH_{0.07}$ synthesised under high hydrogen-pressure was studied by neutron diffraction, using the D1B diffractometer at ILL and the high-resolution Fourier diffractometer HRFD at JINR (Dubna) [2]. The cubic unit-cell of the α-Mn structure, space group $I\bar{4}3m$, contains 58 atoms located on the four crystallographically inequivalent sites 2a, 8c, $24g_1$, and $24g_2$. A profile analysis of the diffraction patterns of $MnH_{0.07}$ showed that hydrogen randomly occupies interstitial positions 12e (0,0,0.538) inside distorted octahedra of manganese atoms on $24g_1$ and $24g_2$ sites, as schematically shown by the drawing in the upper right corner of Fig. 1. These sites form dumb-bells positioned rather far apart, at the centres of the edges and faces of the unit cell of α-Mn with a = 8.9403 Å, see the upper left drawing in Fig. 1. Because of the small distance of 2ℓ = 0.68 Å between the 12e sites in a dumb-bell; each dumb-bell can accommodate only one hydrogen atom. An occupancy of half of the 12e sites corresponds to an H/Mn atomic ratio of x = 6/58 ≈ 0.103. In the studied $MnH_{0.07}$ sample hydrogen therefore filled about 70% of the accessible interstices.

An inelastic neutron-scattering study [2] of α-$MnH_{0.07}$ at 90 K with the KDSOG-M spectrometer at JINR revealed a band of optical hydrogen vibrations split into three peaks, in accordance with the low site symmetry of the hydrogen positions, and also a strong peak at 6.4 meV which was tentatively attributed to the splitting of the vibrational ground-state of hydrogen due to tunnelling between the adjacent 12e sites. Further results of inelastic neutron scattering studies strongly corroborated the assumption of the tunnelling origin of the 6.4 meV peak. These results are partly published in Ref. [3] and include the temperature and the neutron momentum-transfer dependences of the spectra of α-$MnH_{0.07}$ at 5–200 K measured with the TFXA at ISIS, MARI at ISIS and IN6 at ILL and the spectra of α-$MnD_{0.05}$ at 1.7–180 K measured with the IN6 and IN1BeF ILL-spectrometers.

A representative inelastic neutron-scattering spectrum measured with TFXA is shown in Fig. 1 at the bottom. The peaks of the fundamental H optical modes in α-$MnH_{0.07}$ are observed at 74, 107 and 130 meV, in reasonable agreement with the KDSOG-M data. The intensity of the peak at 6.2 meV decreases with increasing temperature and at 200 K the peak exhibits relaxation behaviour.

Figure 2 shows the difference between the inelastic neutron-scattering spectra in energy gain of an α-$MnD_{0.05}$ sample and a sample of pure α-Mn which were measured with IN6

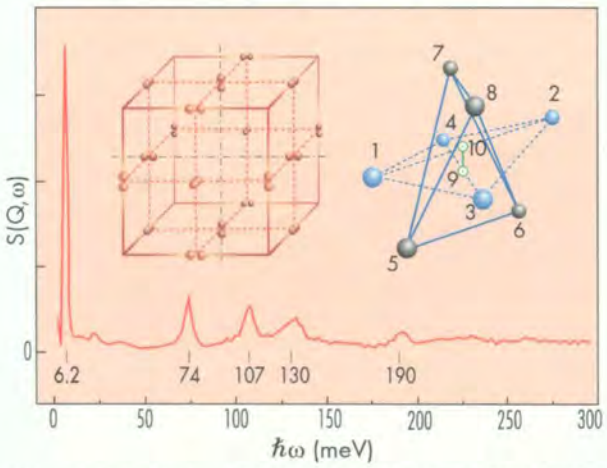

Figure 1: The α-$MnH_{0.07}$ solid solution. On the right: two adjacent positions 12e partly occupied by hydrogen (open circles ⊙ 9 and 10) and their nearest environment of two tetrahedra formed by manganese atoms on positions $24g_1$ (blue circles ● 1 to 4) and on positions $24g_2$ (black circles ● 5 to 8); the Mn atoms 1-4, 5, and 6 form a distorted octahedron around the H atom on position 9. On the left: the arrangement of dumb-bells of 12e positions in the unit cell of α-Mn. Bottom: The inelastic neutron-scattering spectrum measured at 23 K with the TFXA spectrometer at ISIS.

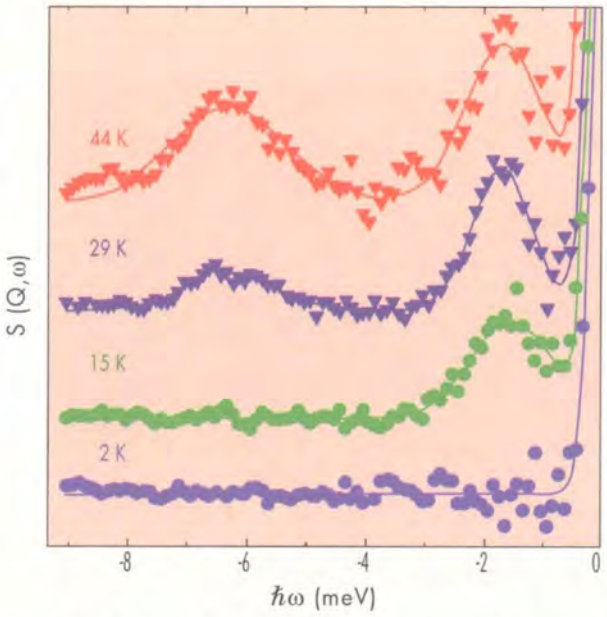

Figure 2: *The differences between the inelastic neutron-scattering spectra of α-$MnD_{0.05}H_{0.005}$ and α-Mn measured in energy gain with the IN6 spectrometer at ILL. The curves are shifted along the y-axis. The α-$MnD_{0.05}$ sample was contaminated with about 0.5at.% H which manifested itself by the peak at 6.3 meV. The peak at 1.6 meV is due to 5at.% D.*

under the same conditions. The positions of these H and D peaks agree with roughly estimated values, $\Delta_0^H = 5$ meV and $\Delta_0^D = 1.5$ meV, for the splitting of the hydrogen and deuterium vibrational ground-states due to tunnelling. These values follow from the relation [4]:

$$\Delta_0 \approx (1/2)\,\hbar\omega_0 \exp(-m\omega_0\ell^2/\hbar)$$

if one substitutes the measured energies $\hbar\omega_0^H = 73$ meV and $\hbar\omega_0^D = 51$ meV of H and D local vibrations along the line $2\ell = 0.68$ Å which connects the 12e sites in a dumb-bell; m is the mass of the H or D atom.

The intensity of the 6.3 meV peak of hydrogen in α-Mn measured with MARI as a function of momentum transfer, Q, can also be described fairly well by the Q-dependence characteristic of tunnelling peaks [5]:

$$S(Q,\omega_{tun}) \propto [1/2 - \sin(2\ell Q)/(4\ell Q)] \exp(-Q^2u^2).$$

The value of u^2, the effective mean-square displacement of H atoms, obtained by fitting was 0.16^2 Å^2.

The temperature dependences of the integrated intensities of the H and D tunnelling peaks are shown in Fig. 3 and can be well explained by a Boltzmann thermal population of the corresponding ground-states (solid curves in Fig. 3).

The most remarkable features of the hydrogen tunnelling peak in the inelastic neutron-scattering spectrum of α-$MnH_{0.07}$ are its occurrence in a very large temperature interval up to 100 K, its anomalously large integrated intensity compared to that of the optical hydrogen band and its anomalously high energy of 6.3 meV. This energy is about 30 times higher than that of tunnelling splittings found for hydrogen in other metals [5]. Hydrogen tunnelling in metals was observed earlier only at temperatures below 10 K, and this is the first time that deuterium tunnelling in metals was measured using neutron spectroscopy.

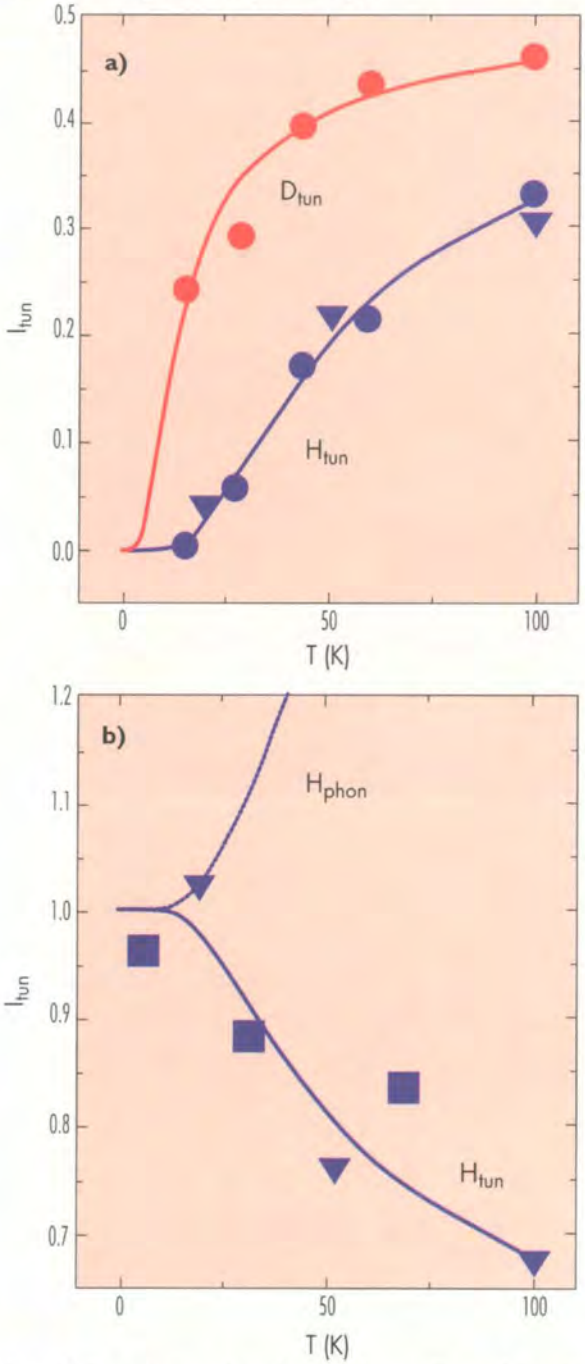

Figure 3: *The temperature dependences of the tunnelling peak intensities for hydrogen (blue symbols) and deuterium (red symbols) in α-Mn obtained from the INS spectra collected in the regime of neutron energy gain **a)** and loss **b)**. The spectra were measured with the spectrometers IN6, ILL (circles), MARI, ISIS (triangles) and TFXA, ISIS (squares). The solid lines represent the Boltzmann thermal population factors, $\exp(-\Delta_0/k_BT)/[1 + \exp(-\Delta_0/k_BT)]$ for the upper ground-state (Fig. 3a) and $1/[1 + \exp(-\Delta_0/k_BT)]$ for the lower ground-state (Fig. 3b). The dashed line in Fig. 3b is the dependence: $1/[\exp(\Delta_0/k_BT) - 1] + 1$ valid for phonons and harmonic oscillators.*

References

■ [1] V. E. Antonov et al., Scripta Materialia 34 (1996) 1331 ■ [2] V. K. Fedotov et al., J. Phys.: Condens. Matter 10 (1998) 5255 ■ [3] A. I. Kolesnikov et al., Physica B 263-264 (1999) 421 ■ [4] S. I. Drechsler et al., J. Phys. F 14 (1984) L243 ■ [5] A. Magerl et al., Phys. Rev. Let. 56 (1986) 159.

Emmanuel Farhi (right) shows the 'virtual' ILL to visitors during the French science week "La Science en fête".

The ILL thesis students (from left) Darius Sullivan, Charlotte Anderson, Jörg Holzinger, Alexandre Sicard enjoy the break during the clip session.

"A hit, a very palpable hit"*, Alan Leadbetter in his lecture about glass.

Shakespeare, Hamlet, act 5 (1601)

Recollection of the old days: Pierre Chieux, Jean-Louis Soubeyroux, CNRS Grenoble, and Jacques Bouillot, Annecy.

WORKSHOPS

2

Workshops and Meetings in which ILL played a major role in the organisation

Frontiers in SAXS and SANS	organised by B. Demé (ILL), O. Diat, Th. Naraynan (ESRF), Th. Zemb (CEA Saclay)	ESRF	12-13 Feb. 99
Powder-diffraction instruments review	organised by A. Hewat (ILL) and C-H. De Novion (LLB Saclay)	ILL	22-23 Mar. 99
Informal workshop on 'Inelastic Scattering with the Neutron Resonant Spin Echo (NRSE) Technique'	organised by R. Currat (ILL)	ILL	23 Jul. 99
'Clip session' of thesis students	organised by G. Brotons	ILL	23 Nov. 99
5th EU Residual Stress Standards Steering Committee Meeting (RESTAND)	organised by T. Pirling	ILL	9-10 Dec. 99

Frontiers in SAXS and SANS

Small-angle scattering is a well established technique to characterise structures ranging from nanoscopic (10 Å) to microscopic (a few microns) scales. The combination of small-angle x-ray scattering (SAXS) and small-angle neutron scattering (SANS) provides complementary (contrast) structural information in numerous systems belonging to hard, soft, as well as biological matter. On the 12-13 February 1999, the workshop *frontiers in SAXS and SANS* gathered 120 scientists at the ILL for a comprehensive overview of the state-of-the-art instruments existing at ESRF and ILL.

The first session was dedicated to the current status of the instruments, whereas the other sessions discussed the present limits in spatial and time resolutions presenting recent developments in optics, detectors and sample environments, and emphasising the need for further improvements. The closing session demonstrated the power of small-angle scattering as applied to two different situations involving the triple isomorphous substitution method in SANS of biological samples and the use of SAXS in polymer processing.

Exciting discussion during the poster session of the small-angle workshop; from left: Marie Forêt, Montpellier, Olivier Dhez and Olivier Diat, both ESRF.

Furthermore, the workshop stressed the usefulness of bringing both x-ray and neutron communities together for joint endeavours.

Powder-diffraction Instruments Review

On 22-23 March 1999, the scientific council's *review of powder and liquids/amorphous materials diffraction* (www.ill.fr/dif/powder-review) hosted 50 participants. There were sessions dedicated to individual instruments, D2B, D20, D4, and the two CRGs: D1A and D1B, and sessions on 'continuous versus TOF neutron sources', 'synchrotrons versus neutrons', and 'data-acquisition and software'.

The final report congratulated the ILL on its world-class instruments, with D2B, D20 and D4 being the best in their categories. Nevertheless, it was found that the total capacity for powder diffraction at ILL is smaller than it should be, taking into account the size of the community and the scientific results. However, at present, the situation is aggravated by the shut-down of D20. The report concluded that the first priority was, of course, to repair D20, but that high priority should be given to improving the efficiency, especially of D2B and D4. D1A, at present scheduled half time, should remain available for powder diffraction at least until the definitive repair of D20. A new powder diffractometer would be desirable, but the characteristics of such a machine requires further discussion.

The D4C upgrade, providing 10 times more flux, should be finished by the end of this year. It was recommended that the upgrade of D2B, presented within the ILL 'Millennium Programme', should become the first priority to allow the routine use of D2B in its highest resolution mode. The need for a dedicated full-time strain scanner was emphasised, totally independent of D1A, with more space, for example behind D1B.

The general discussion concluded that x-rays are better for structure determination, but neutrons are preferable for the refinement to obtain quantitative and precise data, e.g. atomic positions of oxygen in oxides. This is specially true for instruments on continuous sources due to the great stability of their neutron flux, e.g. D4. Finally, data acquisition and refinement software is increasingly important, with the need for neutron laboratories to develop and maintain software such as FullProf and CCP14 in a collaborative network.

"When shall we three meet again. In thunder, lightning, or in rain?"; from left: David Martin, ISIS, John Loveday, Edinburgh, and Adrian Barnes, Bristol.*

**Shakespeare, Macbeth, act 1 (1606)*

The Neutron Resonant Spin Echo (NRSE) Technique

On 23 July an informal workshop on *Inelastic Scattering with the Neutron Resonant Spin Echo (NRSE) Technique* was held at the ILL attended by 20 participants interested in the NRSE technique and its potential applications for inelastic scattering. The specific objectives of the meeting were as follows:

– to assess the scientific case for developing a spin echo set-up optimised for inelastic work (study of excitation linewidths, anharmonic frequency shifts, and others),

– to define the optimum characteristics of such a set-up, in terms of energy and momentum transfer range, energy and momentum resolution, luminosity, polarisation characteristics),

– to review the principles and capabilities of the NRSE method and its technical requirements in the context of inelastic scattering in the light of the instrumentation efforts in this area currently underway at HMI, FRM-II and LLB,

– to discuss the opportunity of developing a NRSE set-up on a polarised-beam three-axis spectrometer at ILL (first on the test instrument IN3, later to be transported as an option onto IN20, IN14, IN22) and to explore possible collaborations in that direction.

After various presentations the workshop participants discussed the feasibility of developing a spin-echo set-up dedicated to inelastic scattering on the test instrument IN3. It was generally felt that:

– the resonant technique appeared better suited in order to take advantage of the increase in luminosity associated with the use of focusing geometries, both the resonant and precession techniques should address, at some stage, the question of how to properly correct for second-order dispersion effects resulting from the local curvature of the dispersion surface.

– a NRSE set-up on IN3 will serve a useful purpose if it becomes operational in 2001 at the latest.

Discussion of the NRSE set-up on IN3; from left: Roland Gähler, Philippe Malbert, Roland Currat, Bruno Dorner and Arno Hiess.

"Clip Session" of Thesis Students

On 23 November, ILL's thesis students invited to a clip and poster session. Since the students work in various disciplines this gathering gave the opportunity to exchange ideas and to help to know each other better. During the session "Physique en Clips" in December 1999, Guillaume Brotons was awarded the prize for the best short presentation by the Grenoble section of the French Physical Society (SFP).

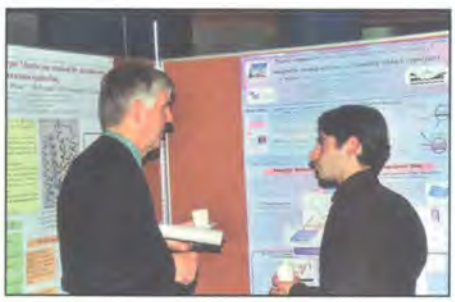

Guillaume Brotons (right) discusses his results with Heinrich Stuhrmann, IBS Grenoble.

5th EU Residual Stress Standards Meeting

On 9-10 December the ILL hosted *the 5th EU Residual Stress Standards (RESTAND) Steering Committee meeting*, chaired by Professor A.G. Youtsos (Petten). Engineers and scientists from various institutions and companies participated: HMI, ILL, ISIS, Petten, Risø, Studsvik, the Universities of Cambridge, London (Imperial College), Salford, and AEA Technology, British Aerospace Airbus, Rolls Royce, Schunk Kohlenstofftechnik, Sintec Keramik, Volkswagen. They have embarked on an EU contract to establish European standards for the measurement of residual stress using neutron diffraction. This is done by comparing measurements on standard samples provided by industry to the neutron laboratories. In addition, developing strategies and procedures for measurements and analysis of data are discussed.

Since many large European companies are participating in this effort, we expect that the new standards will encourage greater interest in neutron diffraction by industry. Moreover, this will help neutron centres to better understand the needs of commercial applications. The RESTAND contract is a follow up of the international VAMAS-TWA20 working group to promote the use of neutron strain scanning; ILL hosted the inaugural meeting of VAMAS in 1995.

These initiatives are particularly timely in view of the proposal (by a consortium of UK Universities to EPSRC) to construct a dedicated neutron strain scanner at ILL, building on the present instrument on D1A (see also AR97, p. 87). This is one of the ILL's Millennium programme projects, on which work will start in 2000.

Working for IN13's upgrade: Frédéric Marchal (left) and Jérome Locatelli.

"And José Dianoux said, 'Let there be light' ...and there was light".*
Giovanna Cicognani, Luigi Cristofolini, Univ. Parma, Jérôme Combet, José Dianoux (from left) setting up a light scattering experiment on IN10.

** Genesis ch. 1, v.1*

"Life is just one damn thing after another."*
Paul Martin (left) sorting out furnace problems on D1A for Maria Jesus Martinez Lope, ICM Madrid, Teresa Fernandez-Diaz and Clemens Ritter (from right).

**E. Hubbard 'Philistine', Dec. 1909 P.32*

Pierre Palleau adjusts the crystal analysers (pyrolithic graphite) on IN1.

NEW DEVELOPMENTS

3

With the advent of the new millennium, the ILL has prepared a programme of instrument renewal. Proposals for new methods and instrument upgrades were made by ILL users and ILL scientists during the last year. Feasibility studies have been undertaken, as described in the following. After discussions through ad-hoc committees (Instrument Subcommittee and Scientific Council), 5 projects were approved by the last Steering Committee. These projects include: the construction of the thermal LADI instrument and the implementation of a strain scanner in collaboration with the British associate; the development of a fast detector for SANS experiments, the rebuild of the D3 diffractometer and the upgrade of the IN20 neutron optics. This phase of the ILL Millennium Programme, which should start in 2000, is a first step to bring the ILL instruments suite up to users expectations. The Millennium Programme will later be extended to other instruments and general infrastructure of the ILL.

Other instrumentation projects are well under way, such as the new IN8 spectrometer, the time-of-flight option on IN15 and the upgrade of the IN13 CRG instrument. New methods are also tested and exploited. The development of instrumentation and techniques is an essential activity at a facility such as the ILL; the outstanding results achieved last year have been made possible by the dedication of the whole staff from technicians and engineers to scientists.

TECHNICAL DEVELOPMENTS

Review of developments

Some notable developments accomplished in 1999, but which are not mentioned in the articles on the following pages, are reviewed below.

- **The new neutron guides H17 and H18** which supply the new diffractometers D16 and D17B, respectively, were commissioned in November 1998. Flux measurements show that the flux on H17 is 5 to 12% higher than on the identical H16 guide, and the flux on H18 is 27 to 45% higher than on the new H17 guide (note the supermirror coating is only on the horizontal surfaces of the guide).

  The H17 and H18 guides have the same geometry as the H14 to H16 guides, section of 200 x 30 mm^2, curvature radius of 2700 m, length 25 m from the rear plate in the swimming pool. The natural nickel coated H17 guide is followed by the 10 m long straight H171 guide with a section of 150 x 30 mm^2. The H18 guide has a natural nickel coating on the vertical faces and a m=2 nickel-titanium supermirror coating on top and bottom. The last 3 m have m=3 supermirror coating on top and bottom and are converging to 150 x 30 mm^2.

- **The 'upgrade of PF1 on H113'** started in 1998. The H113 guide is of a non-conventional design with cross section varying over its length such as to improve its transmission properties. The guide in the out-of-pile has a geometry diverging from 200 x 60 mm^2 to 200 x 90 mm^2, curvature radius of 4000 m, length of 72 m from the rear plate in the swimming pool and m = 2 nickel-titanium supermirror coating on the total surface. The housings in the neutron-guide hall are ready to receive the glass elements. The delivery and mounting of the supermirror-coated glass-elements by the University of Heidelberg is scheduled for the next winter shutdown. The project is co-financed by the Universities of Heidelberg and Munich.

  As compared to the old PF1 station on H53, on H113 the gain in neutron flux can be doubled due to the supermirror coating. Further gains can be achieved by installing a focusing device (which is not yet financed) and by dedicating the beam to PF1 without having further instruments upstream, so that an overall gain of more than ten times can be expected. The missing parts will be installed during the long shut-down end of 1999, and the new beam-position will be properly equipped in the course of the year 2000. As most neutron-particle physics experiments are statistics limited, this new installation should give some additional impetus to the field.

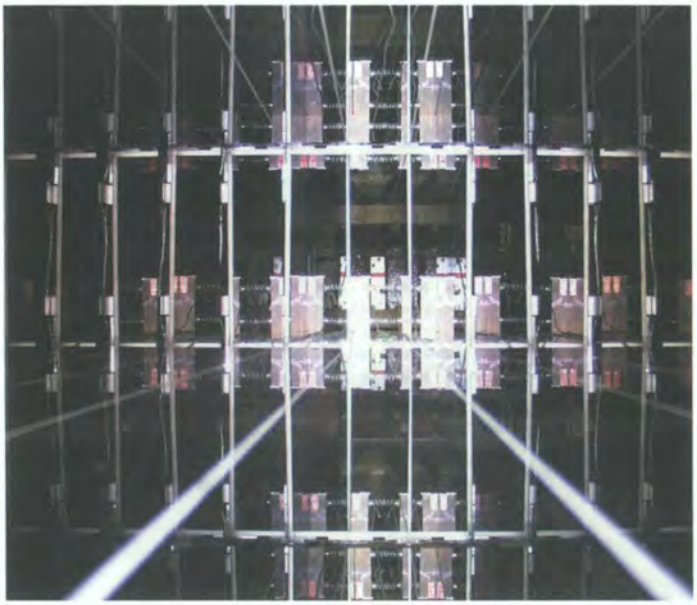

Multiple reflections looking into the new supermirror guide H113 (during installation in August 1999).

- **The new detectors** of the liquids diffractometer D4C were assembled during 1999 and first tests are foreseen in spring 2000.
- **D16, the upgraded 2-axis diffractometer** for medium-resolution work on biological materials, was fully commissioned during 1999. First results of experiments carried out on D16 are presented in the scientific highlights.
- **D17B, the new reflectometer**, was partially commissioned during 1999. The installation of the monochromator mode, including polarised neutrons, is under completion during the winter shutdown (Dec. 1999/Jan. 2000).

Commissioning D17B. From left to right: Loïc Pajou, Bob Cubitt, Eric Beloeuvre, EMBL, André Gabriel, EMBL, Frédéric Descamps.

- **The position-sensitive detector (PSD)** of D20 is currently under repair. After the breakdown of D20's detector, the microstrip-gas-chamber detector-plates were investigated by Auger electron spectrometry. This showed that the anodes transformed from chromium to chromium oxide while working at high voltage. The fact that this oxide appears only on the anodes but not on the cathodes suggests an electrolytic reaction in the glass or on its surface. Due to the reduction of the width of chromium on several anode strips, discharges appeared which led to the progressive destruction of the anodes. This electrochemical effect is now controlled by an enforced cleaning of the glass surface and/or the replacement of chromium strips by strips of gold. This will allow the reconstruction of the detector with a longer lifetime. A prototype of the new microstrip-gas-chamber detector-plates has been tested and all plates are delivered. After mounting these plates into the PSD housing, followed by a heat treatment under vacuum, the PSD will be filled with the detection gas and brought into the reactor hall after the first reactor cycle. Before adjusting and calibrating the PSD's electronics the protection has to be mounted. D20's re-operation is foreseen for June 2000.
- **The time-of-flight spectrometer IN4C** saw its first user experiments during the last cycle of '99 using the low-energy range. During the first half of 1999, the optimisation of the operational parameters, alignment, focussing and chopper speeds has been carried out over the full available wavelength range. Most recent efforts are concentrated on the minimisation of the background, eliminating parasitic scattering and search for the best resolution conditions. Unfortunately, the performance of the instrument is severely limited by the safety restrictions concerning the background choppers. The loss of flux due to the limited transmission of the Al-shield is most severe at longer wavelengths (> 2.5 Å), while the imposed speed limit of 10,000 rpm requires to operate with a 1/2 speed ratio (background choppers/Fermi chopper) at short wavelengths (< 2 Å), with a corresponding loss of intensity on sample, as well as degraded background conditions. The maximum flux on sample was found to be of the order of $1.4 \cdot 10^5$ n/cm^2/s (at λ = 1.1 Å).

  The replacement of the actual background choppers with discs - that should allow the suppression of the safety restrictions - is in progress and the installation of the new choppers is foreseen for July 2000. Meanwhile, we have planned to install a secondary diaphragm before the monochromator position in order to try to improve the energy resolution that seems to be degraded due to the broadening of the incident divergence caused by the 9 cm thick Al-shield.
- **A circular ^{3}He detector** for forward scattering with a central hole for the direct beam is close to completion. It will cover an angular range of approximately 3 to 9°. After beam tests and checks of the electronics it will be mounted on the instrument at the beginning of 2000.
- **The rebuild of the primary spectrometer IN5B**, the time-of-flight instrument, is going ahead as foreseen. The choppers are under design, the magnetic bearings and the supermirror guide are ordered.

An image-plate Laue diffractometer for physics and chemistry

C. Wilkinson (Kings College London),
G. J. McIntyre, J. A. Cowan (ILL),
D. A .A. Myles (EMBL),
M. de Boissieu (LTPCM/ENSEEG Grenoble),
O. Nimz (Freie Universität Berlin),
P. Schobinger-Papamantellos (ETH Zürich).

Test experiments on LADI have shown that a Laue diffractometer adapted to difficult sample environments would be a powerful tool for physics and chemistry, offering rapid collection of complete diffraction data from new materials, from weakly scattering samples, and through phase transitions.

A detector employing neutron-sensitive image-plates is comparatively cheap, offers high spatial resolution, has good homogeneity, a large dynamical range and extended linearity, and can be constructed to subtend very large angles at the specimen. When used with the Laue technique to exploit the full flux of a white neutron beam, such a detector allows collection of single-crystal diffraction data 10 to 100 times faster than on a conventional monochromatic diffractometer, with only a modest loss in precision. The image-plate LAue DIffractometer (LADI) was constructed by the ILL and EMBL to exploit these advantages [1]. It is now in scheduled operation on a cold-neutron beam giving good structural information for macromolecular crystallography [2].

An image-plate Laue diffractometer on a thermal-neutron beam would also have wide application in the small unit-cell problems of physics, chemistry and mineralogy. The possibility to observe complete volumes of reciprocal space rapidly will allow, for example, structural studies of small or weakly scattering crystals in an acceptable time, or complete data collections as a function of temperature or pressure of structural or magnetic phase transitions, which often result in complex incommensurable structures.

LADI has occasionally been moved to the thermal beam H22 for test experiments on problems in physics and chemistry. Some recent highlights are given below.

Quasi-crystals

The structure of a quasi-crystal can be described in a six-dimensional (6D) space where translational periodicity is recovered. The 6D periodic lattice is divided into two 3D spaces: physical space, also called parallel space, and the complementary perpendicular space. The 6D lattice is decorated by a set of 3D atomic objects lying in perpendicular space. The reciprocal lattice observed by diffraction can also be described by a 6D lattice, defined by $Q_{parallel}$ and Q_{perp} and is consequently infinitely densely packed in the observational 3D physical space. Fortunately the intensity of reflections falls off as $|Q|_{perp}^{-6}$, which allows reasonable resolution of quasi-crystal reflections, sufficiently so that the first known quasi-crystal structures could be solved by x-ray powder diffraction using isomorphous replacement [3]. Further detail comes from single-crystal diffraction, especially by exploiting the contrast of the different relative scattering powers of the constituent elements by neutrons vis-à-vis x-rays to detect chemical order in the structure.

Despite the projection of the diffraction pattern into 2D in the Laue technique, the high flux, large dynamic range, large detector surface, and uniform resolution of LADI should prove to be a useful tool for study of quasi-crystals. Figure 1 shows the full image of one Laue diffraction pattern of the new magnetic icosahedral phase Zn_6M_3Y. The five-fold axis is readily identified, and the enlarged region in inset hints at the detail that we will be able to extract routinely from such patterns. The unique area of the pattern is outlined in bold, and is repeated several times in the pattern, but with different wavelengths contributing to the different reflections.

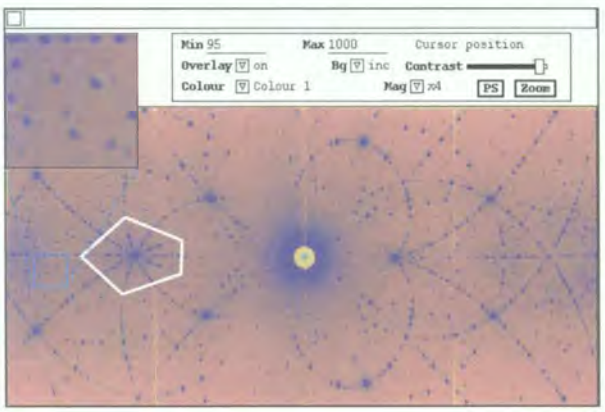

Figure 1: Laue diffraction pattern from icosahedral Zn_6M_3Y obtained in two hours on LADI at the end of the thermal guide H22. The five-fold axis is indicated.

Hydrogen bonding in a large cyclodextrin

Synchrotron x-ray data of the cycloamylose:

$$(C_6H_{10}O_5)_{10} + 23.5H_2O$$

showed that two of the ten glucose units are flipped by 180° around the glycosidic bond to give a distinctive boat-shaped structure with narrow slit-like cavities. Hydrogen bonding involving the hydroxyl O atoms undoubtedly plays an important role in stabilising the orientation of the flipped glucose units, but the positions of the hydroxyl H atoms could not be localised from the x-ray data, possibly due to dynamic disorder.

Just two and a half days of data collection from a very small (for neutron diffraction) crystal of volume 0.2 mm^3 at room

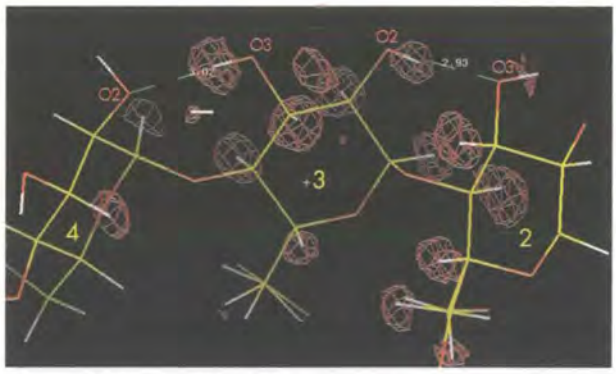

***Figure 2**: Part of the 3D Fourier map of the cycloamylose $(C_6H_{10}O_5)_{10} + 23.5H_2O$, showing the hydrogen atoms in the neighbourhood of the flipped glucose unit (3). Yellow, white and red on the stick model denote carbon, hydrogen and oxygen atoms repectively. The (red) negative isocontours correspond to hydrogen atoms.*

temperature on LADI on H22 yielded some 2000 unique reflections from which the positions of the hydroxyl H atoms and the direction of hydrogen bonding could be unambiguously determined (Fig. 1). In addition, the H atoms in a water-mediated bridge between two cycloamylose molecules could be located. Neutrons are competitively complementary to x-rays!

The modulated structure of $La_2Co_{1.7}$

LADI gives a complete survey of reciprocal space, so that any additional reflections present, which are not predicted in a conventional monochromatic data collection strategy, become evident.

In the idealised atomic structure of $La_2Co_{1.7}$ the Co atoms would form chains along the c-axis; however the c lattice parameter (4.13 Å) is too short to accommodate two Co atoms of radius 2.37 Å in close contact. Previous studies suggested that the Co atoms do form continuous chains with inter-atomic spacing of 2.37 Å, but with only weak correlation between the chains, to give rise to planes of diffuse scattering perpendicular to c [4]. Laue diffraction patterns from LADI revealed that the planes of diffuse scattering are in fact satellites corresponding to a charge density wave with propagation vector $0.113a^* + 0.203c^*$. Six domains are formed in the hexagonal crystal to produce a twelve-fold prism of satellite reflections around each fundamental reflection position, which is seen in projection in the Laue pattern (Fig. 3). Modelling the intensities of the satellite and fundamental reflections shows that the charge-density wave does indeed arise from the lack of space for two Co atoms to be in close contact along the c axis. The Co atoms lie at incommensurate positions along *c*, and adjust to the long-range 3-D lattice by leaving inclined planes of vacancies perpendicular to $0.113a^* + 0.203c^*$.

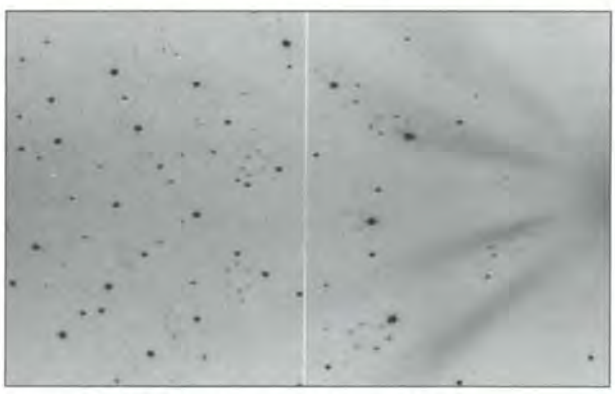

***Figure 3**: Laue diffraction pattern of $La_2Co_{1.7}$ at 15 K.*

An image-plate Laue diffractometer (Fig. 4) for use with difficult sample-environments is one of the projects proposed in the ILL's Millennium Programme. This instrument will cover studies such as magnetism, charge (nuclear) density waves, high-pressure studies and structural phase-transitions. When (even small) single crystals of a material are available, it will offer more detail than powder diffraction in the preliminary investigation of new materials. It will provide a tool for development of new diffraction experiments and will be complementary to existing ILL diffractometers.

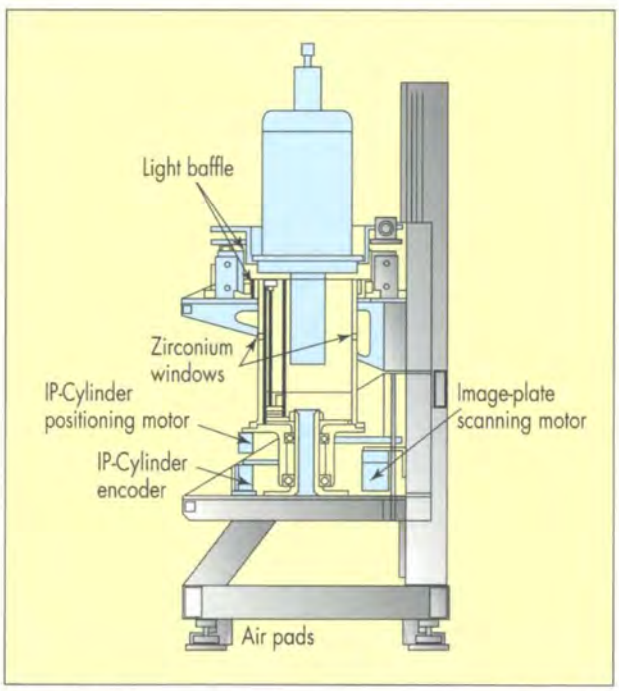

***Figure 4**: A schematic of the proposed thermal-beam Laue Diffractometer. The main difference compared with LADI is that the detector cylinder will be vertical to allow free access for different sample holders such as cryostats, furnaces, magnets or pressure cells.*

References

■ [1] F. Cipriani, J.-C. Castagna, C. Wilkinson, P.Olienek and M.S. Lehmann, J. Neutron Research 4 (1996) 79 ■ [2] N. Niimura, Y. Minezaki, T. Nonaka, J.-C. Castagna, F. Cipriani, P. Høghøj, M.S. Lehmann and C. Wilkinson, Nature Structural Biology 4 (1997) 909 ■ [3] M. Boudard, M. de Boissieu, C. Janot, G. Heger, C. Beeli, H. Nissen, H. Vincent, R. Ibberson, M. Audier and J.M. Dubois, J. Phys. Cond. Matter 4 (1992) 10149 ■ [4] J. Schweizer, K.A. Strnat and J. Tsui, 9th Rare-Earth Res. Conf. Blacksburg, Virginia, USA (1971).

Progress on the IN8C upgrade

A. Hiess, R. Currat (ILL),
F. J. Bermejo (CSIC Madrid).

ILL's first fully optimised thermal-neutron three-axis spectrometer IN8C is soon to be installed on site and will be operational in the year 2000. Here we report on the progress made during the design and prototyping phase of the project.

The following objectives have motivated the current upgrade [1] of the thermal three-axis spectrometer IN8:

(a) the monochromatic flux at the sample position is expected to increase more than six times [2] as a result of using large double-focusing monochromators [3], short distances and a wider neutron beamtube,

(b) the background level will be reduced by adopting a beam geometry with a horizontal virtual source,

(c) more flexibility will be gained by enlarging the range of accessible scattering angles.

The IN8C project has been undertaken by the ILL in collaboration with Spanish scientific partners, who subcontracted the design study and the manufacturing of the primary protection, monochromator mechanics and optical elements to Spanish industry. On the other hand, the reactor-related elements, the installation on site as well as the monochromator crystals are under ILL's responsibility. The primary casemate of IN8C, the new beamtube H10 and the new platform for the diffractometer D15, which is situated above IN8 in the reactor hall, have already been manufactured and the installation on site will start during the winter shutdown 1999/2000. The manufacturing of the monochromator drum makes progress and its construction will continue into 2000.

The instrument is equipped with three double-focusing monochromators (PG002, Cu200 and bent perfect Si111) mounted on a rotating exchanger. A new design concept for the focusing mechanics has been explored by TEKNIKER, Eibar, Spain. Fig. 1 shows the proposed design. The first two faces (one shown in light blue in Fig.1) consist in 9 x 11 elements of (W x H) 25 mm x 17 mm which will build up an active area of (W x H) 233 mm x 197 mm. The horizontal and vertical curvatures can be varied independently. The Cu200 crystals will have an anisotropic mosaicity of 30' horizontal and 10' vertical, realised by the "onion peal method" recently developed by ILL's Neutron Optics Laboratory.

The crystals will be glued on a so-called transfer plate, which will clip onto the reference plate of the monochromator mechanics. The fixed horizontal curvature of the Si111 face (shown in red in Fig. 1) will be realised by bending a sandwich of several perfect Si blades [4] of (W x H) 260 mm x 17 mm. We use 11 "benders" to realise a variable vertical curvature. The use of perfect crystals together with the large active area requires high mechanical precision.

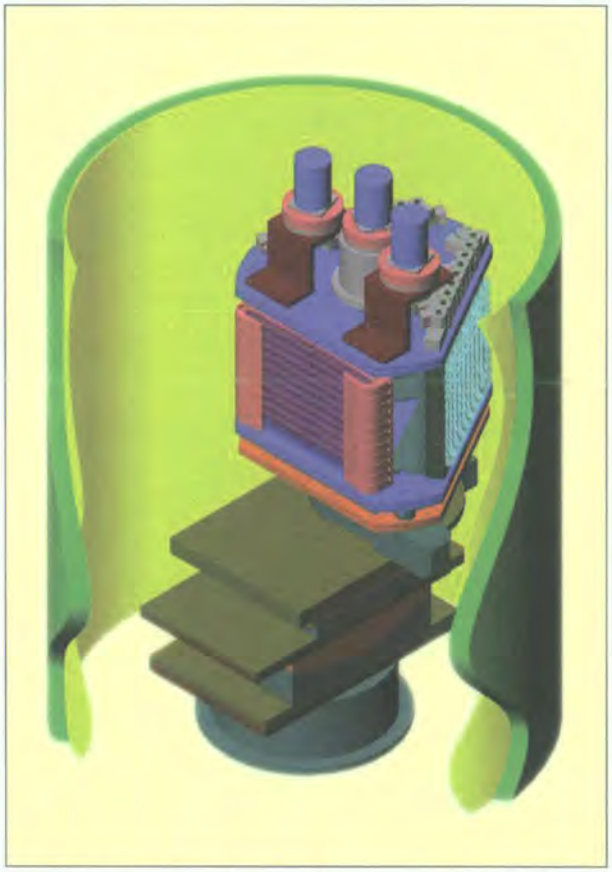

***Figure 1**: Proposed design of the three-face monochromator of IN8C.*

To gain experience with such a novel monochromator mechanics and to identify possible problems with the design, a prototype has been built recently. It consists in the outermost 3 x 3 (out of 9 x 11) elements for the PG002 and the Cu200 faces, and in 2 (out of 11) "benders" for the Si111. The overall precision for the 3 x 3 elements including zero position repeatability and absolute positioning precision is $< 0.03°$, well within specifications. The repeatability in the positioning of the Si face is also $< 0.03°$. Only the error in the linearity of the positioning is higher (0.1°), but it is possible to account for this effect in the instrument control programme.

The precision on the Si horizontal curvature has been determined mechanically. The deviation from a perfect circular bending appears to be 5 mm in a radius of 8000 mm i.e. smaller than 0.1%. The performance of the Si111 "bender" has been checked on the spectrometer IN3 at ILL. One single bender has been installed as an analyser instead of the standard

IN3 PG002 analyser. We performed energy scans using a vanadium cylinder at the sample position. We find that the elastic intensity with the Si bender reaches about 50% of the intensity with the PG002 analyser (normalised to identical active area), and the energy resolution is slightly better with Si111 than with the PG002 analyser. This is consistent with the performance of the other Si analysers in use on ILL three-axis spectrometers instruments [4].

A 2D multi-detector has been used to verify the focusing properties of the analyser in monochromatic focusing mode. The image in the detector is sharper than with a PG002 analyser.

The clip system to fix the crystals on the focusing mechanics works with high precision and appears to be reliable. Further tests will be performed to check if it also allows compensating for the misorientation of the crystals after gluing (by re-machining the back face of the transfer plates).

Given those promising results from the prototype, the manufacturing is now under progress. The future of IN8C will be bright!

Acknowledgements

We thank the ILL technical services and our Spanish partners for their work, enthusiasm and help with the IN8C project.

References

■ [1] A. Hiess et al., submitted to Physica B, ECNS 1999 proceedings ■ [2] J. Saroun; ILL report 1997 ■ [3] L. Pintschovius; Nuc. Inst. and Meth. A338 (1994) 136 ■ [4] J. Kulda, J. Saroun; Nuc. Inst. and Meth. A379 (1996) 155.

The first time-of-flight spin echo

■ B. Farago, G. Ehlers (ILL),
■ G. Kali (HMI Berlin),
■ A. Wischnewski (FZ Jülich).

IN15 was operated for the first time in time-of-flight mode and has shown an excellent instrumental resolution. As well as proving the feasibility of the neutron spin-echo technique on a pulsed source, it offers even more flexibility: a larger than ever dynamical range in one single run and variable monochromatisation. It is especially well suited for the study of relaxations in the small-angle range.

IN15 is a joint venture between the ILL, HMI Berlin and FZ Jülich to push further the limits of neutron spin-echo spectroscopy. Substantial progress has been already achieved by reaching 350 nsec Fourier times (or the equivalent sub neV energy resolution) [1]. This November we passed a new milestone, for the first time IN15 has been operated in time-of-flight mode. This mode of operation is not only a feasibility test for future pulsed sources, but can offer some real advantages depending on the physical problem studied.

The main advantages of neutron spin-echo are that a) the energy resolution is decoupled from the monochromatisation of the incoming beam b) the intermediate scattering function S(Q,t) is the directly measured quantity c) the maximum Fourier time is proportional to the magnetic field integral and to the third power of the wavelength [2].

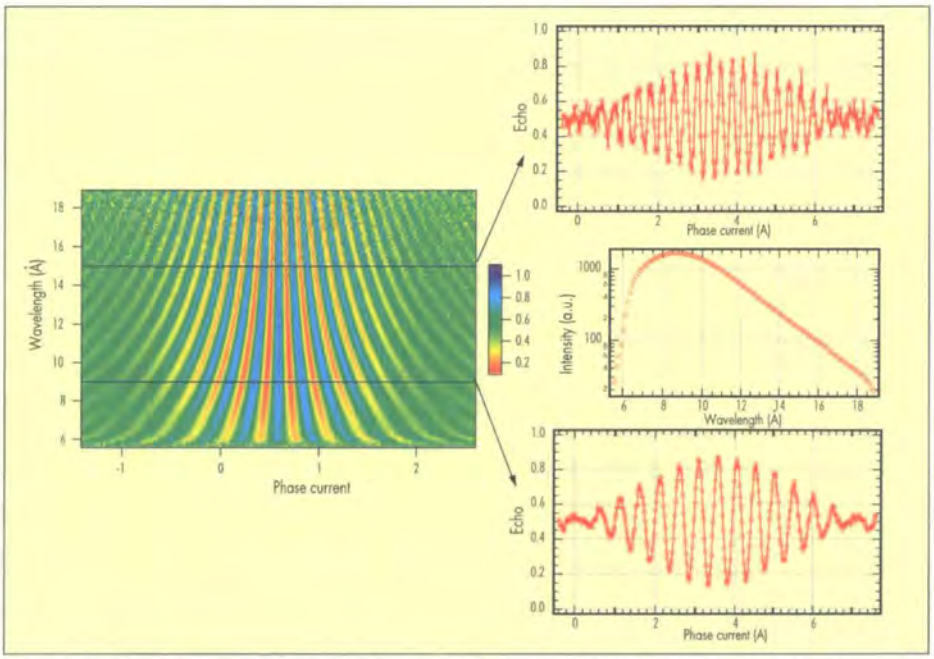

***Figure 1**: Echo group in all time channels as a function of the symmetry (phase current) between the two precession fields on the two sides of the spectrometer. Insert shows a cut at 9 and 15 Å. The periodicity gives the mean wavelength.*

At a given wavelength with a now routinely applied configuration (double echo) [3] three orders of magnitude in time can be covered. This range can be further extended by changing the wavelength due to the strong $t \sim \lambda^3$ dependence. While this possibility has been exploited already both on IN11 and IN15 [4], in practice typically two or maximum three wavelengths were used because for each wavelength the instrument has to be tuned and calibrated, which is rather time consuming.

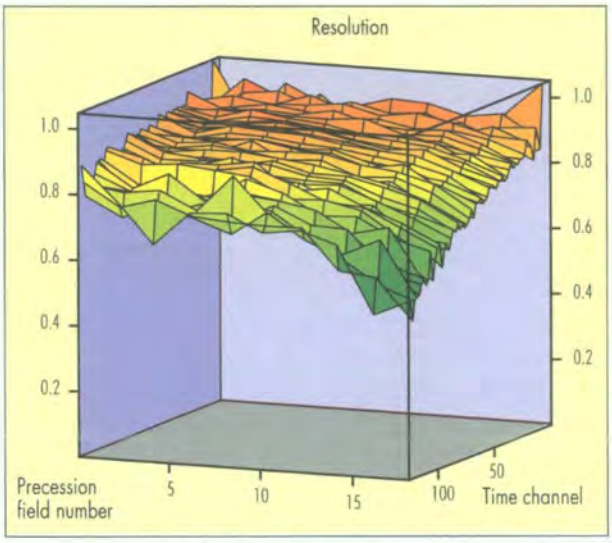

***Figure 2**: Resolution surface for all time channels and precession currents For clarity it was not plotted against Q and time (see Fig. 3).*

In the TOF version of IN15 the usual velocity selector is replaced by four choppers. The first three (triple chopper) produce a neutron pulse with variable monochromatisation (2-15% FWHM). The fourth chopper selects a wavelength band and avoids frame overlap. In fact the time-of-flight enables only the use of a wide range of wavelength, the energy analysis is still made by the spin-echo technique. By the time the neutrons reach the detector the neutron pulse is spread and the detector is continuously counting. The wide wavelength band with the $t \sim \lambda^3$ dependence covers an even larger dynamical range in one single run.

To produce the echo group we have to ensure that the magnetic field integral in the two arms of the spectrometer is identical to 10^{-5} precision, and we have to operate the three flippers ($\pi/2 - \pi - \pi/2$) for all wavelength. The symmetry condition once satisfied does not depend on the wavelength as long as all currents contributing to the field integral are constant. On the other hand the three flippers at any time have different wavelength neutrons just crossing them, so their action must depend on time. This was achieved by fast power supplies which have programmable current profiles, synchronised to a trigger from the choppers. The profiles were adjusted to produce the desired action π or $\pi/2$. This sounds not too difficult, however, for a given precession field we need to optimise at least 12 other correction currents. Thus it was not evident that a common set can be found which will work for all wavelengths.

In the test configuration the choppers were turning at a repetition rate of about 13 Hz and with a nominal wavelength band of 6-19 Å. Due to the cut-off of the neutron guide, in practice only the 7-19 Å band proved to be useable. The TOF electronics was set up to 128 time channels allowing 128 S(Q,t) curves to be measured.

As a first test the symmetry between the two sides was scanned (phase current) at a fixed precession field, to see if the echo group is found for all wavelengths. Figure 1 shows a 2D image of the scan with a horizontal cut at the time channels corresponding to 9 and 15 Å. As expected the centre of the echo group is at the same position for all wavelength.

Encouraged by this success the instrumental resolution was measured at 8.2 scattering angle on the usual standard graphite elastic scatterer. For better visibility, the resolution surface is shown in Fig. 2 at different precession currents and time channels. As can be seen even at the longest wavelength (time channel = 128) the resolution drops only to about 0.5. Finally for the real test we measured a polymer melt sample (15% protonated PEO in the deuterated PEO matrix at T = 140°). Figure 3 shows the S(Q,t) map as measured at one single detector position. The colouring gives an idea about the decay. There is a very favourable match between the wavelength dependence of Q and instrumental resolution. Indeed at a given scattering angle long wavelength yields

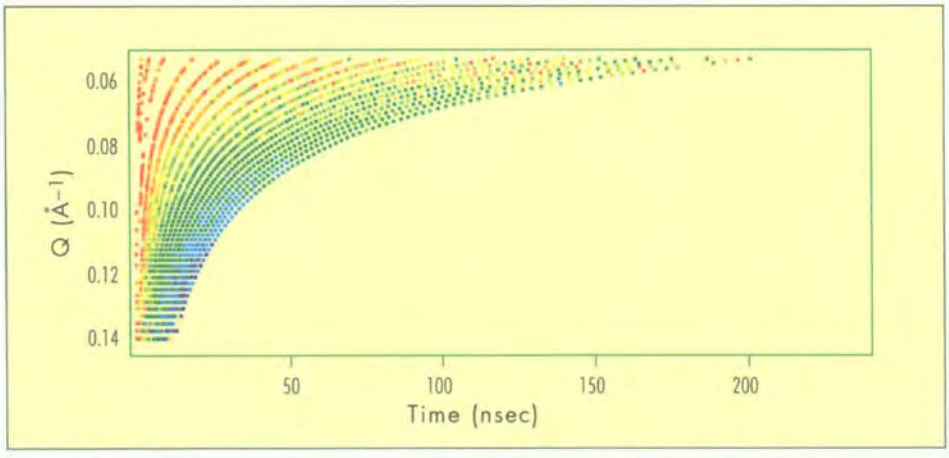

***Figure 3**: S(Q,t) map in Q,t space as measured at one given detector angle on the PEO test sample.*

small Q and long Fourier time and vice versa. In the case of polymer melt dynamics the relaxation time increases very fast about $1/\tau \sim Q^4$ so the resolution is well matched to this physical problem.

A further advantage is that at low Q (long wavelength) the scattered intensity (S(Q)) is high, partially compensating the lower incoming flux. Figure 4 shows a comparison of one S(Q,t) as measured on IN15 in TOF mode and the same sample on the Jülich NSE spectrometer at the same Q value. As a final demonstration we show the result of a fit of $\exp(-t/\tau)$ at all Q values in Fig. 5. While the fitted function is not really appropriate for the polymer dynamics, nevertheless it illustrates the wide dynamical range which can be obtained in one single measurement.

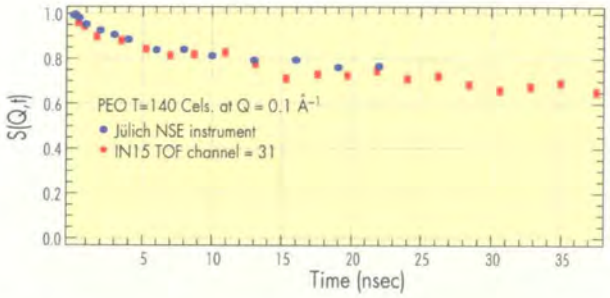

***Figure 4**: Comparison of S(Q,t) measured in Jülich and on IN15 at the same Q value.*

Despite a promising start still a lot remains to be done. Instrument tuning, data treatment has to be refined taking advantage of all related informations in the data set. Instrument stability and monitoring becomes even more essential as acquisition times become longer. For the data storage a new compressed format is under development as using the multidetector of IN15 each run takes up 136Mbyte of space without compression.

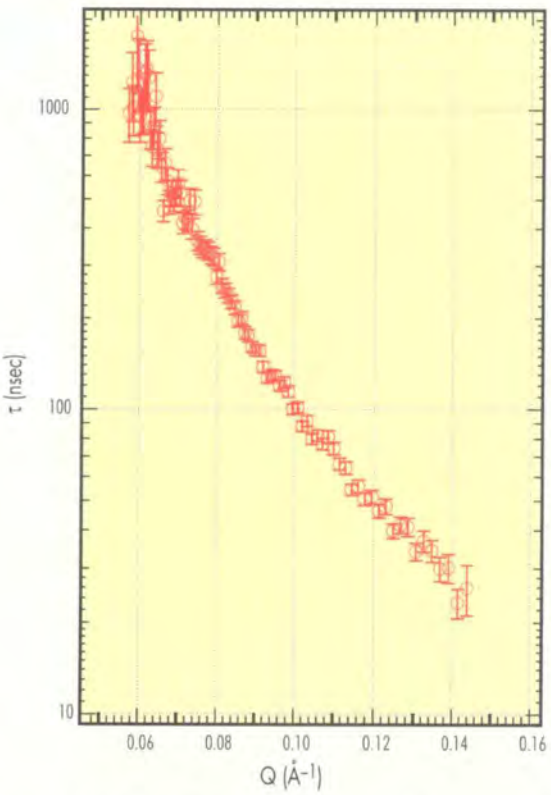

***Figure 5**: Decay time (t) as a function of Q from one measurement. It illustrates the dynamical range covered. In double-echo setup at least another decade can be gained.*

Acknowledgement

This successful start is evidently a result of a teamwork where the hard work of everybody has to be acknowledged. First of all C. Lartigue and A. Kollmar who started the construction. Later P. Schleger effectively started up the instrument and made the first real experiment [1]. The ILL technical staff helped with design, testing, making the choppers and electronics work together; the Jülich technical staff was responsible for the time-dependent power supplies. There was continuous support by the "shareholders" F. Mezei from HMI Berlin, T. Springer and D. Richter from FZ Jülich.

References

■ [1] P. Schleger , G. Ehlers, A. Kollmar, B. Alefeld, J.F. Barthelemy, H. Casalta, B. Farago, P. Giraud, C. Hayes, C. Lartigue, F. Mezei, D. Richter, - The sub-neV resolution NSE Spectrometer IN15 at the Institute Laue-Langevin, Physica B 266 (1999) 49 ■ [2] Neutron Spin Echo Ed. F. Mezei Lecture Notes in Physics 128, Springer-Verlag 1979 ■ [3] B. Farago Annual Report ILL (1988) 103 ■ [4] H. Casalta, P. Schleger, C. Bellouard, M. Hennion, I. Mirebeau, G. Ehlers, B. Farago, J.L. Dormann, M. Kelsch, M. Linde, F. Phillipp, - Direct measurement of superparamagnetic fluctuations in monodomain Fe particles via neutron spin-echo spectroscopy - Phys. Rev. Lett. 82 (1999) 1301.

The upgraded IN13

C. Pfister (IBS and Univ. J. Fourier, Grenoble),
A. Paciaroni (INFM, Operative Group Grenoble).

The backscattering spectrometer IN13 at the ILL became a CRG instrument in July 1998 under a contract between the Université J. Fourier Grenoble and the ILL. A major upgrade of the electronics and instrument control programs has been performed in August 1999. A new auto-adaptative temperature controller for the monochromator furnace allows now for an energy stabilisation of the neutron beam to ca. 0.1 μeV. The temperature of the sample, also regulated by an autoadaptative controller, is stable to better than 0.05 K. The previous instrument characteristics are retained: energy resolution of about 10 μeV, Q-range of 0.3-5.5 Å^{-1}, energy transfer up to ca. 250 μeV. These characteristics are exceptionally well suited for the study of large molecular assemblies held together by weak interactions.

The upgrade of the instrument

The instrument was previously controlled by CAMAC electronics, and operated by a VMS computer. All these elements have become obsolete and therefore, the instrument was completely modernised.

For the electronics, VME-organised controls for all parts of the instrument have been installed. The instrument control program now runs on a PC under Visual Basic. The structure of the written program is clearer and faster in execution; data can be saved every 5 seconds, and transferred to the ILL archive every minute; it presents a much more convivial interaction with the user, not only for the writing of experiment programs but also for survey of the runs and for the availability of the results "on line".

Because of the overall faster speed of the processes, we could improve the measurement of the monochromator temperature: now, the temperatures of 5 thermocouples installed at different positions on the monochromator crystals are measured by a fast-reading Keithley, and the program takes the mean of the obtained values, which is a much more relevant parameter.

The major limitation of the upgrade instrument remains its low flux. Long accumulation times are necessary to reach good statistics (typically, for 200 mg of a given biological sample at one fixed temperature, one needs at least 2 hours of counting for data relative to elastic scattering, and 3-4 days to record a quasielastic spectrum from – 100 μeV to + 100 μeV). The CRG is highly interested by the ILL project of coating the neutron guide with supermirrors (ca. 4-fold gain in flux with little loss in energy resolution on IN13).

Biophysical studies in the frame of the CRG

In the following we present the study of two examples of investigations carried out in CRG-time: the dynamics of biological macromolecules and complex systems, as a function of their environment (hydration, temperature, pressure,

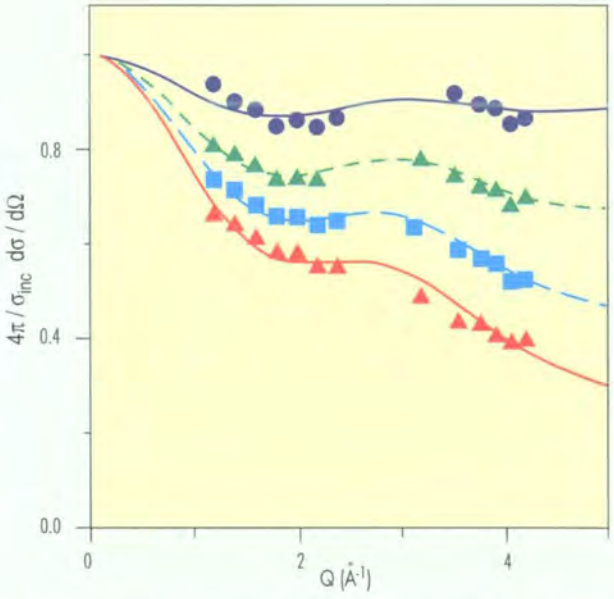

Figure 1: Elastically scattered intensity by ice Ih at 20 K (blue dots), 100 K (green triangles), 180 K (blue squares) and 260 K (red triangles). Lines are fits by a model in which protons are able to jump between two sites of different energies. (The experiments have been carried out by L. Bove, F. Sacchetti and A. Paciaroni, Perugia, Italy and INFM-OGG-Grenoble, France)

additives as salts, protectants, ligands) to find correlations with their characteristics in stability and function. These studies are related to hydrogen-bonded networks in biological matter and in ice.

The first example (Fig. 1, Bove et al.), shows results of ice Ih at different temperatures; this represents a simple prototype serving as reference system for the behaviour of protons in more complex hydrogen-bonded networks like hydrated proteins. The scattering appeared as totally elastic, even at the highest temperature studied (260 K); its integrated intensity (in the energy range –20 μeV to +20 μeV), shown in the Figure, appeared as nonharmonic even at the lowest temperature studied (20 K); this could be fitted by a model

in which the protons are able to jump between two sites of different energies, possibly along the oxygen-oxygen bonds in hexagonal loops present in the disordered ice structure.

For the second example (Fig. 2a, Di Bari et al.), we show the elastically scattered intensity by amylose and amylopectine (main components of starch) at different hydration levels (water, the "plasticiser" as in spaghettis, and involved in "gelification" as in gelly, is obviously of major importance in food science). The good quality of the data and the large Q-range available allow to analyse the results in term of conformational transitions in a double-well potential (Fig. 2a). The derived mean-square displacements (<u^2>, Fig. 2b) show a harmonic behaviour in the dry sample up to 320 K, whereas in hydrated samples a "glass-like" kinetic transition (TG) appears at ca. 230 K. The observed transition temperatures vary markedly with hydration, and they are systematically higher than those observed in globular proteins (typically 150-180 K).

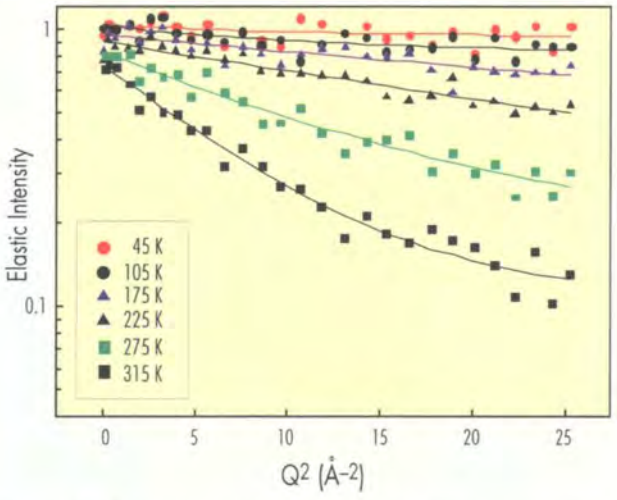

Figure 2: a) *Elastic scattered intensity vs. Q^2 at different temperatures for an amylose sample hydrated at 0.47 ($g.D_2$)/g. dry saccharide). The solid lines are fits to an asymetric double-well potential.*

These observations will have major industrial impact: the modern "food polymer science" approach for successful moisture management of food systems involve kinetically metastable, dynamically constrained glassy states rather than equilibrium thermodynamics; the glass transition temperature (TG) is a relevant parameter for product properties, stability and safety.

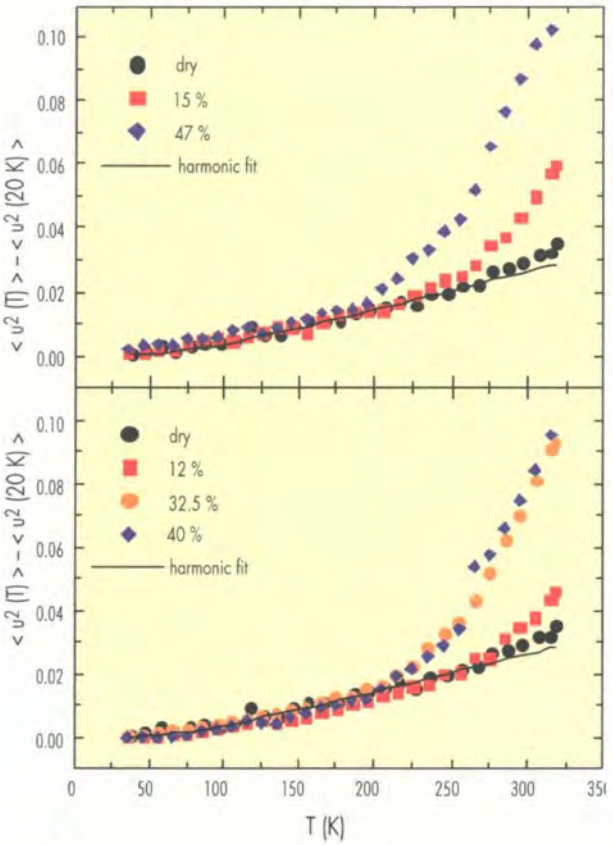

Figure 2: b) *Temperature dependence of the proton mean square displacement <u^2> (normalised to 20 K) for amylose (top) and amylopectine (bottom). The hydration is expressed as $g.D_2O$/g.dry polysaccharide. The continous line is a fit of the low temperature data to an Einstein model of independent harmonic oscillators.*
(The experiments have been carried out by M-T. Di Bari, G. Allbanese, F. Cavatorta and A. Deriu, Parma, Italy)

On-line rheometry and small-angle neutron scattering from complex fluids

P. Lindner, J. Zipfel (ILL)
J. Berghausen, F. Nettesheim, W. Richtering (Univ. Freiburg).

A technological important extension of classical scattering techniques is to investigate soft-matter systems under non-equilibrium conditions. Especially, mechanical deformation is known to have a strong influence on the morphology of complex fluids as e.g. colloidal dispersions, polymer and surfactant solutions or liquid crystals. In order to be able to directly correlate flow properties of complex fluids with the microstructure of the material in the mechanical field we installed a commercial Bohlin rheometer at D11. This rheometer allows to perform many different rheological tests as e.g. simple shear flow, creep as well as low or large amplitude oscillatory deformation. As an example, we demonstrate the influence of added, water-soluble polymer on the structure and flow behaviour of a lyotropic lamellar phase.

The influence of shear flow on the structure of complex fluids (such as surfactants in solution or block copolymer melts) has attracted interest recently [1-3]. Samples consisting of anisotropic mesophases of polymers and surfactants of macroscopic size usually display a polydomain structure and a typical texture is observed in polarising microscopy. The texture strongly influences the rheological properties and often complex flow behaviour is found because the flow field itself can alter the structure of the sample. Consequently, it is necessary to monitor the structure under flow in order to understand rheological properties of these materials. However, although many different systems have been studied during the last few years, the exact influence of the particular experimental parameters like shear rate, stress, strain of frequency remains to be investigated properly.

A further aspect that has to be considered is the type of flow the material is subjected to. In studies on block copolymer melts, large amplitude oscillatory shear has been used. But even the "simple" shear flow can be performed under different conditions, namely at constant stress or at constant shear rate. It has been reported that in some systems different results were obtained when the stress or the shear rate was constant [4-5].

It is obvious that the combination of the powerful small-angle neutron scattering (SANS) instrumentation at the ILL with a state-of-the-art rheometer will provide a unique possibility to directly correlate rheological properties of complex fluids with the underlying microstruture. For this purpose we installed a commercial rheometer at D11, see Fig. 1, which allows to perform many different rheological tests as e.g. simple shear flow either at constant shear stress or constant shear rate, creep and creep recovery as well as long and large amplitude oscillatory shear deformation.

A Couette-type shear-cell with a 1 mm gap was developed that fits into the rheometer fixtures such that two different beam-configurations can be achieved: one where the incident beam is aligned along the direction of the velocity gradient (often called "radial" beam configuration) and a second one where the beam is along the flow direction ("tangential" beam configuration). The latter beam configuration is extremely important in studies on samples with lamellar morphology. Since high quality quartz cylinders are used for the shear cell, excellent scattering data can be obtain even in the range of very low Q available at D11. The rheometer was mounted on a translation table which enables a precise computer-controlled positioning of the shear cell with respect to the neutron beam.

***Figure 1**: Picture of the BOHLIN Rheometer installed on the small-angle neutron scattering instrument D11.*

Figure 2 shows flow curves of the lyotropic lamellar phase without and with added, water soluble polymer. Obviously, the flow behaviour of the sample was extremely altered when 0.5 wt% of poly(N-isopropylacrylamide, PNIPAM) was added. Without polymer, the sample was shear thinning only whereas shear thickening and shear thinning was observed when the polymer was present. The microstructure of the samples under shear was investigated by SANS simultaneously to the rheological measurement.

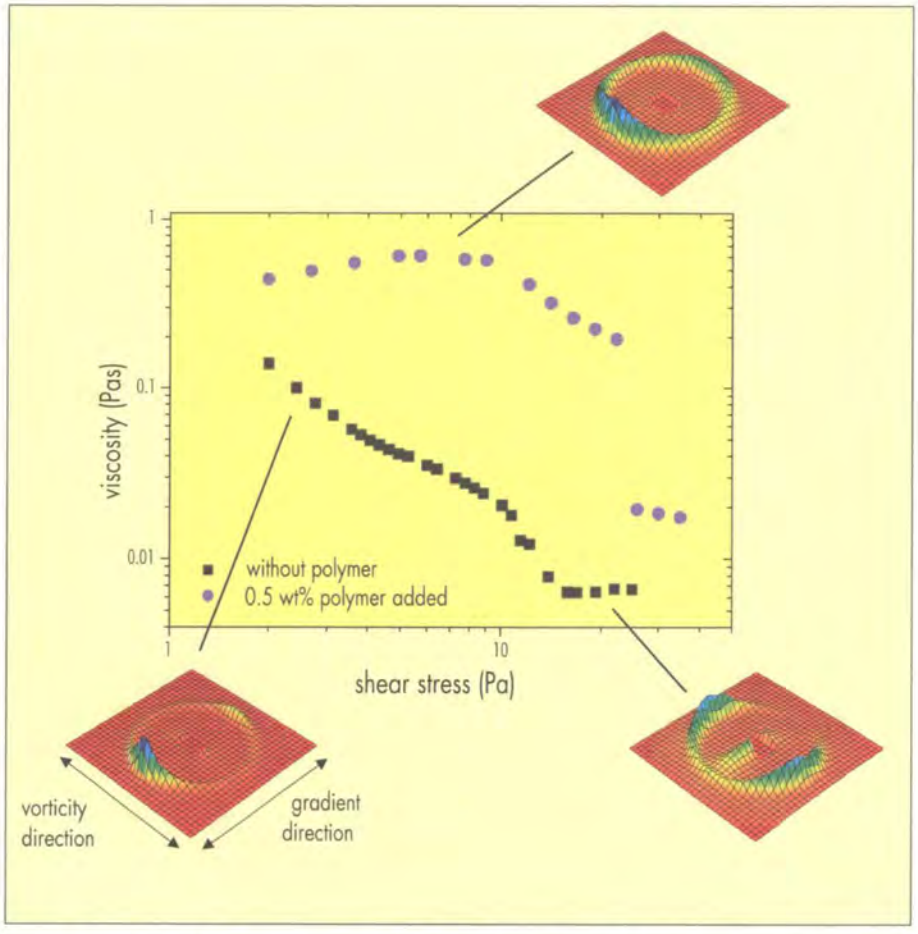

***Figure 2**: Flow curve of the lyotropic lamellar phase. Viscosity as a function of shear stress without polymer and with 0.5 wt% polymer present, together with corresponding SANS spectra as measured at D11.*

In Fig. 2, SANS spectra are shown that were obtained beam-configuration with increasing shear stress. For the sample without polymer a shear induced alignment of the lamellae was found, which can be characterised by comparing the orientation of the layer normal with the direction of flow, the direction of the velocity gradient and the vorticity (neutral) direction, respectively. The real-space orientation is denoted parallel when the layer normal points along the velocity gradient direction, and perpendicular when the layer normalpoints along the vorticity direction. At low shear stresses, the Bragg peak is observed along the velocity gradient direction thus the lamellae are aligned parallel to the walls of the shear cell. With increasing shear, the layers flip to the perpendicular orientation which is characterized by the scattering peak along the neutral (vorticity) direction. The data clearly show that the shear thinning is correlated with a reorientation process of the surfactant double layers.

A different behaviour was observed when a small amount of the water-soluble polymer was added to the aqueous surfactant solution. The SANS spectra obtained at the low and high shear stresses were similar to those obtained from the sample without polymer. At intermediate shear stressses, however, the Bragg peak was observed along the entire azimuthal trace of the two dimensional multidetector in the tangential beam configuration as show in the upper part of Fig.2.

From the isotropic Bragg scattering one can deduce the presence of multilamellar vesicles because the radial symmetry of such "onions" gives rise to an isotropic distributions of layer normals. Again, the simultaneous detection of rheological data and SANS spectra allows a direct correlation of flow properties with the (shear induced) microstructure. Obviously, the vesicles are destroyed at high shear and a perpendicular orientation of planar layers was found.

This is a first example of the new opportunities to explore the differences between rate and stress controlled shear deformations by using the recently installed commercial rheometer.

References

■ [1] G. H. Fredrickson, F. S. Bates, Ann. Rev. Mater. Sci. 26 (1996) 501 ■ [2] O. Diat, D. Roux, F. Nallet, J. Phys. II 3 (1993) 1427 ■ [3] J. Zipfel, J. Berghausen, P. Lindner, W. Richtering, J. Phys. Chem. B 103 (1999) 2841 ■ [4] J. Bergenholtz, N. J. Wagner, Langmuir 12 (1996) 3122 ■ [5] G. Schmidt, S. Müller, C. Schmidt, W. Richtering, Rheol. Acta 38 vol. 8 (1999) 486.

New gravity UCN spectrometer

- I. V. Bondarenko, A. I. Frank (FLNP, Dubna),
- S. V. Masalovich, S. N. Balashov (RRC "Kurchatov Institute", Moscow),
- J. Butterworth, P. Geltenbort P. Høghøj (ILL),
- A. Cimmino, A. G. Klein (School of Physics, Melbourne University).

A gravity spectrometer for ultra-cold neutrons (UCN) using neutron interference filters has been installed and tested. Energy resolution of the order of 6.5 neV has been obtained, which is adequate for a number of proposed fundamental experiments in UCN optics.

The neutron interference filter is analogous to the optical Fabry-Perot interferometer for light. It was first proposed by A. Seregin [1] and manufactured and tested by A. Steyerl et al. [2,3]. The operation of the filter is based on the specific quantum properties of a one-dimensional potential structure.

The long wavelength neutron interaction with matter can be described by the introduction of an effective potential, associated with the medium $U = \frac{2\pi\hbar^2}{m}\rho b$, where m is the neutron mass, ρ is the density of nuclei and b the coherent scattering length. In the simplest case, the filter is made of a three-layered structure of thin films deposited onto a substrate transparent to UCN. Since the outer layers have a greater value of ρb than the inner layer, the potential structure of a filter has a two-humped barrier with a well in between. For a sufficient thickness of the middle layer, the width of the gap is large enough for quasi-bound states to be formed. As a result, the transmission function of the filter has an essentially resonant behaviour as shown in Fig. 1.

For UCN spectrometry, two horizontally oriented interference filters, each having only one resonance, are placed at different heights, one above the other, inside a vertical neutron guide. UCNs, which pass through the first filter, are accelerated in the Earth's gravitational field.

The second filter has a different value of the resonant energy so as to compensate for the change of energy caused by gravity. By changing the position of this analysing filter, it is possible to scan the energy of the transmitted neutrons. Recently, a spectrometer based on this idea [4,5] was constructed and tested (see Fig. 2).

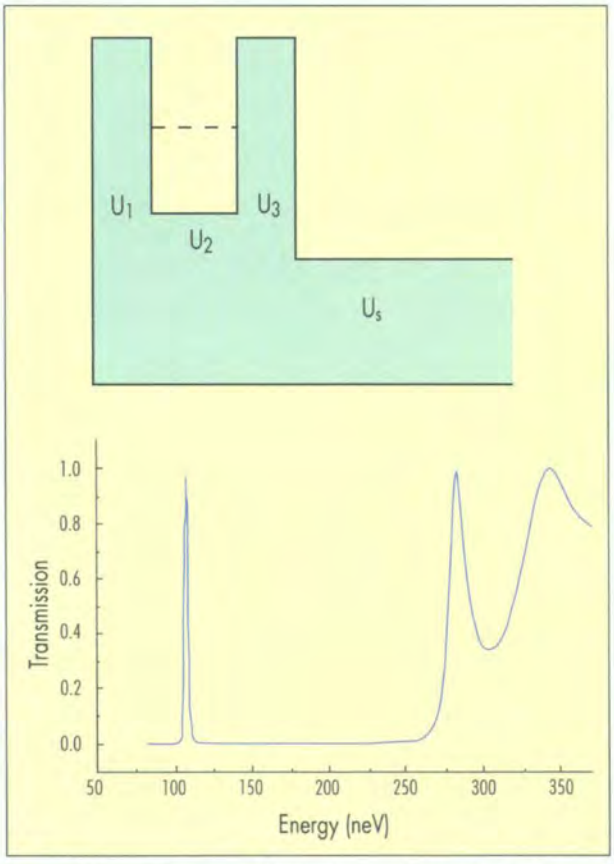

***Figure 1**: Potential structure of the simplest interference filter and its transmission function. The narrow peak on the left corresponds to tunneling through the barriers.*

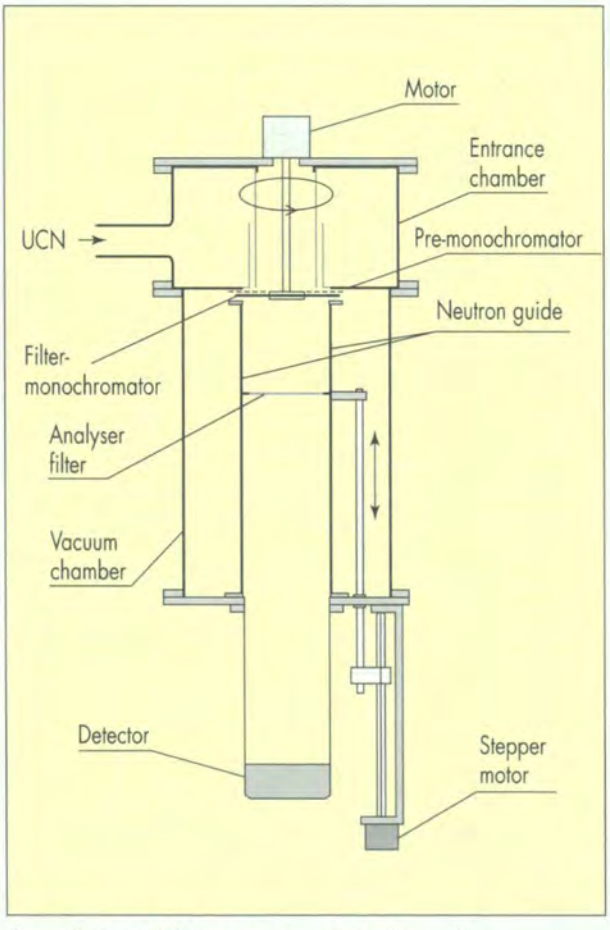

***Figure 2**: Gravity UCN spectrometer with interference filters.*

UCNs enter the spectrometer from the source and after several reflections off the walls of the entrance chamber pass through the cylindrical channel. The channel guides the neutrons to the filter-monochromator. UCNs irradiate only the peripheral region of the filter.

The fitter may be rotated by the motor which is necessary for certain types of experiment (see details in [4,5]).

It is also possible to install an additional filter-premonochromator between the exit of the channel and the main monochromator. UCNs which are transmitted through the filter enter the hexagonal glass neutron guide with vertical walls. They have a relatively narrow energy spectrum, with a width of the order of 4 neV. Inside this guide a second filter-analyser is located. A precise stepper motor driver can change the position of the analyser. The neutrons transmitted through the analyser filter are counted with a ^{3}He proportional detector.

A set of interference filters of different types [5] were designed and manufactured by magnetron sputtering on silicon wafers at the ILL's sputtering machine [6].

The spectrometer was installed at the test beam of the PF2 instrument. The obtained resolution was about 6.5 neV, the maximum count rate was 1.5-3 c/s and the background was 0.2 c/s (see Fig. 3). These parameters make it possible to measure line shifts (arising from any physical effects) down to the order of 10^{-11} eV. This allows us to perform a number of experiments in UCN optics.

The first experiment, which was performed with this device, aimed to test the validity of the commonly accepted neutron dispersion law in matter for the case of very small neutron energies.

Furthermore, the Gravity Spectrometer may be used for the investigation of a number quantum phenomena, namely:

a) controlled change of neutron energy caused by diffraction of neutrons on a moving grating, b) neutron time focusing, which may used in future for the creaton of new intense UCN sources at pulsed neutron sources, c) observation of neutron energy changed due to transmission through an accelerating plate etc.

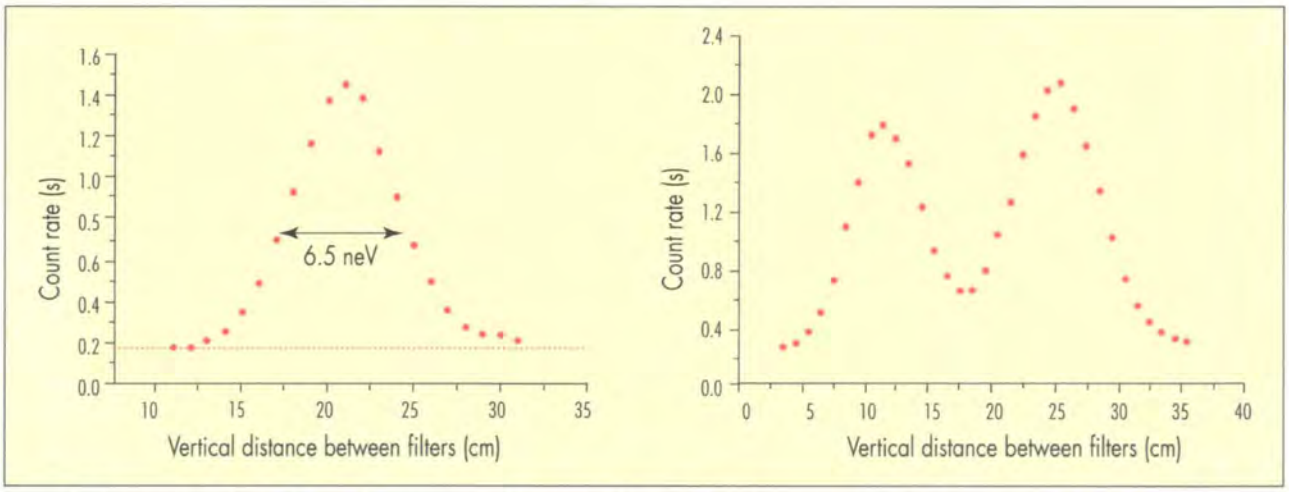

***Figure 3** : Scanning curve for two filters with resonance at 107 nev and 127 neV (left) and demonstration of the level splitting which appeared in a pair of coupled resonators (right). In this last case a double-well five layer Ni(N)-Ti structure was used as the monochromator.*

References

■ [1] A.A. Seregin, JETP 73 (1977) 1634 ■ [2] K.-A. Steinhauser, A. Steyerl, H. Scheckenhofer, S.S. Malik, Phys. Rev. Lett. 44 (1980) 1306 ■ [3] A. Steyerl, W. Drexel, S.S. Malik, E. Gutsmiedel, Physica B 151 (1988) 36 ■ [4] I.V. Bondarenko et al., JETP Letters 67 (1998) 786 ■ [5] I.V. Bondarenko et al., Physics of Atomic Nuclei 62 (1999) 721 ■ [6] I. Anderson, P. Høghøj, ILL Annual Report (1996) 84.

"The one that got away: it was this big."
Giuseppe Zaccai, IBS/ILL.

Michel Ferrand (right), CEA Grenoble,
offering a quick shave to Peter Geltenbort.

"If I talk to it nicely it might work",
Béatrice Nicolaï, LLB Saclay,
looking after her cryostat experiment.

Jean-Rémy Villard, Jean-Louis Champon
and Peter Suttling (from right to left)
test the shutters on IN22.

EXPERIMENTAL PROGRAMME

4

1 Instrument list

2 Reactor operation

3 Beam-time allocation

4 Instrument availability

5 Instrument performance

List of instruments (Dec. 99)

ILL instruments

D1A (1/2)	powder diffractometer	operational
D2B	powder diffractometer	operational
D3	single-crystal diffractometer	operational
D4 (1/2 with IN1)	liquids diffractometer	operational
D7	diffuse-scattering spectrometer	operational
D9	single-crystal diffractometer	operational
D10	single-crystal diffractometer	operational
D11	small-angle scattering diffractometer	operational
D16	small momentum-transfer diffractometer	operational
D17	reflectometer	commissioning
D19	single-crystal diffractometer	operational
D20	powder diffractometer	under repair
D22	small-angle scattering diffractometer	operational
IN1 (1/2 with D4)	three-axis spectrometer	operational
IN4	time-of-flight spectrometer	commissioning
IN5	time-of-flight spectrometer	operational
IN6	time-of-flight spectrometer	operational
IN8	three-axis spectrometer	under reconstruction
IN10	backscattering spectrometer	operational
IN11	spin-echo spectrometer	operational
IN14	three-axis spectrometer	operational
IN16	backscattering spectrometer	operational
IN20	three-axis spectrometer	operational
PF1	neutron beam for particle physics	operational
PF2	ultracold neutron source for particle physics	operational
PN1	fission product mass-spectrometer	operational
PN3	gamma-ray spectrometer	operational

Jointly funded instruments

DB21 (1/2)	single-crystal diffractometer	operational, with EMBL
LADI (1/2)	LAUE diffractometer	operational, with EMBL
IN15	spin-echo spectrometer	operational, with FZ Jülich and HMI Berlin

CRG instruments

ADAM	reflectometer	CRG-B operational
BRISP	Brillouin spectrometer	CRG-B under construction
D1A	powder diffractometer	potential CRG
D1B	powder diffractometer	CRG-A operational
D15	single-crystal diffractometer	CRG-B operational
D23	single-crystal diffractometer	CRG-B operational
EVA	reflectometer	CRG-B operational
IN12	three-axis spectrometer	CRG-B operational
IN13	backscattering spectrometer	CRG-A operational
IN22	three-axis spectrometer	CRG-B operational
S18	interferometer	CRG-C operational
S51	Avogadro	CRG-C operational

Test beams

CT1, CT2	detector test-facility
IN3	three-axis test spectrometer
S42	Laue crystal alignment facility
T3	neutron optic test-facility
T13A,C	monochromator test-facility
T17 test	cold neutron-beam test-facility
S10, S34,	uninstrumented beam-positions

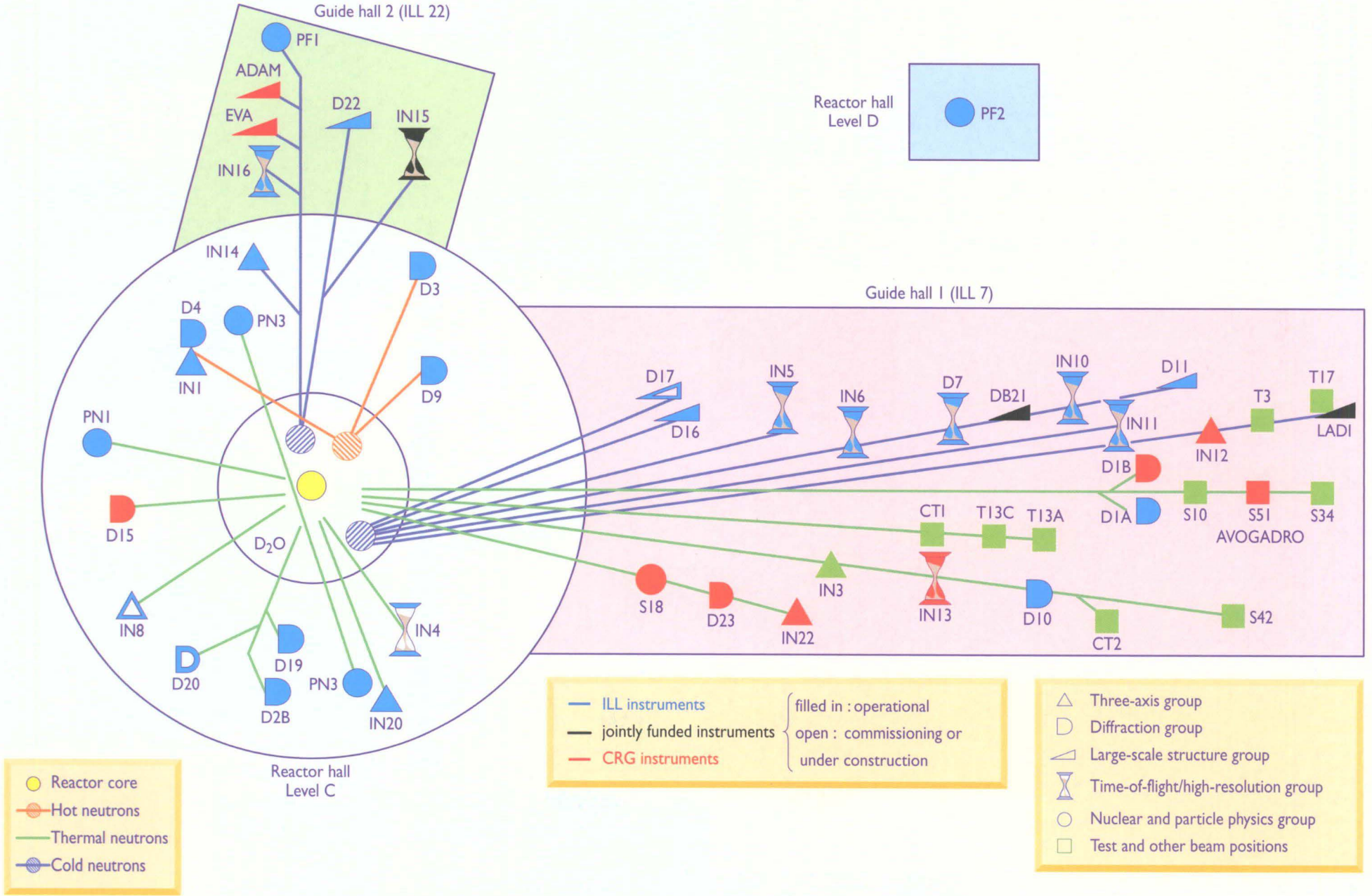
Guide hall 2 (ILL 22)
PF1
ADAM
EVA
IN16
D22
IN15
IN14
D3
D4
PN3
IN1
D9
PN1
D15
D2O
IN8
D20
D19
D2B
PN3
IN4
IN20
Reactor hall
Level C
Reactor hall
Level D
PF2
Guide hall 1 (ILL 7)
D17
D16
IN5
IN6
D7
DB21
IN10
IN11
D11
T3
T17
LADI
IN12
D1B
D1A
S10
S51
S34
AVOGADRO
CT1
T13C
T13A
S18
D23
IN22
IN3
IN13
D10
CT2
S42
Reactor core
Hot neutrons
Thermal neutrons
Cold neutrons
ILL instruments
jointly funded instruments
CRG instruments
filled in : operational
open : commissioning or
under construction
Three-axis group
Diffraction group
Large-scale structure group
Time-of-flight/high-resolution group
Nuclear and particle physics group
Test and other beam positions

Reactor operation

cycle n°	start date	finish date	days scheduled	days of operation	unscheduled shutdowns
117-2	02/02/99	28/02/99	25	24.5	1
118	16/03/99	05/05/99	50	50	0
119	25/05/99	16/07/99	50	50	1
120	12/08/99	09/10/99	50	50	2
121-1	19/10/99	23/11/99	50	33.5	2

Table 1: *Reactor operation in 1999.*

In 1999, the reactor provided scientists with 208 operating days. Apart from the loss of half a day in the first cycle, all time lost due to unscheduled shutdowns during the first four cycles was recovered and the operating schedule was respected until cycle 121-1. This cycle was suspended due to divergent readings on certain temperature measurements on the hot source. Investigations revealed that the hot source would have to be dismantled before the reactor could be restarted. Therefore, the hot source was removed on 15 December 1999.

Owing to administrative problems in connection with the transport container, delivery of the new fuel element for cycle 121-1 was delayed. Nevertheless, the cycle started on schedule.

An important project, completed end of 1999, was the installation of the new neutron guide H113 (see also page 74), which had to pass through both of the containment walls of the reactor building.

The simultaneous removal of three fuel elements is now possible with the new transport container which was used for the first time at the end of 1999. Three elements in storage at ILL and six at the Cadarache site were delivered to COGEMA for reprocessing in 1999.

André Rimet helps putting the dismantled hot source into storage.

Beam-time allocation for 1999

Overall the subcommittees of the scientific council (meetings in Oct. 98 and Apr. 99) scrutinised almost 1000 proposals, out of which 685 proposals received beam time, allocating about 4500 instrument days of beam time on the different instruments; about 730 experiments were carried out. Table 2 shows the request and allocation of beam time per instrument.

Note that D4 and IN1 share a beam and that the CRG instruments offer a reduced number of days for ILL users. For PF2 several experiments share the beam taking neutrons alternatively, so the table contains the beam-days allocated but gives the total number of experiments running simultaneously.

Table 3 shows the distribution of beam-time request and allocation amongst the member and scientific-member countries.

In 1999, the following countries were members: France, Germany, UK, Spain, Switzerland, Austria, Italy, and the

country	requested days	requested in %	allocated days	allocated in %
AUT+CZ	198.6	2.4%	114.3	2.6%
CH	332.8	4.1%	178.3	4.0%
D	**2250.6**	**27.7%**	**1349.7**	**30.5%**
E	365.7	4.5%	196.1	4.4%
F	**2039.0**	**25.1%**	**1143.0**	**25.8%**
GB	**1997.7**	**24.6%**	**1042.0**	**23.5%**
I	365.8	4.5%	139.5	3.2%
RUS	584.0	7.2%	264.3	6.0%
Total	**8134.1**	**100.0%**	**4427.3**	**100.0%**

Table 3: *Beam-time request and allocation by country.*

Czech Republic. In calculating the above statistics of beam time per country, the attribution is based on the location of the laboratory of the proposers, not their individual nationality. For a proposal involving laboratories from more than one member country, the total number of days is divided equally among the collaborating countries. When a proposal involves a collaboration with a non-member country, the allocated time is attributed entirely to the collaborating member country (or countries). When ILL scientists are proposers or co-proposers, the allocated 'ILL time' is attributed among the member countries according to their financial contributions to ILL. Local contacts are not counted as proposers.

The ILL welcomed about 1200 visitors in 1999. Three quarters came from the member countries including 285 from France, 242 from Germany and 211 from the UK; many of our visitors were received more than once. There were thus almost 1800 visits carrying out about 730 experiments. The distribution of beam time for these experiments amongst the different 'colleges' was as follows: 17% of the days were allocated to nuclear and particle physics (college 3), 16% to structural and magnetic excitations (college 4), 31% to crystal and magnetic structures (college 5), 10% to structure and dynamics of liquids and glasses (college 6), 8% to materials science, surfaces and spectroscopy (college 7), 9% to biology (college 8) and 9% to structure and dynamics of soft-condensed matter (college 9).

"Cheerfulness gives elasticity to the spirit. Spectres fly before it." Herma Büttner (left) and Brigitte Aubert, the organisers of the subcommittee meetings, at the final lunch of the meeting.*

** Self-Help (1859) ch.12*

"There is no such thing as a free lunch." Valeria Arrighi, Univ. Edinburgh, Caterina Petrillo, Univ. Perugia, Carmen Miangos, ICTP-CSIC Madrid, (from left to right) enjoy their lunch after the subcommittee meetings.*

** Axiom in US economics in the 60s. R. Heinlein "The Moon is a Harsh Mistress" (1966)*

instrument	days requested	days allocated	number of experiments
*ADAM**	*181*	*54*	*10*
D10	289	175	21
D11	200	140	60
*D15**	*174*	*57*	6
D16	177	70	11
D17	115	50	10
D19	238	173	16
D1A	204	97	25
*D1B**	*135*	*120*	*48*
D20	126		
D22	358	156	77
*D23**	*0*	*30*	*4*
D2B	339	165	66
D3	264	145	17
D4	171	85	19
*EVA**	*46*	*22*	*3*
D7	362	173	20
D9	243	165	24
DB21	118	87	5
IN1	202	71	12
IN10	163	141	19
*IN12**	*4*	*54*	*5*
*IN13**	*102*	*14*	*2*
IN14	335	172	21
IN15	183	80	9
IN16	302	165	26
IN20	196	145	15
*IN22**	*0*	*26*	*3*
IN4	149	56	14
IN5	333	165	34
IN6	324	161	40
IN8	291	162	19
LADI	183	117	7
PF1	350	225	5
PF2	229,5	175	12
PN1	343	162	14
PN3	423	199	14
Total	**8147.5**	**4427**	**732**

***Table 2:** Beam-time request and allocation by instrument. CRG instruments are marked with an asterisk.*

Instruments

The instrumental facilities at the ILL are shown in the schematic diagram on page 91. Besides the ILL instruments there are CRG-instruments, which are operated by external **C**ollaborating **R**esearch **G**roups. There are currently three different categories of CRG instruments. CRG-A in which the external group leases an instrument owned by ILL. They have 50% of the beam time at their disposal and for the other 50% they support ILL's scientific user programme. The CRG-B category owns their instrument and have 70% of the beam time, supporting the ILL programme for the other 30%. Finally, CRG-C instruments are used full time for specific research programmes by the external group who has exclusive use of the beam.

DB21, LADI and IN15 are a joint venture of ILL with other laboratories: in the case of DB21/LADI with EMBL and for IN15 with FZ Jülich and HMI Berlin.

The list of instruments by type as at December 1999 is summarised below (CRG instruments are marked with an asterisk *):

- powder diffractometers: D1A, D1B*, D2B, (D20, detector in repair)
- liquids diffractometer: D4
- single-crystal diffractometers: D3, D9, D10, D15*, D19, DB21, D23*, LADI
- small-angle scattering: D11, D22
- small momentum-transfer diffractometer: D16
- reflectometers: ADAM*, (D17 in commissioning), EVA*
- diffuse-scattering spectrometer: D7
- three-axis spectrometers: IN1, (IN8 under reconstruction), IN12*, IN14, IN20, IN22*
- time-of-flight spectrometers: IN5, IN6, IN4
- backscattering and spin-echo spectrometers: IN10, IN11, IN13*, IN15, IN16
- nuclear-physics instruments: PN1, PN3
- particle-physics instruments: PF1, PF2

Details of the instruments can be found on the web under http://www.ill.fr.

AVOGADRO* and S18*, an interferometer, are CRG-C instruments and are not available as 'user' instruments.

*"Today is the last day of an era past." * Nick Bernhoeft (left), CEA Grenoble, and Gerry Lander, EITU Karlsruhe, before IN8 was shut down for reconstruction.*

**B. Yeltsin, 'Guardian' 1 Sep. 1994*
(at a Berlin ceremony to end the Soviet military presence)

Instrument performance

Table 4 below gives a summary of instrument performance for 1999.

For each cycle a record is kept of any time lost from the total available beam-time, and the reasons for the lost time are analysed for all the instruments.

The table gives a global summary for the year: Overall about 400 days of the total available beam-time was lost due to various malfunctions. However, most of this time was not lost to users because time for minor breakdowns, tests, calibrations and scheduling difficulties is allowed for by initially scheduling about 80% of the total available beam-time. Thus, the total number of days delivered to users was slightly higher than the number of days originally scheduled: 3730 compared with 3716 originally scheduled. In previous years, the ILL gave even 80 days more than originally scheduled.

But unfortunately, in 1999 we experienced several unforeseen shutdowns and therefore the overall loss of beam time was a bit higher than usual. Please note that CRG instruments are not included, because they are not operated by ILL.

Detailed comments on the larger beam-time losses (10% or greater) are as follows:

- Unfortunately, D3's change over of the control computer did not work as smoothly as expected and some time was lost. In addition, beam time could not be used efficiently due to problems on the user side; it was impossible to find replacement experiments.
- D1A faced user problems, too, and could not fill the gap with allocated beam time.
- Also DB21 suffered time loss due to samples which could not be made available in time.
- D11 had various problems mainly due to malfunctioning of the electronics and the selector. However, the selector is replaced now and the electronics will be replaced beginning of 2000.
- IN6 experienced problems with the new temperature regulation and the electronics of the monochromator drive.
- IN15 struggled with the mechanics and electronics of its chopper for the time-of-flight option. But finally, the instrument team succeeded to operate IN15 successfully in time-of-flight mode as you can see on page 79.
- PN1's breakdown was due to failures in the high-voltage components (400kV).
- In 1999's last cycle, PN3 had to be shutdown earlier because of a protection default at the sample waste container.

instruments	days lost	% lost	sched. days	days used	instruments
D1A	14.0	11.3%	110.0	101.0	D1A
D2B	8.5	4.0%	161.0	174.0	D2B
D3	32.0	15.2%	138.0	126.0	D3
D4	7.9	8.3%	89.0	90.3	D4
D7	20.0	9.5%	162.0	145.0	D7
D9	15.5	7.4%	169.0	183.0	D9
D10	10.1	4.8%	177.0	181.5	D10
D11	33.9	16.2%	160.0	149.3	D11
D19	8.0	3.8%	171.0	184.0	D19
DB21	29.8	32.8%	87.0	103.0	DB21
D22	14.9	7.1%	149.0	145.5	D22
LADI	9.0	8.5%	104.0	106.0	LADI
IN1	6.0	5.2%	74.0	86.0	IN1
IN5	13.0	6.2%	147.0	145.0	IN5
IN6	22.0	10.5%	184.0	177.0	IN6
IN8	15.5	7.4%	162.0	174.0	IN8
IN10	8.0	3.8%	138.0	132.0	IN10
IN11	12.7	6.0%	161.0	174.0	IN11
IN14	9.2	4.4%	160.0	168.0	IN14
IN15	41.0	19.5%	131.0	122.0	IN15
IN16	12.8	6.1%	146.0	147.0	IN16
IN20	10.5	5.0%	168.0	168.0	IN20
PF1	2.0	1.0%	210.0	208.0	PF1
PF2	5.0	2.4%	*	*	PF2
PN1	32.5	15.5%	167.0	171.0	PN1
PN3	21.0	10.0%	191.0	170.0	PN3
Total	**414.7**		**3716.0**	**3730.7**	

Table 4: *Instrument performance. (*PF2 consists of several long-term experiments so comparison of days scheduled and used is not meaningful).*

Resto Basler (left) and Hanspeter Aebersold, both Univ. Bern, change their sample on IN5.

The lady scientists of the large-scale structure group: Laurence Perino, Isabelle Grillo and Giovanna Fragneto-Cusani (from left).

Francis Tasset (right) discusses dilution-fridge set-ups with Serge Pujol.

Red shirt, white wine, white shirt, red wine: Ted Forgan (left), Univ. Birmingham, and Bob Cywinski, Univ. St. Andrews.

FACTS AND FIGURES

5

Sculpture by Ipoustéguy "Man Accomplishing Unity" in front of the ILL main building.

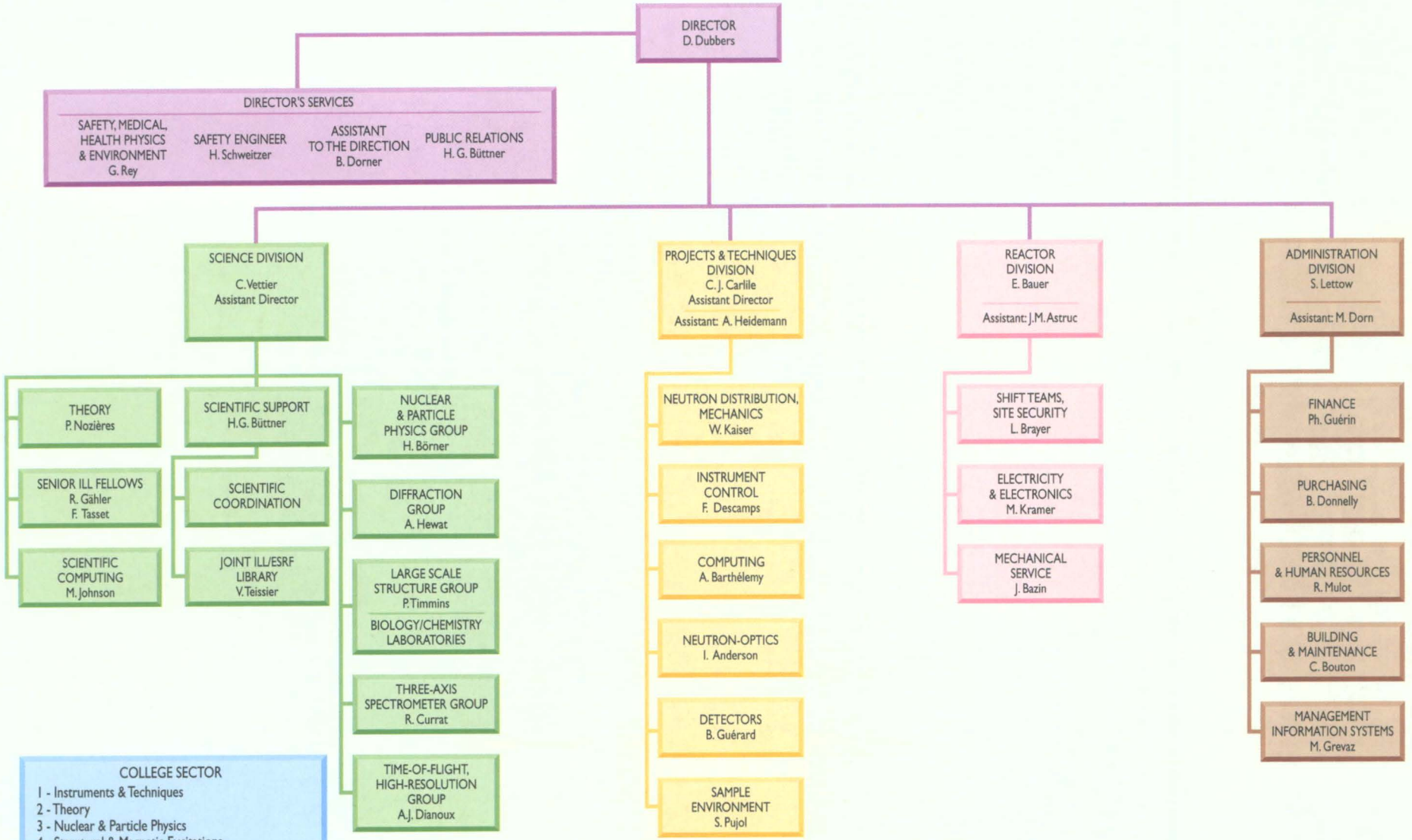

ILL organisation chart on 31/12/99

Facts and Figures for 1999

Name: **Institut** Max von **Laue** - Paul **Langevin (ILL)**

Founded: 1967

Associates: France: Commissariat à l'Energie Atomique (CEA)
Centre National de la Recherche Scientifique (CNRS)
Federal Republic of Germany: Forschungszentrum Jülich
United Kingdom: Engineering and Physical Sciences Research Council (EPSRC)

Countries with Scientific Membership:
Spain: Oficina de Ciencia y Tecnologia (OCYT)
Switzerland: Schweizer Bundesamt für Bildung und Wissenschaft (SBBW)
Italy: Istituto Nazionale per la Fisica della Materia (INFM)
Russia: MINATOM
MENI (Middle European Neutron Initiative) Consortium, composed of:
a) Austria: Österreichische Akademie der Wissenschaften
b) Czech Republic: Charles University of Prague

Staff: 394 people including 48 experimentalists in the scientific sector
254 French, 49 German, 53 British, 38 others

Budget: 373.6 MF (excluding taxes)

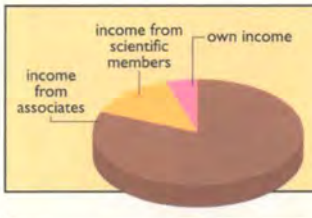

Income in MF

304.6	81.53%	from associates (divided: F 37.87%; D 37.13%; UK 25%)
50.5	13.52%	from scientific members
18.5	4.95%	own income

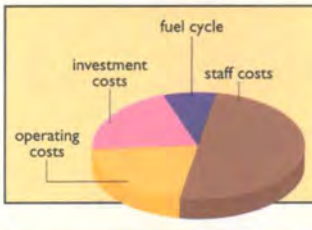

Expenditure in MF

190.2	50.91%	staff costs
77.9	20.85%	operating costs
35.5	9.50%	investment costs
70.0	18.74%	fuel cycle

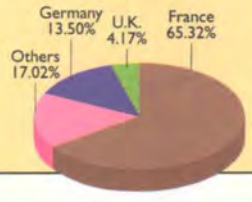

Purchases in MF (total 68.1 MF)

51.8	65.32%	France
10.7	13.50%	Germany
3.3	4.17%	UK
13.5	17.02%	Others

Bodies: Steering Committee, meeting twice a year
Scientific Council with 8 Subcommittees, meeting twice a year
Management Board, meeting weekly

Reactor: 58 MW, running 4.5 reactor cycles per year (with cycles of 50 days)

Experimental Programme:
about 730 experiments (allocated by subcommittees) on 25 ILL-funded and 8 CRG instruments
about 1200 visitors coming from 30 countries
about 1000 proposals submitted and 685 accepted

Experiment Selection by the Scientific Council via its 8 Subcommittees:
nuclear and particle physics (college 3)
structural and magnetic excitations (college 4)
crystallographic structures (college 5a)
magnetic structures (college 5b)
structure and dynamics of liquids and glasses (college 6)
materials science, surfaces and spectroscopy (college 7)
biology (college 8)
structure and dynamics of soft-condensed matter (college 9)

Scientific Life: based on 10 colleges, 8 of which correspond to the subcommittees plus:
instruments and techniques (college 1), theory (college 2)

Dietmar Puschner replacing the paper clip on the He cryostat.

Kazu Kakurai (left), Univ. Tokyo, and Louis-Pierre Regnault, CEA Grenoble, set up IN22.

"Something must be done."* Project meeting of D17B, Peter Høghøj, Gills Pastrello, Michel Bonnaud, Luc Didier, Bob Cubitt (from left to right).

**Edward VIII in 'Western Mail' 19 Nov. 1936*

Jacques Previtali, CEA Grenoble, installs the new 4 Tesla horizontal field cryomagnet on IN12.

PUBLICATIONS

6

In 1999, the ILL received notice of 437 publications by ILL staff and users of which 283 were published as journal articles, and 154 as conference proceedings in journals, books or reports. The distribution by subject is as follows: 48 in instruments and methods, 7 in theory, 29 in particle and nuclear physics, 48 in structural and magnetic excitations, 54 in crystallographic structures, 116 in magnetic structures, 35 in structure and dynamics of liquids and glasses, 57 in materials science, surfaces and spectroscopy, 14 in biology and 54 in structure and dynamics of soft-condensed matter.

This list gives publications received during 1999 resulting from research carried out at the ILL. It was generated from the library database LORIS-DORIS and can be consulted on the Web at http://www.ill.fr

PAPERS PUBLISHED IN SCIENTIFIC PERIODICALS, BOOKS AND CONFERENCE PROCEEDINGS

ABAD E., PIQUE C., BLANCO J.A., ARTIGAS M., BURRIEL R., FERNANDEZ-DIAZ M.T. Magnetic structures of RFe_xMn_{12-x} compounds (R = Tb and Y).
Journal of Magnetism and Magnetic Materials **196-197**, 745-747 (1999)

ALLMAN B.E., CIMMINO A., GRIFFIN S.L., KLEIN A.G., NUGENT K.A., ANDERSON I.S., HØGHØJ P. Novel optics for conditioning neutron beams II: Focusing neutrons with a "Lobster-Eye" optic.
Neutron News **10**, 20-23 (1999)

ALLMAN B.E., CIMMINO A., GRIFFIN S.L., KLEIN A.G., NUGENT K.A., ANDERSON I.S., HØGHØJ P., PEELE A.G. Focussing neutrons with a "Lobster-eye" optic.
Proceedings SPIE **3449**, 165-174 (1998)

ALONSO J.A., GARCIA-MUNOZ J.L., FERNANDEZ-DIAZ M.T., ARANDA M.A.G., MARTINEZ-LOPE M.J., CASAIS M.T. Charge disproportionation in $RNiO_3$ perovskites: Simultaneous metal-insulator and structural transition in $YNiO_3$.
Physical Review Letters **82**, 3871-3874 (1999)

ALONSO J.A., MARTINEZ J.L., MARTINEZ-LOPE M.J., CASAIS M.T., FERNANDEZ-DIAZ M.T. Room temperature magnetoresistance and cluster-glass behavior in the $Tl_{2-x}Bi_xMn_2O_7$ ($0 \le x \le 0.5$) pyrochlore series.
Physical Review Letters **82**, 189-192 (1999)

ALONSO J.A., MARTINEZ-LOPE M.J., CASAIS M.T., ARANDA M.A.G., FERNANDEZ-DIAZ M.T. Metal-insulator transitions, structural and microstructural evolution of $RNiO_3$ (R = Sm, Eu, Gd, Dy, Ho, Y) perovskites: Evidence for room-temperature charge disproportionation in monoclinic $HoNiO_3$ and $YNiO_3$.
Journal of the American Chemical Society **121**, 4754-4762 (1999)

AMORETTI G., CACIUFFO R., SANTINI P., LANDER G.H., KULDA J., DU PLESSIS P. DE V. Polarized neutron scattering study of the magnetic response across T_N in a single crystal of UO_2.
Journal of Applied Physics **85**, 4524-4526 (1999)

ANDERSON C.R., ANDERSEN K.H., BOSSY J., STIRLING W.G., DIMEO R.M., SOKOL P.E., COOK J.C., BROWN D.W. High-resolution neutron-scattering study of the roton in confined superfluid ^{4}He.
Physical Review B **59**, 13588-13591 (1999)

ANDRES H., CLEMENTE-JUAN J.M., AEBERSOLD M., GÜDEL H.U., CORONADO E., BÜTTNER H., KEARLY G., MELERO J., BURRIEL R. Magnetic excitations in polyoxometalate clusters observed by inelastic neutron scattering: Evidence for anisotropic ferromagnetic exchange interactions in the tetrameric cobalt(II) cluster $[Co_4(H_2O)_2(PW_9O_{34})_2]^{10-}$. Comparison with the magnetic and specific heat properties.
Journal of the American Chemical Society **121**, 10028-10034 (1999)

ANGLARET E., ROLS S., SAUVAJOL J.L. Comment on "Effect of the growth temperature on the diameter distribution and chirality of single-wall carbon nanotubes".
Physical Review Letters **81**, 4780 (1998)

ANTONIADIS A., BERRUYER J., FILHOL A. Estimation semi-paramétrique dans les familles doublement poissonniennes et application aux spectres de diffraction.
Revue de Statistique Appliquée **47**, 57-80 (1999)

APRAHAMIAN A., DE HAAN R.C., LESHER S.R., DÖRING J., BRUCE A.M., BÖRNER H.G., JENTSCHEL M., LEHMANN H. Collective $K^\pi = 0^+$ vibrational excitations in ^{178}Hf.
Journal of Physics G: Nuclear and Particle Physics **25**, 685-689 (1999)

ARBE A., COLMENERO J., GOMEZ D., RICHTER D., FARAGO B. Reply to "Comment on 'Merging of the α and β relaxations in polybutadiene: A neutron spin echo and dielectric study'".
Physical Review E **60**, 1103-1105 (1999)

ARGYRIOU D.N., MITCHELL J.F., RADAELLI P.G., BORDALLO H.N., COX D.E., MEDARDE M., JORGENSEN J.D. Lattice effects and magnetic structure in the layered colossal magnetoresistance manganite $La_{2-2x}Sr_{1+2x}Mn_2O_7$, $x = 0.3$.
Physical Review B **59**, 8695-8702 (1999)

ARZUMANOV S.S., BELYAEV S.T., BONDARENKO L.N., IVANOV S.M., KOROBKINA E.I., LYUBIMOV A.N., MOROZOV V.I., RYAZANOV A.I., PANIN Y.N., FOMIN A.I., CHERNYAVSKII S.M., GELTENBORT P., PENDLEBURY J., SCHRECKENBACH K. Cluster structure of the material surface as the cause of the selective enhancement of ultracold-neutron capture associated with subbarrier reflection.
Journal of Experimental and Theoretical Physics **88**, 72-78 (1999)

AYRES DE CAMPOS J., FERREIRA L.P., CRUZ M.M., GIL J.M., MENDES P.J., FERREIRA I.C., BACMANN M., SOUBEYROUX J.L., FRUCHART D., GODINHO M., AYRES DE CAMPOS N. Study of $RFe_{12-x}Mo_x$ (R = Y, Ho) compounds by neutron powder diffraction, ac susceptibility and magnetization.
Journal of Physics Condensed Matter **11**, 687-701 (1999)

BAFILE U., HOCHGESAND K., WINTER R., BAROCCHI F., CONVERT P., HANSEN T., FISCHER H.E. Neutron diffraction on mercury: density dependence of the static structure factor.
Journal of Non-Crystalline Solids **250-252**, 35-39 (1999)

BAKO I., PALINKAS G., DORE J., FISCHER H. Investigation of liquid 1,4-dioxane: An X-ray and neutron diffraction study.
Molecular Physics **96**, 743-747 (1999)

BAKO I., PALINKAS G., DORE J.C., FISCHER H.E. Structural studies of a water/dioxane mixture by neutron diffraction with hydrogen/deuterium substitution.
Chemical Physics Letters **303**, 315-319 (1999)

BAO W., RAYMOND S., SHAPIRO S.M., MOTOYA K., FÅK B., ERWIN R.W. Unconventional ferromagnetic and spin-glass states of the reentrant spin glass $Fe_{0.7}Al_{0.3}$.
Physical Review Letters **82**, 4711-4714 (1999)

BASCH H., MUSAEV D.G., MOROKUMA K., FRYZUK M.D., LOVE J.B., SEIDEL W.W., ALBINATI A., KOETZLE T.F., KLOOSTER W.T., MASON S.A., ECKERT J. Theoretical predictions and single-crystal neutron diffraction and inelastic neutron scattering studies on the reaction of dihydrogen with the dinuclear dinitrogen complex of zirconium $[P_2N_2]Zr(\mu\text{-}\eta^2\text{-}N_2)Zr[P_2N_2]$, $P_2N_2 = PhP(CH_2SiMe_2NSiMe_2CH_2)_2PPh$.
Journal of the American Chemical Society **121**, 523-528 (1999)

BECVAR F. Simulation of γ cascades in complex nuclei with emphasis on assessment of uncertainties of cascade-related quantities.
Nuclear Instruments and Methods in Physics Research A **417**, 434-449 (1998)

BENITES G.M., AURELIO G., FERNANDEZ GUILLERMET A., CUELLO G.J., BERMEJO F.J. Atomic ordering and systematics of bonding lengths in the Ti-V omega phase: A neutron diffraction study.
Journal of Alloys and Compounds **284**, 251-255 (1999)

BENSCH W., NÄTHER C., HELMER O., RITTER C. The magnetic structures of $Tl_3Cr_5Se_8$ ($x = 1$ and 0.2) as determined by neutron scattering.
Journal of Alloys and Compounds **290**, 41-51 (1999)

BERNHOEFT N. Geometrical effects in diffraction analysis.
Acta Crystallographica A **55**, 274-288 (1999)

BERNHOEFT N., ROESSLI B., SATO N., ASO N., HIESS A., LANDER G.H., ENDOH Y., KOMATSUBARA T. Magnetic fluctuations above and below T_c in the heavy fermion superconductor UPd_2Al_3.
Physica B **259-261**, 614-620 (1999)

BIEBER R., WAGEMANS C., GOEMINNE G., WAGEMANS J., DENECKE B., LOISELET M., GAELENS M., GELTENBORT P., OBERHUMMER H. Thermal neutron induced (n,p) and (n,α) reactions on ^{37}Ar.
Nuclear Physics A **647**, 3-11 (1999)

BIENFAIT M., ZEPPENFELD P., RAMOS R.C. Jr., GAY J.M., VILCHES O.E., CODDENS G. Isotopic ordering in adsorbed hydrogen monolayers.
Physical Review B **60**, 11773-11782 (1999)

BLANCO J.A., ESPESO J.I., GARCIA SOLDEVILLA J., GOMEZ SAL J.C., IBARRA M.R., MARQUINA C., FISCHER H.E. Magnetic structure of GdCu through the martensitic structural transformation: A neutron-diffraction study.
Physical Review B **59**, 512-518 (1999)

BON C., LEHMANN M.S., WILKINSON C. Quasi-Laue neutron-diffraction study of the water arrangement in crystals of triclinic hen egg-white lysozyme.
Acta Crystallographica D **55**, 978-987 (1999)

BONDARENKO I.V., KRASNOPEROV A.V., FRANK A.I., BALASHOV S.N., MASALOVICH S.V., NOSOV V.G., GELTENBORT P., HØGHØJ P., KLEIN A.G., CIMMINO A. Experimental check of the dispersion law for ultracold neutrons.
JETP Letters **67**, 786-792 (1998)

BÖNI P., LORENZO J.E., ROESSLI B., SHIRANE G., WERNER S.A., WILDES A. Polarization analysis of low-energy excitations in single-domain Cr.
Physica B **267-268**, 255-258 (1999)

BÖRNER H.G., JENTSCHEL M., ZAMFIR N.V., CASTEN R.F., KRTICKA M., ANDREJTSCHEFF W. Ultrahigh resolution study of collective modes in ^{158}Gd.
Physical Review C **59**, 2432-2439 (1999)

BOUCHERLE J.X., GIVORD F., SCHWEIZER J., GUKASOV A., MIGNOT J.M., LELIEVRE-BERNA E., AOKI H., OCHIAI A. Polarized neutron investigation in the mixed-valence compound Sm_3Te_4.
Physica B **267-268**, 37-40 (1999)

BOUCHERLE J.X., GIVORD F., SCHWEIZER J., MIGNOT J.M., LELIEVRE-BERNA E., AOKI H., OCHIAI A. A polarized neutron investigation of charge-ordering in mixed-valence Sm_4Bi_3.
Physica B **267-268**, 47-50 (1999)

BOULLAY P., GREBILLE D., HERVIEU M., RAVEAU B., SUARD E. Incommensurate nuclear and magnetic structure of the oxygen-deficient perovskites $(Ba_{2-3x}Bi_{3x-1})(Fe_{2x}Bi_{1-2x})O_{2+3/2x}$ ($0.43 \le x \le 0.50$).
Journal of Solid State Chemistry **147**, 450-463 (1999)

BOURDAROT F., BOMBARDI A., BURLET P., CALEMCZUK R., LANDER G.H., LAPIERRE F., SANCHEZ J.P., MATTENBERGER K., VOGT O. Collapse of the magnetic ordering and structural anomalies in the $U_xLa_{1-x}S$ system: Neutron diffraction and specific heat measurements.
European Physical Journal B **9**, 605-611 (1999)

BRION S. DE, CIORCAS F., CHOUTEAU G., LEJAY P., RADAELLI P., CHAILLOUT C. Magnetic and electric properties of $La_{1-\delta}MnO_3$.
Physical Review B **59**, 1304-1310 (1999)

BROWN A.B.D., CLARKE S.M., RENNIE A.R. Measurement of the flow alignment of clay dispersions by neutron diffraction.
In: "Dynamics of Complex Fluids", ADAMS M.J., MASHELKAR R.A., PEARSON J.R.A., RENNIE A.R. (Eds) (Imperial College Press, 1998) pp.330-337

BROWN P.J., BARGAWI A.Y., CRANGLE J., NEUMANN K.U., ZIEBECK K.R.A. Direct observation of a band Jahn-Teller effect in the martensitic phase transition of Ni_2MnGa.
Journal of Physics Condensed Matter **11**, 4715-4722 (1999)

BROWN P.J., BARGAWI A.Y., CRANGLE J., NEUMANN K.U., ZIEBECK K.R.A. The induced moment distribution in atomically ordered and disordered Pt_3V.
Solid State Communications **109**, 329-332 (1999)

BROWN P.J., FORSYTH J.B., TASSET F. Precision determination of antiferromagnetic form factors.
Physica B **267-268**, 215-220 (1999)

BRUCKNER G., CZERMAK A., RAUCH H., WEILHAMMER P. Position sensitive detection of thermal neutrons with solid state detectors (Gd Si planar detectors).
Nuclear Instruments and Methods in Physics Research A **424**, 183-189 (1999)

BRUNAUER G., BOYSEN H., FREY F., HANSEN T. Hochtemperatur-Strukturanalyse von 3:2-Mullit.
Zeitschrift für Kristallographie Supplement **16**, 100 (1999)

BUCHER R., SCHÖNFELD B., KOSTORZ G., ZOLLIKER M. Short-range order in Ni-rich Ni-Ti studied by diffuse neutron scattering.
Physica Status Solidi (a) **175**, 527-536 (1999)

BUMAJDAD A., EASTOE J., GRIFFITHS P., STEYTLER D.C., HEENAN R.K., LU J.R., TIMMINS P. Interfacial compositions and phase structures in mixed surfactant microemulsions.
Langmuir **15**, 5271-5278 (1999)

BURIAN A., DORE J.C., FISCHER H.E., SLOAN J. Structural studies of multiwall carbon nanotubes by neutron diffraction.
Physical Review B **59**, 1665-1668 (1999)

BURIAN A., DORE J.C., FISCHER H.E., SLOAN J., SZCZYGIELSKA A. Structural studies of carbon nanotubes by wide-angle neutron scattering.
Proceedings SPIE **3725**, 107-110 (1999)

BURLET P., HENRY J.Y., REGNAULT L.P. In-plane magnetic anisotropy in antiferromagnetic YBa_2Cu3O_{6+x}.
Physica C **296**, 205-209 (1998)

BURLET P., REGNAULT L.P., VETTIER C. To the editor and readers of Neutron News.
Neutron News **10**, 2 (1999)

BYRNE J., GELTENBORT P. Particle physics with slow neutrons. Workshop held at Grenoble.
Neutron News **10**, 5-6 (1999)

CACIUFFO R., AMORETTI G., MURANI A., SESSOLI R., CANESCHI A., GATTESCHI D. Neutron spectroscopy for the magnetic anisotropy of molecular clusters.
Physical Review Letters **81**, 4744-4747 (1998)

CACIUFFO R., AMORETTI G., SANTINI P., LANDER G.H., KULDA J., DU PLESSIS P. DE V. Magnetic excitations and dynamical Jahn-Teller distortions in UO_2.
Physical Review B **59**, 13892-13900 (1999)

CACIUFFO R., MIRA J., RIVAS J., SENARIS-RODRIGUEZ M.A., RADAELLI P.G., CARSUGHI F., FIORANI D., GOODENOUGH J.B. Transition from itinerant to polaronic conduction in $La_{1-x}Sr_xCoO_3$ perovskites.
Europhysics Letters **45**, 399-405 (1999)

CAIGNAERT V., MILLANGE F., DOMENGES B., RAVEAU B., SUARD E. A new ordered oxygen-deficient manganite perovskite: $LaBaMn_2O_{5.5}$. Crystal and magnetic structure.
Chemistry of Materials **11**, 930-938 (1999)

CAMPBELL S.I., KEMALI M., ROSS D.K., BULL D.J., FERNANDEZ J.F., JOHNSON M.R. Quasi-elastic neutron scattering study of the hydrogen diffusion in the C15 laves structure, $TiCr_{1.85}$.
Journal of Alloys and Compounds **293-295**, 351-355 (1999)

CANTON P., FAGHERAZZI G., FRATTINI R., RIELLO P. Stabilization of cubic Na-modified ZrO_2: A neutron diffraction study.
Journal of Applied Crystallography **32**, 475-480 (1999)

CARLSSON P., ZORN R., ANDERSSON D., FARAGO B., RICHTER D., TORELL L.M., BÖRJESSON L., JACOBSSON P. The segmental dynamics of a polymer electrolyte investigated by neutron spin echo technique.
In: "CP469, Slow Dynamics in Complex Systems: Eighth Tohwa University International Symposium", TOKUYAMA M., OPPENHEIM I. (Eds) (American Institute of Physics, 1999) pp. 607-614

CASALTA H., SCHLEGER P., BELLOUARD C., HENNION M., MIREBEAU I., EHLERS G., FARAGO B., DORMANN J.L., KELSCH M., LINDE M., PHILLIPP F. Direct measurement of superparamagnetic fluctuations in monodomain Fe particles via neutron spin-echo spectroscopy.
Physical Review Letters **82**, 1301-1304 (1999)

CAVADINI N., HENGGELER W., FURRER A., GÜDEL H.U., KRÄMER K., MUTKA H. Magnetic excitations in the quantum spin system $KCuCl_3$.
European Physical Journal B **7**, 519-522 (1999)

CENDOYA I., ALEGRIA A., ALBERDI J.M., COLMENERO J., GRIMM H., RICHTER D., FRICK B. Effect of blending on the PVME dynamics. A dielectric, NMR and QENS investigation.
Macromolecules **32**, 4065-4078 (1999)

CHAHID A., MCGREEVY R.L., WICKS J., MUTKA H. Critical narrowing of molten $^7Li_{0.62}Na_{0.38}$ alloy - II. Approach to the low Q limiting behaviour.
Physica B **266**, 121-125 (1999)

CHARITAT T., BELLET-AMALRIC E., FRAGNETO G., GRANER F. Adsorbed and free lipid bilayers at the solid-liquid interface.
European Physical Journal B **8**, 583-593 (1999)

CHARRIER B., SCHMITT D. Investigation of the local atomic order in i-$RE_8Mg_{42}Zn_{50}$ quasicrystals (RE = rare earth).
In: "Proceedings of the International Conference on Aperiodic Crystals - Aperiodic'97", BOISSIEU M. DE, VERGER-GAUGRY J.L., CURRAT R. (Eds) (World Scientific, 1998) pp.733-737

CHATTERJI T., MCINTYRE G.J., SURYANARAYANAN R., DHALENNE G., REVCOLEVSCHI A. Spin correlations in the bilayer manganite $La_{1.2}Sr_{1.8}Mn_2O_7$.
Solid State Communications **112**, 235-239 (1999)

CHATTERJI T., REGNAULT L.P., THALMEIER P., SURYANARAYANAN R., DHALENNE G., REVCOLEVSCHI A. Spin waves in the quasi-two-dimensional ferromagnetic bilayer manganite $La_{1.2}Sr_{1.8}Mn_2O_7$.
Physical Review B **60**, R6965-R6968 (1999)

CHATTERJI T., THALMEIER P., MCINTYRE G.J., VAN DE KAMP R., SURYANARAYANAN R., DHALENNE G., REVCOLEVSCHI A. Low-energy magnetic excitations in double-layered manganite $La_{1.2}Sr_{1.8}Mn_2O_7$.
Europhysics Letters **46**, 801-807 (1999)

CHAUMAT V., RESSOUCHE E., OULADDIAF B., DESRE P., MORET F. Experimental study of phase equilibria in the Nb-Ti-Al system.
Scripta Materiala **40**, 905-911 (1999)

CHAZEAU L., CAVAILLE J.Y., TERECH P. Mechanical behaviour above T_g of a plasticised PVC reinforced with cellulose whiskers; a SANS structural study.
Polymer **40**, 5333-5344 (1999)

CHRISTENSEN A.N., FJELLVÅG H. Neutron powder diffraction study of the dehydration of zeolite N.
Acta Chemica Scandinavica **53**, 85-89 (1999)

CICOGNANI G., DIANOUX A.J., FONTANA A., ROSSI F., MONTAGNA M., SCOPIGNO T., PELOUS J., TERKI F., PILLIEZ J.N., WOIGNIER T. Low frequency dynamics of silica xerogel porous system.
Philosophical Magazine B **79**, 2091-2102 (1999)

CIMMINO A., ALLMAN B.E., BRUMBY S.P., IRVING T.H.K., KLEIN A.G., NUGENT K.A., ANDERSON I.S., HØGHØJ P., PEELE A.G. Square micro-channel arrays for focussing neutrons and X-rays. Proceedings SPIE **3511**, 393-400 (1998)

CIMMINO A., ALLMAN B.E., KLEIN A.G., HAMILTON W.A., ANDERSON I.S., HAMELIN B., HØGHØJ P., BASTIE P. Micro-array collimators for X-rays and neutrons.
Proceedings SPIE **3511**, 376-384 (1998)

CLEMENTE-JUAN J.M., ANDRES H., BORRAS-ALMENAR J.J., CORONADO E., GÜDEL H.U., AEBERSOLD M., KEARLY G., BÜTTNER H., ZOLLIKER M. Magnetic excitations in polyoxometalate clusters observed by inelastic neutron scattering: Evidence for ferromagnetic exchange interactions and spin anisotropy in the tetrameric nickel(II) cluster $[Ni_4(H_2O)_2(PW_9O_{34})_2]^{10-}$ and comparison with the magnetic properties.
Journal of the American Chemical Society **121**, 10021-10027 (1999)

CLEMENTYEV E.S., BRADEN M., LAZUKOV V.N., ALEKSEEV P.A., MIGNOT J.M., SADIKOV I.P., HIESS A., LAPERTOT G. Anomalous phonon softening in intermediate-valence CeNi.
Physica B **259-261**, 42-43 (1999)

CODDENS G., LYONNARD S., HENNION B., CALVAYRAC Y. Phason dynamics in perfect icosahedral quasicrystals.
In: "Proceedings of the International Conference on Aperiodic Crystals - Aperiodic'97", BOISSIEU M. DE, VERGER-GAUGRY J.L., CURRAT R. (Eds) (World Scientific, 1998) pp.629-638

COMBET J., MORELON N.D., FERRAND M., BEE M. Dynamical transition and molecular motions in a channel-like inclusion compound under hydrostatic pressure.
Physica B **266**, 56-59 (1999)

CORNELL K., WIPF H., COOK J.C., KEARLEY G.J., NEUMAIER K. Local and long-range hydrogen diffusion in $Nb(OH)_{0.011}$.
Journal of Alloys and Compounds **293-295**, 275-278 (1999)

COURTOIS P. Characterization of Heusler crystals for polarized neutrons monochromators.
Physica B **267-268**, 363-366 (1999)

CREMILLIEUX Y., BERTHEZENE Y., HUMBLOT H., VIALLON M., CANET E., BOURGEOIS M., ALBERT T., HEIL W., BRIGUET A. A combined ^1H perfusion/^3He ventilation NMR study in rat lungs.
Magnetic Resonance in Medicine **41**, 645-648 (1999)

CRISTOFOLINI L., CICOGNANI G., DIANOUX A.J., FACCI P., FONTANA M.P., RICCO M. Li diffusion and fullerene dynamics in lithium fulleride $Li_{12}C_{60}$ from inelastic neutron scattering experiments.
Philosophical Magazine B **79**, 2065-2071 (1999)

CYWINSKI R., KILCOYNE S.H., STEWART J.R. Diffuse magnetic scattering of polarised neutrons.
Physica B **267-268**, 106-114 (1999)

CZIHAK C., MÜLLER M., SCHOBER H., HEUX L., VOGL G. Dynamics of water adsorbed to cellulose.
Physica B **266**, 87-91 (1999)

DAHLBORG U., SFN ADMINISTRATION BOARD The french neutron community meets at Albé.
Neutron News **10**, 3-4 (1999)

DALMAS DE REOTIER P., YAOUANC A., VAN DER LAAN G., KERNAVANOIS N., SANCHEZ J.P., SMITH J.L., HIESS A., HUXLEY A., ROGALEV A. Probing the magnetic 5*f* density of states above the Fermi level in metallic uranium compounds by X-ray magnetic circular dichroism.
Physical Review B **60**, 10606-10609 (1999)

DANZIG A., RUPP A. The ^{3}He filter project at HMI Berlin.
Physica B **267-268**, 344-347 (1999)

D'ASTUTO M., BOURGES P., CASALTA H., IVANOV A., PETITGRAND D. Low-energy magnetic dynamics of Nd-moments in Nd_2CuO_4.
Physica B **259-261**, 875-876 (1999)

DAVIDSON M.G., GOETA A.E., HOWARD J.A.K., LEHMANN C.W., MCINTYRE G.M., PRICE R.D. Low temperature neutron and X-ray diffraction study of imino(triphenyl)phosphorane.
Journal of Organometallic Chemistry **550**, 449-452 (1998)

DE BERNABE A., CAPITAN M.J., FISCHER H.E., LEQUIEN S., MOMPEAN F.J., PRIETO C., QUIROS C., COLINO J., LEFEBVRE S., BESSIERE M., SANZ J.M. Oxidation study of Co/Cu multilayers by resonant X-ray reflectivity.
Vacuum **52**, 109-113 (1999)

DE BERNABE A., CAPITAN M.J., FISCHER H.E., QUIROS C., PRIETO C., COLINO J., MOMPEAN F., SANZ J.M. Combination of specular and off-specular low-angle X-ray diffraction in the study of Co/Cu multilayers: Mesoscopic structure and layer oxidation.
Surface and Interface Analysis **27**, 1-7 (1999)

DE COSTER C., DECROIX B., HEYDE K., JOLIE J., LEHMANN H., WOOD J.L. Particle-hole excitations in the interacting boson model (IV). The U(5)-SU(3) coupling.
Nuclear Physics A **651**, 31-55 (1999)

DEME B. SAXS and SANS techniques discussed in Grenoble.
Neutron News **10**, 15 (1999)

DERVENAGAS P., HIESS A., LANDER G.H., WASTIN F., REBIZANT J. Neutron diffraction study of the magnetic structure of $U_{0.1}Np_{0.9}Ru_2Si_2$.
Solid State Communications **109**, 35-39 (1999)

DERVENAGAS P., KACZOROWSKI D., BOURDAROT F., BURLET P., CZOPNIK A., LANDER G.H. Neutron diffraction on a UGa_3 single crystal.
Physica B **269**, 368-372 (1999)

DIMEO R.M., SOKOL P.E., ANDERSON C.R., STIRLING W.G., ADAMS M.A. Confinement effects on superfluid helium.
Journal of Low-Temperature Physics **113**, 369-374 (1998)

DIMEO R.M., SOKOL P.E., ANDERSON C.R., STIRLING W.G., ANDERSEN K.H., ADAMS M.A. Localized collective excitations in superfluid helium in Vycor.
Physical Review Letters **81**, 5860-5863 (1998)

DJURADO D., NICOLAU Y.F., RANNOU P., LUZNY W., SAMUELSEN E.J., TERECH P., BEE M., SAUVAJOL J.L. An overall view of the structure of an heterogeneous medium: The conducting polyaniline.
Synthetic Metals **101**, 764-767 (1999)

DOLL C., BÖRNER H.G., JAAG S., KÄPPELER F., ANDREJTSCHEFF W. Lifetime measurement in ^{176}Lu and its astrophysical consequences.
Physical Review C **59**, 492-499 (1999)

DÖNNI A., FISCHER P., FAUTH F., CONVERT P., AOKI Y., SUGAWARA H., SATO H. Antiferromagnetic ordering in the cubic superconductor $YbPd_2Sn$.
Physica B **259-261**, 705-706 (1999)

DÖNNI A., KELLER L., FISCHER P., AOKI Y., SATO H., FAUTH F., ZOLLIKER M., KOMATSUBARA T., ENDOH Y. Magnetic order and crystal-field excitations in $Nd_3Pd_{20}Ge_6$.
Journal of Physics Condensed Matter **10**, 7219-7229 (1998)

DORNER B., PETITGRAND D., GÜDEL H.U. Minute splitting of magnetic excitations due to dipolar interactions in $CsFeCl_3$ and $RbFeCl_3$ observed with polarised neutrons.
Physica B **267-268**, 263-265 (1999)

DÖRR M., GERLACH H., KALUS J., KARL N., MONKENBUSCH M., NATKANIEC I., SCHMELZER U., SCHMIDT W., STEZOWSKI J.J., VORDERWISCH P., VOSS G., WARTH M. Structure and lattice dynamics of dipolarly disordered 2,3-dimethylanthracene crystals.
Journal of Physics Condensed Matter **10**, 10879-10899 (1998)

DÖRR M., LOEWENHAUPT M., HAHN W., BRÜCK E., HAGMUSA I.H., KLAASSE J.C.P., ROTTER M. Specific heat of $DyCu_2$ single crystals in high magnetic fields.
Physica B **262**, 340-347 (1999)

DUBBERS D. Fundamental interactions (Experiments).
Nuclear Physics A **654**, 297c-314c (1999)

DUBOIS M., DEDIEU J.C., DEME B., GULIK-KRZYWICKI T., ZEMB T. Phase diagram of positively charged catanionic surfactant aggregates: The myristic acid-cetyltrimethylammonium hydroxide-water system.
ACS Symposium Series **736**, 86-101 (1999)

DUGAIN F., BOISSIEU M. DE, HRADIL K., SHIBATA K., CURRAT R., KORTAN A.R., TSAI A.P., SUCK J.B., FREY F. Inelastic neutron scattering study of the dynamics of the decagonal AlNiCo phase.
In: "Proceedings of the International Conference on Aperiodic Crystals - Aperiodic'97", BOISSIEU M. DE, VERGER-GAUGRY J.L., CURRAT R. (Eds) (World Scientific, 1998) pp.651-655

DUGAIN F., BOISSIEU M. DE, SHIBATA K., CURRAT R., SATO T.J., KORTAN A.R., SUCK J.B., HRADIL K., FREY F., TSAI A.P. Inelastic neutron scattering study of the dynamics of the AlNiCo decagonal phase.
European Physical Journal B **7**, 513-516 (1999)

DUVAL E., SAVIOT L., SUROVTSEV N., WIEDERSICH J., DIANOUX A.J. Observation of propagating acoustic vibrational modes in glasses by Raman scattering.
Philosophical Magazine B **79**, 2051-2056 (1999)

EBEL C., FAOU P., FRANZETTI B., KERNEL B., MADERN D., PASCU M., PFISTER C., RICHARD S., ZACCAI G. Molecular interactions in extreme halophiles - The solvation - Stabilization hypothesis for halophilic proteins.
In: "Microbiology and Biogeochemistry of Hypersaline Environments", OREN A. (Eds) (CRC Press, 1998) pp.227-237

EBEL C., FAOU P., ZACCAI G. Protein-solvent and weak protein-protein interactions in halophilic malate dehydrogenase.
Journal of Crystal Growth **196**, 395-402 (1999)

EGELHAAF S.U., SCHURTENBERGER P. Micelle-to-vesicle transition: A time-resolved structural study.
Physical Review Letters **82**, 2804-2807 (1999)

EHLERS G., RITTER C., KRUTJAKOW A., MIEKELEY W., STÜSSER N., ZEISKE T., MALETTA H. Anomalous transition from antiferromagnetic to ferromagnetic order in $Tb_{1-x}Y_xNiAl$.
Physical Review B **59**, 8821-8827 (1999)

EILHARD J., ZIRKEL A., TSCHÖP W., HAHN O., KREMER K., SCHÄRPF O., RICHTER D., BUCHENAU U. Spatial correlations in polycarbonates: Neutron scattering and simulation.
Journal of Chemical Physics **110**, 1819-1830 (1999)

ENGBERG D., WISCHNEWSKI A., BUCHENAU U., BÖRJESSON L., DIANOUX A.J., SOKOLOV A.P., TORELL L.M. Origin of the boson peak in a network glass B_2O_3.
Physical Review B **59**, 4053-4057 (1999)

FÅK B., BOSSY J. Excitations and their temperature dependence in superfluid ^{4}He beyond the roton.
Journal of Low-Temperature Physics **113**, 531-536 (1998)

FÅK B., FARAGO B., VAN DIJK N.H. Neutron spin-echo study of URu_2Si_2.
Physica B **259-261**, 644-645 (1999)

FARAGO B. Recent neutron spin-echo developments at the ILL (IN11 and IN15).
Physica B **267-268**, 270-276 (1999)

FEDOTOV V.K., ANTONOV V.E., ANTONOVA T.E., BOKHENKOV E.L., DORNER B., GROSSE G., WAGNER F.E. Atomic ordering in the hcp cobalt hydrides and deuterides.
Journal of Alloys and Compounds **291**, 1-7 (1999)

FERNANDEZ-DIAZ M.T., MARTINEZ J.L., ALONSO J.M., HERRERO E. Structural, thermal, transport, and magnetic properties of the charge-ordered $La_{1/3}Ca_{2/3}MnO_3$ oxide.
Physical Review B **59**, 1277-1284 (1999)

FIORETTO D., BUCHENAU U., COMEZ L., SOKOLOV A., MASCIOVECCHIO C., MERMET A., RUOCCO G., SETTE F., WILLNER L., FRICK B., RICHTER D., VERDINI L. High-frequency dynamics of glass-forming polybutadiene.
Physical Review E **59**, 4470-4475 (1999)

FISCHER H.E., BERMEJO F.J., CUELLO G.J., FERNANDEZ-DIAZ M.T., DAWIDOWSKI J., GONZALEZ M.A., SCHOBER H., JIMENEZ-RUIZ M. Quantitative evaluation of anharmonic and disorder effects on glassy dynamics.
Physical Review Letters **82**, 1193-1196 (1999)

FISCHER H.E., BERMEJO F.J., CUELLO G.J., FERNANDEZ-DIAZ M.T., DAWIDOWSKI J., JIMENEZ-RUIZ M., SCHOBER H. An experimental separation of anharmonic and disorder effects on glassy dynamics.
Europhysics Letters **46**, 643-648 (1999)

FISCHER P., FAUTH F., BÖTTGER G., SKRIPOV A.V., KOZHANOV V.N. Neutron diffraction study of the location of deuterium in the deuterium-stabilized $HfTi_2D_4$ phase.
Journal of Alloys and Compounds **282**, 184-186 (1999)

FITTER J. The temperature dependence of internal molecular motions in hydrated and dry α-amylase: The role of hydration water in the dynamical transition of proteins.
Biophysical Journal **76**, 1034-1042 (1999)

FITTER J., LECHNER R.E., DENCHER N.A. Interactions of hydration water and biological membranes studied by neutron scattering.
Journal of Physical Chemistry B **103**, 8036-8050 (1999)

FONG H.F., BOURGES P., SIDIS Y., REGNAULT L.P., BOSSY J., IVANOV A., MILIUS D.L., AKSAY I.A., KEIMER B. Effect of nonmagnetic impurities on the magnetic resonance peak in $YBa_2Cu_3O_7$.
Physical Review Letters **82**, 1939-1942 (1999)

FONG H.F., BOURGES P., SIDIS Y., REGNAULT L.P., IVANOV A., GU G.D., KOSHIZUKA N., KEIMER B. Neutron scattering from magnetic excitations in $Bi_2Sr_2CaCu_2O_{8+\delta}$.
Nature **398**, 588-591 (1999)

FORET M., HEHLEN B., COURTENS E., VACHER R., CASALTA H., DORNER B. Is there a Ioffe-Regel limit for sound propagation in glasses?
Physica B **263-264**, 264-267 (1999)

FORGAN E.M., KEALEY P.G., RISEMAN T.M., LEE S.L., PAUL D.MCK., AEGERTER C.M., CUBITT R., SCHLEGER P., PAUTRAT A., SIMON C., JOHNSON S.T. Fluxoids and neutron polarisation effects.
Physica B **267-268**, 115-121 (1999)

FÖRSTER S., HERMSDORF N., LEUBE W., SCHNABLEGGER H., REGENBRECHT M., AKARI S., LINDNER P., BÖTTCHER C. Fusion of charged block copolymer micelles into toroid networks.
Journal of Physical Chemistry B **103**, 6657-6668 (1999)

FÖRSTER S., NEUBERT I., SCHLÜTER A.D., LINDNER P. How dendrons stiffen polymer chains: A SANS study.
Macromolecules **32**, 4043-4049 (1999)

FORTIN J.Y., BELLISSARD J., GUSMAO M., ZIMAN T. De Haas-van Alphen oscillations and magnetic breakdown: Semiclassical calculation of multiband orbits.
Physical Review B **57**, 1484-1497 (1998)

FREUDENBERGER J., KREYSSIG A., RITTER C., NENKOV K., DRECHSLER S.L., FUCHS G., MÜLLER K.H., LOEWENHAUPT M., SCHULTZ L. Suppression of superconductivity by nonmagnetic impurities, structural properties and magnetic ordering in $Ho_xLa_{1-x}Ni_2B_2C$.
Physica C **315**, 91-98 (1999)

FREY F., WEIDNER E., HRADIL K., BOISSIEU M. DE, CURRAT R. Über das diffuse Schichtliniensystem in dekagonalen AlCoNi Phasen.
Zeitschrift für Kristallographie Supplement **16**, 140 (1999)

FRICK B., ALBA-SIMIONESCO C. Comparison of the pressure and temperature dependence of the elastic incoherent scattering for the polymers polybutadiene and polyisobutylene.
Physica B **266**, 13-19 (1999)

GABRYS B.J. Applications of polarized neutrons to non-magnetic materials.
Physica B **267-268**, 122-130 (1999)

GAPINSKI J., STEFFEN W., PATKOWSKI A., SOKOLOV A.P., KISLIUK A., BUCHENAU U., RUSSINA M., MEZEI F., SCHOBER H. Spectrum of fast dynamics in glass forming liquids: Does the "knee" exist?
Journal of Chemical Physics **110**, 2312-2315 (1999)

GARCIA-HERNANDEZ M., MOMPEAN F.J., SCHÄRPF O., ANDERSEN K.H., FÅK B. Collective excitations in liquid para-H_2: A neutron polarization-analysis study.
Physical Review B **59**, 958-964 (1999)

GARCIA-LANDA B., RITTER C., IBARRA M.R., BLASCO J., ALGARABEL P.A., MAHENDIRAN R., GARCIA J. Magnetic and magnetotransport properties of the ordered perovskite Sr_2FeMoO_6.
Solid State Communications **110**, 435-438 (1999)

GARCIA-MUNOZ J.L., LLOBET A., FRONTERA C., FONTCUBERTA J., OBRADORS X., RITTER C. Charge localization and magnetic dynamics in manganites.
Journal of Magnetism and Magnetic Materials **196-197**, 477-478 (1999)

GARCIA-MUNOZ J.L., LLOBET A., FRONTERA C., RITTER C. Charge localization and magnetic dynamics in ferromagnetic and charge-ordered manganites.
Journal of Applied Physics **85**, 5639-5641 (1999)

GARCIA SOLDEVILLA J., ESPESO J.I., RODRIGUEZ FERNANDEZ J., GOMEZ SAL J.C., BLANCO J.A., FERNANDEZ-DIAZ M.T. The role of magnetic interactions on the stability of magnetic structures in RCu compounds (R = Ce, Pr and Nd).
Journal of Magnetism and Magnetic Materials **196-197**, 898-900 (1999)

GARRETT P.E., LEHMANN H., JOLIE J., MCGRATH C.A., YEH M., YATES S.W. Quadrupole-octupole coupled states in ^{112}Cd.
Physical Review C **59**, 2455-2461 (1999)

GEISSLER E., HORKAY F., HECHT A.M., ROCHAS C. Effect of solvent on chain unfolding in polymer networks.
The Wiley Polymer Networks Group Series **1**, 433-443 (1998)

GELTENBORT P., NESVIZHEVSKY V.V., KARTASHOV D.G., LYCHAGIN E.V., MUZYCHKA A.Y., NEKHAEV G.V., SHVETSOV V.N., STRELKOV A.V., KHARITONOV A.G., SEREBROV A.P., TAL'DAEV R.R., PENDLEBURY J.M. A new escape channel for ultracold neutrons in traps.
JETP Letters **70**, 170-175 (1999)

GENET F., LORIDANT S., RITTER C., LUCAZEAU G. Phase transitions in $BaCeO_3$: Neutron diffraction and Raman studies.
Journal of Physics and Chemistry of Solids **60**, 2009-2021 (1999)

GENEVEY J., IBRAHIM F., PINSTON J.A., FAUST H., FRIEDRICHS T., GROSS M., OBERSTEDT S. Identification of μs isomers in the fission products of $^{241}Pu(n_{th}, f)$.
Physical Review C **59**, 82-89 (1999)

GIANNINI E., BELLINGERI E., PASSERINI R., FLÜKIGER R. *In-situ* high temperature neutron diffraction study of Bi,Pb(2223) phase formation in Ag-sheathed monofilamentary tapes.
International Journal of Modern Physics B **13**, 1067-1072 (1999)

GIBBS M.R., ANDERSEN K.H., STIRLING W.G., SCHOBER H. The collective excitations of normal and superfluid ^4He: The dependence on pressure and temperature.
Journal of Physics Condensed Matter **11**, 603-628 (1999)

GIVORD F., BOUCHERLE J.X., DREYER J., ISIKAWA Y., OULADDIAF B., PUJOL S., SCHWEIZER J., TASSET F. A complex modulated magnetic structure in $CeNi_2Al_5$ persisting at very low temperatures.
Journal of Physics Condensed Matter **11**, 7327-7338 (1999)

GLISS C., CASALTA H., BAYERL T.M. Surfactant-induced alterations of lecithin molecular dynamics in bilayers studied by quasielastic neutron scattering and solid-state NMR.
Journal of Physical Chemistry B **103**, 8908-8914 (1999)

GÖBEL A., WANG D.T., CARDONA M., PINTSCHOVIUS L., REICHARDT W., KULDA J., PYKA N.M., ITOH K., HALLER E.E. Effects of isotope disorder on energies and lifetimes of phonons in germanium.
Physical Review B **58**, 10510-10522 (1998)

GONCHARENKO I.N., MIREBEAU I., IRODOVA A.V., SUARD E. Magnetic and hydrogen ordering in the frustrated laves hydrides $RMn_2H_{4.5}$ (R = Y, Gd, Tb, Dy, Ho): A neutron-diffraction study.
Physical Review B **59**, 9324-9331 (1999)

GONZALEZ M.A., ENCISO E., BERMEJO F.J., BEE M. Ethanol force fields: A molecular dynamics study of polarization effects on different phases.
Journal of Chemical Physics **110**, 8045-8059 (1999)

GOUTENOIRE F., RETOUX R., SUARD E., LACORRE P. *Ab initio* determination of the novel perovskite-related structure of $La_7Mo_7O_{30}$ from powder diffraction.
Journal of Solid State Chemistry **142**, 228-235 (1999)

GRATZ E., GOREMYCHKIN E., LATROCHE M., HILSCHER G., ROTTER M., MÜLLER H., LINDBAUM A., MICHOR H., PAUL-BONCOUR V., FERNANDEZ-DIAZ T. New magnetic phenomena in $TbNi_2$.
Journal of Physics Condensed Matter **11**, 7893-7905 (1999)

GRENIER B., RENARD J.P., VEILLET P., REGNAULT L.P., LORENZO J.E., PAULSEN C., DHALENNE G., REVCOLEVSCHI A. Universal phase diagram of Si-, Zn-, Mg- and Ni-doped $CuGeO_3$: Spin-Peierls order and antiferromagnetism.
Physica B **259-261**, 954-955 (1999)

GROSS M., HABS D., KESTER O., OTT J., RAO R., THIROLF P., VON EGIDY T., KIENLE P., KÖSTER U., STEICHELE E. The status of the Munich Fission Fragment Accelerator Project.
In: "CP447 Nuclear Fission and Fission-Product Spectroscopy: Second International Workshop", FIONI G.et al (Eds) (American Institute of Physics, 1998) pp.126-134

GUKASOV A., PLAKHTY V.P., DORNER B., KOKOVIN S.Y., SYROMYATNIKOV V.N., SMIRNOV O.P., CHERNENKOV Y.P. Inelastic neutron scattering study of spin waves in the garnet $Mn_3Al_2Ge_3O_{12}$ with a triangular magnetic structure.
Journal of Physics Condensed Matter **11**, 2869-2878 (1999)

GÜNTHER R., DONNER W., TOPERVERG B.P., DOSCH H. Birefringent Bragg diffraction of evanescent neutron states in magnetic films.
Physical Review Letters **81**, 116-119 (1998)

GUTT C., ASMUSSEN B., PRESS W., MERKL C., CASALTA H., GREINERT J., BOHRMANN G., TSE J.S., HÜLLER A. Quantum rotations in natural methane-clathrates from the Pacific sea-floor.
Europhysics Letters **48**, 269-275 (1999)

GUZIK A., PIERRE J., KACZMARSKA K., OULADDIAF B. Magnetic structures of $Ce(Ag_xCu_{1-x})_{1.8}Sb_2$ Kondo compounds.
Journal of Magnetism and Magnetic Materials **196-197**, 891-892 (1999)

HAHN K., JOBIC H., KÄRGER J. Investigating one-dimensional diffusion by quasielastic neutron scattering: A theoretical approach.
Physical Review E **59**, 6662-6671 (1999)

HALM T., NOMSSI NZALI J., HOYER W., MAY R.P. Neutron small-angle scattering on molten Ga-Tl alloys.
Journal of Non-Crystalline Solids **250-252**, 293-296 (1999)

HECHT A.M., GEISSLER E., HORKAY F. Structure of silica-filled poly(dimethyl siloxane) gels and solutions.
Physical Review E **59**, 1976-1981 (1999)

HEIL W., DREYER J., HOFMANN D., HUMBLOT H., LELIEVRE-BERNA E., TASSET F. ^3He neutron spin-filter.
Physica B **267-268**, 328-335 (1999)

HEIL W., HUMBLOT H., HOFMANN D., KRASNOSCHEKOVA I., LELIEVRE-BERNA E., PETOUKHOV A., PETROV G., SEREBROV A., TASSET F., VALSKY G. Neutron optics P-violation effects near p-wave resonance.
Physica B **267-268**, 289-293 (1999)

HENGGELER W., ROESSLI B., FURRER A., VORDERWISCH P., CHATTERJI T. Henggeler et al. Reply to comment on "Correlations of the Nd magnetic moments and their influence on the specific heat in $Nd_{2-x}Ce_xCuO_4$".
Physical Review Letters **82**, 2218 (1999)

HERRMANNSDÖRFER T., DÖNNI A., FISCHER P., KELLER L., BÖTTGER G., GUTMANN M., KITAZAWA H., TANG J. Successive magnetic ordering of the Tb sublattices in $Tb_3Pd_{20}Si_6$.
Journal of Physics Condensed Matter **11**, 2929-2936 (1999)

HIESS A., COAD S., BUSCHINGER B., TROVARELLI O., BOUCHERLE J.X., GIVORD F., HANSEN T., LELIEVRE-BERNA E., SUARD E., GEIBEL C., STEGLICH F. Magnetism in $R_2T_3X_9$ (R = Ce, Yb, U; T = Rh, Ir; X = Al, Ga) intermetallic compounds.
Physica B **259-261**, 343-344 (1999)

HØGHØJ P., ANDERSON I., SIEBRECHT R., GRAF W., BEN-SAIDANE K. Neutron polarizing Fe/Si mirrors at ILL.
Physica B **267-268**, 355-359 (1999)

HORKAY F., HECHT A.M., GEISSLER E. Fine structure of polymer networks as revealed by solvent swelling.
Macromolecules **31**, 8851-8856 (1998)

HUXLEY A., VAN DIJK N.H., PAUL D. MCK., CUBITT R., LEJAY P. A low field study of the flux line lattice in $CeRu_2$.
Physica B **259-261**, 696-698 (1999)

IGA F., BOUVET A., REGNAULT L.P., TAKABATAKE T., HIESS A., KASUYA T. Magnetic excitations in a single crystal of the Kondo semiconductor YbB_{12}.
Journal of Physics and Chemistry of Solids **60**, 1193-1196 (1999)

IRODOVA A.V., SUARD E. Evolution of hydrogen superstructure with k = (1/2 1/2 1/2) in $ZrV_2D_{2+\delta}$, $-0.8 < \delta < 0.2$.
Journal of Alloys and Compounds **291**, 184-189 (1999)

IVANOV A.S., BOURGES P., PETITGRAND D. In-plane copper spin wave gap in Pr_2CuO_4.
Physica B **259-261**, 879-881 (1999)

JANOT C. Clusters and properties in quasicrystals.
In: "Proceedings of the International Conference on Aperiodic Crystals - Aperiodic'97", BOISSIEU M. DE, VERGER-GAUGRY J.L., CURRAT R. (Eds) (World Scientific, 1998) pp. 699-714

JANOT C., PATERA J. Simple physical generation of aperiodic structures.
Journal of Non-Crystalline Solids **232-234**, 234-238 (1998)

JIMENEZ-RUIZ M., CRIADO A., BERMEJO F.J., CUELLO G.J., TROUW F.R., FERNANDEZ-PEREA R., LÖWEN H., CABRILLO C., FISCHER H.E. Purely dynamical signature of the orientational glass transition.
Physical Review Letters **83**, 2757-2760 (1999)

JOBIC H., KÄRGER J., BEE M. Simultaneous measurement of self- and transport diffusivities in zeolites.
Physical Review Letters **82**, 4260-4263 (1999)

JOHNSON M.R., PRAGER M., GRIMM H., NEUMANN M.A., KEARLEY G.J., WILSON C.C. Methyl group dynamics in paracetamol and acetanilide: Probing the static properties of intermolecular hydrogen bonds formed by peptide groups.
Chemical Physics **244**, 49-66 (1999)

JOHNSON S.T., FORGAN E.M., LLOYD S.H., AEGERTER C.M., LEE S.L., CUBITT R., KEALEY P.G., AGER C., TAJIMA S., RYKOV A., PAUL D.MCK. Flux-line lattice structures in untwinned $YBa_2Cu_3O_{7-\delta}$.
Physical Review Letters **82**, 2792-2795 (1999)

JOUBERT J.M., LATROCHE M., PERCHERON-GUEGAN A., BOUREE VIGNERON F. Thermodynamic and structural comparison between two potential metal-hydride battery materials $LaNi_{3.55}Mn_{0.4}Al_{0.3}Co_{0.75}$ and $CeNi_{3.55}Mn_{0.4}Al_{0.3}Co_{0.75}$.
Journal of Alloys and Compounds **275-277**, 118-122 (1998)

JOUMARD I., MARCUS J., KLEIN T., CUBITT R. Small angle neutron scattering and magnetization measurements in the cubic $(K,Ba)BiO_3$ superconductor.
Physical Review Letters **82**, 4930-4933 (1999)

KAISER I., ROTHENHÄUSLER C., BOYSEN H., FREY F., LERCH M., CONVERT P., HANSEN T. Anionen- und Leerstellenordnung in γ-Zirkonoxinitrid (Zr_3ON_2).
Zeitschrift für Kristallographie Supplement **16**, 113 (1999)

KARLA I., PIERRE J., MURANI A.P., NEUMANN M. Crystalline electric field in RNiSb compounds investigated by inelastic neutron scattering.
Physica B **271**, 294-303 (1999)

KATAOKA M., FERRAND M., GOUPIL-LAMY A.V., KAMIKUBO H., YUNOKI J., OKA T., SMITH J.C. Dynamical and structural modifications of staphylococcal nuclease on C-terminal truncation.
Physica B **266**, 20-26 (1999)

KAZIMIROV V.Y., SARIN V.A., RITTER C., SHUVALOV L.A. Neutron diffraction study of the atomic structure of the ferroelectric phase of $(CH_3)_2NH_2Al(SO_4)_2{\cdot}6H_2O$ ferroelectric-ferroelastic (DMAAS).
Crystallography Reports **44**, 56-61 (1999)

KEIMER B., BOURGES P., FONG H.F., SIDIS Y., REGNAULT L.P., IVANOV A., MILIUS D.L., AKSAY I.A., GU G.D., KOSHIZUKA N. Resonant spin excitations in $YBa_2Cu_3O_{6+x}$ and $Bi_2Sr_2CaCu_2O_{8+\delta}$.
Journal of Physics and Chemistry of Solids **60**, 1007-1011 (1999)

KELLER L., DÖNNI A., ZOLLIKER M., KOMATSUBARA T. Crystalline electric field excitations in $R_3Pd_{20}Ge_6$ (R = Ce, Pr, Nd).
Physica B **259-261**, 336-337 (1999)

KESSLER E.G. Jr., DEWEY M.S., DESLATTES R.D., HENINS A., BÖRNER H.G., JENTSCHEL M., DOLL C., LEHMANN H. The deuteron binding energy and the neutron mass.
Physics Letters A **255**, 221-229 (1999)

KING S.M. Small-angle neutron scattering.
In: "Modern Techniques for Polymer Characterisation", PETHRICK R.A., DAWKINS J.V. (Eds) (John Wiley & Sons, Ltd, 1999) pp.171-232

KÖBLER U., HOSER A., GRAF H.A., FERNANDEZ-DIAZ M.T., FISCHER K., BRÜCKEL T. Investigations of the sublattice magnetizations $M_{sub}(T)$ in antiferromagnets with fourth-order exchange interactions: $Eu_xSr_{1-x}Te$.
European Physical Journal B **8**, 217-224 (1999)

KÖBLER U., HOSER A., KAWAKAMI M., CHATTERJI T., REBIZANT J. An unified view of the spin dynamics in two- and three-dimensional magnetic systems.
Journal of Magnetism and Magnetic Materials **205**, 343-356 (1999)

KOHLMANN H., FAUTH F., YVON K. Hydrogen order in monoclinic $ZrCr_2H_{3.8}$.
Journal of Alloys and Compounds **285**, 204-211 (1999)

KOHLMANN H., GINGL F., HANSEN T., YVON K. The first determination of Eu-H distances by neutron diffraction on the novel hydrides $EuMg_2H_6$ and $EuMgH_4$.
Angewandte Chemie International Edition English **38**, 2029-2032 (1999)

KOLESNIKOV A.I., ANTONOV V.E., BENNINGTON S.M., DORNER B., FEDOTOV V.K., GROSSE G., LI J.C., PARKER S.F., WAGNER F.E. The vibrational spectrum and giant tunnelling effect of hydrogen dissolved in α-Mn.
Physica B **263-264**, 421-423 (1999)

KÖSTER U., FAUST H., FIONI G., FRIEDRICHS T., GROSS M., OBERSTEDT S. Ternary fission yields of $^{241}Pu(n_{th}, f)$.
Nuclear Physics A **652**, 371-387 (1999)

KOZA M., SCHOBER H., TÖLLE A., FUJARA F., HANSEN T. Formation of ice XII at different conditions.
Nature **397**, 660-661 (1999)

KRÄMER K.W., GÜDEL H.U., ROESSLI B., FISCHER P., DÖNNI A., WADA N., FAUTH F., FERNANDEZ-DIAZ M.T., HAUSS T. Noncollinear two-and three-dimensional magnetic ordering in the honeycomb lattices of ErX_3 (X = Cl, Br, I).
Physical Review B **60**, R3724-R3727 (1999)

KRAMP S., PYKA N.M., LOEWENHAUPT M., ROTTER M. Temperature and field dependence of the spin wave gap in $NdCu_2$.
Journal of Applied Physics **85**, 5645-5647 (1999)

KREYSSIG A., LOEWENHAUPT M., FREUDENBERGER J., MÜLLER K.H., RITTER C. Evidence of tetragonal to orthorhombic distortion of $HoNi_2B_2C$ in the magnetically ordered state.
Journal of Applied Physics **85**, 6058-6060 (1999)

KRIMMEL A., LOIDL A., KLEMM M., HORN S., SCHOBER H. Dramatic change of the magnetic response in LiV_2O_4: Possible heavy fermion to itinerant d-metal transition.
Physical Review Letters **82**, 2919-2922 (1999)

KRINITSINA T.P., KRAVTSOV E.A., LAUTER-PASSIOUK V.V., LAUTER H.J., POPOV V.V., ROMASHEV L.N., TSURIN V.A., BURKHANOV A.M., USTINOV V.V. Morphology of crystallites and magnetic structure of non-collinear Fe/Cr multilayers.
Journal of Magnetism and Magnetic Materials **203**, 181-183 (1999)

KRÜGER E., NISTLER W., WEIRAUCH W. Determination of the fine-structure constant by a precise measurement of h/m_n: The final result.
Metrologia **35**, 203-209 (1998)

KUHS W.F., BAUER F.C., AHSBAHS H., MCINTYRE G.J. Neutron single crystal diffraction on KDP at 20 K and 1.7 GPa.
The Review of High Pressure Science and Technology **7**, 307-309 (1998)

KUHS W.F., CHAZALLON B., KLAPPROTH A., PAUER F. Filling-isotherms in clathrate-hydrates.
The Review of High Pressure Science and Technology **7**, 1147-1149 (1998)

KUHS W.F., LOBBAN C., FINNEY J.L. Partial H-ordering in high pressure ices III and V.
The Review of High Pressure Science and Technology **7**, 1141-1143 (1998)

KULDA J., HEIL W., HUMBLOT H., TASSET F., WILDES A., PLAKHTY V., MOSKVIN E., BURLET P., DREYER J., FÅK B. Use of the ^3He filter in search of the in-chain spin correlations in $YBa_2Cu_3O_{6+1}$.
Physica B **267-268**, 252-254 (1999)

LANGAN P. ACA hosts "New directions in neutron scattering instrumentation for structural biology".
Neutron News **10**, 8-10 (1999)

LANGAN P., LEHMANN M., WILKINSON C., JOGL G., KRATKY C. Neutron Laue diffraction studies of coenzyme cob(II)alamin.
Acta Crystallographica D **55**, 51-59 (1999)

LANGAN P., NISHIYAMA Y., CHANZY H. A revised structure and hydrogen-bonding system in cellulose II from a neutron fiber diffraction analysis.
Journal of the American Chemical Society **121**, 9940-9946 (1999)

LANGRIDGE S., PAIXAO J.A., BERNHOEFT N., VETTIER C., LANDER G.H., GIBBS D., SØRENSEN S.A., STUNAULT A., WERMEILLE D., TALIK E. Changes in 5d band polarization in rare-earth compounds.
Physical Review Letters **82**, 2187-2190 (1999)

LANZARA A., SAINI N.L., BIANCONI A., DUC F., BORDET P. Anomalous local atomic correlations in $HgBa_2CuO_{4+\delta}$.
Physical Review B **59**, 3851-3854 (1999)

LAPPAS A., BROWN C.M., KORDATOS K., SUARD E., TANIGAKI K., PRASSIDES K. Neutron diffraction study of the polymeric structure of Na_2RbC_{60}.
Journal of Physics Condensed Matter **11**, 371-381 (1999)

LATROCHE M., JOUBERT J.M., PERCHERON-GUEGAN A., NOTTEN P.H.L. Crystal structure of nonstoichiometric copper-substituted $La(Ni_{1-z}Cu_z)_x$ compounds studied by neutron and synchrotron anomalous powder diffraction.
Journal of Solid State Chemistry **146**, 313-321 (1999)

LATROCHE M., PAUL-BONCOUR V., PERCHERON-GUEGAN A., BOUREE-VIGNERON F. Temperature dependence study of $YMn_2D_{4.5}$ by means of neutron powder diffraction.
Journal of Alloys and Compounds **274**, 59-64 (1998)

LATROCHE M., PERCHERON-GUEGAN A., CHABRE Y. Etude par diffraction de neutrons *in situ* de l'influence de la teneur en cobalt sur le comportement des électrodes négatives des batteries nickel-hydrure de type $MMNi_{4.3-x}Mn_{0.3}Al_{0.4}Co_x$.
In: "Proceedings des Journées d'Etudes SEE-ENSEEG" (1999) pp.45-54

LAUTER-PASYUK V., LAUTER H.J., LORENZ M., AKSENOV V.L., LEIDERER P. Magnetic flux distribution inside an $YBa_2Cu_3O_7$ superconducting thin film in the mixed state.
Physica B **267-268**, 149-153 (1999)

LEFMANN K., NIELSEN K. McStas, a general software package for neutron ray-tracing simulations.
Neutron News **10**, 20-23 (1999)

LEHMANN H., BÖRNER H.G., CASTEN R.F., CORMINBOEUF F., DOLL C., JENTSCHEL M., JOLIE J., ZAMFIR N.V. On the importance of the *SU*(3) description for the interpretation of the first excited $K^{\pi} = 0^+$ band in deformed nuclei.
Journal of Physics G: Nuclear and Particle Physics **25**, 827-830 (1999)

LEHMANN H., NORD A., DE ALMEIDA PINTO A.E., BECK O., BESSERER J., VON BRENTANO P., DRISSI S., ECKERT T., HERZBERG R.D., JÄGER D., JOLIE J., KNEISSL U., MARGRAF J., MASER H., PIETRALLA N., PITZ H.H. Dipole excitations in the vibrational nucleus ^{112}Cd.
Physical Review C **60**, 024308-1/024308-10 (1999)

LEHNERT H., BOYSEN H., FREY F., RADAELLI P. Ordnungsparameterkopplungen und Debye-Waller-Faktoren in $PbTiO_3$.
Zeitschrift für Kristallographie Supplement **16**, 113 (1999)

LELIEVRE-BERNA E. French neutron community meets.
Neutron News **10**, 8-9 (1999)

LELIEVRE-BERNA E., TASSET F. The D3C project: Improvements and new fields of science.
Physica B **267-268**, 21-26 (1999)

LERCH M., BOYSEN H., HANSEN T. Neutronenbeugungsuntersuchungen zur Sauerstoff-diffusion in reinem und dotiertem $LaGaO_3$.
Zeitschrift für Kristallographie Supplement **16**, 46 (1999)

LEVELUT C., SCHEYER Y., PELOUS J., PROCHAZKA F. Brillouin and neutron inelastic scattering investigation of the relaxational processes in glass- and gel-forming polymers.
Journal of Non-Crystalline Solids **235-237**, 375-382 (1998)

LI Z.X., WELLER A., THOMAS R.K., RENNIE A.R., WEBSTER J.R.P., PENFOLD J., HEENAN R.K., CUBITT R. Adsorption of the lamellar phase of aerosol-OT at the solid/liquid and air/liquid interfaces.
Journal of Physical Chemistry B **103**, 10800-10806 (1999)

LINDNER P. ILL for industry held in Grenoble.
Neutron News **10**, 4 (1999)

LISS K.D., MAGERL A., HOCK R., WAIBEL B., REMHOF A. The investigation of ultrasonic fields by time resolved X-ray diffraction.
Proceedings SPIE **3451**, 117-127 (1998)

LLOBET A., GARCIA-MUNOZ J.L., FRONTERA C., RITTER C. Tetragonal to monoclinic transition in the metallic antiferromagnet $Pr_{0.5}Sr_{0.5}MnO_3$.
Physical Review B **60**, R9889-R9892 (1999)

LLOBET A., RITTER C., FRONTERA C., OBRADORS X., GARCIA-MUNOZ J.L., ALONSO J.A. Structural instability vs. bandwidth-controlled charge ordering in $x = 1/2$ manganites.
Journal of Magnetism and Magnetic Materials **196-197**, 549-551 (1999)

LOEWENHAUPT M., PYKA N.M. Design of the triple-axis spectrometer PANDA at the high-flux reactor FRM-II of Garching.
Physica B **267-268**, 336-340 (1999)

LORENZO J.E., REGNAULT L.P., BOUCHER J.P., HENNION B., DHALENNE G., REVCOLEVSCHI A. Anisotropy of the spin interactions in the spin-Peierls compound $CuGeO_3$: A new magnetic excitation branch.
Europhysics Letters **45**, 619-625 (1999)

LOSILLA E.R., SALVADO M.A., ARANDA M.A.G., CABEZA A., PERTIERRA P., GARCIA-GRANDA S., BRUQUE S. Layered acid arsenates α-$M(HAsO_4)_2{\cdot}H_2O$ (M = Ti, Sn, Pb): Synthesis optimization and crystal structures.
Journal of Molecular Structure **470**, 93-104 (1998)

LOVESEY S.W., BALCAR E. The scattering of polarized neutrons by a magnetic material.
Physica B **267-268**, 221-226 (1999)

LUTTERBACH N., VERSMOLD H., REUS V., BELLONI L., ZEMB T., LINDNER P. Charge-stabilized liquidlike ordered binary colloidal suspensions. 2. Partial structure factors determined by small-angle neutron scattering.
Langmuir **15**, 345-352 (1999)

MA G., BARLOW D.J., LAWRENCE M.J., TIMMINS P. Small angle neutron scattering studies of non-ionic surfactant vesicles.
Journal of Pharmacy and Pharmacology **50**, 148 (1998)

MADIH-AYADI K., RAKOTOZAFY S., CEVA T., CROSET B., DUPONT-PAVLOVSKY N., CONVERT P., MIREBEAU I., RESSOUCHE E. Growth mode of dichloromethane physisorbed on graphite. Thermodynamic and structural characterizations.
Surface Science **436**, 99-106 (1999)

MADSEN G.K.H., WILSON C., NYMAND T.M., MCINTYRE G.J., LARSEN F.K. The structure of nitromalonamide: A combined neutron-diffraction and computational study of a very short hydrogen bond.
Journal of Physical Chemistry A **103**, 8684-8690 (1999)

MAGERL A., ZABEL H., FRICK B., LINDNER P. Flow dynamics of sheared liquids explored by inelastic neutron scattering.
Applied Physics Letters **74**, 3474-3476 (1999)

MALAMAN B., VENTURINI G., WELTER R., SANCHEZ J.P., VULLIET P., RESSOUCHE E. Magnetic properties of RMn_6Sn_6 (R = Gd-Er) compounds from neutron diffraction and Mössbauer measurements.
Journal of Magnetism and Magnetic Materials **202**, 519-534 (1999)

MALEYEV S.V., PETITGRAND D., BOURGES P., IVANOV A.S. Pseudodipolar interaction in noncollinear antiferromagnets and spin waves in Pr_2CuO_4.
Physica B **259-261**, 870-874 (1999)

MALIK S.S., SARKISOV D., STEYERL A., BRENNER T., BUTTERWORTH J., GELTENBORT P., HINO M., OKUMURA K., UTSURO M. Unconventional trapping of ultracold neutrons.
Physics Letters A **260**, 328-334 (1999)

MARGADONNA S., BROWN C.M., LAPPAS A., PRASSIDES K., TANIGAKI K., KNUDSEN K.D., LE BIHAN T., MEZOUAR M. Pressure and temperature evolution of the structure of the superconducting Na_2CsC_{60} fulleride.
Journal of Solid State Chemistry **145**, 471-478 (1999)

MARIN C., CHARVOLIN T., BRAITHWAITE D., CALEMCZUK R. Properties of a large $La_{1.92}Sr_{0.08}CuO_{4+\delta}$ single crystal grown by the travelling-solvent floating-zone method.
Physica C **320**, 197-205 (1999)

MARMEGGI J.C., CURRAT R., BOUVET A., LANDER G.H. Phonon softening in alpha-uranium associated with the CDW transition.
Physica B **263-264**, 624-626 (1999)

MARTIN-MARTIN A., PEREIRA L.C.J., LANDER G.H., REBIZANT J., WASTIN F., SPIRLET J.C., DERVENAGAS P., BROWN P.J. Neutron-diffraction studies of single crystals of U_2T_2In (T = Ni, Pd, Pt).
Physical Review B **59**, 11818-11825 (1999)

MAZET T., WELTER R., VENTURINI G., RESSOUCHE E., MALAMAN B. Neutron diffraction study of the $ZrMn_6Ge_6$, $LuMn_6Ge_6$ and $ScMn_6Ge_6$ compounds.
Solid State Communications **110**, 407-412 (1999)

MCGREEVY R.L. Nyköping welcomes QENS'98.
Neutron News **10**, 10-11 (1999)

MEIJER G.I., ECCLESTON R.S., MUTKA H., ROSSEL C., KARPINSKI J., KAZAKOV S., WACHTER P. Magnetic excitations in the quasi-one-dimensional magnet $Sr_{0.73}CuO_2$: Coexistence of the spin gap and long-range magnetic order.
Physical Review B **60**, 9260-9263 (1999)

MEIJER G.I., HENGGELER W., BROWN J., BECKER O.S., BEDNORZ J.G., ROSSEL C., WACHTER P. Reduction of ordered moment in strongly correlated $LaTiO_{3+\delta}$ upon band filling.
Physical Review B **59**, 11832-11836 (1999)

MELINON P., KEGHELIAN P., PEREZ A., CHAMPAGNON B., GUYOT Y., SAVIOT L., RENY E., CROS C., POUCHARD M., DIANOUX A.J. Phonon density of states of silicon clathrates: Characteristic width narrowing effect with respect to the diamond phase.
Physical Review **59**, 10099-10104 (1999)

MENTRE O., DHAUSSY A.C., ABRAHAM F., SUARD E., STEINFINK H. Crystal structure of $Pb_2V_3O_9$: Rietveld refinement and electron lone-pair localization. The magnetic susceptibility of Sr^{2+}-substituted phases.
Chemistry of Materials **11**, 2408-2416 (1999)

METZ A., PYKA N.M., LOEWENHAUPT M., MENOVSKY A.A., VAN DE KAMP R. Temperature dependence of the magnetic excitations in Nd_2CuO_4.
Journal of Magnetism and Magnetic Materials **196-197**, 473-474 (1999)

MEYER A., BUSCH R., SCHOBER H. Time-temperature superposition of structural relaxation in a viscous metallic liquid.
Physical Review Letters **83**, 5027-5029 (1999)

MILLANGE F., CAIGNAERT V., DOMENGES B., RAVEAU B., SUARD E. Order-disorder phenomena in new $LaBaMn_2O_{6-x}$ CMR perovskites. Crystal and magnetic structure.
Chemistry of Materials **10**, 1974-1983 (1998)

MILLANGE F., SUARD E., CAIGNAERT V., RAVEAU B. $YBaMn_2O_5$: Crystal and magnetic structure reinvestigation.
Materials Research Bulletin **34**, 1-9 (1999)

MIREBEAU I., HENNION M., CASALTA H., ANDRES H., GÜDEL H.U., IRODOVA A.V., CANESCHI A. Low-energy magnetic excitations of the Mn_{12}-acetate spin cluster observed by neutron scattering.
Physical Review Letters **83**, 628-630 (1999)

MITCHELL J.F., MILLBURN J.E., MEDARDE M., SHORT S., JORGENSEN J.D., FERNANDEZ-DIAZ M.T. $Sr_3Mn_2O_7$: Mn^{4+} parent compound of the $n = 2$ layered CMR manganites.
Journal of Solid State Chemistry **141**, 599-603 (1998)

MONDELLI C., ANDERSEN K., MUTKA H., PAYEN C., FRICK B. Polarized neutron scattering study of the kagome antiferromagnet $SrCr_8Ga_4O_{19}$.
Physica B **267-268**, 139-141 (1999)

MONDELLI C., MUTKA H., FRICK B., PAYEN C. Spin freezing in the kagomé system $SrCr_8Ga_4O_{19}$ - high resolution study of the elastic and low-energy dynamic responses.
Physica B **266**, 104-107 (1999)

MORENO A.J., ALEGRIA A., COLMENERO J., FRICK B. Isotope effect on the rotational tunneling transitions of methyl groups in glassy polymers.
Physical Review B **59**, 5983-5986 (1999)

MORFIN I., LINDNER P., BOUE F. Temperature and shear rate dependence of small angle neutron scattering from semidilute polymer solutions.
Macromolecules **32**, 7208-7223 (1999)

MURANI A.P., BROWN P.J. Comment on "X-ray magnetic circular dichroism study on $CeFe_2$" by A. Delobbe et al.
Europhysics Letters **48**, 353-354 (1999)

MURANI A.P., OULADDIAF B., ECCLESTON R.S. Single-ion 4f-spectral response from Ce-ions in the compound $CeFe_2$.
Physica B **259-261**, 1167-1168 (1999)

MURANI A.P., SCHÄRPF O., ANDERSEN K.H., RICHARD D., RAPHEL R. Atomic and magnetic correlations in a Cu-5 at % Mn spin-glass alloy.
Physica B **267-268**, 131-133 (1999)

MUTKA H. Influence of defects and impurities on charge density wave systems.
In: "Advances in the Crystallographic and Microstructural Analysis of Charge Density Wave Modulated Crystals", BOSWELL F.W., BENNETT J.C. (Eds) (Kluwer Academic Publishers, 1999) pp.153-184

MUZYCHKA A.Y., POKOTILOVSKII Y.N., GELTENBORT P. Search for anomalous transmission of ultracold neutrons through metal foils.
JETP Letters **67**, 459-463 (1998)

MUZYCHKA A.Y., POKOTILOVSKI Y.N., GELTENBORT P. Search for low-energy upscattering of ultracold neutrons from a beryllium surface.
Journal of Experimental and Theoretical Physics **88**, 79-83 (1999)

NABEREZHNOV A., VAKHRUSHEV S., DORNER B., STRAUCH D., MOUDDEN H. Inelastic neutron scattering study of the relaxor ferroelectric $PbMg_{1/3}Nb_{2/3}O_3$ at high temperatures.
European Physical Journal B **11**, 13-20 (1999)

NAKAMURA H., KIM N., SHIGA M., KMIEC R., TOMALA K., RESSOUCHE E., SANCHEZ J.P., MALAMAN B. The partially disordered state of the frustrated face-centred cubic antiferromagnet $GdInCu_4$.
Journal of Physics Condensed Matter **11**, 1095-1104 (1999)

NEE I., BUSE K., HAVERMEYER F., RUPP R.A., FALLY M., MAY R.P. Neutron diffraction from thermally fixed gratings in photorefractive lithium niobate crystals.
Physical Review B **60**, R9896-R9899 (1999)

NEMIROVSKY D., MOREH R., ANDERSEN K.H., MAYERS J. Anomalous kinetic energies of adsorbed ^4He on active carbon fibre (ACF).
Journal of Physics Condensed Matter **11**, 6653-6660 (1999)

NESVIZHEVSKY V.V., STRELKOV A.V., GELTENBORT P., IAYDJIEV P.S. Investigation of storage of ultra-cold neutrons in traps.
European Physical Journal Applied Physics **6**, 151-154 (1999)

NESVIZHEVSKY V.V., STRELKOV A.V., GELTENBORT P., IAYDJIEV P.S. Observation of a new mechanism of ultracold-neutron losses in traps.
Physics of Atomic Nuclei **62**, 776-786 (1999)

NEUMANN M.A., JOHNSON M.R., RADAELLI P.G., TROMMSDORFF H.P., PARKER S.F. Rotional dynamics of methyl groups in durene: A crystallographic, spectroscopic, and molecular mechanics investigation.
Journal of Chemical Physics **110**, 516-527 (1999)

NOGALES A., EZQUERRA T.A., BATALLAN F., FRICK B., LOPEZ-CABARCOS E., BALTA CALLEJA F.J. Restricted dynamics in poly(ether ether ketone) as revealed by incoherent quasielastic neutron scattering and broad-band dielectric spectroscopy.
Macromolecules **32**, 2301-2308 (1999)

NOTTEN P.H.L., LATROCHE M., PERCHERON-GUEGAN A. The influence of Mn on the crystallography and electrochemistry of nonstoichiometric AB_5-type hydride-forming compounds.
Journal of the Electrochemical Society **146**, 3181-3189 (1999)

NOVION C. DE ., HEWAT A. ILL reviews powder and liquids/amorphous materials diffraction.
Neutron News **10**, 5 (1999)

NOZIERES P., PISTOLESI F. From semiconductors to superconductors: A simple model for pseudogaps.
European Physical Journal B **10**, 649-662 (1999)

OAKLEY G.S., POUGET S., HARRISON A., FRUNZKE J., VISSER D. Neutron spin echo study of magnetic fluctuations in the kagome antiferromagnet $(D_3O)Fe_3(SO_4)_2(OD)_6$.
Physica B **267-268**, 145-148 (1999)

OAKLEY G.S., VISSER D., FRUNZKE J., ANDERSEN K.H., WILLS A.S., HARRISON A. A polarised neutron scattering study of the magnetic correlations in the kagome antiferromagnet $AFe_3(SO_4)_2(OD)_6$ (A = D_3O, K).
Physica B **267-268**, 142-144 (1999)

OBERSTEDT S. Retrospective radon dosimetry.
Il Nuovo Cimento C **22**, 341-344 (1999)

OBERSTEDT S., HAMBSCH F.J., VIVES F. Fission-mode calculations for ^{239}U, a revision of the multimodal random neck-rupture model.
Nuclear Physics A **644**, 289-305 (1998)

ODENBACH S., GILLY H., LINDNER P. The use of magnetic small angle neutron scattering for the detection of flow profiles in magnetic fluids.
Journal of Magnetism and Magnetic Materials **201**, 353-356 (1999)

OSBORN R., ARONSON M.C., RAINFORD B.D., MAPLE M.B., CHAU R., ANDERSEN K.H. Quantum critical scattering in uranium non-Fermi liquid compounds.
Physica B **241-243**, 859-861 (1998)

OSBORN R., GOREMYCHKIN E.A., SASHIN I.L., MURANI A.P. Inelastic neutron scattering study of the spin dynamics of $Yb_{1-x}Lu_xAl_3$.
Journal of Applied Physics **85**, 5344-5346 (1999)

PAIXAO J.A., ROBINSON R.A., LANDER G.H., BROWN P.J. Magnetic site susceptibilities in UPdSn.
Journal of Physics Condensed Matter **11**, 2127-2138 (1999)

PAOLASINI L., CACIUFFO R., ROESSLI B., LANDER G.H., MYERS K., CANFIELD P. Iron spin waves in YFe_2 and UFe_2.
Physical Review B **59**, 6867-6872 (1999)

PAPPAS C., KALI G., BÖNI P., KISCHNIK R., MERTENS L.A., GRANZ P., MEZEI F. Performance of the multidetector NSE spectrometer SPAN at BENSC.
Physica B **267-268**, 285-288 (1999)

PARK J.G., ADROJA D.T., MCEWEN K.A., BI Y.J., KULDA J. Crystal field excitation of single crystal CeNiSn.
Physica B **259-261**, 288-289 (1999)

PAUL-BONCOUR V., GUENEE L., LATROCHE M., PERCHERON-GUEGAN A., OULADDIAF B., BOUREE-VIGNERON F. Elaboration, structures, and phase transitions for YFe_2D_x compounds (x = 1.3, 1.75, 1.9, 2.6) studied by neutron diffraction.
Journal of Solid State Chemistry **142**, 120-129 (1999)

PETRENKO O.A., PAUL D.MCK., RITTER C., ZEISKE T., YETHIRAJ M. Magnetic frustration and order in gadolinium gallium garnet.
Physica B **266**, 41-48 (1999)

PETRI I., SALMON P.S., FISCHER H.E. Structure of the liquid semiconductor GeSe.
Journal of Physics Condensed Matter **11**, 7051-7060 (1999)

PFLEIDERER T., WALDNER I., BERTAGNOLLI H., TÖDHEIDE K., KIRCHNER B., HUBER H., FISCHER H.E. The structure of fluid argon from high-pressure neutron diffraction and *ab initio* molecular dynamics simulations.
Journal of Chemical Physics **111**, 2641-2646 (1999)

PHILIPPOT E., ARMAND P., YOT P., CAMBON O., GOIFFON A., MCINTYRE G.J., BORDET P. Neutron and X-ray structure refinements between 15 and 1073 K of piezoelectric gallium arsenate, $GaAsO_4$: Temperature and pressure behavior compared with other α-quartz materials.
Journal of Solid State Chemistry **146**, 114-123 (1999)

PIMPINELLI A., JENSEN P., LARRALDE H., PEYLA P. Scaling and crossovers in models for thin film growth.
In: "Morphological Organization in Epitaxial Growth and Removal", ZHANG Z., LAGALLY M.G. (Eds) (World Scientific, 1998) pp.121-148

PINTSCHOVIUS L., BLASCHKO O., KREXNER G., PYKA N. Bulk modulus of C_{60} studied by single-crystal neutron diffraction.
Physical Review B **59**, 11020-11026 (1999)

PLAKHTY V.P., MALEYEV S.V., BURLET P., GAVRILOV S.V., SMIRNOV O.P. Spin-flop transition in Pr_2CuO_4 by neutron diffraction.
Physics Letters A **250**, 201-204 (1998)

PLAKHTY V.P., MALEYEV S.V., WOSNITZA J., KREMER B.K., VISSER D., KULDA J., SMIRNOV O.P., GOUKASSOV A.G., ZOBKALO I.A., MOSKVIN E. Polarized neutron scattering study of the spin chirality.
Physica B **267-268**, 259-262 (1999)

PONTILLON Y., AKITA T., GRAND A., KOBAYASHI K., LELIEVRE-BERNA E., PECAUT J., RESSOUCHE E., SCHWEIZER J. Experimental and theoretical spin density in a ferromagnetic molecular complex presenting interheteromolecular hydrogen bonds.
Journal of the American Chemical Society **121**, 10126-10133 (1999)

PONTILLON Y., CANESCHI A., GATTESCHI D., RESSOUCHE E., SCHWEIZER J., SESSOLI R. Spin density in a ferromagnetic nitronyl nitroxide free radical.
Physica B **267-268**, 51-55 (1999)

PONTILLON Y., CANESCHI A., GATTESCHI D., SESSOLI R., RESSOUCHE E., SCHWEIZER J., LELIEVRE-BERNA E. Magnetization density in an iron(III) magnetic cluster. A polarized neutron investigation.
Journal of the American Chemical Society **121**, 5342-5343 (1999)

PÖTSCHKE D., BALLAUFF M., LINDNER P., FISCHER M., VÖGTLE F. Analysis of the structure of dendrimers in solution by small-angle neutron scattering including contrast variation.
Macromolecules **32**, 4079-4087 (1999)

POUGET S., ALBA M. NSE investigation of the spin dynamics in the nearly percolating frustrated insulating compound $CdCr_{2(1-x)}In_{2x}S_4$ (x = 0.10).
Physica B **267-268**, 304-307 (1999)

POWELL A.V., COLGAN D.C., RITTER C. Magnetic structure and spin reorientation in the ternary sulfides $Ni_xCr_{3-x}S_4$ (x = 1/4, 1/2, 3/4).
Journal of Solid State Chemistry **143**, 163-173 (1999)

POWELL A.V., RITTER C., VAQUEIRO P. A powder neutron diffraction study of the magnetic structure of FeV_2S_4.
Journal of Solid State Chemistry **144**, 372-378 (1999)

PRAGER M., SCHIEBEL P., JOHNSON M., GRIMM H., HAGDORN H., IHRINGER J., PRANDL W., LALOWICZ Z. The isotope effect and phase transitions in ammonium hexachloropalladate studied by neutron tunnelling spectroscopy.
Journal of Physics Condensed Matter **11**, 5483-5495 (1999)

PTASIEWICZ-BAK H., OLOVSSON I., MCINTYRE G.J. Charge density in $NiCl_2.4H_2O$ at 295 and 30 K.
Acta Crystallographica B **55**, 830-840 (1999)

PYKA N.M., LOEWENHAUPT M., METZ A. Dispersion of Nd spin correlations in heavy-fermion like $Nd_{1.85}Ce_{0.15}CuO_4$.
Journal of Applied Physics **85**, 5347-5349 (1999)

PYKA N.M., METZ A., LOEWENHAUPT M., SCHMIDT W., MENOVSKY A.A., VAN DE KAMP R. Magnetic field dependence of low-energy magnetic correlations in $Nd_{2-x}Ce_xCuO_4$.
Physica B **259-261**, 877-878 (1999)

RADAELLI P.G., COX D.E., CAPOGNA L., CHEONG S.W., MAREZIO M. Wigner-crystal and bi-stripe models for the magnetic and crystallographic superstructures of $La_{0.333}Ca_{0.667}MnO_3$.
Physical Review B **59**, 14440-14450 (1999)

RADLINSKI A.P., RADLINSKA E.Z., AGAMALIAN M., WIGNALL G.D., LINDNER P., RANDL O.G. Fractal geometry of rocks.
Physical Review Letters **82**, 3078-3081 (1999)

RAUCH H., ZAWISKY M., STELLMACH C., GELTENBORT P. Giant absorption cross section of ultracold neutrons in gadolinium.
Physical Review Letters **83**, 4955-4958 (1999)

RAYMOND S., RAOELISON D., KAMBE S., REGNAULT L.P., FÅK B., CALEMCZUK R., FLOUQUET J., HAEN P., LEJAY P. Magnetic instabilities in $CeRu_2Si_2$ compounds.
Physica B **259-261**, 48-53 (1999)

RAYMOND S., YOKOO T., ZHELUDEV A., NAGLER S.E., WILDES A., AKIMITSU J. Polarized-neutron observation of longitudinal Haldane-gap excitations in Nd_2BaNiO_5.
Physical Review Letters **82**, 2382-2385 (1999)

REEHUIS M., GERDES M., JEITSCHKO W., OULADDIAF B., STÜSSER N. Crystal and magnetic structure of the ternary carbides $Ho_2Mo_2C_3$ and $Er_2Mo_2C_3$.
Zeitschrift für Kristallographie Supplement **16**, 166 (1999)

REEHUIS M., GERDES M., JEITSCHKO W., OULADDIAF B., STÜSSER N. Crystal and magnetic structures of the ternary carbides $Ho_2Mo_2C_3$ and $Er_2Mo_2C_3$.
Journal of Magnetism and Magnetic Materials **195**, 657-666 (1999)

REGNAULT L.P., BOUCHER J.P., MOUDDEN H., LORENZO J.E., HIESS A., AMMERAHL U., DHALENNE G., REVCOLEVSCHI A. Spin dynamics in the magnetic chain arrays of $Sr_{14}Cu_{24}O_{41}$: A neutron inelastic scattering investigation.
Physical Review B **59**, 1055-1059 (1999)

REGNAULT L.P., MOUDDEN A.H., BOUCHER J.P., LORENZO E., HIESS A., VIETKIN A., REVCOLEVSCHI A. Spin dynamics of the spin ladder system $Sr_{14}Cu_{24}O_{41}$.
Physica B **259-261**, 1038-1039 (1999)

REGNAULT L.P., TASSET F., LORENZO J.E., ROBERTS T., DHALENNE G., REVCOLEVSCHI A. Polarized neutron inelastic scattering on the spin-Peierls system $CuGeO_3$: "three-directional" versus "three-dimensional" polarization analysis.
Physica B **267-268**, 227-235 (1999)

REMHOF A., SONG G., SUTTER C., SCHREYER A., SIEBRECHT R., ZABEL H., GÜTHOFF F., WINDGASSE J. Hydrogen and deuterium in epitaxial Y(0001) films: Structural properties and isotope exchange.
Physical Review B **59**, 6689-6699 (1999)

RENKER B., SCHOBER H., BRADEN M. Alignment of polymer chains in RbC_{60} by uniaxial pressure.
Solid State Communications **109**, 423-426 (1999)

RENKER B., SCHOBER H., LEBEDKIN S. Microscopic dynamics of C_{60}-polymers.
Synthetic Metals **103**, 2443-2444 (1999)

REQUARDT H., NAD F.Y., MONCEAU P., CURRAT R., LORENZO J.E., GRÜBEL G., VETTIER C. Current conversion in the sliding charge density wave state of $NbSe_3$.
Synthetic Metals **103**, 2586-2588 (1999)

RICHARD O., SCHUDDINCK W., VAN TENDELOO G., MILLANGE F., HERVIEU M., CAIGNAERT V., RAVEAU B. Room-temperature and low-temperature structure of $Nd_{1-x}Ca_xMnO_3$ ($0.3 \leq x \leq 0.5$).
Acta Crystallographica A **55**, 704-718 (1999)

RICHTER D., MONKENBUSCH M., ALLGEIER J., ARBE A., COLMENERO J., FARAGO B., CHEOL BAE Y., FAUST R. From Rouse dynamics to local relaxation: A neutron spin echo study on polyisobutylene melts.
Journal of Chemical Physics **111**, 6107-6120 (1999)

RICHTER D., MONKENBUSCH M., ARBE A., COLMENERO J., FARAGO B., FAUST R. Space time observation of the α-process in polymers by quasielastic neutron scattering.
Journal of Physics Condensed Matter **11**, A297-A306 (1999)

RIGHI A., AYALA A.P., BOURSON P., OULADDIAF B., MOREIRA R.L. High temperature neutron diffraction study of $LiK_{1-x}Rb_xSO_4$ crystals.
Journal of Physics Condensed Matter **11**, 6859-6866 (1999)

RISEMAN T.M., KEALEY P.G., FORGAN E.M., MACKENZIE A.P., GALVIN L.M., TYLER A.W., LEE S.L., AGER C., PAUL D.MCK., AEGERTER C.M., CUBITT R., MAO Z.Q., AKIMA T., MAENO Y. Observation of a square flux-line lattice in the unconventional superconductor Sr_2RuO_4.
Nature **396**, 242-245 (1998)

RITTER C., IBARRA M.R., MARQUINA C. The influence of doping on the stability of a new magnetic ground state in RMn_2-compounds.
Journal of Magnetism and Magnetic Materials **196-197**, 721-722 (1999)

ROBERTS T.W., ZOCHOWSKI S.W., TASSET F., MCEWEN K.A. Magnetic moment directions in the 3-*q* phase of neodymium from neutron polarimetry with CRYOPAD.
Physica B **267-268**, 243-247 (1999)

ROCHAS C., HECHT A.M., GEISSLER E. Scattering properties of agarose gels.
Macromolecules Symposium **138**, 157-163 (1999)

ROEPKE M., HOLLAND-MORITZ E., BÜCHNER B., BERG H., LECHNER R.E., LONGEVILLE S., FITTER J., KAHN R., CODDENS G., FERRAND M. 4*f*-spin dynamics in $La_{2-x-y}Sr_xNd_yCuO_4$.
Physical Review B **60**, 9793-9800 (1999)

ROLS S., ALMAIRAC R., HENRARD L., ANGLARET E., SAUVAJOL J.L. Diffraction by finite-size crystalline bundles of single wall nanotubes.
European Physical Journal B **10**, 263-270 (1999)

ROLS S., ALMAIRAC R., HENRARD L., ANGLARET E., SAUVAJOL J.L. Structure of single-wall carbon nanotubes: Neutron powder diffraction and simulations.
Synthetic Metals **103**, 2517-2518 (1999)

ROMERO DE PAZ J., FERNANDEZ-DIAZ M.T., HERNANDEZ VELASCO J., SAEZ PUCHE R., MARTINEZ J.L. Crystal and magnetic structure of $PrCaCrO_4$.
Journal of Solid State Chemistry **142**, 29-32 (1999)

ROTHENHÄUSLER C., LERCH M., RAHÄUSER O., HANSEN T. Über Kristallstruktur und Hochtemperaturverhalten von NbNO.
Zeitschrift für Kristallographie Supplement **16**, 59 (1999)

ROZENBERG M.J., GREMPEL D.R. The Ising spin glass in a transverse field and the Kondo model.
Physica B **259-261**, 174-175 (1999)

RUOCCO G., SETTE F. The high-frequency dynamics of liquid water.
Journal of Physics Condensed Matter **11**, R259-R293 (1999)

SAUVAJOL J.L., ANGLARET E., ROLS S., JOURNET C., GOZE C., BERNIER P., MASER W.K., MUNOZ E., BENITO A.M., MARTINEZ M.T., CODDENS G., DIANOUX A.J. Structure and vibrational properties of single wall carbon nanotubes.
Synthetic Metals **103**, 2537-2539 (1999)

SAVIOT L., DUVAL E., SUROVTSEV N., JAL J.F., DIANOUX A.J. Propagating to nonpropagating vibrational modes in amorphous polycarbonate.
Physical Review B **60**, 18-21 (1999)

SAYETAT F., DEPORTES J., OULADDIAF B., KESSLER M., SAOUDI M., REEHUIS M. Fe magnetism in $Ti_{1-x}Sc_xFe_2$ ($x \leq 0.2$)1.
Journal of Magnetism and Magnetic Materials **192**, 100-104 (1999)

SCHAD R., BELIËN P., VERBANCK G., MOSHCHALKOV V.V., BRUYNSERAEDE Y., FISCHER H.E., LEFEBVRE S., BESSIERE M. Giant magnetoresistance dependence on the lateral correlation length of the interface roughness in magnetic superlattices.
Physical Review B **59**, 1242-1248 (1999)

SCHAD R., BELIËN P., VERBANCK G., TEMST K., FISCHER H., LEFEBVRE S., BESSIERE M., BAHR D., FALTA J., DEKOSTER J., LANGOUCHE G., MOSHCHALKOV V.V., BRUYNSERAEDE Y. Giant magnetoresistance in Fe/Cr superlattices with and without bulk scattering.
Journal of Magnetism and Magnetic Materials **198-199**, 104-106 (1999)

SCHEYER Y., LEVELUT C., PELOUS J., DURAND D. Cross-link density influence on the relaxations in glass- and gel-forming polyurethanes by neutron and Brillouin scattering.
Physical Review B **57**, 11212-11220 (1998)

SCHLEGER P., EHLERS G., KOLLMAR A., ALEFELD B., BARTHELEMY J.F., CASALTA H., FARAGO B., GIRAUD P., HAYES C., LARTIGUE C., MEZEI F., RICHTER D. The sub-neV resolution NSE spectrometer IN15 at the Institute Laue-Langevin.
Physica B **266**, 49-55 (1999)

SCHMITT D., OULADDIAF B., ROUTSI C.D., YAKINTHOS J.K., GAMARI-SEALE H. Magnetic properties of $RPdGe_2$ (R = Y, Gd, Tb, Dy) compounds.
Journal of Alloys and Compounds **292**, 21-26 (1999)

SCHOBER H., RENKER B. On how to do solid state chemistry with inelastic neutron scattering: The example of network formation in fullerenes.
Neutron News **10**, 28-33 (1999)

SCHOBER H., RENKER B. Pressure dependence of the external mode spectrum of solid C_{60}.
Physical Review B **59**, 3287-3290 (1999)

SCHOBER H., RENKER B., HEID R. Vibrational behavior of Na_4C_{60} in the monomer and two-dimensional polymer states.
Physical Review B **60**, 998-1004 (1999)

SCHOBINGER-PAPAMANTELLOS P., BUSCHOW K.H.J., DE GROOT C.H., DE BOER F.R., BÖTTGER G., RITTER C. Magnetic ordering of $Pr_6Fe_{13}Si$ and $Nd_6Fe_{13}Au$ studied by neutron diffraction.
Journal of Physics Condensed Matter **11**, 4469-4481 (1999)

SCHOBINGER-PAPAMANTELLOS P., BUSCHOW K.H.J., HAGMUSA I.H., DE BOER F.R., RITTER C., FAUTH F. Magnetic ordering of $TbFe_4Al_8$ studied by neutron diffraction. I.
Journal of Magnetism and Magnetic Materials **202**, 410-425 (1999)

SCHOBINGER-PAPAMANTELLOS P., BUSCHOW K.H.J., RITTER C. The (T, x) magnetic phase diagram of $TbNi_xGe_2$ ($0.4 < x < 1$) compounds. A neutron study.
Journal of Alloys and Compounds **287**, 51-56 (1999)

SCHOLPP T., WEIDNER E., FREY F., GILLE P., HRADIL K., MCINTYRE G., BOISSIEU M. DE, CURRAT R., GRUSHKO B., TSAI A.P. Neutronen und Röntgenbeugungsuntersuchungen an fehlgeordneten dekagonalen Al-Ni-Co Phasen.
Zeitschrift für Kristallographie Supplement **16**, 144 (1999)

SCHOLTEN M., DRONSKOWSKI R., JACOBS H. $InCrBr_3$: A ternary indium bromide containing Jahn-Teller unstable Cr^{2+} and the magnetic structures of $InCrBr_3$ and $InFeBr_3$.
Inorganic Chemistry **38**, 2614-2620 (1999)

SCHREYER A., SIEBRECHT R., ENGLISCH U., PIETSCH U., ZABEL H. ADAM, the new reflectometer at the ILL.
Physica B **248**, 349-354 (1998)

SCHWEIZER J. Historical account of polarized neutrons in Grenoble.
Physica B **267-268**, 9-20 (1999)

SEMADENI F., BÖNI P., ENDOH Y., ROESSLI B., SHIRANE G. Direct observation of spin-flip excitations in MnSi.
Physica B **267-268**, 248-251 (1999)

SERRANO-GONZALEZ H., BRAMWELL S.T., HARRIS K.D.M., KARIUKI B.M., NIXON L., PARKIN I.P., RITTER C. Structural and magnetic characterization of the frustrated triangular-lattice antiferromagnets $CsFe(SO_4)_2$ and $RbFe(SO_4)_2$.
Physical Review B **59**, 14451-14460 (1999)

SFERRAZZA M., HEPPENSTALL-BUTLER M., CUBITT R., BUCKNALL D., WEBSTER J., JONES R.A.L. Interfacial instability driven by dispersive forces: The early stages of spinodal dewetting of a thin polymer film on a polymer substrate.
Physical Review Letters **81**, 5173-5176 (1998)

SIEBRECHT R., SCHREYER A., ENGLISCH U., PIETSCH U., ZABEL H. The new reflectometer ADAM at the ILL.
Physica B **241-243**, 169-171 (1998)

SIEBRECHT R., SCHREYER A., SCHMITTE T., SCHMIDT W., ZABEL H. Investigation of magnetic coupling phenomena in $Fe_{1-x}Cr_x$/Cr-superlattices with spin-polarized neutrons.
Physica B **267-268**, 207-210 (1999)

SIERKS C., LOEWENHAUPT M., TILS P., FREUDENBERGER J., MÜLLER K.H., LOONG C.K., SCHOBER H. Magnetic excitations in the Kondo-lattice $YbNi_2{}^{11}B_2C$.
Physica B **259-261**, 592-593 (1999)

SOKOLOV A.P., BUCHENAU U., RICHTER D., MASCIOVECCHIO C., SETTE F., MERMET A., FIORETTO D., RUOCCO G., WILLNER L., FRICK B. Brillouin and Umklapp scattering in polybutadiene: Comparison of neutron and X-ray scattering.
Physical Review E **60**, R2464-R2467 (1999)

STAUB U., GUTMANN M., FAUTH F., KAGUNYA W. Difficulty of probing the superconducting gap with relaxation measurements on 4f crystal-field transitions with neutron scattering.
Journal of Physics Condensed Matter **11**, L59-L64 (1999)

STELLBRINK J., WILLNER L., RICHTER D., LINDNER P., FETTERS L.J., HUANG J.S. Self-assembling behavior of butadienyllithium headgroups in benzene via SANS measurements.
Macromolecules **32**, 5321-5329 (1999)

STOCKERT O., LÖHNEYSEN H.V., ROSCH A., PYKA N., LOEWENHAUPT M. Spin dynamics at the magnetic instability in $CeCu_{6-x}Au_x$.
Physica B **259-261**, 376-377 (1999)

STOCKERT O., SCHRÖDER A., LÖHNEYSEN H.V., PYKA N., GARCIA-MATRES E., KAMP R.V.D., WELZEL S., LOEWENHAUPT M. Evolution of the magnetic order in $CeCu_{6-x}Au_x$.
Physica B **259-261**, 383-384 (1999)

STREMPFER J., BRÜCKEL T., MCINTYRE G.J., TASSET F., ZEISKE T., BURGER K., PRANDL W. A reinvestigation of the field-induced magnetic form factor of chromium.
Physica B **267-268**, 56-59 (1999)

STRITT N., JOLIE J., JENTSCHEL M., BÖRNER H.G., DOLL C. Investigation of the interatomic potential using the crystal gamma-ray-induced Doppler-broadening method on oriented Ni single crystals.
Physical Review B **59**, 6762-6773 (1999)

STROBEL P., LE CRAS F., SEGUIN L., ANNE M., TARASCON J.M. Oxygen nonstoichiometry in Li-Mn-O spinel oxides: A powder neutron diffraction study.
Journal of Solid State Chemistry **135**, 132-139 (1998)

STUHR U., CORNELL K., WIPF H. Deuterium diffusion in niobium: The influence of coherency stresses.
Physical Review Letters **82**, 2302-2305 (1999)

STUHR U., WIPF H., ANDERSEN K.H., HAHN H. Low-frequency modes in nanocrystalline Pd.
Physical Review Letters **81**, 1449-1452 (1998)

STUHRMANN H.B. Neutron contrast variation and dynamic nuclear polarisation.
Physica B **267-268**, 92-96 (1999)

STUNAULT A., BERGEVIN F. DE, WERMEILLE D., VETTIER C., BRÜCKEL T., BERNHOEFT N., MCINTYRE G.J., HENRY J.Y. K-edge resonant X-ray magnetic scattering from $RbMnF_3$.
Physical Review B **60**, 10170-10179 (1999)

SUNDARESAN A., CAIGNAERT V., MAIGNAN A., RAVEAU B., SUARD E. Anomalous magnetic ordering of Ce and Kondo-like effect in the double-exchange ferromagnet $(Pr_{0.1}Ce_{0.4}Sr_{0.5})MnO_3$.
Physical Review B **60**, 533-537 (1999)`

TAKEDA T., SETO H., KAWABATA Y., OKUHARA D., KRIST T., ZEYEN C.M.E., ANDERSON I.S., HØGHØJ P., NAGAO M., YOSHIZAWA H., KOMURA S., EBISAWA T., TASAKI S., MONKENBUSCH M. Improvement of neutron spin echo spectrometer at C2-2 of JRR3M.
Journal of Physics and Chemistry of Solids **60**, 1599-1601 (1999)

TASSET F., BROWN P.J., LELIEVRE-BERNA E., ROBERTS T., PUJOL S., ALLIBON J., BOURGEAT-LAMI E. Spherical neutron polarimetry with Cryopad-II.
Physica B **267-268**, 69-74 (1999)

TASSET F., LELIEVRE-BERNA E. ILL hosts PNCMI'98.
Neutron News **10**, 2-3 (1999)

TAYLOR J.W., SMITH T.J., ANDERSEN K.H., CAPELLMANN H., KREMER R.K., SIMON A., SCHÄRPF O., NEUMANN K.U., ZIEBECK K.R.A. Spin-spin correlations in the insulating and metallic phases of the Mott system V_2O_3.
European Physical Journal B **12**, 199-207 (1999)

TERECH P., COUTIN A. Structure of a transient network made up of entangled monomolecular organometallic wires in organic liquids. Effects of an endcapping molecule.
Langmuir **15**, 5513-5525 (1999)

TERECH P., TRZNADEL M., RANNOU P., TRAVERS J.P., NECHTSCHEIN M., LEGRAND J.F., DJURADO D. Preliminary SANS studies of PANI-CSA films.
Synthetic Metals **101**, 839 (1999)

TERECH P., WEISS R.G. Low-mass luminescent organogels.
In: "Surface Characterization Methods. Principles, Techniques, and Applications", MILLING A.J. (Eds) (Marcel Dekker, Inc., 1999) pp.285-344

TERKI F., PILLIEZ J.N., WOIGNIER T., PELOUS J., FONTANA A., ROSSI F., MONTAGNA M., FERRARI M., CICOGNANI G., DIANOUX A.J. Low-frenquency light scattering in silica xerogels: Influence of the heat treatment.
Philosophical Magazine B **79**, 2081-2089 (1999)

TIETZE-JAENSCH H., VAN DE KAMP R., SCHMIDT W. Magnetic excitation mode splitting and finite size effects in Rb_2MnCl_4.
Physica B **241-243**, 566-569 (1998)

TOLLA B., DEMOURGUES A., POUCHARD M., RABARDEL L., FOURNES L., WATTIAUX A. Oxygen exchange properties in the new pyrochlore solid solution $Ce_2Sn_2O_7$-$Ce_2Sn_2O_8$.
Comptes Rendus de l'Academie des Sciences **2**, 139-146 (1999)

TOPERVERG B., VOROBYEV A., GORDEYEV G., LAZEBNIK A., REKVELDT T., KRAAN W. Use of the optical theorem in polarized neutron small angle scattering from ferrofluid.
Physica B **267-268**, 203-206 (1999)

TOPERVERG B.P., RÜHM A., DONNER W., DOSCH H. Polarized neutron grazing angle birefrigent diffraction from magnetic stratified media.
Physica B **267-268**, 198-202 (1999)

TSEKHANOVICH I., DENSCHLAG H.O., DAVI M., BÜYÜKMUMCU Z., WÖSTHEINRICH M., GÖNNENWEIN F., OBERSTEDT S., FAUST H.R. Mass and charge distributions in the very asymmetric thermal neutron induced fission of the odd-Z nucleus $^{242m}Am^*$.
Nuclear Physics A **658**, 217-239 (1999)

TSUKADA I., SASAGO Y., UCHINOKURA K., ZHELUDEV A., MASLOV S., SHIRANE G., KAKURAI K., RESSOUCHE E. $BaCu_2Si_2O_7$: A quasi-one-dimensional $S = 1/2$ antiferromagnetic chain system.
Physical Review B **60**, 6601-6607 (1999)

TUINIER R., TEN GROTENHUIS E., HOLT C., TIMMINS P.A., DE KRUIF C.G. Depletion interaction of casein micelles and an exocellular polysaccharide.
Physical Review E **60**, 848-856 (1999)

TURNER S.F., CLARKE S.M., RENNIE A.R., THIRTLE P.N., COOKE D.J., LI Z.X., THOMAS R.K. Adsorption of sodium dodecyl sulfate to a polystyrene/water interface studied by neutron reflection and attenuated total reflection infrared spectroscopy.
Langmuir **15**, 1017-1023 (1999)

UHLIG H., SUCK J.B. Quasielastic neutron scattering experiments on icosahedral $Al_{71}Pd_{19}Mn_{10}$ at different temperatures.
In: "Proceedings of the International Conference on Aperiodic Crystals - Aperiodic'97", BOISSIEU M. DE, VERGER-GAUGRY J.L., CURRAT R. (Eds) (World Scientific, 1998) pp.657-661

VAN DER GRINTEN M.G.D., PENDLEBURY J.M., SHIERS D., BAKER C.A., GREEN K., HARRIS P.G., IAYDJIEV P.S., IVANOV S.N., GELTENBORT P. Characterization and development of diamond-like carbon coatings for storing ultracold neutrons.
Nuclear Instruments and Methods in Physics Research A **423**, 421-427 (1999)

VANNIER R.N., ABRAHAM F., NOWOGROCKI G., MAIRESSE G. New structural and electrical data on Bi-Mo mixed oxides with a structure based on $[Bi_{12}O_{14}]_\infty$ columns.
Journal of Solid State Chemistry **142**, 294-304 (1999)

VANNIER R.N., THERY O., KINOWSKI C., HUVE M., VAN TENDELOO G., SUARD E., ABRAHAM F. Zr substituted bismuth uranate.
Journal of Materials Chemistry **9**, 435-443 (1999)

VERDIERE M., M'SAAD M. Commande prédictive en température de cryostats.
In: "JDA'99, Journées Doctorales d'Automatique" (1999) pp.149-152

VERSMOLD H., MUSA S., DUX C., LINDNER P. On the structure of shear-ordered colloidal dispersions: Bragg-rod intensity distribution.
Langmuir **15**, 5065-5067 (1999)

VERT R., BOUOUDINA M., FRUCHART D., GIGNOUX D., KALYCHAK Y., OULADDIAF B., SKOLOZDRA R.V. Magnetisation and neutron diffraction studies of $HoFe_{12-x}Ta_xX_y$ ($0.5 \leq x \leq 0.7$, X = H, C).
Journal of Alloys and Compounds **285**, 56-63 (1999)

VISSER D., CARLING S.G., WATTS I.D., DAY P., ANDERSEN K.H. Neutron polarisation analysis of the magnetic ordering of the quasi-two-dimensional honeycomb network d_{20}-$(P(C_6D_5)_4)Fe^{II}Fe^{III}(C_2O_4)_3$.
Physica B **267-268**, 266-269 (1999)

WAGEMANS C., WAGEMANS J., GELTENBORT P., ZIMMER O. Experimental determination of the $^{234}U(n_{th}, f)$ cross section.
Nuclear Science and Engineering **132**, 308-311 (1999)

WAGNER J., JANSSEN S., RUPP R., MAY R., HEMPELMANN R. Characterization of nanoscale titanium nitride dispersions by small-angle neutron scattering.
Journal of the American Ceramic Society **81**, 3313-3317 (1998)

WESTERMANN S., KREITSCHMANN M., PYCKHOUT-HINTZEN W., RICHTER D., STRAUBE E., FARAGO B., GOERIGK G. Matrix chain deformation in reinforced networks: A SANS approach.
Macromolecules **32**, 5793-5802 (1999)

WILDES A.R. The polarizer-analyzer correction problem in neutron polarization analysis experiments.
Review of Scientific Instruments **70**, 4241-4245 (1999)

WILKINS C.J.T., RAINFORD B.D., GOFF J.P., WARD R.C.C., WELLS M.R., MCMORROW D.F., MCINTYRE G.J. Magnetic characterisation of Tm/Y and Tm/Lu superlattices.
Journal of Magnetism and Magnetic Materials **198-199**, 509-512 (1999)

WILSON R.W., BAILEY L., CUBITT R., GONSALVES M., GLIDLE A., HILLMAN A.R., VOS J.G., HOGAN C., WEBSTER J.R.P. A study of $[Os(bipy)_2(PVP)_{3.3}(PS)_{6.7}Cl]^+$ polymer film modified electrodes using neutron reflectivity.
Physical Chemistry - Chemical Physics **1**, 843-853 (1999)

WILSON R.W., CUBITT R., GLIDLE A., HILLMANN A.R., SAVILLE P.M., VOS J.G. A neutron reflectivity study of $[Os(bipy)_2(PVP)_{10}C1]^+$ polymer film modified electrodes: Effect of redox state and counter ion.
Electrochimica Acta **44**, 3533-3548 (1999)

WÖSTHEINRICH M., PFISTER R., GÖNNENWEIN F., DENSCHLAG H.O., FAUST H., OBERSTEDT S. Yields of ternary particles from the reactions $^{229}Th(n_{th}, f)$, $^{233}U(n_{th}, f)$ and $^{239}Pu(n_{th}, f)$.
Acta Physica Slovaca **49**, 117-124 (1999)

WÜRGER A. Tunneling systems with dipolar interactions.
Physica B **263-264**, 253-257 (1999)

WUTTKE J. Improved sample holder for multidetector neutron spectrometers.
Physica B **266**, 112-114 (1999)

Y MARERO D.M., ENGBERG D. OSIRIS: The polarisation analysis spectrometer and diffractometer at ISIS.
Physica B **267-268**, 134-138 (1999)

YOKOO T., RAYMOND S., ZHELUDEV A., MASLOV S., RESSOUCHE E., ZALIZNYAK I., ERWIN R., NAKAMURA M., AKIMITSU J. Magnetic ordering, spin waves, and Haldane gap excitations in $(Nd_xY_{1-x})_2BaNiO_5$ linear-chain mixed-spin antiferromagnets.
Physical Review B **58**, 14424-14435 (1998)

ZAKHAROVA S.S., EGELHAAF S.U., BHUIYAN L.B., OUTHWAITE C.W., BRATKO D., VAN DER MAAREL J.R.C. Multivalent ion-DNA interaction: Neutron scattering estimates of polyamine distribution.
Journal of Chemical Physics **111**, 10706-10716 (1999)

ZEMB T., DUBOIS M., DEME B., GULIK-KRZYWICKI T. Self-assembly of flat nanodiscs in salt-free catanionic surfactant solutions.
Science **283**, 816-819 (1999)

ZEYEN C.M.E. Spin echo three-axes spectrometers for improved energy and momentum resolution.
Journal of Physics and Chemistry of Solids **60**, 1573-1578 (1999)

ZHELUDEV A. Haldane spin chains in a staggered field: 2-1-1-5 rare earth nickelates.
Neutron News **10**, 16-19 (1999)

ZIMMER O. A method for precise neutron beam polarisation analysis using an opaque spin filter.
Physics Letters B **461**, 307-314 (1999)

ZIMMER O., MÜLLER T.M., HAUTLE P., HEIL W., HUMBLOT H. High-precision neutron polarization analysis using opaque spin filters.
Physics Letters B **455**, 62-68 (1999)

ZIPFEL J., BERGHAUSEN J., LINDNER P., RICHTERING W. Influence of shear on lyotropic lamellar phases with different membrane defects.
Journal of Physical Chemistry B **103**, 2841-2849 (1999)

ZIPFEL J., BERGHAUSEN J., SCHMIDT G., LINDNER P., ALEXANDRIDIS P., TSIANOU M., RICHTERING W. Shear induced structures in lamellar phases of amphiphilic block copolymers.
Physical Chemistry - Chemical Physics **1**, 3905-3910 (1999)

ZIPFEL J., LINDNER P., TSIANOU M., ALEXANDRIDIS P., RICHTERING W. Shear-induced formation of multilamellar vesicles ("onions") in block copolymers.
Langmuir **15**, 2599-2602 (1999)

BOOKS PUBLISHED

BOISSIEU M. DE, VERGER-GAUGRY J.L., CURRAT R. Proceedings of the International Conference on Aperiodic Crystals - Aperiodic'97.
World Scientific, 1998

GIVORD F., REGNAULT L. P., RESSOUCHE E. Proceedings of the Second International Workshop on Polarised Neutrons for Condensed Matter Investigations-PNCMI'98. (TASSET F., chairman).
Physica B, 1999

JOHNSON M. R., KEARLEY G. J., BÜTTNER H. G. Neutrons and Numerical Methods-N_2M.
AIP Conference Proceedings 479, 1999

THESES AND HABILITATIONS

JOHNSON M.R. De l'effet tunnel des protons à la modélisation de la surface d'énergie potentielle.
Institut Laue-Langevin, Grenoble, France.
Mémoire présenté pour un diplôme d'habilitation à diriger les recherches. Université Joseph Fourier, Grenoble I, France (1999)

KREISEL J. Etude d'hexaferrites de baryum substitués $BaFe_{12-2x}A_xCo_xO_{19}$ (A = Ir, Ti) - Synthèse de monocristaux, structures cristallines et magnétiques, spectroscopie Raman -
Thèse présentée pour obtenir le titre de Docteur de l'Institut National Polytechnique de Grenoble, France (1999)

MORELON N.D. Dynamique moléculaire du composé d'inclusion TANO-heptane. Une étude combinée : simulation numérique/diffusion quasiélastique incohérente des neutrons.
Thèse présentée pour obtenir le titre de Docteur de l'Université Joseph FOURIER-Grenoble 1, France (1999)

MORFIN I. Structures induites par l'écoulement dans une solution viscoélastique de polymère.
Thèse présentée pour obtenir le grade de Docteur de l'Université Joseph Fourier, Grenoble, France (1999)

NICOLAÏ B. Dynamique rotationnelle des groupements méthyles et structure cristalline à basse température, étude par diffusion des neutrons et modélisation.
Thèse présentée pour obtenir le grade de Docteur de l'Université Paris 7-Denis Diderot, France (1998)

PICHLMAIER A.C. Messung der Lebensdauer freier Neutronen mittels Speicherung von ultrakalten Neutronen.
Vollständiger Abdruck der von der Fakultät für Physik der Technischen Universität München zur Erlangung des akademischen Grades eines Doktors der Naturwissenschaften genehmigten Dissertation, München, Germany (1999)

PORTES DE ALBUQUERQUE M. Mesure optimisée de densités d'aimantation.
Thèse présentée pour obtenir le titre de Docteur de l'Institut National Polytechnique de Grenoble - INPG, France (1999)

STEGMANN R. Untersuchung des Chaperonsystems GroE mit Neutronenkleinwinkelstreuung.
Vollständiger Abdruck der von der Fakultät für Physik der Technischen Universität München zur Erlangung des akademischen Grades eines Doktors der Naturwissenschaften (Dr. rer. nat.) genehmigten Dissertation, München, Germany (1998)

STELLMACH C. Anderson-Lokalisierung und Hochfrequenzinduzierte Polarisation von ultrakalten Neutronen.
Inaugural - Dissertation zur Erlangung der Doktorwürde der Naturwissenschaftlich-Mathematischen Gesamtfakultät der Ruprecht-Karls-Universität Heidelberg, Germany (1998)

WILSON R.W. Neutron reflectivity studies of polymer modified electrodes.
Thesis submitted for the degree of Doctor of Philosophy at the University of Leicester, Great Britain (1999)

WÖSTHEINRICH M. Emission von ternären Teilchen aus den Reaktionen $^{229}Th(n_{th},f)$, $^{233}U(n_{th},f)$ und $^{239}Pu(n_{th},f)$.
Dissertation zur Erlangung des Grades eines Doktors der Naturwissenschaften der Fakultät für Physik der Eberhard-Karls-Universität zu Tübingen, Germany (1999)

Editors: Herma G. Büttner, Christian Vettier
Design and typesetting: Soft Office – www.softoffice.fr
Photography by J.L. Baudet, H.G. Büttner, P. Convert, S. Claisse (ILL), Studio de la Revirée
Printing: France Quercy
April 2000

Acknowledgement
We would like to thank all the people who helped make this report.

Further copies can be obtained from:
Institut Laue-Langevin
Scientific **C**oordination **O**ffice (SCO)
BP 156 – F-38042 Grenoble Cedex 9 (France)
tel: +33 (0)4 76 20 72 40 – fax: +33 (0)4 76 48 39 06
email: kjenkins@ill.fr or sco@ill.fr
web: www.ill.fr

NEUTRONS
FOR SCIENCE

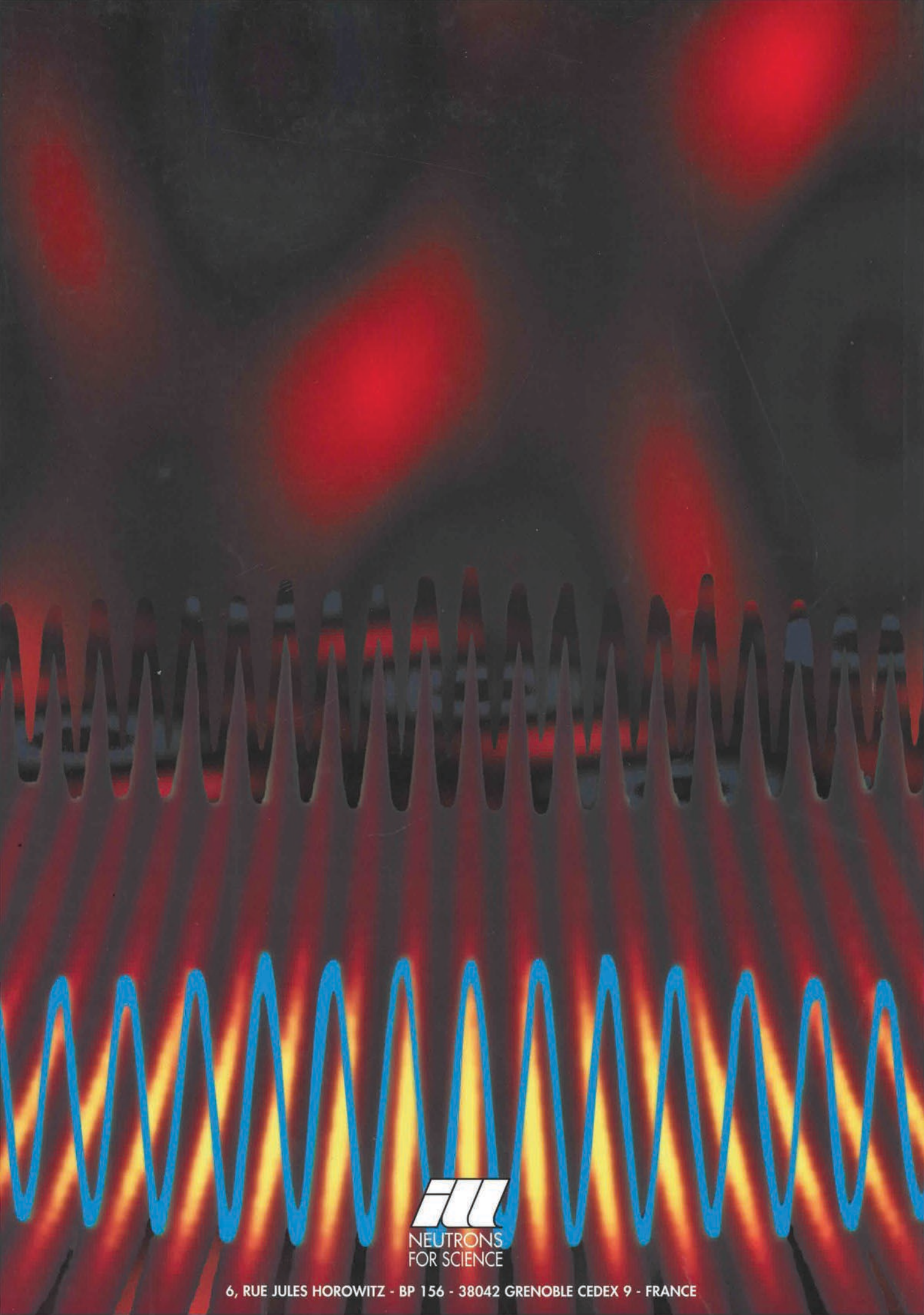

NEUTRONS
FOR SCIENCE

6, RUE JULES HOROWITZ - BP 156 - 38042 GRENOBLE CEDEX 9 - FRANCE